INVESTIGATION AND ASSESSMENT OF THE INTEGRATED COPPER CHLORINE CYCLE FOR HYDROGEN PRODUCTION WITH A NEW SEPARATION PROCESS

by

Faran Razi

A thesis submitted to the
School of Graduate and Postdoctoral Studies in partial
fulfillment of the requirements for the degree of

Doctor of Philosophy in Mechanical Engineering

Faculty of Engineering and Applied Science

University of Ontario Institute of Technology (Ontario Tech University)

Oshawa, Ontario, Canada

August 2021

THESIS EXAMINATION INFORMATION

Submitted by: **Faran Razi**

Doctor of Philosophy in **Mechanical Engineering**

Thesis title: Investigation and Assessment of the Integrated Copper Chlorine Cycle for Hydrogen Production with a New Separation Process

An oral defense of this thesis took place on July 31, 2021 in front of the following examining committee:

Examining Committee:

Chair of Examining Committee	Dr. Martin Agelin-Chaab
Research Supervisor	Dr. Ibrahim Dincer
Research Co-supervisor	Dr. Kamiel Gabriel
Examining Committee Member	Dr. Haoxiang Lang
Examining Committee Member	Dr. Dipal Patel
University Examiner	Dr. Remon Pop-Iliev
External Examiner	Dr. Ali Elkamel, University of Waterloo

The above committee determined that the thesis is acceptable in form and content and that a satisfactory knowledge of the field covered by the thesis was demonstrated by the candidate during an oral examination. A signed copy of the Certificate of Approval is available from the School of Graduate and Postdoctoral Studies.

ABSTRACT

The production of hydrogen as a clean fuel is anticipated to have a major impact on the development of the environmentally benign generation of energy. At present, a significant portion of hydrogen generation is based on the exploitation of fossil fuels thereby contributing to an increase in global greenhouse gas emissions. Thus, hydrogen production through non-fossil fuel sources is essential for sustainable development. In this thesis, green hydrogen generation is considered via a four-step copper-chlorine thermochemical water-splitting cycle. The lab-scale integrated copper-chlorine cycle at the Clean Energy Research Laboratory is investigated in this regard. The integrated cycle is comprehensively studied through the energy and exergy, thermal management, exergoeconomic, exergoenvironmental, and multi-objective optimization approaches for performance assessment. A new approach for the anolyte separation step of the integrated cycle is also investigated and the flash vaporization process is proposed as a feasible option in this regard. The integrated cycle is also conceptually modified with the flash vaporization process and investigated through the energy and exergy, thermal management, exergoeconomic, and exergoenvironmental approaches and the performances of the integrated cycle at the Clean Energy Research Laboratory and the cycle conceptually modified with the flash vaporization process are comparatively assessed as well. Moreover, a standalone experimental setup is developed and the flash vaporization process is experimentally investigated. The overall energy and exergy efficiencies of the integrated cycle are evaluated as 6.6 and 10.2%, respectively while those of the cycle conceptually modified with flash vaporization are evaluated as 7.2 and 11%, respectively. The average unit hydrogen cost for the integrated cycle is evaluated to be 4.94 $/kg while that for the conceptually modified cycle is 4.7 $/kg. Moreover, the average unit hydrogen cost for the modified cycle with the incorporation of waste heat recovery is evaluated to be 2 $/kg for a production capacity of 1.3 T/h. In the context of the experimental assessment of the flash vaporization process, the flash chamber design with a higher length-to-diameter ratio results in a higher volume of the separated species.

Keywords: Hydrogen; thermochemical; copper-chlorine cycle; flash vaporization; exergy

AUTHOR'S DECLARATION

I hereby declare that this thesis consists of original work of which I have authored. This is a true copy of the thesis, including any required final revisions, as accepted by my examiners.

I authorize the University of Ontario Institute of Technology (Ontario Tech University) to lend this thesis to other institutions or individuals for the purpose of scholarly research. I further authorize University of Ontario Institute of Technology (Ontario Tech University) to reproduce this thesis by photocopying or by other means, in total or in part, at the request of other institutions or individuals for the purpose of scholarly research. I understand that my thesis will be made electronically available to the public.

_____ FARAN RAZI

STATEMENT OF CONTRIBUTIONS

Some parts of this thesis have been published in the following research publications:

F. Razi, I. Dincer, and K. Gabriel, “Energy and exergy analyses of a new integrated thermochemical copper-chlorine cycle for hydrogen production,” Energy, vol. 205, p. 117985, 2020.

F. Razi, I. Dincer, and K. Gabriel, “Thermal management of a new integrated copper-chlorine cycle for hydrogen production,” Energy Conversion and Management, vol. 212, p. 112629, 2020.

F. Razi, I. Dincer, and K. Gabriel, “A multiobjective optimization of the integrated copper-chlorine cycle for hydrogen production,” Computers and Chemical Engineering, vol. 140, p. 106889, 2020.

F. Razi, I. Dincer, and K. Gabriel, "A Specific exergy costing assessment of the integrated copper-chlorine cycle for hydrogen production," International Journal of Hydrogen Energy, vol. 45, No. 56, p. 31425-31439, 2020.

F. Razi, I. Dincer, and K. Gabriel, "Exergoeconomic analysis of a new integrated copper-chlorine cycle for hydrogen production," International Journal of Hydrogen Energy, vol. 45, No. 55, p. 30042-30055, 2020.

F. Razi, I. Dincer, and K. Gabriel, “Exergoenvironmental analysis of the integrated copper-chlorine cycle for hydrogen production”, Energy, vol. 226, p. 120426, 2021.

F. Razi, I. Dincer, and K. Gabriel, “Process Improvement and Analysis of an Integrated Four-Step Copper–Chlorine Cycle Modified with a Flash Vaporization Process for Hydrogen Production”, Energy and Fuels, vol. 35, No. 10, p. 9038–9046, 2021.

ACKNOWLEDGEMENTS

I would like to begin by expressing my deepest gratitude, love, and respect for my supervisor, teacher, and mentor Professor Ibrahim Dincer who inspired me by his example and showed me to the path of excellence. Professor Dincer has been a major source of inspiration for me during this journey. He provided me with the confidence and self-belief without which I would not have come this far. There are not enough words with me to thank him for his continuous support and his conviction in my abilities. His extraordinary comprehension and immensely vast experience guided me through the toughest obstacles during my research.

I would also like to thank my co-supervisor Professor Kamiel Gabriel who has also supported, guided, and mentored me during my Ph.D. journey.

I would like to express my deepest gratitude and love for my beloved wife Dr. Marium Tahir and my dearest daughter Madina Faran who have been the pillars of immense support to me during this journey. My wife has always been there for me during the toughest days of this journey and has constantly provided me with unconditional love and support through thick and thin. I would have never achieved this big milestone of my life without the support of my wife.

I am also very thankful to my beloved parents Mr. Razi Badshah and Mrs. Rehman Bibi for their constant prayers, love, and unconditional support during this journey. I would also like to thank my elder brother Cdr (R) Anees Muhammad Khan who encouraged me to pursue a Ph.D. degree. He dreamed that I should be a Ph.D. degree holder one day. Apart from him, I would also like to thank all my brothers and sisters who have extended their unconditional support to me throughout.

Last but not the least, I am also grateful to all my colleagues and friends at the ACE3030 and Clean Energy Research Laboratory for being extremely helpful and supportive throughout.

.

TABLE OF CONTENTS

LIST OF FIGURES

LIST OF TABLES

NOMENCLATURE

A	area (m^2)
b	specific environmental impact (mPt/kJ or mPt/kWh)
$\dot{B}$	environmental impact rate (mPt/h or Pt/s)
c	unit exergy cost ($/kJ or $/MJ), cost rate of electricity ($/kWh)
$\dot{C}$	heat cost rate/exergy cost ($/h)
$\dot{CA}$	annual capital cost ($/year)
CRF	capital recovery factor
CuCl	cuprous chloride
$CuCl_2$	cupric chloride
Cu_2OCl_2	copper-oxychloride
$\dot{E}x$	exergy rate (kJ/s or kW or MW)
ex	specific exergy (kJ/kg)
f	exergoeconomic factor/exergoenvironmental factor
h	specific enthalpy (kJ/kg)
HCl	hydrochloric acid
H_2	hydrogen
i	interest rate (%)
j	salvage value ratio (%)
K	capital cost ($)
$\dot{L}$	thermodynamic loss rate (kJ/s or kW or MW)
$\dot{m}$	mass flow rate (g/s or kg/s)
n	lifetime (years)
N	annual operating hours
O_2	oxygen
P	product, pressure (kPa)
PEC	purchased equipment cost ($)
PW	present worth ($)
PWF	present worth factor
$\dot{Q}$	heat rate (kJ/s or kW or MW)
r	relative cost difference/ relative difference of specific environmental impact
$\dot{R}$	Ratio of thermodynamic loss rate to capital cost (kW/$)
S	stream/state point, salvage value ($)
T	temperature (°C or K)
TCC	total capital cost ($)
$\dot{V}$	volume flow rate (l/s or m^3/s)
$\dot{W}$	work rate (kJ/s or kW or MW)
$\dot{Y}$	component-related environmental impact rate (mPt/h or Pt/s)
$\dot{Z}$	capital cost rate ($/h)

Greek letters

η	energy efficiency
ψ	exergy efficiency
τ	number of annual operating hours at full load
φ	operating and maintenance cost factor

ρ	density (kg/m^3)

Subscripts

0	ambient condition
ac	accumulated
ADA	atmospheric distillation unit of anolyte
ADU	anolyte drying unit
b	source
c	cycle
con	concentrator/consumption
cond	condenser
Des	destruction
Dry	dryer
e	exit
en	energy
Elec	electrolyzer
elec	electricity
ex	exergy
F	fuel
Gen	generation/generated
H	heater
HCl-cond	HCl condenser
Hyd	hydrolysis
i,in	inlet
j,k	location
max	maximum
min	minimum
out	output
P	product, pump
PH	preheater
PSDU	pressure swing distillation unit
Q	heat/thermal
q	heat transfer
QC	quench cell
S	stream/state point
SC	steam condenser
Sep	separation, separator
Therm	thermolysis
th	thermal, throttling valve
w	water, work
W	waste

Acronyms

ADA	atmospheric distillation unit of anolyte
ADU	anolyte drying unit
AMV	anolyte make up vessel

ANN	artificial neural network
C	configuration
CERL	Clean Energy Research Laboratory
Conc	concentrator
Cond	condenser
Cu-Cl	copper-chlorine
EES	engineering equation solver
Elect	electrolyzer
EXCEM	exergy cost energy mass
F	fuel
GA	genetic algorithm
GHG	greenhouse gas
GWP	global warming potential
H	heater
IC	internal combustion
L/D	length-to-diameter
LCA	life cycle assessment
LGS	liquid gas separator
LHV	lower heating value
MSE	mean square error
ORC	organic Rankine cycle
PF	pollutant formation
PSDU	pressure swing distillation unit
PVC	polyvinyl chloride
S/Cu	steam-to-copper
SMR	steam methane reforming
SNG	synthetic natural gas
SOFC	solid oxide fuel cell
SPECO	specific exergy costing
WGSR	water gas shift reaction

CHAPTER 1 : INTRODUCTION

In this chapter, the considerable use of fossil fuels globally and their continuous rise is discussed highlighting the importance of renewable energy resources and their significance in the future of clean energy production. The importance of hydrogen fuel is presented and its potential to be utilized as an effective energy storage medium is discussed. Finally, the potential of thermochemical water-splitting for sustainable green hydrogen production is described.

1.1 Utilization and environmental implications of fossil fuels

The energy requirements in the upcoming years are estimated to significantly increase as a consequence of the rise in human population and industrial activities. This increased demand for energy is expected to come from both the developed as well as developing countries. It is a substantial challenge to maintain an equilibrium between the demand and ample supply of energy particularly with an increased rate of population growth. New and innovative approaches are needed in this regard to ensure an adequate supply of electricity. The primary sources of global power generation are fossil fuels since they are capable of producing energy at higher efficiencies. Despite their effectiveness, the consistent and prolonged combustion of these fossil fuels has increased the global carbon footprint alongside the swift rate of fossil fuel depletion. There is an exceeding uncertainty with regards to the challenge of climate change mitigation in the near future due to the wide range of technological and economic factors [1]. The idea of a sustainable energy-based economy significantly depends upon the hydrogen produced through renewables and is an encouraging solution for both global climate change and fossil fuel exhaustion [2]. The global scientific community has been proactive in exploring innovative and efficient ways of employing alternate energy sources for a reduction in greenhouse gas (GHG) emissions while at the same time meeting the energy demands. Renewable sources hold the potential of exponentially meeting the global energy demand [3]. Nevertheless, the intermittent availability of renewables such as solar and wind energy presents a major challenge for the adoption of these sources at full scale.

1.2 Hydrogen as a potential fuel

Alternate non-carbonaceous fuels, like hydrogen, are considered as a sustainable carbon-free option to counter the issues such as energy sustainability and climate change [4]. Hydrogen, as an energy carrier, possesses a potential solution to the challenge of intermittency associated with renewables. Various manufacturing industries utilize hydrogen [5] and it can effectively be transformed into electrical energy [6]. Moreover, having a lower heating value (LHV) of 120 MJ/kg, hydrogen can be utilized as an efficient and environmentally benign fuel. Thus, hydrogen is becoming an integral part of future global energy policies because of its advantages over conventional carbonaceous fuels. There are numerous approaches for the generation of hydrogen including some commercially and technologically mature methods as well as a few techniques that are still in the developing stages. A process involving the combustion of natural gas in the presence of a catalyst commonly known as steam methane reforming (SMR) is one of the most widely used, effective, and economic methodology for producing hydrogen on a larger scale [7]. Alongside the advantages of SMR, it involves the emission of large quantities of carbon dioxide (CO_2). According to an estimation, for every kg of produced hydrogen, SMR emits 11 to 13 kg of CO_2. Also, being an essential GHG, methane possesses 21 times higher global warming potential (GWP) compared with CO_2 [8]. Thus, there is a need for a cleaner route of hydrogen production.

According to the obtained data from reference the numerous methods of cleaner hydrogen generation employing solar energy are comparatively evaluated in terms of their overall efficiencies, sustainability indices, and generation capacities as presented in Figures 1.1, 1.2, and 1.3, respectively. Among the compared methods are solar thermochemical cycles, hybrid thermochemical cycles, solar thermochemical hydrogen sulfide splitting, solar methane cracking, solar high-temperature electrolysis, PV electrolysis, solar thermal energy generation and electrolysis, biophotolysis, photocatalysis, photofermentation, anaerobic digestion, and artificial photosynthesis. The figures show that among the numerous methods considered, the solar and hybrid thermochemical cycles operate at the highest energy efficiency of 35% and exergy efficiency of 38% having considerably higher sustainability indices of above 0.6 as well as higher production capacities ranging between 75 MW and 400 MW. Though, reference [5] considers solar energy as a source of providing

thermal energy for thermochemical hydrogen production, the reported values may remain within a similar range for alternate thermal energy sources for example nuclear or industrial waste heat.

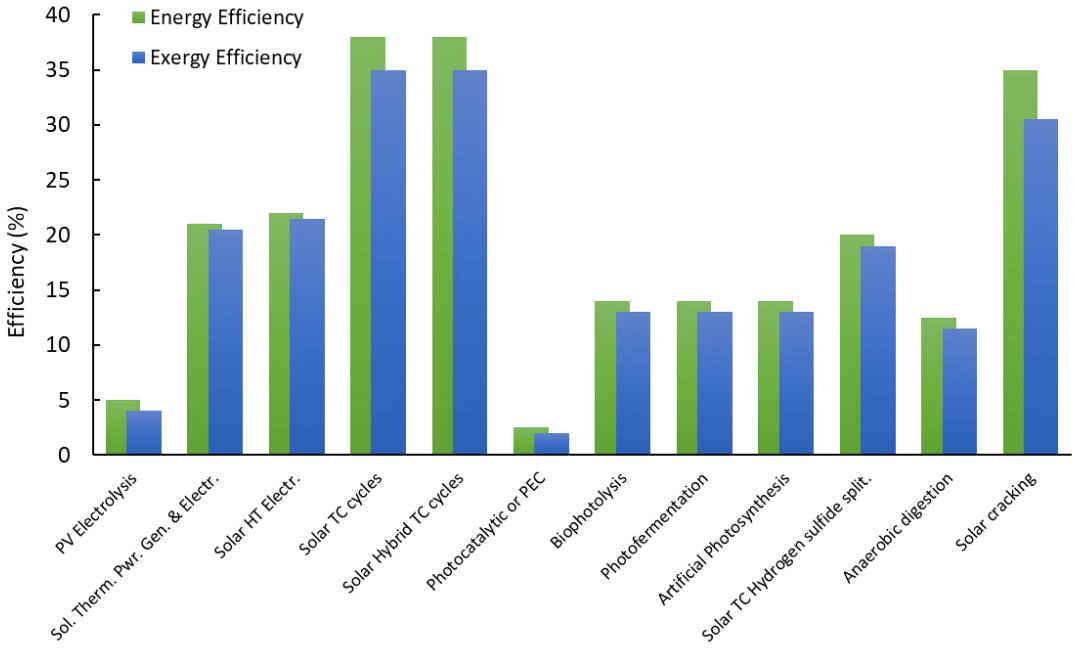

Fig. 1.1. Comparison of efficiencies between the several solar-based hydrogen production methods (modified from [5])

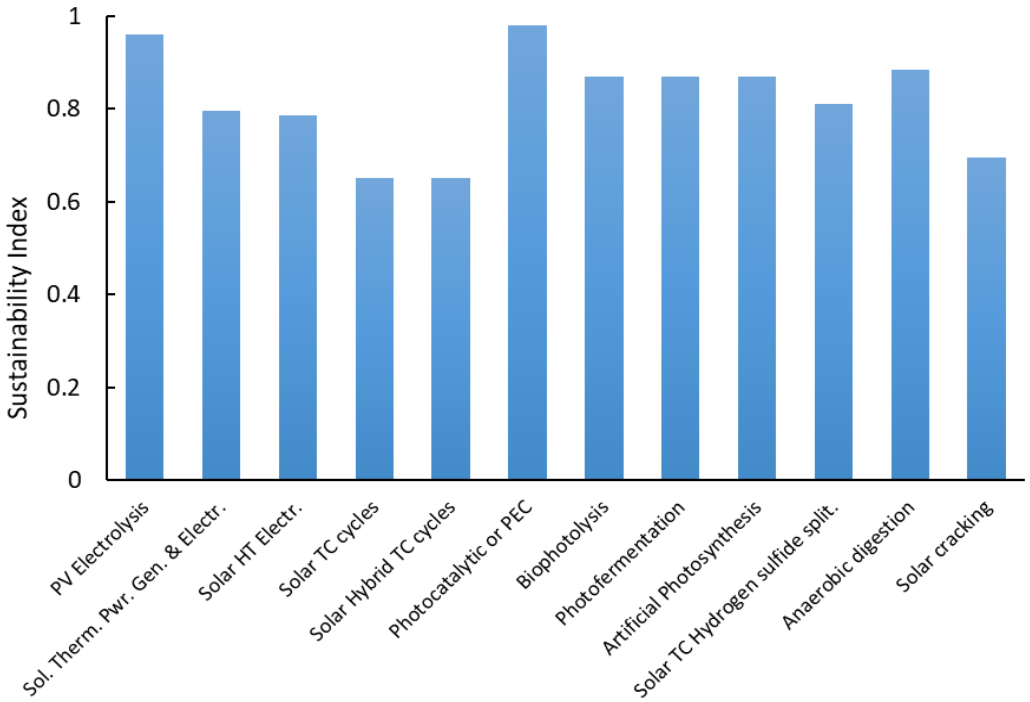

Fig. 1.2. Comparison of the sustainability index between the several solar-based hydrogen production methods (modified from [5])

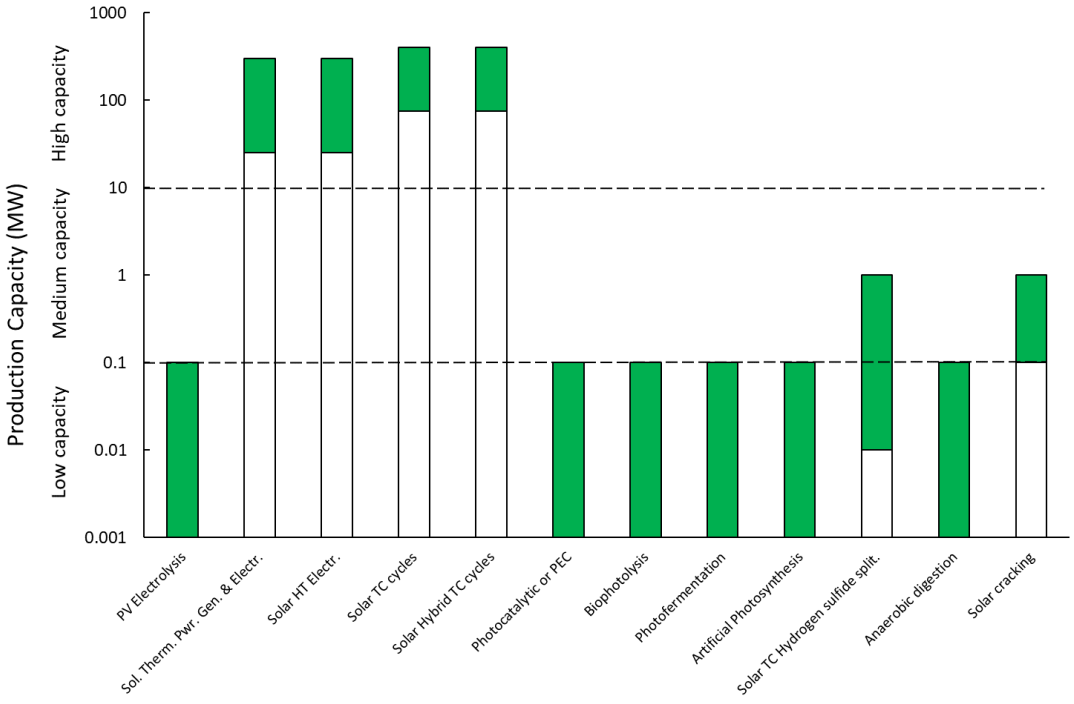

Fig. 1.3. Comparison of the production capacity between various solar-based hydrogen production methods (modified from [5])

1.3 Thermochemical cycles for water splitting

Thermochemical hydrogen generation involves the thermochemical decomposition of water into oxygen and hydrogen as a result of a sequence of certain chemical processes and reactions such that all chemicals are ultimately replenished [9]. Among the various benefits of thermochemical hydrogen generation is no requirement of membrane for separating oxygen and hydrogen, moderate temperature requirement, no and low electrical input requirement for thermochemical and hybrid thermochemical cycles, respectively [10]. The numerous variants of thermochemical cycles include two, three, four, and five-step cycles. A few examples of the two-step cycles are zinc, iron, ceria, germanium-based, and hybrid sulfur cycles. A few examples of the three-step cycles include hybrid-cadmium, magnesium-chlorine, and sulfur-iodine cycles. Four-step cycles include four-step copper-chlorine cycle and UT-3 cycles. A few examples of the five-step cycles are hybrid sulfur ammonia and five-step copper-chlorine cycles. Nearly 200 thermochemical water-splitting cycles have been reported and studied in the open literature, and very few of those have been proposed as reasonable methods for generation of hydrogen at a larger scale [11]. Cycles such as magnesium-chlorine, hybrid-sulfur, and sulfur iodine are amongst the most

commonly studied cycles by several researchers globally in pursuit of sustainable and environmentally benign processes to produce hydrogen. Several studies in the open literature have reported, shortlisted, and suggested the copper-chlorine (Cu-Cl) cycle as one of the most practically feasible and promising options of large-scale thermochemical hydrogen generation. Among the several advantages of the Cu-Cl cycle are its comparatively low requirement of thermal energy allowing relative flexibility in the choice of selection of appropriate materials (which is not possible in cycles operating at much elevated operating temperatures), and flexibility in the choice of exploitation of various thermal energy sources such as renewable or waste heat from industries for providing the required heat energy for the cycle. According to a comprehensive review conducted by Safari and Dincer [10], the Cu-Cl cycle has a lower GWP of 0.55 kg of CO_2 per kg of H_2 and a unit hydrogen cost of 2.2 $/kg making it a promising option to be considered for large-scale green hydrogen generation.

1.4 Motivation

The continuous utilization of hydrocarbon-based fuels not only contributes towards global warming due to excessive GHG emissions but also drastically increases the rate of fossil fuel depletion. Hydrogen, as a fuel, is a promising alternate for addressing both environmental and sustainability issues. Hydrogen production is realized through various routes however, a method that has the potential of producing cleaner hydrogen at higher efficiencies and capacities is thermochemical water-splitting. One of the fundamental motivations of this thesis is to eliminate the usage of fossil fuels and replace it with a cleaner hydrogen production method. Another major motivation of this thesis study is the development of a new and a less energy-intensive technique for the anolyte separation process of the Cu-Cl cycle for improvement in the overall efficiencies of the cycle.

1.5 Objectives

This thesis is generally concerned with the investigation and assessment of the thermochemical hydrogen production via a four-step Cu-Cl cycle through the lab-scale integrated design of the cycle developed at the Clean Energy Research Laboratory (CERL) at the Ontario Tech University. This thesis is also concerned with the development and investigation of the flash vaporization process as an alternate and a less-energy intensive

approach for anolyte separation in the Cu-Cl cycle. In this regard, the specific objectives of this thesis are described as follows:

- To model, simulate, and analyze the existing four-step integrated Cu-Cl cycle at CERL and its modified version through the incorporation of the flash vaporization process in Aspen-plus.
- To analyze the existing and the modified integrated cycles thermodynamically through the energy and exergy analyses. This includes: (a) the performance evaluation of the several components of both versions of the cycle in terms of their heat input, heat rejection, and exergy destruction rates, (b) the overall performance evaluation of both versions of the cycle in terms of the net heat input and overall energy and exergy efficiencies, (c) sensitivity analysis to assess the behavior of different components and processes under various operating conditions, and (d) comparative assessment between the existing and the modified cycles in terms of the various performance parameters.
- To perform thermal management of the existing and the modified integrated cycles through Aspen-plus simulations. This includes: (a) development of different heat recovery configurations incorporating internal heat recovery through different components of the cycle based on different steam-to-copper ratios for the existing integrated cycle, (b) development of various heat recovery configurations incorporating both internal heat recovery and waste heat recovery through a steel furnace for the modified cycle, and (c) comparative evaluation of the considered configurations based on various performance characteristics such as the overall efficiencies, net heat input, and heat recovery temperatures.
- To perform an exergoeconomic assessment of the existing and the modified integrated cycles. This includes: (a) application of the EXCEM and SPECO approaches to the integrated cycles, (b) evaluation of the various exergoeconomic performance parameters, (c) evaluation of the unit cost of hydrogen for a given production capacity, (d) sensitivity analysis to assess the effect of various factors on the overall exergoeconomic performance, and (e) comparative assessment of the unit cost of hydrogen between the existing and the modified integrated cycles.
- To perform an exergoenvironmental assessment of the existing and the modified integrated cycles. This includes: (a) evaluation of the environmental impact of various

components and the overall cycles, (b) sensitivity analysis to assess the effect of various factors on the overall exergoenvironmental performance, (c) assessment of the influence of various electrical energy sources on the GWP of the cycle, and (d) comparative assessment of the environmental impact of various components between the existing and the modified integrated cycles.

- To perform multi-objective optimization of the integrated cycle. This includes: (a) application of the genetic algorithm technique to determine the several optimal solutions in terms of *Pareto Frontier* plots and (b) considering the objective functions of exergy efficiency, cost rate, and hydrogen production rate to maximize the efficiency and hydrogen production rate and minimize the cost rate.
- To develop and experimentally investigate the flash vaporization process as a new approach for anolyte separation. This includes: (a) development of a lab-scale standalone experimental setup for investigating a semi-continuous flash vaporization process, (b) experimental testing of the flash vaporization process in terms of the volume and the mass of the separated HCl and H_2O mixture by varying the operating conditions such as operating temperature (65 to 85ºC) and volume flow rate (0.0025 to 0.005 l/s) of the anolyte solution and operating vacuum pressure (0.2 to 0.5 bar) of the flash chamber, (c) experimental testing of two different flash chamber designs under the same operating conditions, and (d) characterization of the separated HCl and H_2O mixture for percentage concentration of the HCl in the separated sample.
- To develop an empirical correlation for the theoretical estimation of the amount of the separated mixture of HCl and H_2O via the flash vaporization process.

1.6 Novelties

The original work in the present study is described below:

- The four-step integrated Cu-Cl cycle setup at CERL is investigated through thermodynamic, thermal management, exergoeconomic, exergoenvironmental, and multi-objective optimization approaches.
- The flash vaporization process is conceptually incorporated in the integrated cycle and is investigated through thermodynamic, thermal management, exergoeconomic, and exergoenvironmental approaches.

- New internal and waste heat utilization techniques are developed for the existing and the modified versions of the cycle.
- A standalone experimental setup is developed for the flash vaporization process.
- The flash vaporization process is experimentally investigated.
- An empirical model is developed for prediction of the amount of the separated HCl and H_2O mixture via the flash vaporization process.

1.7 Thesis outline

This thesis constitutes seven chapters. The first chapter provides the background and introductory information related to fossil fuel utilization, the potential of hydrogen to be used as a fuel, and the various renewable pathways of hydrogen generation in general and thermochemical water-splitting cycles in particular. Moreover, the motivation, specific thesis objectives, and thesis novelties are also described. The second chapter provides a comprehensive literature review discussing relevant studies conducted in the present research domain and highlights some of the major gaps in the literature. The third chapter provides the detailed operating mechanism of the four-step integrated thermochemical copper-chlorine cycle at CERL as well as of the cycle with some suggested modifications. Moreover, it provides the details of the standalone experimental setup and procedure of the proposed anolyte separation approach for the cycle. The fourth chapter provides the details of the various analyses conducted for the thermodynamic, thermal management, exergoeconomic, exergoenvironmental, and multi-objective optimization of both the actual integrated cycle and the cycle with the proposed conceptual modifications. Moreover, the formulation of an empirical model for predicting the theoretical fraction of the separated anolyte is also discussed. The fifth chapter discusses the results obtained through the modeling and simulation of the cycle for the various analyses as well as the performed experiments. Some of the results are based on the energy and exergy analyses, thermal management, exergoeconomic analysis, exergoenvironmental analysis, and the multi-objective optimization of the integrated cycle while some other results are based on the energy and exergy analyses, thermal management, exergoeconomic analysis, and exergoenvironmental analysis of the cycle with proposed modifications. The results also consider a comparative evaluation of the integrated cycle and the cycle with proposed modifications in terms of several thermodynamic, exergoeconomic, and

exergoenvironmental performance parameters. The results of the performed experimental work are also discussed. Moreover, the results for the comparison between the theoretically calculated and experimentally obtained fraction of the separated anolyte based on the empirical correlation are also presented. Finally, chapter 6 provides the main conclusions of this thesis along with various recommendations for the potential studies for the future.

In closing, this chapter provides a brief overview of the current trends of global fossil fuel utilization and its environmental implications. In this regard, the utility of hydrogen as a promising alternate fuel is also described. Several hydrogen production methods are compared and the advantages of thermochemical water-splitting as a sustainable and environmentally benign hydrogen production process are discussed. In this regard, the motivations and specific objectives of this thesis are also described. The following chapter describes a detailed literature review of thermochemical hydrogen production through copper-chlorine cycle.

CHAPTER 2 BACKGROUND AND LITERATURE REVIEW

In this chapter, a detailed literature survey of various studies that investigated the thermochemical Cu-Cl cycle as a whole or its individual steps is provided. Various integrated systems incorporating the Cu-Cl cycle are also discussed followed by several studies considering different thermal management approaches for the cycle. Investigations regarding the exergoeconomic, exergoenvironmental, and multi-objective optimization of energy systems are also reviewed. Numerous studies considering the investigation of the flash vaporization process are also discussed. The resulting gaps in the literature, specific objectives of this thesis, and the corresponding novelties are also provided in this chapter.

2.1 Thermochemical Cu-Cl cycle

There are three main variants of the thermochemical Cu-Cl cycle which are three-, four-, and five-step processes. The four-step Cu-Cl cycle is based on the four basic processes (i) hydrolysis, (ii) thermolysis, (iii) electrolysis, and (iv) drying. During the hydrolysis step, steam and cupric-chloride ($CuCl_2$) react via an endothermic reaction to produce copper-oxychloride (Cu_2OCl_2) and hydrochloric acid (HCl). This Cu_2OCl_2 then gets thermally decomposed into cuprous chloride (CuCl) and oxygen (O_2) during the thermolysis step. The third step of the cycle results in the production of hydrogen where CuCl and HCl from thermolysis and hydrolysis reactions respectively undergo an electrochemical reaction to produce hydrogen in an electrolyzer. During the drying process, the aqueous $CuCl_2$ solution undergoes drying where $CuCl_2$ gets separated from the rest of the anolyte components such as HCl, CuCl, and water. This step essentially replenishes all the chemicals to be used for the subsequent cycle. Table 2.1 shows the details of the four chemical reactions taking place during a four-step Cu-Cl cycle. The different variants of the Cu-Cl cycle have been studied extensively in the open literature. These studies are categorized as overall cycle analysis, individual steps/processes, integrated systems, and heat recovery.

Table 2.1. Details of the chemical reactions taking place during the cycle

Process	Chemical Reaction	Temperature (°C)
Hydrolysis	$2CuCl_2\,(s) + H_2O\,(g) \rightarrow Cu_2OCl_2\,(s) + 2HCl\,(g)$	370 - 400
Thermolysis	$Cu_2OCl_2\,(s) \rightarrow 2CuCl\,(l) + 0.5O_2\,(g)$	500 - 530
Electrolysis	$2CuCl\,(aq) + 2HCl\,(g) \rightarrow H_2\,(g) + 2CuCl_2\,(aq)$	25 - 90
Drying	$CuCl_2\,(aq) \rightarrow CuCl_2\,(s) + H_2O\,(g)$	100 - 130

2.1.1 Overall cycle analysis

The initial results of experiments performed on a six and a four-step Cu-Cl cycle were reported in [12] and [13], respectively by Lewis et al. where the results pertaining to the electrolysis, thermolysis, and hydrolysis reactions were provided. Further, the feasibility of the cycle was also exhibited as per the preliminary obtained experimental and thermodynamic evaluations.

For a five-step cycle, Wang et al. [14] assessed the thermal requirements of every step of the cycle by making assumptions of stoichiometric reactions. According to their analysis, they reported an evaluation of the net thermal energy requirement of the cycle as 451.65 kJ/mol H_2.

To reduce the excess need of stream for the cycle, Wang et al. [15] suggested a six-step variant of the cycle. According to their obtained results, they concluded that the steam requirement could be minimized by up to ten times compared with orthodox cycles. Nonetheless, among the few challenges encountered with the cycle are prevention of dehydration in the $CuCl_2$ hydrate and efficient mixing of the reactant particles in the oxygen production step.

A comparative assessment through exergy and energy analyses of the three, four, and five-step cycles has been conducted by Ishaq and Dincer [16]. In their evaluation, the energy efficiencies reported for the three, four, and five-step cycles are 40%, 42%, and 39% while the corresponding energy efficiencies are 68%, 76%, and 70%.

Thermodynamic assessment of a four-step (lab-scale) cycle at the Clean Energy Research Lab (CERL) has been conducted by Farsi et al. [17] where energy and exergy evaluation of the various steps and processes of the cycle was performed. As per the results obtained in their investigation, they reported an overall energy efficiency of the cycle to be 12% and overall exergy efficiency of the cycle to be 35%.

2.1.2 Individual steps/processes

Hydrolysis reaction or process is a step of substantial significance in the Cu-Cl cycle impacting the various subsequent steps of the cycle. Numerous investigations have considered a variety of chemical reactors for the process. In this context, a spray reactor

was employed and investigated for the hydrolysis step by Ferrandon et al. [18]. For the characterization of the solid products of the reaction, they utilized a scanning electron microscope and X-ray diffraction. They also studied two different types of atomizers including ultrasonic nozzle and pneumatic nebulizer. Based on their evaluations, they concluded that while employing a pneumatic nebulizer, a counter-current reactor exhibited a substantially higher yield of the copper-oxychloride (Cu_2OCl_2) compared with a co-current reactor as a consequence of higher mas transfer. On the contrary, the ultrasonic nozzle demonstrated better results and more use-friendliness. Another primary conclusion of their study included a yield of Cu_2OCl_2 as high as up to 95% coupled with small quantities of cuprous chloride (CuCl) at a steam-to-copper (S/Cu) ratio of 24 was obtained through exploiting an ultrasonic nozzle with a co-current flow reactor.

Numerous thermochemical cycles for hydrogen generation, in a series of studies, were examined by Lewis et al. [19] where they shortlisted the Cu-Cl cycle for more research and development. Based on their analysis, they presented various insightful conclusions with regards to the utilization of a fixed bed microreactor. As per the results reported by the authors, for Cu_2OCl_2 yields of above 95%, the S/Cu ratio needs to be around 17 at temperatures ranging from 380ºC to 390ºC. On the contrary, a Cu_2OCl_2 yield of only 30% was acquired at a S/Cu ratio of 5 for the same range of operating temperature. Further increase in temperature at this S/Cu ratio resulted in an increase in the Cu_2OCl_2 yields nonetheless, any further augmentation in temperature beyond 390ºC at this S/Cu ratio was not recommended because of an increase in chlorine gas (Cl_2) and CuCl generation. Moreover, an increase in S/Cu ratio beyond 17 was not suggested as it caused an increase in the requirement of energy to vaporize water.

A fixed bed microreactor for the hydrolysis reaction was also studied by Singh et al. [20] employing numerous configurations of the $CuCl_2$ sample. They compared the ball and un-ball milled samples of $CuCl_2$ at similar operating conditions in terms of their percentage conversion. Based on their obtained results, a percentage conversion ranging between 95% and 97% was attained using a ball-milled sample of $CuCl_2$ at an operating temperature of 400ºC.

The electrolysis step of the cycle has also been studied by various researchers and at numerous operating conditions. In this context, an experimental examination of a novel electrolyzer system employing Nafion-based membranes and Pt/C catalysts to prepare electrode assemblies of the membrane was reported by Schatz et al. [21]. According to their obtained results, they maintained that their system could produce hydrogen at efficiencies ranging from 91% to 99% with no deposition of copper on the electrolyzer.

The thermodynamics and efficiencies of an electrolyzer utilized in a Cu-Cl cycle were examined and reported by Hall et al. [22]. In their study, an approach was formulated for predicting the overall efficiencies by comparing the estimated data, as a result of predictions of thermodynamic models with those of the data evaluated through experimental observations of an open circuit potential.

In another study conducted by Gong et al. [23] regarding the electrolysis step, a new design of an electrolyzer was proposed. According to their evaluations, it was concluded that the thermodynamic and experimental data (obtained through employing linear sweep voltammetry) pertaining to open circuit potential showed good agreement. They further reported that an increase in temperatures resulted in better system performance. However, the flow rates of the anolyte and catholyte did not particularly influence the overall performance of the electrolyzer.

Several examinations considering separation methodologies of the oxidized anolyte discharging the anode side of the electrolyzer have been reported in the open literature. In this context, the adoption of a spray drying approach for obtaining solid $CuCl_2$ was considered by Naterer et al. [24]. In their study, they proposed that the necessary heat for the process could be supplied via low-grade waste heat to enhance the efficiency of the cycle.

Evaporative drying of the aqueous $CuCl_2$ droplets was investigated in another study by Naterer et al. [25] in which they assessed the process of droplets (with sizes ranging from 100 µm to 200 µm) being sprayed utilizing air at lower temperatures for a $CuCl_2$ solution with quantities between 8.2 and 2 moles of water/mole of $CuCl_2$. According to the results obtained in their investigation, they reported that the identification and assessment of the

ideal conditions for the drying process via low thermal energy waste heat sources could be accomplished through the predictive formulation.

In yet another study, the utilization of the crystallization process to separate $CuCl_2$ from an aqueous anolyte solution was investigated by Naterer et al. [26] through the application of X-ray diffraction technique for detailed characterization of the recovered $CuCl_2$ solid. Further, they employed the thermogravimetric analysis to examine the decomposition temperature and thermal stability.

The two separation approaches namely crystallization and spray drying under investigation at the Ontario Tech University were comparatively assessed by Wang et al. [27]. In their evaluation, they reported that the crystallization process was more economical compared with spray drying. They also added that it was a more commercially mature technique. Moreover, they maintained that among the numerous challenges in realization the spray drying process was the need for a large number of heat exchangers having large dimensions along with HCl and water recovery from the drying air. Nevertheless, the obtained $CuCl_2$ via spray drying is relatively anhydrous compared with the crystallized $CuCl_2$ which may comprise numerous water molecules.

2.1.3 Integrated systems

As far as the integration of the Cu-Cl cycle with several thermodynamic cycles/processes for multigeneration purposes, several investigations have been carried out and reported in the open literature. In this context, a biomass-based combined cycle integrated with an absorption cooling system and solar-based Cu-Cl cycle was conceptually developed and studied by Ishaq and Dincer [28]. Based on their obtained results, they reported overall exergy and energy efficiencies of their system to be 31.5% and 30%, respectively with a hydrogen production capacity of almost 60 mol/s and a net power generation capacity of 8.3 MW.

A new trigeneration integrated system (for oxygen, hydrogen, and power generation) constituting a stand-alone Cu-Cl cycle coupled with a combined heat and power unit was conceptually developed and studied by Wu et al. [29]. Based on their evaluations, they reported that their system could work at a minimum power efficiency of 48% for the

numerous scenarios considered in their examination which were based on thermal energy integration of the thermochemical cycle and self-heat recovery of the combined heat and power unit.

A gas turbine cycle driven three, four and five-step Cu-Cl cycles were proposed and examined by Wu et al. [30]. According to their analysis, they reported that the pressure and temperature influenced the yields of CuCl and Cu_2OCl_2. They also concluded that even though thermochemical cycles with lesser steps had less equipment, nonetheless, higher energy dissipation was associated with them.

A solar-based Cu-Cl cycle was conceptually proposed and studied by Sayyaadi et al. [31] capable of generating hydrogen at a capacity of 6 T/day. Their system exhibited an improvement in thermal efficiency of 10.2% compared with previously investigated designs. Further, considering their design as the baseline, they examined four different scenarios for optimization for assessing the room for improvement. The objective functions they considered for optimization included exergy and energy efficiencies and unit hydrogen cost. According to their evaluations, the objective functions of their final optimized system had values of 58.2%, 49.8%, and 6.33 $/kg for exergy efficiency, energy efficiency, and unit cost of hydrogen, respectively.

The integration of a high-temperature electrolysis process with various configurations of Cu-Cl cycle was performed by Khalid et al. [32] where they carried out several experiments for assessment and investigation of the feasibility of employing the high-temperature electrolysis for the thermochemical cycle. In another study, an integrated cogeneration system of hydrogen and power generation was thermodynamically analyzed and investigated by Ishaq et al. [33] where their system demonstrated exergy and energy efficiencies of 40% and 38%, respectively.

2.1.4 Heat recovery

In the context of the heat recovery for the Cu-Cl cycle, numerous methodologies for improving the overall efficiencies of the cycle via a reduction in the overall thermal requirements of the cycle were examined by Naterer et al. [34]. Among the different approaches of recovering thermal energy from molten CuCl reviewed and reported by

Ghandehariun et al. [35] were atomization and steam generation via a quenching bath and atomization and droplet descent via counter-current flow.

A new conceptual design employing a combination of numerous heat exchangers for a four-step Cu-Cl cycle was proposed and evaluated by Ozbilen et al. [36]. According to their evaluations, they claimed to cause a potential reduction in the requirement of steam via reducing pressure during the hydrolysis reaction. They also concluded that the S/Cu ratio could be lowered from 16 to 10 while considering a pressure of 0.4 atm and an operating temperature of 390ºC. They further suggested that the performance of the cycle could be significantly improved through internal heat recovery within the cycle. In this context, they reported an exergy efficiency of 66% and an energy efficiency of 55.4% for their proposed thermal management system.

2.2 Exergoeconomic analysis of energy systems

Numerous approaches and methodologies for exergoeconomic evaluations have been formulated, proposed, and reported in the open literature. Some of the frequently applied methods in this regard with particular applications in thermal energy systems include the specific exergy costing (SPECO) and exergy-cost-energy-mass (EXCEM). Numerous studies in the open literature have considered the application of these two exergoeconomic approaches.

A new and detailed exergoeconomic approach based on the quantities of mass, cost, energy, and exergy called the EXCEM was developed by Rosen and Dincer [37]. The foundation of this approach is based on the comprehension of the performance of a system in terms of the examination of the input and output flows of the EXCEM quantities. The fundamental objective of this approach is the assessment of the capital costs and thermodynamic losses of numerous components of a thermal or an energy system. The application of the EXCEM approach for thermoeconomic evaluation of energy systems has been considered in several studies reported in the literature.

In this context, a solar-assisted tea drying system was assessed and evaluated by Ozturk and Dincer [38] where they reported that the ratio of the thermodynamic loss increased when the inlet air flow rate was made to increase. In another investigation employing the

EXCEM approach, the influence of the reference temperature on the exergetic and exergoeconomic performance of a natural gas-driven thermal power plant was evaluated by [39].

The formulation and development of another frequently employed exergoeconomic approach known as the specific exergy costing (SPECO) was done by Lazzaretto and Tsatsaronis [40]. They firstly defined the product and the fuel for every equipment of a given system on the basis of the removal and supply of exergy from each exergy stream of a considered system at all state points. They then estimated the cost of each stream employing the principles of business administration. The application of the SPECO approach for thermoeconomic evaluation of energy systems has been considered in several studies reported in the literature.

In this context, the thermoeconomic performance of a hybrid solar and biomass energy-driven organic Rankine cycle (ORC) was assessed by Oyekale et al. [41] via the SPECO approach. A methane co-feeding-based biomass gasification system was studied by Nakyai et al. [42] where they evaluated the unit hydrogen cost of their system through the application of the SPECO approach. An integrated system considering a coal-based Rankine cycle and a Kalina cycle were exergoeconomically investigated by Singh and Kaushik [43] through employing the SPECO approach. A cogeneration system for steam and power was exergoeconomically studied by Cavalcanti et al. [44] by employing the SPECO approach. An integrated solar combined cycle was exergoeconomically investigated by Baghernejad and Yaghoubi [45] through the application of the SPECO approach. A trigeneration system based on a solid oxide fuel cell (SOFC) for the production of space cooling, heating, and electrical energy was studied by Chitsaz et al. [46] by applying the SPECO methodology. In the context of the Cu-Cl cycle, a four-step conceptual Cu-Cl cycle was exergoeconomically evaluated by Ozbilen et al. [47] by considering the application of the SPECO approach.

2.3 Exergoenvironmental analysis of energy systems

It is also of substantial importance to evaluate the environmental implications of a certain thermal energy system while assessing its energetic/exergetic performance. Thus, an exergoenvironmental analysis is such which considers a combination of the environmental

and energy-exergy analyses. In this context, a three-step-based concept of exergoenvironmental evaluation of thermal energy systems was developed and suggested by Meyer et al. [48]. A detailed exergetic assessment of a given system is carried out during the first step while step two encompasses the environmental impact evaluation of numerous equipment of that system via a suitable methodology for quantitatively expressing the environmental impact for example Eco-indicator 99 method couple with life cycle assessment (LCA). Lastly, step three involves the association of equipment-affiliated environmental impact to all exergy streams of the cycle at each state point thereby allowing the evaluation of each exergoenvironmental variable. In this context, numerous studies in the literature have considered the exergoenvironmental analysis of energy systems.

An exergoenvironmental assessment of a SMR process for hydrogen generation was carried out by Boyano et al. [49]. In their study, several components of their system exhibiting great environmental impact potential were identified. Further, an enhancement in exergetic efficiencies of certain components was suggested for a reduction in their respective environmental impacts. A solar-based combined cycle was exergoenvironmentally evaluated by Cavalcanti [50] where the condenser was reported to require an enhancement in terms of its exergy efficiency for a subsequent reduction in its environmental impact. An exergoenvironmental assessment of a combined cycle powerplant coupled with a chemical looping process was conducted by Petrakopoulou et al. [51] where they suggested an improvement in some of the major components of their system in terms of their exergy efficiency for reducing their electrical energy associated environmental implications. An integrated solar energy-based combined cycle gas turbine system was exergoenvironmentally evaluated by Bonforte et al. [52] where significant environmental advantages of their system were reported due to its lower utilization of fossil fuel. A cogeneration gasification system based on municipal solid waste coupled with a combined cycle was exergoenvironmentally assessed by Casas-Ledon et al. [53] with outputs of thermal and electrical energy. An exergoenvironmental evaluation of an ultra-supercritical coal-based power plant was carried out by Rocha and Silva [54] where it was reported that although their considered system was a much-improved configuration of a coal-driven power generation system compared with its counterpart systems, nevertheless, it demonstrated a higher environmental impact and addition of numerous exhaust gas

treatment components could substantially reduce the system's overall environmental impact. A steam and autothermal reforming system of natural gas for generation of methanol was exergoenvironmentally assessed by Blumberg et al. [55] where they pointed out the need for reduction in exergy destruction in various equipment for a decrease in the system's total environmental impact via addition and utilization of materials possessing enhanced properties. An exergoenvironmental evaluation of a reverse osmosis desalination system with a production capacity of 82000 m^3/day was conducted by Blanco-Marigorta et al. [56] where numerous components of their system were identified to possess the highest exergoenvironmental impact reduction potential. An integrated system comprising an ORC, GT, and SOFC was exergoenvironmentally analyzed by Ghorbani et al. [57] where two different working fluids for the ORC were considered and certain main equipment of their system with higher environmental impact associated with exergy destruction were identified. Another exergoenvironmental study considering integration of gas reforming process with air and gas bottoming cycles for producing hydrogen and electrical power was conducted by Ahmadi et al. [58] where an increase of about 17% in the exergoenvironmental factor was reported when integration of the bottoming cycle with a GT cycle was considered compared with a stand-alone GT cycle. A geothermal energy-based combined heating and power (CHP) system was exergoenvironmentally assessed by Wang et al. [59] where certain main components of their system such as heat exchanger, condenser, and vapor generator were identified to have the maximum environmental impact reduction potential. In context of the Cu-Cl cycle, an exergoenvironmental evaluation of a four-step conceptual Cu-Cl cycle for hydrogen generation was reported by Ozbilen et al. [47].

2.4 Multi-objective optimization of energy systems

Multi-objective optimization is often carried out for the identification of certain key variables which allow enhancement in the performance of a given energy system. Contrary to single-objective optimization, a key benefit of multi-objective optimization is that it simultaneously takes two or more objective functions into consideration. In this context, several multi-objective optimization studies have been performed and reported in the open literature considering various energy systems. A combined-cycle power plant was studied via a multi-objective optimization approach by Ahmadi et al. [60] where they considered

the total cost, cost rate of environmental impact, and exergetic efficiencies as their objective functions through the application of the genetic algorithm. Multi-objective optimization of solar energy driven integrated system for hydrogen generation was carried out by Khanmohammadi et al. [61] considering exergetic efficiency and overall cost as their objective functions. A modeling-based optimization of a dimethyl ether production unit through syngas via a commercial slurry reactor was conducted by Papari et al. [62] by taking dimethyl ether productivity and carbon monoxide conversion into account as their objective functions. A hydrothermal gasification unit via microalgae for the generation of synthetic natural gas (SNG) was studied through the multi-objective approach by Mian et al. [63] by considering the overall efficiencies, economic and environmental impact as objective functions. A multi-objective optimization study considering hydrogen to carbon monoxide mole ratio, carbon monoxide selectivity, and synthesis gas generation with methane conversion as objective functions was carried out by Mohanty [64]. Multi-objective optimization of low-grade waste heat recovery from industrial systems was performed by Deslauriers et al. [65] with objective functions of exergetic efficiency and cost. With the objective functions of excess water volume, life cycle cost, and load probability loss, a water pumping unit based on photovoltaic energy was studied through a multi-objective approach by Muhsen et al. [66]. A solar energy-based Cu-Cl cycle was investigated through a multi-objective approach by Sayyaadi and Boroujeni [31] considering the overall efficiencies and production cost of hydrogen as their objective functions. A multi-objective of a conceptual four-step Cu-Cl cycle was carried out by Ozbilen et al. [67] where they considered exergoeconomic and exergoenvironmental objective functions by employing the genetic algorithm methodology.

2.5 Separation techniques

There is a wide variety of separation methodologies available in the literature. Some of the methods are feasible for separating homogeneous solutions while others are suitable to separate heterogeneous mixtures. Since the anolyte under consideration is an aqueous homogeneous solution, we will only consider processes/techniques suitable for separating homogeneous mixtures. A few of these processes include distillation, extraction, crystallization, and flash vaporization.

Distillation is a method used for the separation of components from liquid mixtures through selective evaporation and condensation. The separation depends on the relative volatility of different constituents of the mixture. Distillation could result in either complete or partial separation of the components. It is widely used commercially for the refining of crude oil. Advantages of distillation include easy implementation and high separation efficiency. The disadvantages associated with the distillation process are that it becomes expensive at an industrial scale due to the requirement of large structures, specialized machinery, and heavy-duty materials.

Extraction is a method for separating compounds or metal complexes based on their relative solubilities in two immiscible liquids such as water and an organic solvent. Generally, this process involves a net transfer of one or more species from aqueous to organic liquid. The driving mechanism for this process is the chemical potential. This method is carried out as both batch and continuous processes. The continuous process is usually multistage and employs centrifugal action which allows the thorough mixing of the two solutions at high RPMs. A disadvantage of this method is the excessive post-processing requirement for extracting the solute from the organic solvent.

Crystallization is a process employed for recovering and separating dissolved solids from a solution where mass transfer of a solute takes place from a homogeneous solution to a solid crystalline phase. There is a wide range of its commercial applications at small scale such as synthesis of specialized chemicals (pharmaceutical products) and large scale such as sugar, salt, and fertilizer production. A big downside to this process is that it is extremely time-consuming and is not very feasible for continuous process operations.

Flash vaporization is a process that involves a reduction in the feed pressure to achieve partial vaporization inside a flash chamber. This results in the separation and instantaneous vaporization of the more volatile components of the feed. The relative difference between the volatility of the components or species in the solution must be considerably high to achieve better separation. The pressure reduction could be achieved through a throttling valve. Moreover, the flash chamber must be maintained at vacuum conditions before the feed is allowed to enter the flash chamber after undergoing pressure reduction in a throttling valve. Vacuum conditions inside the flash chamber are created through a vacuum

pump. The advantage of this technique is that it causes the feed to vaporize at lower temperatures and is thus less energy-intensive. Moreover, the separation efficiency could be improved by ensuring better vacuum conditions inside the flash chamber and significant pressure reduction through the throttling valve. This technique is both suitable for batch and continuous operation processes. Therefore, this technique has been proposed in this thesis proposal as the new method for the anolyte separation process in the integrated Cu-Cl cycle. According to the comprehensive literature review performed on flash vaporization and its applications, it is found that this technique has not been employed as yet for the anolyte separation purposes in a Cu-Cl cycle. Several experimental investigations have been reported in the literature considering flash vaporization techniques. A few of those studies and their key findings are briefly discussed in this section.

The flash vaporization process in a pool of distilled water was evaluated by Saury et al. [68] where they studied the influence of the rate of depressurization and liquid height. For visually observing the flashing phenomena, they employed a charged-couple device (CCD). According to their obtained results, they concluded that the flashing duration was an increasing function of the liquid level at the beginning of the process. They also reported that the equilibrium conditions at a certain constant rate of depressurization were achieved more quickly at a lower initial height of the liquid inside the flash chamber. The steam-carrying effect for pure water and aqueous NaCl solutions in the static flash vaporization process was investigated by Zhang et al. [69] where they studied the water-film equilibrium, water-film height drop, and steam-carrying ratio and their dependence on the initial concentration of water-film and separation height in their performed experiments. Based on their results, they concluded that a reduction in the separation height or an increase in the water-film concentration at the beginning caused an increase in the steam carrying ratio. An experimental and numerical investigation of the flash vaporization process under numerous pressure conditions was carried out by Liao et al. [70]. According to their simulation results, they reported an over-prediction of the increasing rate and maximum steam volume fraction at lower levels of pressure. They also concluded that the mean diameter of the bubble and the rate of evaporation were inversely related to each other. The flash vaporization process through superheated water jets was investigated by

Mutair and Ikegami [71] where they conducted experiments considering a smaller desalination unit capable of producing 15.2 tons/day of fresh water. They reported that an increase in the water temperature at the beginning and the superheat degree resulted in an increase in the intensity of the flash vaporization process. An experimental study examining the energy transformation and separation characteristics of the circulatory flash vaporization process was carried out by Zhang et al. [72]. They conducted experiments by varying pressures from 7.4 to 47.4 kPa and flow rates from 400 to 1200 l/h. Based on their results, it was reported that the efficiency of flash vaporization was improved upon an increase in flow rate and the pressure inside the flash chamber. On the contrary, an increase in the concentration and initial height of water film caused a reduction in efficiency. A new design of flash chamber for flash vaporization process was experimentally studied by Stengler et al. [73] for desalination at low temperature. They suggested incorporating low-grade waste or solar thermal energy to supply the required heat for the process. They considered a flow rate of 1600 l/h of feed water during their experiments. According to their experiments, they proposed that their suggested design of flash chamber exhibited enhanced evaporative expansion. Experimental and theoretical assessment of the flash vaporization process was carried out by Wang et al. [74]. According to their performed experiments, a one-dimensional mathematical model was developed for the flash vaporization process considering physical processes of the outflow of gas due to flash vaporization, mild vaporization, and depressurization. They reported reasonably good agreement between their experimental and theoretical results in terms of liquid temperature and mass of vaporization.

2.6 Main gaps in the literature

The comprehensive literature reviewed resulted in the identification of various key gaps in the literature which are required to be addressed. There exists a gap in the literature with regards to the investigation of an actual lab-scale design of a fully integrated four-step Cu-Cl thermochemical cycle. Several investigations in the literature were focused on the thermodynamic assessments of various conceptual designs of four and five-step cycles [16], [36], [47] however, those designs were very basic and only considered major processes within the cycle.

There exists a gap in the literature with regards to the investigation of alternate approaches for the anolyte separation step of the Cu-Cl cycle. Previous studies focused on the crystallization and spray drying methods which are either time-intensive or energy-intensive and could mostly operate under batch process operation of the cycle. Techniques that are both less energy and time-intensive and could operate conveniently under continuous or semi-continuous process operation of the cycle have not been investigated.

The Flash vaporization process is extensively used commercially for the desalination of sea water. However, the application of this process for the anolyte separation purposes in thermochemical cycles in general and the Cu-Cl cycle, in particular, has not been explored yet. This process has the potential to be used in a continuous or semi-continuous process operation of the cycle. In addition, it is a relatively less energy-consuming process. There exist several experimental investigations in the literature which consider the application of the flash vaporization process for sea water desalination however, there are no studies that carry out an experimental investigation of the flash vaporization process for separation of anolyte in a Cu-Cl cycle which is another gap in the literature.

There are no modeling studies in the literature that consider the incorporation of the flash vaporization process in an integrated design of a four-step Cu-Cl cycle. The thermodynamic, exergoeconomic, exergoenvironmental, and thermal management analyses for a cycle integrated with flash vaporization have not been carried out in the literature which is another major research gap.

Thus, the motivation and the specific objectives under taken in this thesis study are to address all these gaps identified in the literature.

In closing, this chapter provides a comprehensive review of the literature regarding thermochemical hydrogen production via a four-step Cu-Cl cycle. It also discusses the methodologies and various studies employing the exergoeconomic, exergoenvironmental, and multi-objective optimization of thermal energy systems. Several separation approaches are also discussed and compared and the various studies considering the application of flash vaporization process are presented. Moreover, the main research gaps are identified. The following chapter describes the details of the integrated Cu-Cl cycle at the Ontario Tech University.

CHAPTER 3 : SYSTEM DEVELOPMENT AND EXPERIMENTAL INVESTIGATION

This chapter describes the detailed layout and operational mechanism of the four-step integrated Cu-Cl cycle at the CERL at the Ontario Tech University. The details of the four main steps of the cycle along with the operational details of several auxiliary components/processes within the cycle are also discussed. Moreover, the suggested conceptual modification of the integrated Cu-Cl cycle by incorporation of the flash vaporization process as an alternate anolyte separation approach is also described. The modified cycle considers the replacement of certain components/processes in the actual integrated cycle with various new components/processes for realizing the flash vaporization process. Further, the experimental apparatus and procedure to examine the flash vaporization process are also presented and discussed. Various measurement devices and components are presented and their operational details are provided. The details of the experimental procedure are also presented in a step-by-step manner.

3.1 Four-step integrated Cu-Cl cycle at CERL

The schematic of an integrated four-step Cu-Cl thermochemical water-splitting cycle for hydrogen generation at CERL is illustrated in Figure 3.1 and the detailed layout of the integrated cycle modeled and simulated in Aspen-plus is illustrated in Figure 3.2. The foundation of the Cu-Cl thermochemical cycle lies on four fundamental processes or steps which are (i) hydrolysis, (ii) thermolysis, (iii) electrolysis, and (iv) separation/drying. The detailed operation of each of these steps along with the numerous auxiliary processes taking place within the cycle at CERL is described as follows:

Hydrolysis: The cycle begins with the hydrolysis reaction in which $CuCl_2$ is endothermically hydrolyzed. The process is realized such that water is first converted into superheated steam via the heater-1 of the cycle to be transformed into superheated steam (400ºC). Simultaneously, $CuCl_2$ is also allowed to be heated to the same temperature via heater-8 of the cycle. Once, both reactants achieve the desired temperature of the hydrolysis reaction, they are allowed to enter the hydrolysis reactor which is already maintained at the desired reaction temperature of 400ºC. Upon reacting with each other, solid Cu_2OCl_2 and

HCl gas are produced. The HCl product also contains some amount of unreacted steam. The products of the hydrolysis reaction are separated via separator-1 of the cycle.

Thermolysis: The solid Cu_2OCl_2 is then heated via heater-2 of the cycle to the desired thermolysis reaction temperature of 530ºC before it is allowed to enter the reactor which is already maintained at the same temperature such that Cu_2OCl_2 is thermally decomposed into CuCl as the primary product and oxygen (O_2) as the secondary product. The products of the thermolysis reaction are separated via separator-2 of the cycle.

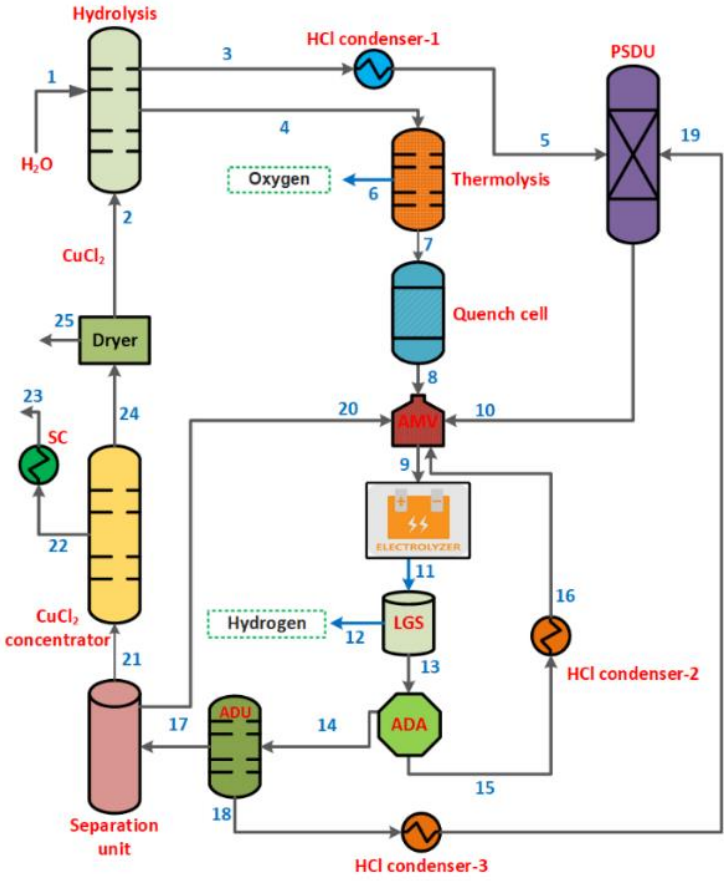

Fig. 3.1. Schematic representation of the four-step integrated Cu-Cl cycle for hydrogen production at the Clean Energy Research Laboratory

Electrolysis: The mixture of the HCl/steam exiting the separator-1 is first condensed to a temperature of 50ºC via the HCl-condenser-1 and then gets separated via the pressure swing distillation unit (PSDU) to get collected in the anolyte makeup vessel (AMV). The CuCl discharging the separator-2 first passes through the quenching cell to solidify thereby also getting collected in the AMV. From AMV, both reactants of the electrolysis reaction are then allowed to enter the electrolyzer to produce hydrogen as the main product of the

reaction as well as of the entire cycle at the electrolyzer's cathode side and the oxidized anolyte at the anode side. The anolyte is an aqueous solution constituting four components i.e., CuCl, HCl, $CuCl_2$, and H_2O. Hydrogen is separated from the oxide anolyte via the liquid-gas separator (LGS).

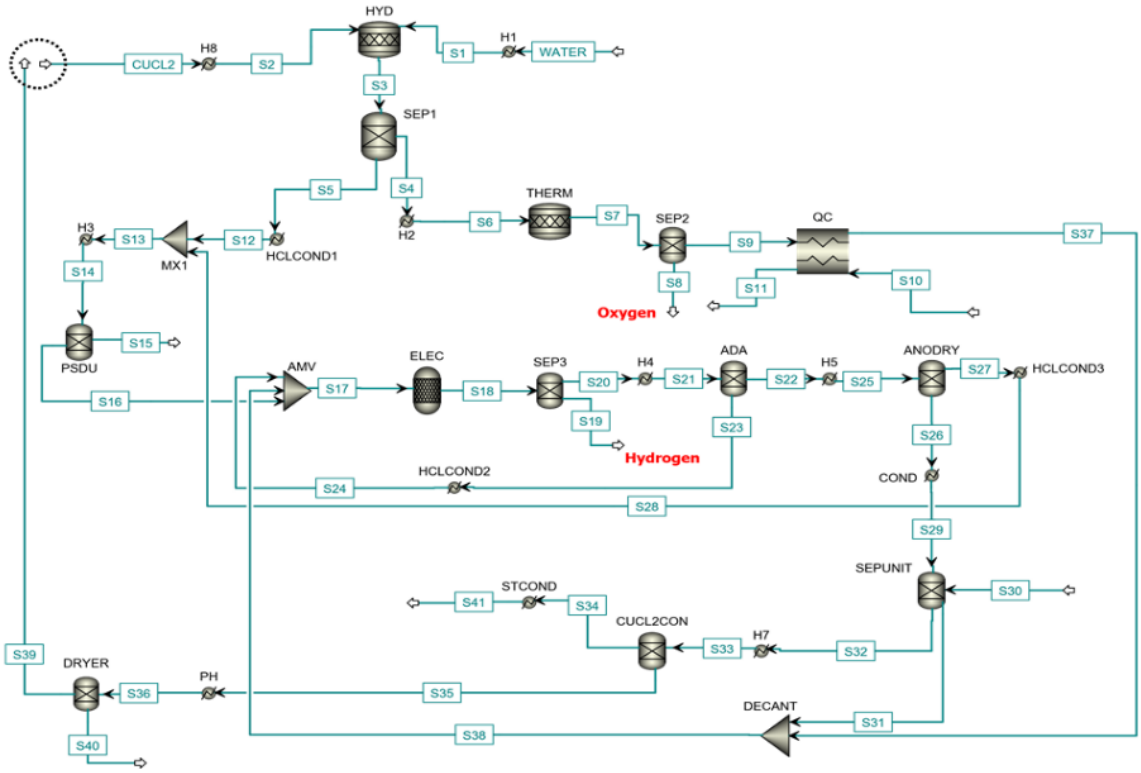

Fig. 3.2. Process flowsheet of the integrated cycle simulated in Aspen-plus

Separation/drying: The separation of the different anolyte components is performed in several steps. The oxidized anolyte exiting the LGS is first heated via the heater-4 and then experiences partial separation through the atmospheric distillation unit of the anolyte (ADA). The partially separated HCl first condenses inside the HCl-condenser-2 and is recycled back to the AMV. The remaining anolyte then again gets heated via the heater-5 and the leftover HCl separates from the anolyte through the anolyte drying unit (ADU). The separated HCl stream exiting the ADU condenses inside the HCl-condenser-3 and is recycled back into the mixer-1. The remaining anolyte discharging the ADU does not contain HCl. This anolyte is then further processed inside the separation unit where some water is being fed to the anolyte such that only $CuCl_2$ gets dissolved in it but not CuCl since it is insoluble in water thereby ensuring convenient separation from $CuCl_2$. The separated CuCl gets collected in the decanter unit to be recycled back to the AMV. After

the separated unit, the anolyte which now only constitutes $CuCl_2$ dissolved in the water passes through the $CuCl_2$-concentrator such that a major percentage of water is removed from the $CuCl_2$ which is then condensed via the steam condenser. The remaining moisture content associated with this $CuCl_2$ is further removed via the dryer unit and the completely anhydrous $CuCl_2$ is recycled back to be used for the subsequent cycle during the hydrolysis step.

3.2 Integrated cycle conceptually modified with flash vaporization process

This section describes the operational mechanism of the cycle conceptually modified with the flash vaporization process. The cycle operation till the electrolysis step is similar to the actual integrated cycle at CERL. The processes following the electrolysis step undergo certain modifications. The main objective of this proposed modification in the actual integrated cycle at CERL is to partially separate the various components of the oxidized anolyte exiting the electrolyzer of the cycle at relatively lower operating temperatures to minimize the thermal requirements of the anolyte separation step.

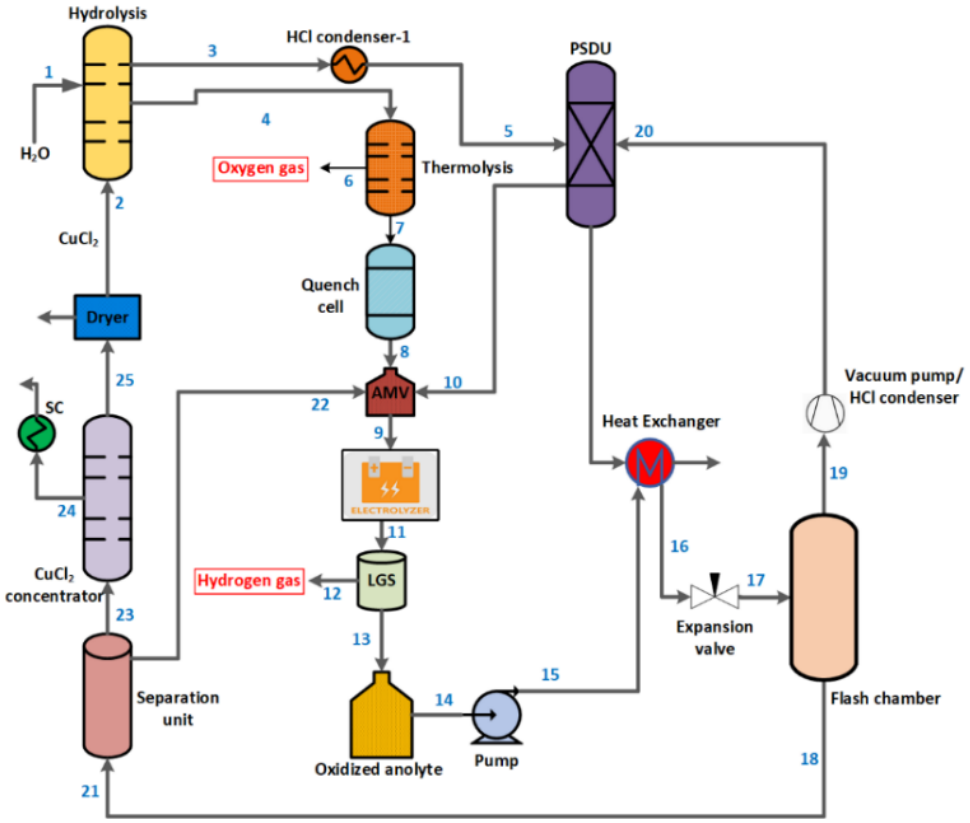

Fig. 3.3. Schematic representation of the integrated Cu-Cl cycle modified with flash vaporization process

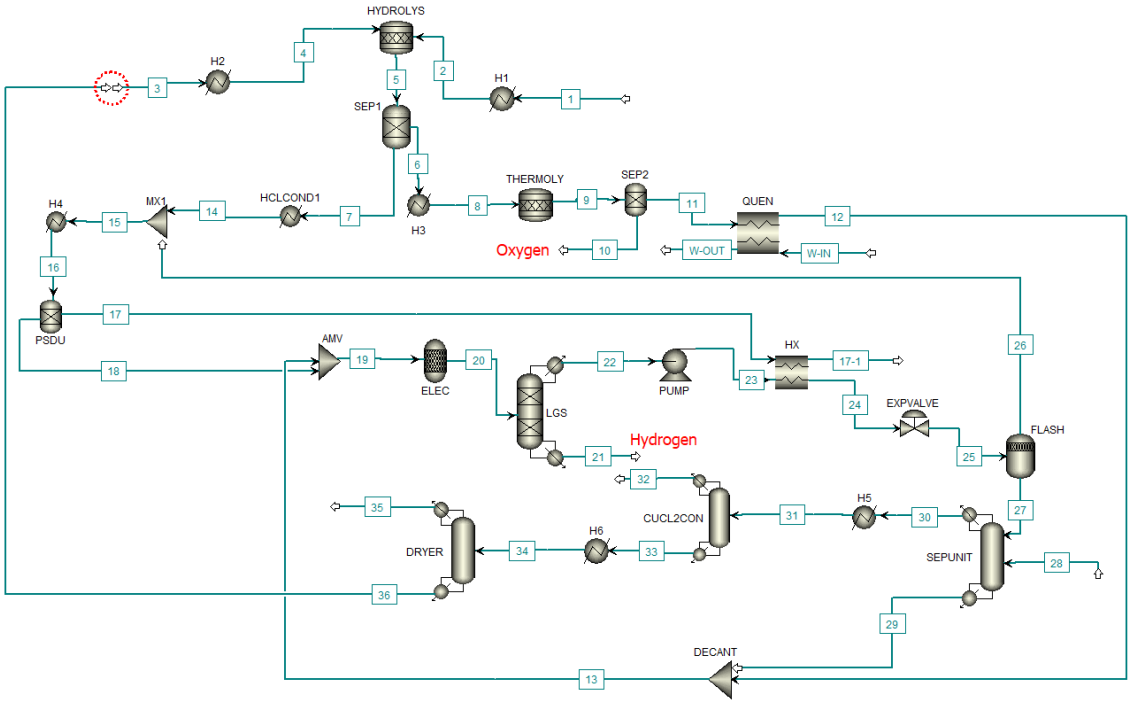

Fig. 3.4. Process flowsheet of the modified integrated cycle simulated in Aspen-plus

This will consequently positively impact the overall efficiencies of the cycle which is the ultimate goal. The oxidized anolyte, after getting separated from H_2 via the LGS, is allowed to gain thermal energy from the steam discharging the PSDU via the heat exchanger before adiabatically expanding through the throttling valve. After the throttling valve, the anolyte makes its way to the flash chamber where the vacuum conditions are already maintained. Upon entering the flash chamber, the anolyte undergoes instantaneous partial vaporization such that a mixture of H_2O and HCl separates from the anolyte. All subsequent processes in the modified cycle are similar to the actual integrated cycle at CERL as discussed in section 3.1. The simplified schematic and the detailed design of the modified cycle simulated in Aspen-plus are illustrated in Figures 3.3 and 3.4, respectively.

3.3 Experimental setup for the standalone flash vaporization process

The experimental setup of the standalone flash vaporization process developed at CERL is shown in Figure 3.5. The individual components of the setup are shown in Figure 3.6. Two different flash chamber designs are considered in this regard having different length to diameter (L/D) ratios for performance comparison purposes. Flash chamber 1 is made of clear polyvinyl chloride (PVC) material while flash chamber 2 is made of glass. Flash

chamber 1 has a length of 55 cm and an internal diameter of 10 cm resulting in a L/D ratio of 5.5. Flash chamber 2 has a length of 36 cm and an internal diameter of 19 cm resulting in a L/D ratio of 1.9. Both flash chambers have one inlet and three outlet ports. The inlet port is used for connecting the flash chamber with the throttling valve. One of the outlet ports is for draining the left-over anolyte solution to be reused for the subsequent experiments. The other two outlet ports are for connecting the vacuum chamber and pressure gauge.

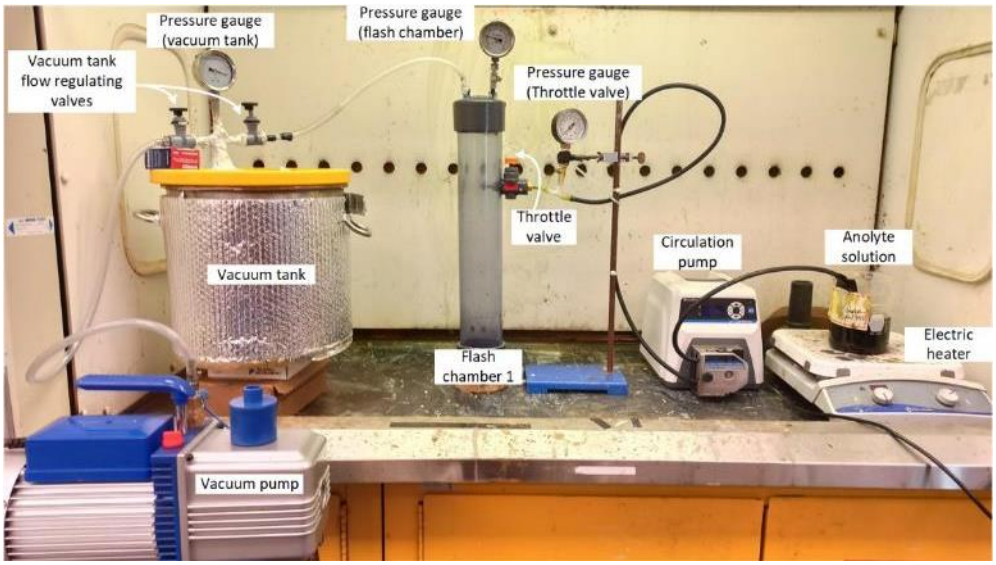

(a)

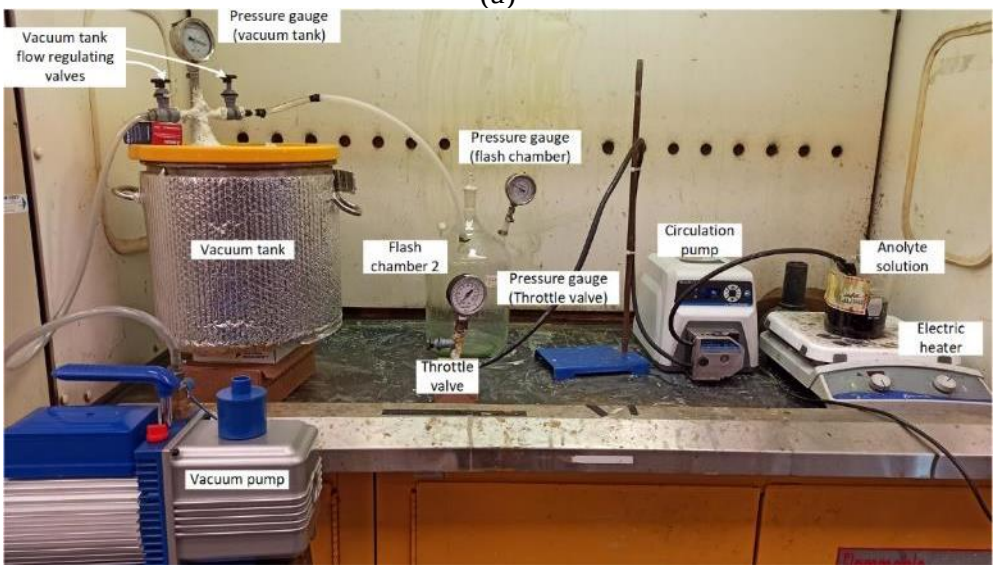

(b)

Fig. 3.5. Complete experimental setup of the stand-alone flash vaporization process with (a) flash chamber 1 and (b) flash chamber 2

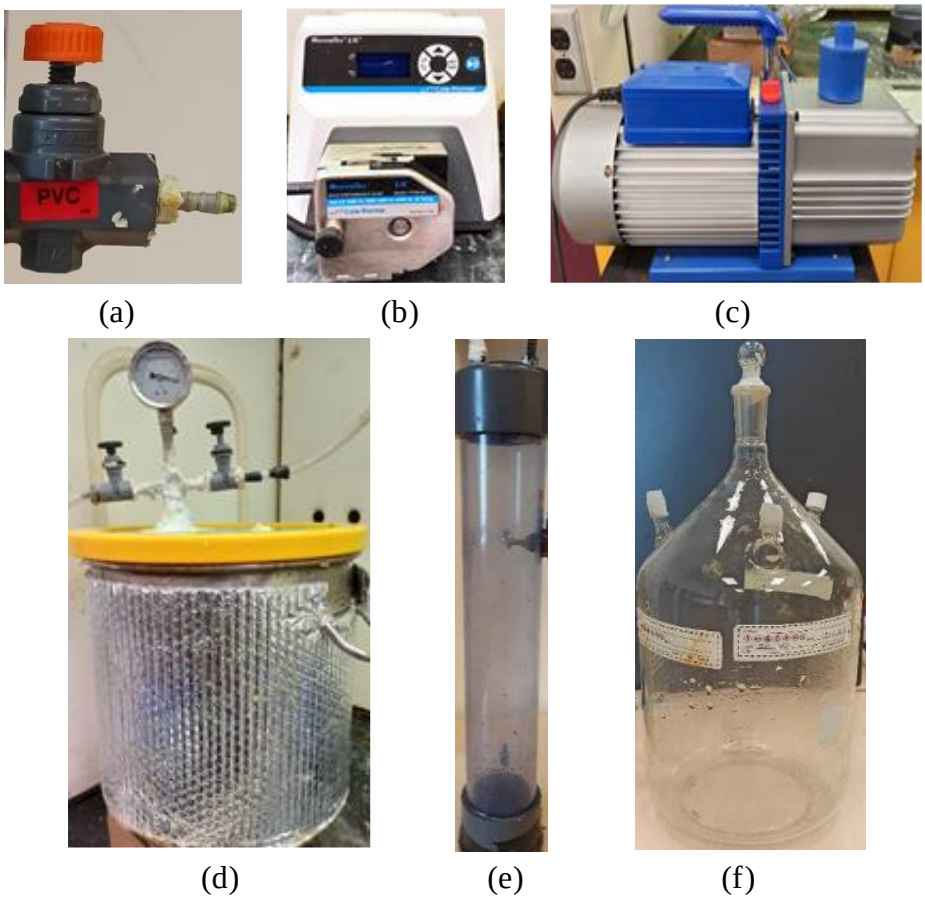

Fig. 3.6. Photographic representation of the various components of the experimental setup (a) throttle valve, (b) circulation pump, (c) vacuum pump, (d) vacuum tank with inlet valves and pressure gage, (e) flash chamber 1, and (f) flash chamber 2

The reason for choosing PVC as the fabrication material for flash chamber 1 is that it is a more economical option from fabrication view point and does not easily fracture. Moreover, various cross-sections are readily available commercially providing a wide range of dimensions to choose from. Also, the throttle valve is fused into the surface of the flash chamber 1 for which glass is not a suitable option. The flash chamber 2 is a glass flask already available in-house with the aforementioned dimensions. The utilization of metallic materials is not recommended for flash chamber fabrication since they can easily corrode while processing the anolyte solution due to its acidic nature. As far as the design of flash chamber 1 is concerned, the reason for choosing a slender shape is based on literature where a chamber with a high length to diameter ratio is recommended. The rationale behind this particular shape is its better flashing behavior compared with a round shaped chamber with a smaller height. The see-through nature of flash chamber materials

is essential for flow visualization purposes for experiments. All the valves used in our experimental setup are made of PVC material to resist corrosion due to the acidic nature of the anolyte solution containing HCl. The vacuum tank is made of stainless steel with an acrylic lid on its top for ensuring better vacuum conditions. A *Cole Palmer Masterflex* pump with model number 77250-62 is used for the circulation of the anolyte solution. The pressure gauge mounted over the vacuum pump and the flash chamber has a pressure measurement range of 0 to -1 bar. The pressure gauge mounted upstream of the throttle valve has a pressure measurement range of 0 to 2 bar. The anolyte solution is prepared such that 200 g of $CuCl_2$ and 20 g of CuCl are dissolved in a flask containing 600 ml of H_2O and 100 ml of HCl. The resulting anolyte solution has a total volume of 850 ml. The same composition of the anolyte solution is used for all experiments.

3.4. Experimental procedure

In this section, the detailed experimental procedure for the flash vaporization process is discussed. Figure 3.7 shows the flow chart of the step-by-step procedure of the flash vaporization process. Firstly, the anolyte solution is heated through the electric heater to the desired temperature. Three temperatures (65ºC, 75ºC, and 85ºC) are considered for the experiments. A digital thermometer is used for obtaining the correct temperature reading of the anolyte. Once the desired anolyte temperature is achieved, the anolyte is pumped through the throttle valve via the circulation pump at a flow rate of 0.0041 l/s. At this flow rate, a gage pressure of 0.25 bar is measured at a location upstream of the throttle valve. Simultaneously, the vacuum pump is switched on to allow the vacuum to be created inside both the vacuum and flash chambers. A maximum vacuum pressure of 0.15 bar is achieved inside both the vacuum and flash chambers. The anolyte then enters the flash chamber through the throttle valve in the form of a spray due to vacuum conditions inside the flash chamber. Upon entering the flash chamber, some of the anolyte instantaneously vaporizes and is collected in a flask placed inside the vacuum tank. The remaining anolyte gets collected at the base of the flash chamber which is then drained through the outlet port near the bottom of the chamber. The drained anolyte is collected in a flask and is again heated to the desired temperature for the next run of the experiment. After completion of experiments, the collected sample of the separated mixture of HCl and H_2O mixture is analyzed. The HCl concentration in the separated sample is obtained through the titration

process. For titration, a 0.1 M sodium hydroxide (NaOH) solution is prepared and is filled into a burette. The separated mixture of HCl and H_2O sample is collected in a glass flask and 2 to 3 drops of phenolphthalein solution are added to it. Phenolphthalein is generally used as an indicator in titration experiments to indicate the end point of the titration. After that, the NaOH solution is gradually added from the burette into the flask containing the mixture of HCl and H_2O sample till the point where the solution in the flask turns pink in color indicating the endpoint of the process. The volume of the NaOH solution added into the mixture of HCl and H_2O sample is then noted from the burette for evaluation of the HCl concentration inside the separated sample solution.

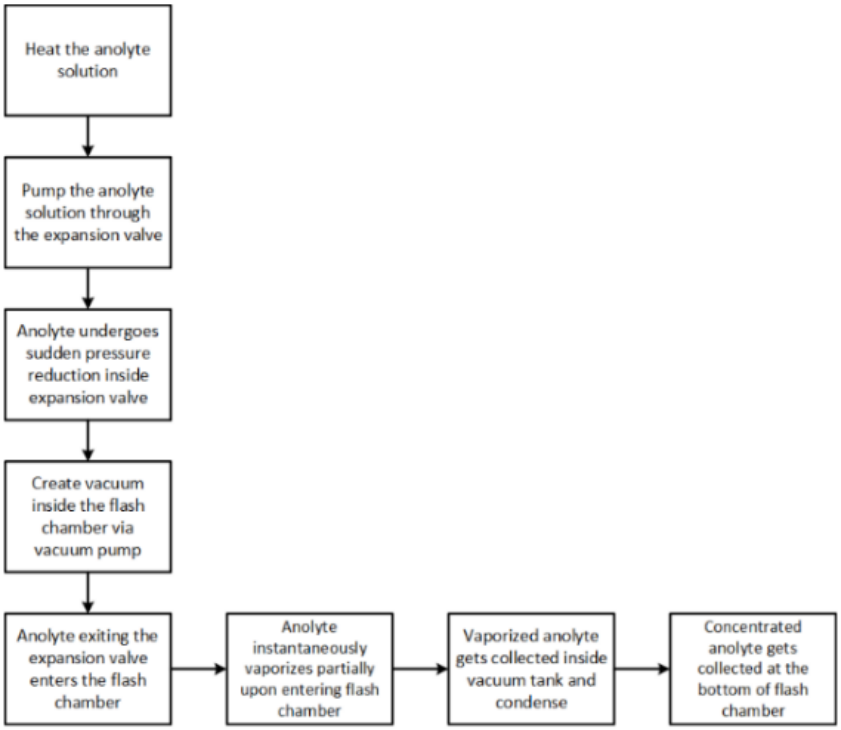

Fig. 3.7. Flowchart of the experimental procedure of the flash vaporization process

In closing, this chapter describes the details and operational mechanisms of the existing integrated four-step Cu-Cl cycle at the Ontario Tech University and its conceptually modified version by incorporating the flash vaporization process. The working of the main components and various auxiliary processes in the cycle is explained. This chapter also provides the details of the various components and their integration for the development of a standalone experimental setup for investigating the flash vaporization process. Moreover, the experimental and characterization procedures are discussed. The following chapter provides the details of the various analyses performed on the cycle.

CHAPTER 4 : ANALYSIS AND MODELING

In this chapter, the energy and exergy analyses, thermal management, multi-objective optimization, exergoeconomic and exergoenvironmental analyses performed on the four-step integrated Cu-Cl cycle at CERL and the cycle modified with flash vaporization process are presented. The modeling and mathematical details for the aforementioned analyses are also provided in detail.

4.1 Modeling and analyses of the integrated cycle at CERL

This section presents the detailed modeling and the various resulting analyses conducted on the four-step integrated Cu-Cl cycle set-up at CERL. The analyses include energy and exergy analyses, thermal management, exergoeconomic, exergoenvironmental and multi-objective optimization of the integrated cycle. Energy and exergy analyses consider the evaluation of all thermodynamic properties and performance parameters of the cycle. Thermal management of the cycle considers internal heat recovery through various components. Exergoeconomic analysis is performed by considering both the SPECO and EXCEM methodologies for evaluation of the various thermoeconomic parameters such as unit hydrogen cost and cost rate of hydrogen production. Exergoenvironmental analysis considers the evaluation of several environmental impact parameters of the cycle. Multi-objective optimization of the cycle is performed by considering three objective functions based on the data obtained through Aspen-plus simulations.

4.1.1 Energy and exergy analyses

The performance of each component of the integrated Cu-Cl cycle at CERL is evaluated based on the balanced exergy and energy equations along with the overall cycle efficiencies. Pressure and temperature of 1 bar and 25°C are considered to be the reference conditions. A few assumptions for simplification in the analysis are described below:

- The variations in potential and kinetic exergies and energies are insignificant.
- The losses in pressure are insignificant and are thus neglected.
- The steady-state conditions exist.

The generalized exergy, exergy, and mass balance equations are provided below:

$$\sum_{in} \dot{m}_{in} = \sum_{e} \dot{m}_{e} \tag{4.1}$$

$$\dot{Q} + \sum_{in} \dot{m}_{in} \left(h_{in} + \frac{V_{in}^2}{2} + gZ_{in} \right) = \dot{W} + \sum_{e} \dot{m}_{e} \left(h_{e} + \frac{V_{e}^2}{2} + gZ_{e} \right) \tag{4.2}$$

$$\dot{E}x^{Q} + \sum_{in} \dot{m}_{in} ex_{in} = \sum_{e} \dot{m}_{e} ex_{e} + \dot{E}x_{w} + \dot{E}x_{d} \tag{4.3}$$

The exergy, energy, and mass balance equations for all components of the integrated cycle are formulated and presented in Table 4.1. Moreover, the overall energy and exergy efficiencies of the integrated cycle are evaluated according to equations 4.4 and 4.6.

$$\eta = \frac{\dot{m}_{H_2} LHV_{H_2}}{\dot{Q}_{net,in} + \dot{W}_{in}} \tag{4.4}$$

$$\dot{Q}_{net,in} = \dot{Q}_{in,Hyd} + \dot{Q}_{in,Therm} + \dot{Q}_{in,Dryer} + \dot{Q}_{in,H1} + \dot{Q}_{in,H2} + \dot{Q}_{in,H3} + \dot{Q}_{in,H4} + \dot{Q}_{in,H5} + \dot{Q}_{in,H7} + \dot{Q}_{in,H8} \tag{4.5}$$

$$\psi = \frac{\dot{m}_{H_2} ex_{H_2}}{\dot{E}x_{\dot{Q}_{net,in}} + \dot{W}_{in}} \tag{4.6}$$

$$\dot{E}x_{\dot{Q}_{net,in}} = \dot{Q}_{net,in} \left(1 - \frac{T_0}{T_{cycle}} \right) \tag{4.7}$$

Table 4.1. Mass, energy, and exergy balance equations for the integrated cycle

Component	Mass balance equation	Energy balance equation	Exergy balance equation
Hydrolysis reactor	$\dot{m}_w + \dot{m}_{CuCl2} = \dot{m}_{s3}$	$\dot{m}_w h_w + \dot{m}_{CuCl2} h_{CuCl2} + \dot{Q}_{in,H1} + \dot{Q}_{in,H8} + \dot{Q}_{in,Hyd} = \dot{m}_{s3} h_{s3}$	$\dot{m}_w ex_w + \dot{m}_{CuCl2} ex_{CuCl2} + \dot{E}x_{\dot{Q}_{in,H1}} + \dot{E}x_{\dot{Q}_{in,H8}} + \dot{E}x_{\dot{Q}_{in,Hyd}} = \dot{m}_{s3} ex_{s3} + \dot{E}x_d$
Thermolysis reactor	$\dot{m}_{s4} = \dot{m}_{s7}$	$\dot{m}_{s4} h_{s4} + \dot{Q}_{in,H2} + \dot{Q}_{in,Therm} = \dot{m}_{s7} h_{s7}$	$\dot{m}_{s4} ex_{s4} + \dot{E}x_{\dot{Q}_{in,H2}} + \dot{E}x_{\dot{Q}_{in,Therm}} = \dot{m}_{s7} ex_{s7} + \dot{E}x_d$
Quenching cell	$\dot{m}_{s9} + \dot{m}_{s10} = \dot{m}_{s37} + \dot{m}_{s11}$	$\dot{m}_{s9} h_{s9} + \dot{m}_{s10} h_{s10} = \dot{m}_{s37} h_{s37} + \dot{m}_{s11} h_{s11}$	$\dot{m}_{s9} ex_{s9} + \dot{m}_{s10} ex_{s10} = \dot{m}_{s37} ex_{s37} + \dot{m}_{s11} ex_{s11} + \dot{E}x_d$
Anolyte make-up vessel	$\dot{m}_{s16} + \dot{m}_{s24} + \dot{m}_{s38} = \dot{m}_{s17}$	$\dot{m}_{s16} h_{s16} + \dot{m}_{s24} h_{s24} + \dot{m}_{s38} h_{s38} = \dot{m}_{s17} h_{s17}$	$\dot{m}_{s16} ex_{s16} + \dot{m}_{s24} ex_{s24} + \dot{m}_{s38} ex_{s38} = \dot{m}_{s17} ex_{s17} + \dot{E}x_d$
Electrolyzer	$\dot{m}_{s17} = \dot{m}_{s18}$	$\dot{m}_{s17} h_{s17} + \dot{W}_{in} = \dot{m}_{s18} h_{s18}$	$\dot{m}_{s17} ex_{s17} + \dot{W}_{in} = \dot{m}_{s18} ex_{s18} + \dot{E}x_d$
Liquid-gas separator	$\dot{m}_{s18} = \dot{m}_{s19} + \dot{m}_{s20}$	$\dot{m}_{s18} h_{s18} = \dot{m}_{s19} h_{s19} + \dot{m}_{s20} h_{s20}$	$\dot{m}_{s18} ex_{s18} = \dot{m}_{s19} ex_{s19} + \dot{m}_{s20} ex_{s20} + \dot{E}x_d$

Atmospheric distillation unit of anolyte	$\dot{m}_{s20} = \dot{m}_{s22} + \dot{m}_{s23}$	$\dot{m}_{s20}h_{s20} + \dot{Q}_{in,H4} = \dot{m}_{s22}h_{s22} + \dot{m}_{s23}h_{s23}$	$\dot{m}_{s20}ex_{s20} + \dot{E}x_{\dot{Q}_{in,H4}} = \dot{m}_{s22}ex_{s22} + \dot{m}_{s23}ex_{s23} + \dot{E}x_d$
Anolyte drying unit	$\dot{m}_{s22} = \dot{m}_{s26} + \dot{m}_{s27}$	$\dot{m}_{s22}h_{s22} + \dot{Q}_{in,H5} = \dot{m}_{s26}h_{s26} + \dot{m}_{s27}h_{s27}$	$\dot{m}_{s22}ex_{s22} + \dot{E}x_{\dot{Q}_{in,H5}} = \dot{m}_{s26}ex_{s26} + \dot{m}_{s27}ex_{s27} + \dot{E}x_d$
Separation unit	$\dot{m}_{s26} + \dot{m}_{s30} = \dot{m}_{s31} + \dot{m}_{s32}$	$\dot{m}_{s26}h_{s26} + \dot{m}_{s30}h_{s30} = \dot{m}_{s31}h_{s31} + \dot{m}_{s32}h_{s32} + \dot{Q}_{e,cond}$	$\dot{m}_{s26}ex_{s26} + \dot{m}_{s30}ex_{s30} = \dot{m}_{s31}ex_{s31} + \dot{m}_{s32}ex_{s32} + \dot{E}x_{\dot{Q}_{e,cond}} + \dot{E}x_d$
$CuCl_2$ concentrator	$\dot{m}_{s32} = \dot{m}_{s34} + \dot{m}_{s35}$	$\dot{m}_{s32}h_{s32} + \dot{Q}_{in,H7} = \dot{m}_{s34}h_{s34} + \dot{m}_{s35}h_{s35}$	$\dot{m}_{s32}ex_{s32} + \dot{E}x_{\dot{Q}_{in,H7}} = \dot{m}_{s34}ex_{s34} + \dot{m}_{s35}ex_{s35} + \dot{E}x_d$
Pressure swing distillation unit	$\dot{m}_{s13} = \dot{m}_{s15} + \dot{m}_{s16}$	$\dot{m}_{s13}h_{s13} + \dot{Q}_{in,H3} = \dot{m}_{s15}h_{s15} + \dot{m}_{s16}h_{s16}$	$\dot{m}_{s13}ex_{s13} + \dot{E}x_{\dot{Q}_{in,H3}} = \dot{m}_{s15}ex_{s15} + \dot{m}_{s16}ex_{s16} + \dot{E}x_d$
HCl-condenser-1	$\dot{m}_{s5} = \dot{m}_{s12}$	$\dot{m}_{s5}h_{s5} = \dot{m}_{s12}h_{s12} + \dot{Q}_{e,HClcond1}$	$\dot{m}_{s5}ex_{s5} = \dot{m}_{s12}ex_{s12} + \dot{E}x_{\dot{Q}_{e,HClcond1}} + \dot{E}x_d$
HCl-condenser-2	$\dot{m}_{s23} = \dot{m}_{s24}$	$\dot{m}_{s23}h_{s23} = \dot{m}_{s24}h_{s24} + \dot{Q}_{e,HClcond2}$	$\dot{m}_{s23}ex_{s23} = \dot{m}_{s24}ex_{s24} + \dot{E}x_{\dot{Q}_{e,HClcond2}} + \dot{E}x_d$
HCl-condenser-3	$\dot{m}_{s27} = \dot{m}_{s28}$	$\dot{m}_{s27}h_{s27} = \dot{m}_{s28}h_{s28} + \dot{Q}_{e,HClcond3}$	$\dot{m}_{s27}ex_{s27} = \dot{m}_{s28}ex_{s28} + \dot{E}x_{\dot{Q}_{e,HClcond3}} + \dot{E}x_d$
Dryer	$\dot{m}_{s35} = \dot{m}_{s39} + \dot{m}_{s40}$	$\dot{m}_{s35}h_{s35} + \dot{Q}_{in,Dryer} = \dot{m}_{s39}h_{s39} + \dot{m}_{s40}h_{s40}$	$\dot{m}_{s35}ex_{s35} + \dot{E}x_{\dot{Q}_{in,Dryer}} = \dot{m}_{s39}ex_{s39} + \dot{m}_{s40}ex_{s40} + \dot{E}x_d$
Steam condenser	$\dot{m}_{s34} = \dot{m}_{s41}$	$\dot{m}_{s34}h_{s34} = \dot{m}_{s41}h_{s41} + \dot{Q}_{e,SC}$	$\dot{m}_{s34}ex_{s34} = \dot{m}_{s41}ex_{s41} + \dot{E}x_{\dot{Q}_{e,SC}} + \dot{E}x_d$

4.1.2 Thermal management

Thermal management of the integrated Cu-Cl cycle is performed by considering six heat recovery schemes. Heat recovery is carried out during two phases. During the first phase, steam, which is exiting the different components of the integrated cycle, is recovered whereas, during the second phase, the recovered steam is allowed to absorb heat via the

excess thermal energy of the HCl-condenser-1 employing the heat-exchanger-1 in the integrated cycle. The numerous considered configurations of heat recovery are presented in Table 4.2.

Table 4.2. Heat recovery schemes and their corresponding S/Cu ratios

Configuration	S/Cu molar ratio
C-1	17.4
C-2	15.1
C-3	13.6
C-4	12.9
C-5	15.2
C-6	16.7

The steam and heat recovery processes are carried out in a step-by-step manner through three complete cycles. The first cycle constitutes the steam recovery from the several components of the cycle including the dryer unit, the quenching cell, the PSDU, and the $CuCl_2$-concentrator. The second cycle constitutes the recovery of heat by passing the steam recovered during the first cycle through the heat exchanger-1. The third cycle constitutes the input of the superheated steam obtained during the second cycle for the hydrolysis reaction. The recovered steam during the second cycle recovers heat in the third cycle and the process continues. Hence, the utilization of heat recovery in the integrated cycle takes place after the completion of the first two cycles. The S/Cu ratio considered for the initial two cycles is 12.5. The S/Cu ratio of the third and subsequent cycles is based on individual heat recovery configurations. The process flowsheet showing the operation of the cycle modeled in Aspen-plus for configuration C-1 is shown in Figure 4.1. The process flowsheets showing the operation of the first cycle for the remaining five configurations are shown in Figure 4.2 demonstrating the mixing process of the steam recovered via numerous streams in the cycle. The second and third cycle's representation for every configuration is similar as presented in Figure 4.1. The considered heat recovery schemes are different combinations of the streams recovered through several components of the cycle due to which their temperatures and S/Cu ratios are different as well. The temperature of streams exiting the PSDU, the $CuCl_2$-concentrator, the quenching cell, and the dryer unit are 106, 110, 100, and 130°C, respectively whereas their corresponding mass flow rates are 0.09, 0.03, 0.02, and 0.01 kg/s. To achieve steam recovery via the $CuCl_2$-concentrator, the steam condenser of the original integrated cycle was removed during the modeling

phase of this analysis. The details of heat recovery of the various configurations are discussed as follows:

- ***Configuration C-1:*** Streams discharging the quenching cell, the PSDU, and the $CuCl_2$-concentrator are first recovered and then mixed to obtain an output stream having a steam recovery temperature of 100°C. This output stream then recovers heat from stream S5 (HCl/H_2O) at 400°C via the heat-exchanger-1 to achieve a temperature of 196.4°C.
- ***Configuration C-2:*** Streams discharging the PSDU, and the $CuCl_2$-concentrator are first recovered and then mixed to obtain an output stream having a steam recovery temperature of 107°C. This output stream then recovers heat from stream S5 (HCl/H_2O) at 400°C via the heat-exchanger-1 to achieve a temperature of 342.3°C.
- ***Configuration C-3:*** Streams discharging the PSDU, and the quenching cell are first recovered and then mixed to obtain an output stream having a steam recovery temperature of 100°C. This output stream then recovers heat from stream S5 (HCl/H_2O) at 400°C via the heat-exchanger-1 to achieve a temperature of 220°C.
- ***Configuration C-4:*** Streams discharging the PSDU, and the dryer unit are first recovered and then mixed to obtain an output stream having a steam recovery temperature of 109°C. This output stream then recovers heat from stream S5 (HCl/H_2O) at 400°C via the heat-exchanger-1 to achieve a temperature of 391.3°C.
- ***Configuration C-5:*** Streams discharging the PSDU, and the dryer unit are first recovered and then mixed to obtain an output stream having a steam recovery temperature of 100°C. This output stream then recovers heat from stream S5 (HCl/H_2O) at 400°C via the heat-exchanger-1 to achieve a temperature of 210.5°C.
- ***Configuration C-6:*** Streams discharging the PSDU, the $CuCl_2$-concentrator, and the dryer unit are first recovered and then mixed to obtain an output stream having a steam recovery temperature of 109.4°C. This output stream then recovers heat from stream S5 (HCl/H_2O) at 400°C via the heat-exchanger-1 to achieve a temperature of 329.5°C.

Finally, the output stream recovered after heat recovery for each configuration is then heated via the heater-1 to achieve a temperature of 400°C to be utilized as the feed for the hydrolysis reaction.

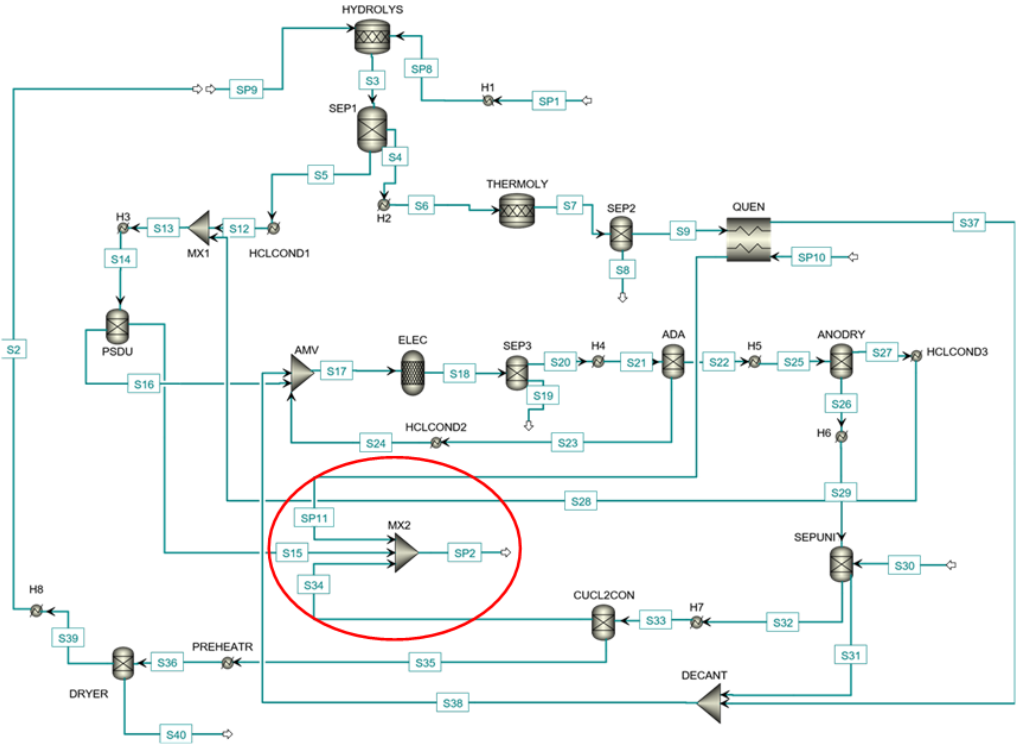
HYDROLYS
SP9
SP8
S3
H1
SP1
SEP1
S4
S5
THERMOLY
H3
S13
S12
H2
S6
S7
SEP2
QUEN
S37
MX1
HCLCOND1
S14
S9
SP10
S8
PSDU
S2
AMV
ELEC
SEP3
H4
ADA
H5
ANODRY
S27
HCLCOND3
S17
S18
S20
S21
S22
S25
S16
S19
S26
HCLCOND2
H6
S24
S23
S28
S29
SP11
MX2
SEPUNI
S15
SP2
S30
S34
H8
CUCL2CON
H7
S33
S32
S39
PREHEATR
S36
S35
S31
DRYER
DECANT
S38
S40

(a)

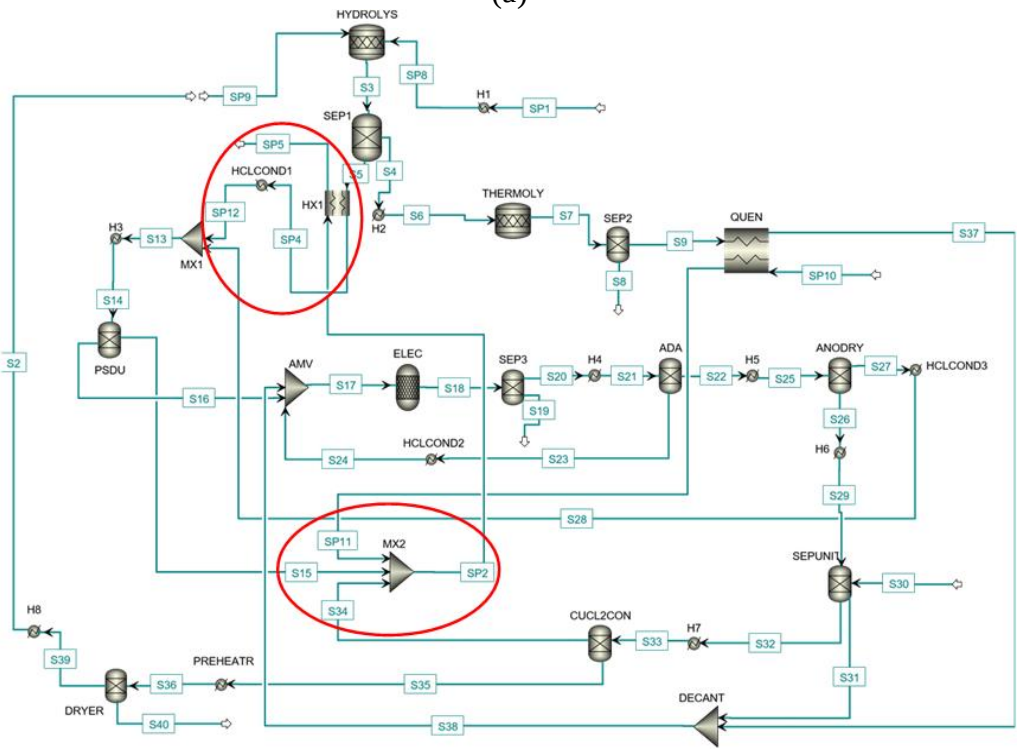
HYDROLYS
SP9
SP8
S3
H1
SP1
SEP1
SP5
HCLCOND1
S4
HX1
SP12
H2
S6
THERMOLY
S7
SEP2
QUEN
S37
H3
S13
SP4
MX1
S9
SP10
S8
S14
PSDU
S2
AMV
ELEC
SEP3
H4
ADA
H5
ANODRY
S27
HCLCOND3
S17
S18
S20
S21
S22
S25
S16
S19
S26
HCLCOND2
H6
S24
S23
S28
S29
SP11
MX2
SEPUNIT
S15
SP2
S30
S34
H8
CUCL2CON
H7
S33
S32
S39
PREHEATR
S36
S35
S31
DRYER
DECANT
S38
S40

(b)

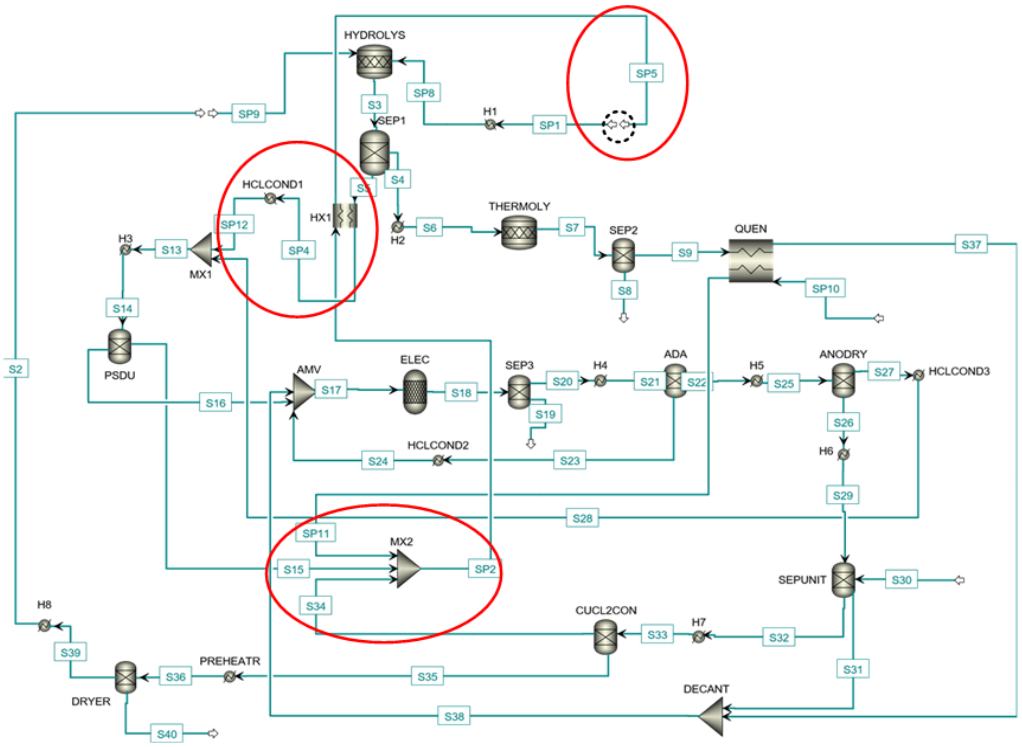

(c)

Fig. 4.1. Aspen-plus process flowsheet of the cycle operation for the configuration C-1: (a) 1st cycle (b) 2nd cycle and (c) 3rd cycle

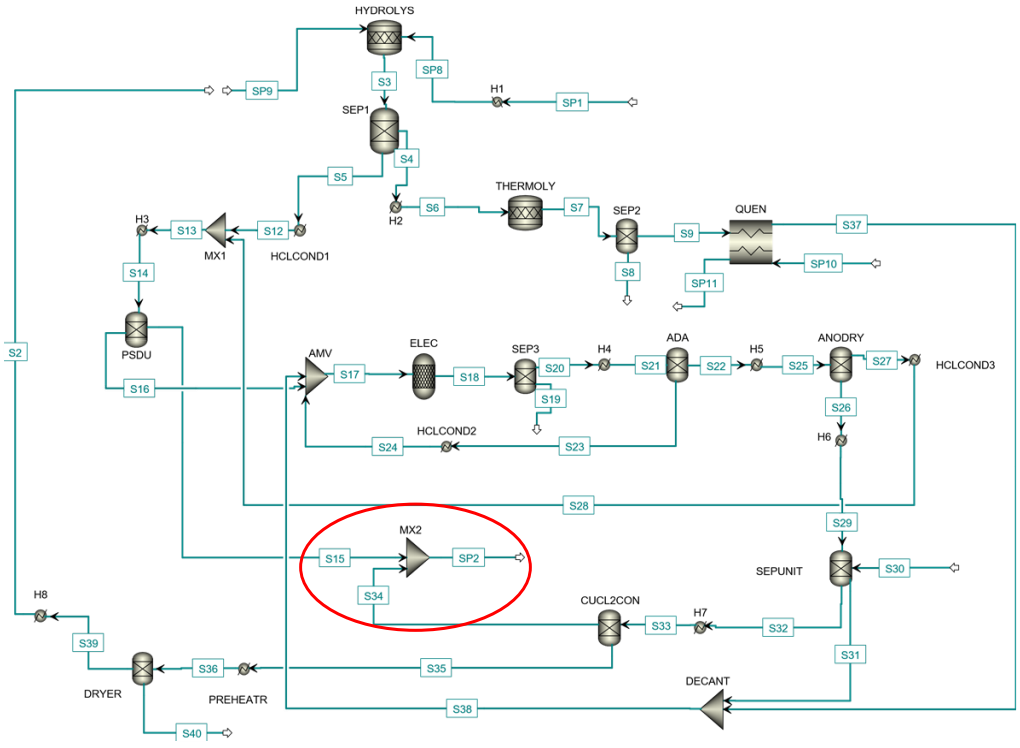

(a)

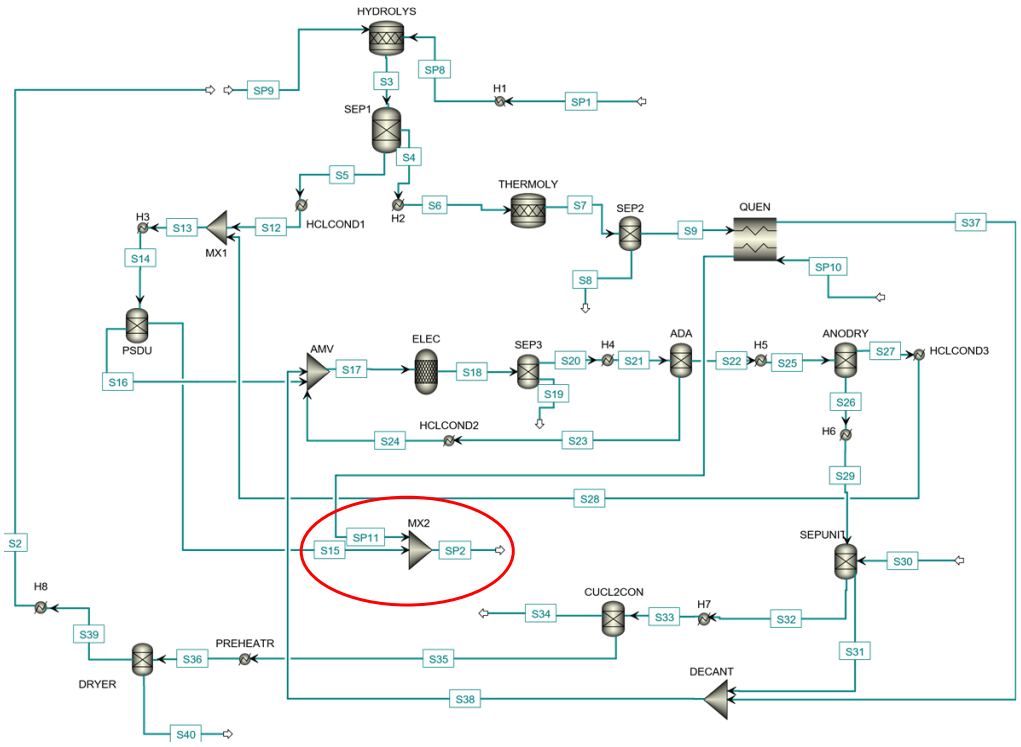
HYDROLYS
SP9
SP8
S3
H1
SP1
SEP1
S4
S5
THERMOLY
S6
S7
SEP2
QUEN
S37
H3
S13
S12
HCLCOND1
H2
MX1
S14
S9
SP10
S8
PSDU
AMV
ELEC
SEP3
H4
ADA
H5
ANODRY
S27
HCLCOND3
S16
S17
S18
S20
S21
S22
S25
S19
S26
HCLCOND2
H6
S24
S23
S29
S28
MX2
SP11
S15
SP2
SEPUNIT
S30
S2
H8
CUCL2CON
S34
S33
H7
S32
S39
PREHEATR
S36
S35
S31
DRYER
DECANT
S38
S40

(b)

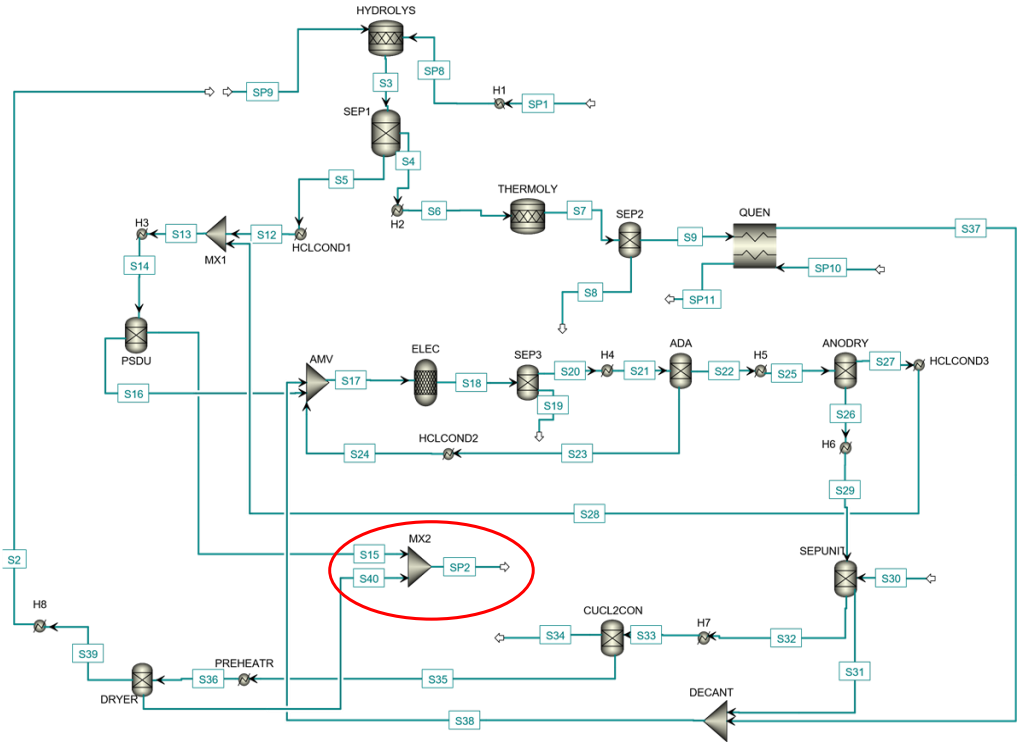
HYDROLYS
SP9
SP8
S3
H1
SP1
SEP1
S4
S5
THERMOLY
S6
S7
SEP2
QUEN
S37
H3
S13
S12
HCLCOND1
H2
MX1
S14
S9
SP10
SP11
S8
PSDU
AMV
ELEC
SEP3
H4
ADA
H5
ANODRY
S27
HCLCOND3
S16
S17
S18
S20
S21
S22
S25
S19
S26
HCLCOND2
H6
S24
S23
S29
S28
MX2
S15
S40
SP2
SEPUNIT
S30
S2
H8
CUCL2CON
S34
S33
H7
S32
S39
PREHEATR
S36
S35
S31
DRYER
DECANT
S38

(c)

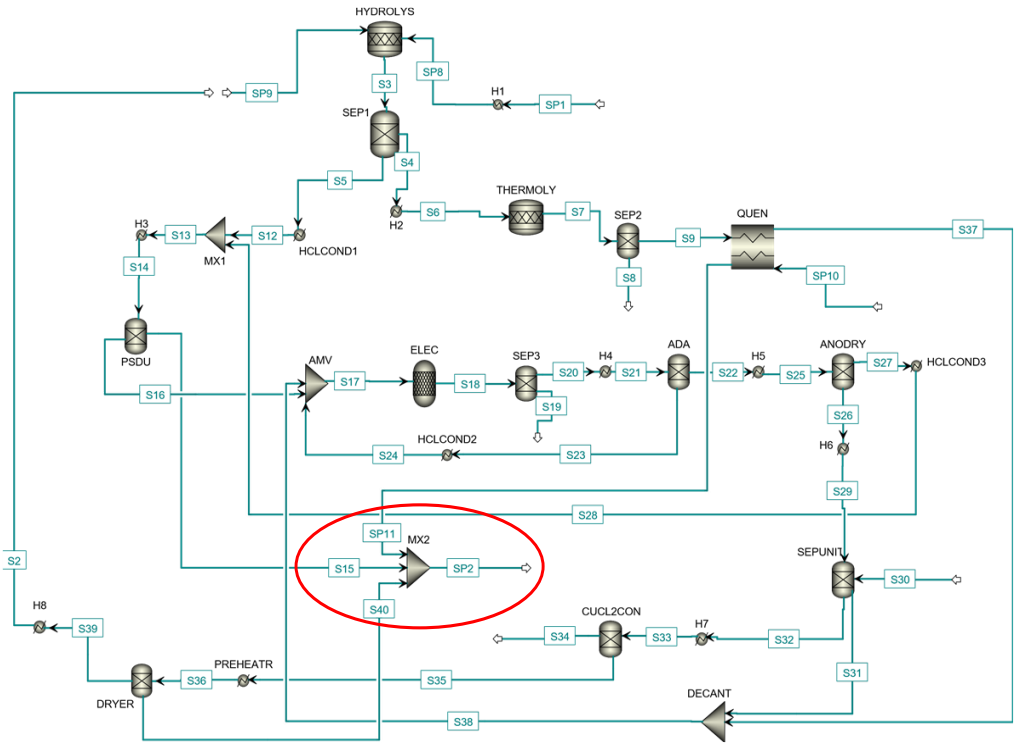

(d)

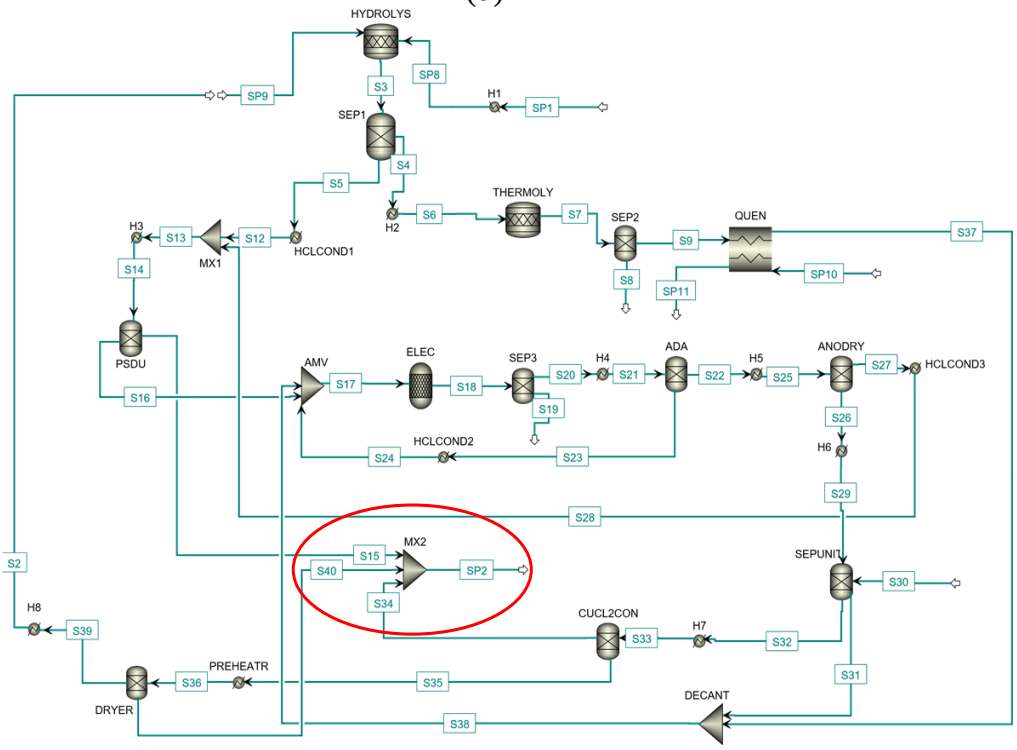

(e)

Fig. 4.2. Aspen-plus process flowsheet representing cycle operation of the 1st cycle for the configurations: (a) C-2 (b) C-3 (c) C-4 (d) C-5 and (e) C-6

4.1.3 Exergoeconomic analysis

Along with the assessment of the exergetic and energetic performances of a given system and its associated components, an economic analysis of energy systems is also imperative to evaluate their financial feasibility. The outcome of the combination of economic and exergy-energy assessments is termed as exergoeconomic analysis. There are numerous approaches and methods of exergoeconomic analysis formulated and suggested in the literature. There are four major categories of the numerous approaches for exergoeconomic evaluation according to Tsatsaronis [75]. These include exergy-economic similarity number, calculus analysis, cost accounting, and product/cost efficiency diagrams. The two most frequently applied approaches in this context are the SPECO and the EXCEM. Hence, in this thesis, these two methods are applied to a four-step integrated Cu-Cl cycle.

4.1.3.1 Exergy-cost-energy-mass (EXCEM) approach

The foundation of the EXCEM approach is based on the comprehension of the performance of a system in terms of the examination of the input and output flows of the EXCEM quantities at the system level as well as at every point within the system. An illustration of the analysis concept of the EXCEM approach is provided in Figure 4.3. The formulation of the generalized balances equations employed for the Cu-Cl cycle is based on the concept described in [76]. Of the four specified EXCEM quantities, only mass and energy are subject to conservation due to their very nature. However, exergy and cost are not subject to conservation such that the former either manages to stay the same or tends to reduce while the latter either remains constant or tends to increase.

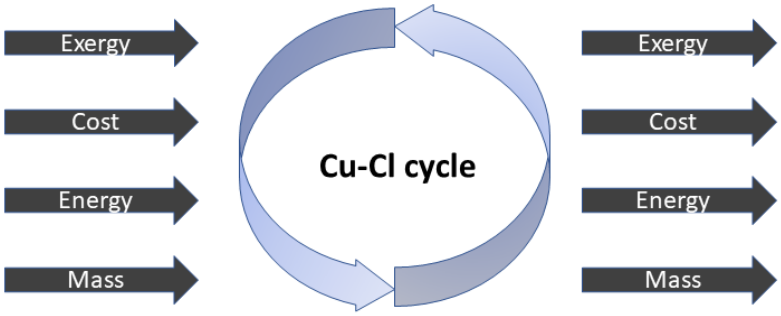

Fig. 4.3. Application of the EXCEM approach to a four-step Cu-Cl cycle

A general balanced equation for a quantity may be represented as

$$Input + Generation - Output - Consumption = Accumulation \quad (4.8)$$

In the above equation, the output and the input terms represent the quantities that discharge and enter respectively the boundaries of a given system. While the production and utilization of quantities in a given system are represented by the terms generation and consumption, respectively. The build-up of a quantity (positive or negative) in a given system is represented with the accumulation term. The representation of these general equations can either be done in an integral or in a differential form which are respectively expressed as:

Amount input + Amount generated – Amount output – Amount consumed = Amount accumulated (4.9)

Input rate + Generation rate – Output rate – Consumption rate = Accumulation rate (4.10)

Due to the principles of mass and energy conservation, neither are they produced nor expended. Further, due to the irreversibilities of a given process, exergy is subject to consumption and is thus affiliated with the generation of entropy. Hence, the mass, energy, and exergy balance equations are represented as:

$$\dot{m}_{in} - \dot{m}_{out} = \dot{m}_{ac} \tag{4.11}$$

$$\dot{E}_{in} - \dot{E}_{out} = \dot{E}_{ac} \tag{4.12}$$

$$\dot{E}x_{in} - \dot{E}x_{out} - \dot{L}_{ex} = \dot{E}x_{ac} \tag{4.13}$$

The output terms shown in Eqs. 4.12 and 4.13 may further be classified as product and waste as:

$$\dot{E}_{out} = \dot{E}_{out,P} - \dot{E}_{out,W} \tag{4.14}$$

$$\dot{E}x_{out} = \dot{E}x_{out,P} - \dot{E}x_{out,W} \tag{4.15}$$

The general balanced equation for cost can be represented as

$$K_{in} + K_{gen} - K_{out} = K_{ac} \tag{4.16}$$

where K symbolizes cost, the subscripts *out*, *in*, and *ac* denote output, input, and accumulation, respectively while the subscript *gen* symbolizes the corresponding capital and secondary costs for creating and maintaining a certain system. Exergy and energy losses are the two categories of losses taken into account in this analysis. Equations 4.12 and 4.14 are employed for the evaluation of energy losses. The loss rate is denoted as $\dot{L}$ and the energy loss rate is obtained as:

$$\dot{L}_{en} = \dot{E}_{out,W} \tag{4.17}$$

Furthermore, equations 4.13 and 4.15 represent the exergy losses which are further classified as consumption of exergy (loss of exergy due to various irreversibilities during a certain process) and output of waste exergy (loss of exergy from a given system) respectively described through equations 4.15 and 4.13. The mathematical expression showing the sum of these categories of exergy losses is represented as:

$$\dot{L}_{ex} = \dot{E}x_{out,W} + \dot{E}x_{con} \tag{4.18}$$

Equation 4.16 provides the mathematical representation of the capital cost (K) as:

$$K = \text{ Capital cost of the system} \tag{4.19}$$

The accumulation terms (equations 4.8 to 4.13 and 4.16) in any given energy system operating under the assumption of steady-state-steady-flow mode equals zero. Therefore, all the losses associated with the terms described previously ($\dot{L}_{en}$ and $\dot{L}_{ex}$) are mathematically expressed below as:

$$\dot{L}_{en} = \sum_{in} \text{Energy flow rates} - \sum_{P} \text{Energy flow rates} \tag{4.20}$$

$$\dot{L}_{ex} = \sum_{in} \text{Exergy flow rates} - \sum_{P} \text{Exergy flow rates} \tag{4.21}$$

The ratio of the thermodynamic loss rate ($\dot{L}$) to capital cost (K) is defined as a parameter R and is expressed as

$$\dot{R} = \dot{L}/K \tag{4.22}$$

The parameter $\dot{R}$, in terms of energy loss and exergy loss, is expressed mathematically as

$$\dot{R}_{en} = \dot{L}_{en}/K \tag{4.23}$$

$$\dot{R}_{ex} = \dot{L}_{ex}/K \tag{4.24}$$

4.1.3.2 Specific exergy costing (SPECO) approach

The foundation of the SPECO approach of the exergoeconomic analysis lies on three fundamental steps that are described as follows:

1) Identification of each exergy stream of a system.
2) Definition of fuel and product for each equipment of a system.
3) Formulation of balanced exergetic cost equations for each equipment of a system.

The evaluation of the rate of exergy at each state point for all streams of the integrated cycle is carried out through Aspen-plus. The definition of exergy of products and fuels for all cycle equipment is provided in Table 4.3. The cost balance equations are formulated based on the principles laid down by Lazzaretto and Tsatsaronis [40]. The generalized representation of the exergetic cost balance equation for each equipment of a system is provided as:

$$\sum_e \left(c_e \dot{E}x_e\right)_k + c_{elec,k}\dot{W}_k = c_{q,k}\dot{E}x_{q,k} + \sum_{in}\left(c_{in}\dot{E}x_{in}\right)_k + \dot{Z}_k \tag{4.25}$$

The cost of inlet and outlet exergy streams of matter, electrical power, and heat transfer are given via equations 4.26 through 4.29 as:

$$\dot{C}_{in} = c_{in}\dot{E}x_{in} \tag{4.26}$$

$$\dot{C}_e = c_e\dot{E}x_e \tag{4.27}$$

$$\dot{C}_{elec} = c_{elec}\dot{W} \tag{4.28}$$

$$\dot{C}_q = c_q\dot{E}x_q \tag{4.29}$$

where the unit exergy cost, rate of exergy, electrical power, and capital cost rate are symbolized respectively as c, $\dot{E}x$, $\dot{W}$, and $\dot{Z}_k$. The subscript k denotes the *kth* equipment of a system. The sum of both the capital investment and the operation and maintenance costs equals the capital cost rate. To evaluate the cost at each state point of a system, it is imperative to develop auxiliary equations as the number of streams exceeds the number of equipment. In this context, the formulation of the auxiliary equations is accomplished through the application of product (*P*) and fuel (*F*) rules as described in [40]. As per the *F* rule, the specific cost linked with the removal of exergy from a given stream acting as fuel needs to be the same as the average specific cost at which the exergy that is removed is transferred to the stream discharging the same equipment. As per the *P* rule, each exergy stream linked with the product that is discharging given equipment is being allocated the same specific cost of exergy. Table 4.4 provides the balanced cost rate and auxiliary equations for all equipment of the integrated cycle at CERL. The hourly levelized cost rate for the *kth* equipment of the Cu-Cl cycle is mathematically expressed as:

$$\dot{Z}_k^T = \dot{Z}_{Cu-Cl}^T \frac{PEC_k}{\sum_{Cu-Cl} PEC} \tag{4.30}$$

Here, the cost of purchased equipment is represented as *PEC*. The hourly levelized total cost rate of equipment of a given system is symbolized as $\dot{Z}_{Cu-Cl}^T$ and is mathematically expressed as:

$$\dot{Z}_{Cu-Cl}^T = \frac{\emptyset \dot{CA}_{Cu-Cl}}{\tau} \tag{4.31}$$

where the annual operational hours, the operating and maintenance cost factor, and the annual capital cost of a given system are denoted as τ, $\emptyset$, and $\dot{CA}_{Cu-Cl}$ respectively. The annual capital cost is mathematically defined as:

$$\dot{CA}_{Cu-Cl} = PW_{Cu-Cl} CRF(i, n) \tag{4.32}$$

Table 4.3. Definition of exergy of fuel and product for different components

Component	Fuel	Product
Hydrolysis	$\dot{E}x_{Q,Hyd}$	$(\dot{E}x_{S4} + \dot{E}x_{S5}) - (\dot{E}x_{S1} + \dot{E}x_{S2})$
Thermolysis	$\dot{E}x_{Q,Therm}$	$(\dot{E}x_{S8} + \dot{E}x_{S9}) - (\dot{E}x_{S6})$
Dryer	$\dot{E}x_{Q,PH}$	$(\dot{E}x_{S39} + \dot{E}x_{S40}) - (\dot{E}x_{S35})$
ADU	$\dot{E}x_{Q,H5}$	$(\dot{E}x_{S26} + \dot{E}x_{S27}) - (\dot{E}x_{S22})$
ADA	$\dot{E}x_{Q,H4}$	$(\dot{E}x_{S22} + \dot{E}x_{S23}) - (\dot{E}x_{S20})$
HCl-cond-1	$\dot{E}x_{Q,HCl-cond1}$	$\dot{E}x_{S12} - \dot{E}x_{S5}$
HCl-cond-2	$\dot{E}x_{Q,HCl-cond2}$	$\dot{E}x_{S24} - \dot{E}x_{S23}$
HCl-cond-3	$\dot{E}x_{Q,HCl-cond3}$	$\dot{E}x_{S28} - \dot{E}x_{S27}$
Quench Cell	$\dot{E}x_{S11} - \dot{E}x_{S10}$	$\dot{E}x_{S9} - \dot{E}x_{S37}$
Electrolyzer	$\dot{W}_{Elec}$	$(\dot{E}x_{S19} + \dot{E}x_{S20}) - (\dot{E}x_{S17})$
$CuCl_2$-concentrator	$\dot{E}x_{Q,H7}$	$(\dot{E}x_{S34} + \dot{E}x_{S35}) - (\dot{E}x_{S32})$
PSDU	$\dot{E}x_{Q,H3}$	$(\dot{E}x_{S15} + \dot{E}x_{S16}) - (\dot{E}x_{S13})$
Steam condenser	$\dot{E}x_{Q,SC}$	$\dot{E}x_{S41} - \dot{E}x_{S34}$
Heater-1	$\dot{E}x_{Q,H1}$	$\dot{E}x_{S1} - \dot{E}x_{water}$
Heater-2	$\dot{E}x_{Q,H2}$	$\dot{E}x_{S6} - \dot{E}x_{S4}$
Heater-8	$\dot{E}x_{Q,H8}$	$\dot{E}x_{S2} - \dot{E}x_{CuCl_2}$
Condenser	$\dot{E}x_{Q,Cond}$	$\dot{E}x_{S29} - \dot{E}x_{S26}$

Here, the capital recovery factor is represented as $CRF(i, n)$. The terms in parenthesis *i* and *n* denote the interest rate and lifetime of a given system in years, respectively. The capital recovery factor is mathematically defined as:

$$CRF = \frac{i(i+1)^n}{(i+1)^n - 1} \tag{4.33}$$

Table 4.4. Balanced exergetic cost rate and auxiliary equations for different components

Component	Balanced equation for exergetic cost rate	Auxiliary equation
Hydrolysis	$\dot{C}_{S1} + \dot{C}_{S2} + \dot{Z}_{Hyd,Sep1} + \dot{E}x_{Q,Hyd}c_{th} = \dot{C}_{S4} + \dot{C}_{S5}$	$\frac{\dot{C}_{S4}}{\dot{E}x_{S4}} = \frac{\dot{C}_{S5}}{\dot{E}x_{S5}}$
Thermolysis	$\dot{C}_{S6} + \dot{Z}_{Therm,Sep2} + \dot{E}x_{Q,Therm}c_{th} = \dot{C}_{S8} + \dot{C}_{S9}$	$\frac{\dot{C}_{S8}}{\dot{E}x_{S8}} = \frac{\dot{C}_{S9}}{\dot{E}x_{S9}}$
Quench cell	$\dot{C}_{S9} + \dot{C}_{S10} + \dot{Z}_{QC} = \dot{C}_{S37} + \dot{C}_{S11}$	$\frac{\dot{C}_{S9}}{\dot{E}x_{S9}} = \frac{\dot{C}_{S37}}{\dot{E}x_{S37}}$ $\frac{\dot{C}_{S10}}{\dot{E}x_{S10}} = \frac{\dot{C}_{S11}}{\dot{E}x_{S11}}$
PSDU	$\dot{C}_{S13} + \dot{Z}_{PSDU,H3} + \dot{E}x_{Q,H3}c_{th} = \dot{C}_{S15} + \dot{C}_{S16}$	$\frac{\dot{C}_{S15}}{\dot{E}x_{S15}} = \frac{\dot{C}_{S16}}{\dot{E}x_{S16}}$
Electrolyzer	$\dot{C}_{S17} + \dot{Z}_{Elec,Sep3} + \dot{W}_{Elec}c_{elec} = \dot{C}_{S19} + \dot{C}_{S20}$	$\frac{\dot{C}_{S19}}{\dot{E}x_{S19}} = \frac{\dot{C}_{S20}}{\dot{E}x_{S20}}$
ADA	$\dot{C}_{S20} + \dot{Z}_{ADA,H4} + \dot{E}x_{Q,H4}c_{th} = \dot{C}_{S22} + \dot{C}_{S23}$	$\frac{\dot{C}_{S22}}{\dot{E}x_{S22}} = \frac{\dot{C}_{S23}}{\dot{E}x_{S23}}$
ADU	$\dot{C}_{S22} + \dot{Z}_{ADU,H5} + \dot{E}x_{Q,H5}c_{th} = \dot{C}_{S26} + \dot{C}_{S27}$	$\frac{\dot{C}_{S26}}{\dot{E}x_{S26}} = \frac{\dot{C}_{S27}}{\dot{E}x_{S27}}$
$CuCl_2$-concentrator	$\dot{C}_{S32} + \dot{Z}_{CuCl_2-con,H7} + \dot{E}x_{Q,H7}c_{th} = \dot{C}_{S34} + \dot{C}_{S35}$	$\frac{\dot{C}_{S34}}{\dot{E}x_{S34}} = \frac{\dot{C}_{S35}}{\dot{E}x_{S35}}$
Dryer	$\dot{C}_{S35} + \dot{Z}_{Dryer,PH} + \dot{E}x_{Q,PH}c_{th} = \dot{C}_{S39} + \dot{C}_{S40}$	$\frac{\dot{C}_{S39}}{\dot{E}x_{S39}} = \frac{\dot{C}_{S40}}{\dot{E}x_{S40}}$
Separation unit	$\dot{C}_{S29} + \dot{C}_{S30} + \dot{Z}_{Sep-unit} = \dot{C}_{S31} + \dot{C}_{S32}$	$\frac{\dot{C}_{S31}}{\dot{E}x_{S31}} = \frac{\dot{C}_{S32}}{\dot{E}x_{S32}}$
Steam condenser	$\dot{C}_{S34} + \dot{Z}_{SC} + \dot{E}x_{Q,SC}c_w = \dot{C}_{S41}$	-
HCl-condenser-1	$\dot{C}_{S5} + \dot{Z}_{HCl-cond1} + \dot{E}x_{Q,HCl-cond1}c_w = \dot{C}_{S12}$	-
HCl-condenser-2	$\dot{C}_{S23} + \dot{Z}_{HCl-cond2} + \dot{E}x_{Q,HCl-cond2}c_w = \dot{C}_{S24}$	-
HCl-condenser-3	$\dot{C}_{S27} + \dot{Z}_{HCl-cond3} + \dot{E}x_{Q,HCl-cond3}c_w = \dot{C}_{S28}$	-
Heater-1	$\dot{C}_{water} + \dot{Z}_{H1} + \dot{E}x_{Q,H1}c_{th} = \dot{C}_{S1}$	-

Heater-2	$\dot{C}_{S4} + \dot{Z}_{H2} + \dot{E}x_{Q,H2} c_{th} = \dot{C}_{S6}$	-
Heater-8	$\dot{C}_{CuCl_2} + \dot{Z}_{H8} + \dot{E}x_{Q,H8} c_{th} = \dot{C}_{S2}$	-
Condenser	$\dot{C}_{S26} + \dot{Z}_{Cond} + \dot{E}x_{Q,Cond} c_w = \dot{C}_{S29}$	-

PW_{Cu-Cl} represents the present worth of the system and is defined as

$$PW_{Cu-Cl} = TCC_{Cu-Cl} - S_{Cu-Cl} PWF(i,n) \tag{4.34}$$

where the capital cost, salvage value, and the present worth factor of a given system are symbolized as TCC_{Cu-Cl}, S_{Cu-Cl}, and $PVF(i,n)$, respectively. The salvage value and the present worth factor are expressed as:

$$S_{Cu-Cl} = TCC_{Cu-Cl}\, j \tag{4.35}$$

$$PWF(i,n) = \frac{1}{(i+1)^n} \tag{4.36}$$

where the salvage value ratio of a given system is denoted as *j*. The cost rate associated with exergy destruction for given equipment of a system is obtained as:

$$\dot{C}_{D,k} = c_{F,k} \dot{E}x_{D,k} \tag{4.37}$$

where the cost associated with exergy destruction of the *kth* equipment and the unit exergy cost are denoted as $\dot{E}x_{D,k}$ and $c_{F,k}$, respectively.

The exergoeconomic factor (f_k) relates the exergy destruction cost rate and the non-exergetic cost rate (capital and operating and maintenance cost rate) for the *kth* component and is defined as

$$f_k = \frac{\dot{Z}_k}{\dot{Z}_k + \dot{C}_{D,k}} \tag{4.38}$$

A comparative increase or change in the average cost of unit exergy between the fuel and the product of certain *kth* equipment of a given system is expressed as the relative cost difference symbolized as r_k and mathematically represented as:

$$r_k = \frac{c_{P,k} - c_{F,k}}{c_{F,k}} \tag{4.39}$$

4.1.4 Exergoenvironmental analysis

The exergoenvironmental analysis comprises an assessment of the environmental effect of numerous equipment associated with a given system and the sources of that impact via a combination of a comprehensive technique for environmental assessment and exergy analysis. Through the application of the LCA methodology, the environmental influence of every equipment of a given system and their corresponding input streams are evaluated. To quantitatively analyze and represent the environmental impact as a function of exhaustion and the related emissions of a given natural resource, there are numerous approaches being used in the open literature. The impact assessment in the present analysis is carried out in terms of the Eco-indicator 99 points which is used and suggested by numerous authors [77] as a feasible option for LCA purposes. The exergoenvironmental analysis, much like the exergoeconomic analysis, follows a similar approach of allocating the environmental impact to exergy streams [78]. The environmental impact balances and the auxiliary equations for every equipment of the cycle are provided in Table 4.5. The symbolic representation of the environmental impact of an exergy stream as a function of Eco-indicator points/time (Pt/h or mPt/h) is done through $\dot{B}_j$ while the representation of the specific environmental impact of a stream as a function of the Eco-indicator points/exergy (Pt/kJ or mPt/kJ) is done through b_j. The rate of environmental impact related to the *jth* material stream of a given system is described as a product of the unit or specific environmental impact and rate of exergy of the *jth* stream and is defined mathematically as:

$$\dot{B}_j = \dot{E}x_j b_j \tag{4.40}$$

Similarly, the environmental impact rate in terms of work and heat transfers can be mathematically defined respectively as:

$$\dot{B}_w = \dot{W} b_w \tag{4.41}$$

$$\dot{B}_q = \dot{E}x_q b_q \tag{4.42}$$

The environmental impact rate associated with *kth* equipment of a given system is denoted as $\dot{Y}_k$ having units of Pt or mPt/h and is mathematically expressed for certain equipment as:

$$\dot{Y}_k = \frac{Y_k}{n.N} \tag{4.43}$$

Here, the lifetime of a system/equipment, annual operating hours, and environmental impact related to the *kth* equipment is denoted as *N*, *n*, and Y_k, respectively. An LCA study conducted in [47] for a conceptual four-step Cu-Cl cycle considered the similar process equipment as the integrated cycle at CERL. Thus, as per the defined criteria for every equipment, the values of the environmental impact of several components in [47] are normalized for the integrated cycle at CERL based on its requirements.

Table 4.5. Balanced environmental impact and auxiliary equations for different components

Equipment	Balanced environmental impact equation	Auxiliary equation
Hydrolysis	$\dot{B}_{S1} + \dot{B}_{S2} + \dot{Y}_{Hyd} + \dot{E}x_{Q,Hyd} b_{th} = \dot{B}_{S4} + \dot{B}_{S5}$	$\frac{\dot{B}_{S4}}{\dot{E}x_{S4}} = \frac{\dot{B}_{S5}}{\dot{E}x_{S5}}$ [P rule]
Thermolysis	$\dot{B}_{S6} + \dot{Y}_{Therm} + \dot{E}x_{Q,Therm} b_{th} = \dot{B}_{S8} + \dot{B}_{S9}$	$\frac{\dot{B}_{S8}}{\dot{E}x_{S8}} = \frac{\dot{B}_{S9}}{\dot{E}x_{S9}}$ [P rule]
Quench cell	$\dot{B}_{S9} + \dot{B}_{S10} + \dot{Y}_{QC} = \dot{B}_{S37} + \dot{B}_{S11}$	$\frac{\dot{B}_{S9}}{\dot{E}x_{S9}} = \frac{\dot{B}_{S37}}{\dot{E}x_{S37}}$ [P rule] $\frac{\dot{B}_{S10}}{\dot{E}x_{S10}} = \frac{\dot{B}_{S11}}{\dot{E}x_{S11}}$ [F rule]
PSDU	$\dot{B}_{S13} + \dot{Y}_{H3} + \dot{E}x_{Q,H3} b_{th} = \dot{B}_{S15} + \dot{B}_{S16}$	$\frac{\dot{B}_{S15}}{\dot{E}x_{S15}} = \frac{\dot{B}_{S16}}{\dot{E}x_{S16}}$ [P rule]
Electrolyzer	$\dot{B}_{S17} + \dot{Y}_{Elec} + \dot{W}_{elec} b_{elec} = \dot{B}_{S19} + \dot{B}_{S20}$	$\frac{\dot{B}_{S19}}{\dot{E}x_{S19}} = \frac{\dot{B}_{S20}}{\dot{E}x_{S20}}$ [P rule]
ADA	$\dot{B}_{S20} + \dot{Y}_{H4} + \dot{E}x_{Q,H4} b_{th} = \dot{B}_{S22} + \dot{B}_{S23}$	$\frac{\dot{B}_{S22}}{\dot{E}x_{S22}} = \frac{\dot{B}_{S23}}{\dot{E}x_{S23}}$ [P rule]
ADU	$\dot{B}_{S22} + \dot{Y}_{H5} + \dot{E}x_{Q,H5} b_{th} = \dot{B}_{S26} + \dot{B}_{S27}$	$\frac{\dot{B}_{S26}}{\dot{E}x_{S26}} = \frac{\dot{B}_{S27}}{\dot{E}x_{S27}}$ [P rule]
$CuCl_2$-concentrator	$\dot{B}_{S32} + \dot{Y}_{H7} + \dot{E}x_{Q,H7} b_{th} = \dot{B}_{S34} + \dot{B}_{S35}$	$\frac{\dot{B}_{S34}}{\dot{E}x_{S34}} = \frac{\dot{B}_{S35}}{\dot{E}x_{S35}}$ [P rule]
Dryer	$\dot{B}_{S35} + \dot{Y}_{PH} + \dot{E}x_{Q,PH} b_{th} = \dot{B}_{S39} + \dot{B}_{S40}$	$\frac{\dot{B}_{S39}}{\dot{E}x_{S39}} = \frac{\dot{B}_{S40}}{\dot{E}x_{S40}}$ [P rule]
Separation unit	$B_{S29} + \dot{B}_{S30} = \dot{B}_{S31} + \dot{B}_{S32}$	$\frac{\dot{B}_{S31}}{\dot{E}x_{S31}} = \frac{\dot{B}_{S32}}{\dot{E}x_{S32}}$ [P rule]

Steam condenser	$\dot{B}_{S34} + \dot{Y}_{SC} + \dot{E}x_{Q,SC} b_w = \dot{B}_{S41}$	-
HCl-condenser-1	$\dot{B}_{S5} + \dot{Y}_{HCl-cond1} + \dot{E}x_{Q,HCl-cond1} b_w = \dot{B}_{S12}$	-
HCl-condenser-2	$\dot{B}_{S23} + \dot{Y}_{HCl-cond2} + \dot{E}x_{Q,HCl-cond2} b_w = \dot{B}_{S24}$	-
HCl-condenser-3	$\dot{B}_{S27} + \dot{Y}_{HCl-cond3} + \dot{E}x_{Q,HCl-cond3} b_w = \dot{B}_{S28}$	-
Heater-1	$\dot{B}_{water} + \dot{Y}_{H1} + \dot{E}x_{Q,H1} b_{th} = \dot{B}_{S1}$	-
Heater-2	$\dot{B}_{S4} + \dot{Y}_{H2} + \dot{E}x_{Q,H2} b_{th} = \dot{B}_{S6}$	-
Heater-8	$\dot{B}_{CuCl_2} + \dot{Y}_{H8} + \dot{E}x_{Q,H8} b_{th} = \dot{B}_{S2}$	-
Condenser	$\dot{B}_{S26} + \dot{Y}_{Cond} + \dot{E}x_{Q,Cond} b_w = \dot{B}_{S29}$	-

The balanced equation for the environmental impact rate for the *kth* component is defined as:

$$\sum_{j=1}^{n} \dot{B}_{j,k,in} + \dot{Y}_k = \sum_{j=1}^{n} \dot{B}_{j,k,out} \tag{4.44}$$

Here, we define a term accounting for pollutant formation ($\dot{B}^{PF}$) as:

$$\dot{B}^{PF} = \sum_j b_j (\dot{m}_{out} - \dot{m}_{in}) \tag{4.45}$$

This term signifies any deposition or accumulation of pollutants during a certain process or within certain equipment in a given system including SO_x, NO_x, CO_2, CO, and CH_4. As these pollutants are not relevant to the Cu-Cl cycle, thus this term in such a case can be ignored.

Much similar to the exergoeconomic evaluation methodology, the representation of the specific environmental impacts associated with the fuel and the product for the *kth* equipment is done as:

$$b_{F,k} = \frac{\dot{B}_{F,k}}{\dot{E}x_{F,k}} \tag{4.46}$$

$$b_{P,k} = \frac{\dot{B}_{P,k}}{\dot{E}x_{P,k}} \tag{4.47}$$

For the *kth* equipment, the environmental impact rate affiliated with exergy destruction is symbolized as $\dot{B}_{D,k}$ which is a product of the unit environmental impact of fuel and the rate of exergy destruction of the *kth* equipment and is represented mathematically as:

$$\dot{B}_{D,k} = \dot{E}x_{D,k} b_{F,k} \quad (4.48)$$

For the *kth* equipment, the total or cumulative environmental impact rate ($\dot{B}_{T,k}$) is defined as a sum of the component associated and exergy destruction environmental impact rates and is expressed mathematically as:

$$\dot{B}_{T,k} = \dot{B}_{D,k} + \dot{Y}_k \quad (4.49)$$

For the *kth* equipment, the ratio of the equipment related and the total or cumulative environmental impact is termed as the exergoenvironmental factor ($f_{b,k}$) and is expressed mathematically as:

$$f_{b,k} = \frac{\dot{Y}_k}{\dot{B}_{D,k} + \dot{Y}_k} \quad (4.50)$$

The relative difference of the unit environmental impact denoted as $r_{b,k}$ is given as:

$$r_{b,k} = \frac{b_{P,k} - b_{F,k}}{b_{F,k}} \quad (4.51)$$

4.1.5 Multi-objective optimization

To evaluate the best design parameters required for the optimal performance of the integrated cycle at CERL, multi-objective optimization is carried out employing a genetic algorithm (GA). Methodology, design parameters, objective functions, and constraints are described in detail in this section.

4.1.5.1 Evolutionary algorithm: genetic algorithm

To obtain an optimal solution based on the evolutionary principles of biology, a stochastic and iterative search mechanism is employed in the GA [79]. A differentiating characteristic of evolutionary algorithm is that the decision variable values are incorporated in an individual objective function which is a possible solution for an optimization problem [80]. Two or more than two objective functions need to be either maximized or minimized corresponding to one another whenever carrying out multi-objective optimization. The objective functions are most frequently conflicting in nature and increase upon decreasing the other and vice versa. Multi-objective optimization proposes certain optimal design variable numerical values which have the capacity to satisfy certain pre-defined objective

functions [81]. These optimal values are most commonly subjective and are dependent upon the requirements of a given system and their anticipated outcomes.

4.1.5.2 Optimization methodology

Figure 4.4 presents a methodology flowchart of multi-objective optimization constituting numerous steps. Firstly, a parametric study is carried out in Aspen-plus for obtaining the output values. Then, the decision variable and the objective function values are employed in MATLAB as inputs and outputs, respectively. One of the most essential steps of multi-objective optimization is obtaining a relationship between the objective functions and decision variables in terms of a mathematical function. This objective is accomplished by employing the artificial neural network (ANN) of MATLAB by using the neural net fitting application. Figure 4.5 shows an illustration of the ANN employed for the integrated Cu-Cl cycle. The input and output data obtained through the parametric study results of Aspen-plus are applied to the ANN model for training. Numerous methods of training are available in ANN and among those various methods, the *Bayesian Regularization* method is selected for this analysis as suggested in several investigations in the literature since it generates accurate results and has a better performance. Once the mathematical function is acquired, the optimization application in MATLAB is employed by utilizing the *multi-objective optimization using genetic algorithm* solver and the constraint objective function and decision variable values are entered for obtaining the *Pareto Frontier* graphs. Every point represented in a *Pareto Frontier* graph is one of the best-suggested solutions for a given optimization problem. The optimal point can be any point of a *Pareto Frontier* graph since it is subjective and is solely up to the particular criteria of the decision-maker.

4.1.5.3 Objectives

There are three objective functions selected for the multi-objective optimization of the integrated Cu-Cl cycle. These are heat cost rate, exergy efficiency, and hydrogen production rate symbolized as $\dot{C}$, ψ, and $\dot{m}_{H_2}$, respectively. The objectives to be maximized are the hydrogen production rate and exergy efficiency while the heat cost rate is to be minimized. Equation 4.6 is used for evaluating the exergy efficiency while the heat cost rate is defined as the cost rate of the net heat input of the cycle and is obtained as:

$$\dot{C} = \dot{Q}_{net,in} c \tag{4.52}$$

Here, *c* symbolizes the average unit electrical energy cost rate ($/kWh) in Ontario during the winters and the summers.

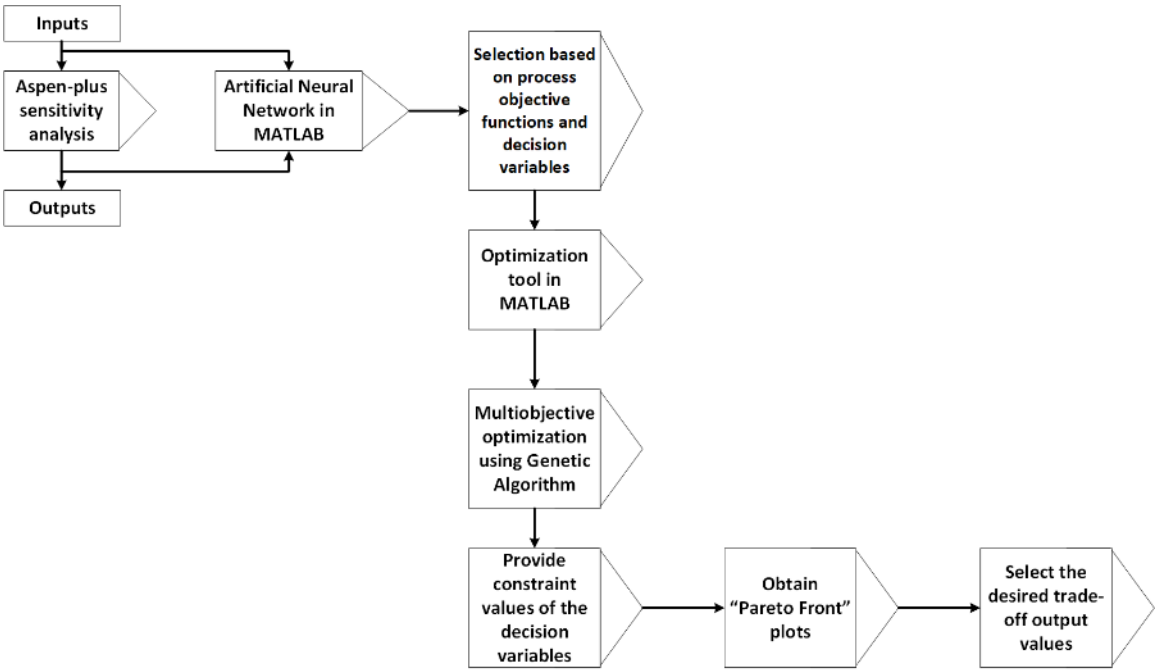

Fig. 4.4. Flowchart representation of the step-by-step methodology of multi-objective optimization

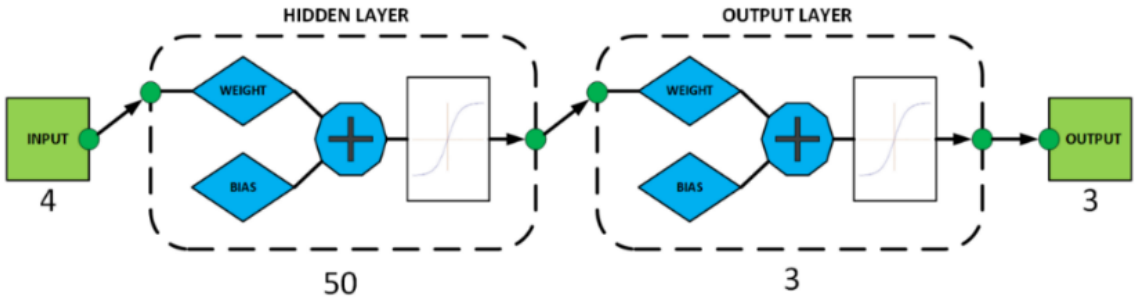

Fig. 4.5. Illustration of the Neural Network applied for generating relationships between the inputs and the outputs for all cases

4.1.5.4 Decision variables

Net heat input rate, input temperature of steam, and S/Cu ratio are the three decision variables used for the optimization problem. Four different cases of optimization are considered in this regard which is shown through Table 4.6. Each case corresponds to a different input value of the steam temperature input and net heat input rate for the same range of the S/Cu ratio. The constraint values are obtained through the simulations carried out in Aspen-plus based on the operating conditions of the cycle. The values for the input

temperature of steam are considered as plausible and attainable temperatures through the recovery of thermal energy in the cycle. The specific range of the S/Cu values is considered for attaining an insight for their possible application in future experiments to be conducted on the integrated cycle at CERL. There is a certain influence of the input temperature of steam on the heat cost rate and the exergy efficiency at a given hydrogen production rate the details of which are discussed in section 5.1.6.

Table 4.6. Decision variables and constraint values for the different optimization cases

Multi-objective optimization		**Decision variables with constraint values**		
		S/Cu	T_{steam} **(°C)**	$\dot{Q}_{net,in}$ **(kW)**
Case	1	10.7-22.9	25	771.33 - 4115.16
	2		100	564.60 - 2629.24
	3		200	549.28 - 2519.15
	4		300	424.14 - 2258.61

4.2 Modeling and analysis of the cycle conceptually modified with flash vaporization

This section presents the detailed modeling and the various resulting analyses conducted on the integrated Cu-Cl cycle conceptually modified with flash vaporization process. The analyses include energy and exergy analyses, thermal management, exergoeconomic, and exergoenvironmental analyses. A similar approach for all analyses has been applied to the modified cycle as the actual integrated cycle at CERL.

4.2.1 Energy and exergy analyses

The energy and exergy analyses of the modified integrated cycle are carried out by the application of balanced energy and exergy equations for each cycle component. A temperature of 25°C and a pressure of 1 bar are considered as the reference conditions. For the purposes of analysis facilitation, a few assumptions are made, as follows:

- The potential and kinetic energies are insignificant and are thus neglected.
- Pressure losses are insignificant.
- Steady-state conditions are assumed to exist.

Table 4.7. Exergy and energy balance equations for the cycle modified with flash vaporization

Component	Energy balance equation	Exergy balance equation
Hydrolysis reactor	$\dot{m}_1 h_1 + \dot{m}_3 h_3 + \dot{Q}_{in,H1} + \dot{Q}_{in,H2} + \dot{Q}_{in,Hyd} = \dot{m}_5 h_5$	$\dot{m}_1 ex_1 + \dot{m}_3 ex_3 + \dot{E}x_{\dot{Q}_{in,H1}} + \dot{E}x_{\dot{Q}_{in,H2}} + \dot{E}x_{\dot{Q}_{in,Hyd}} = \dot{m}_5 ex_5 + \dot{E}x_d$
Thermolysis reactor	$\dot{m}_6 h_6 + \dot{Q}_{in,H3} + \dot{Q}_{in,Therm} = \dot{m}_9 h_9$	$\dot{m}_6 ex_6 + \dot{E}x_{\dot{Q}_{in,H3}} + \dot{E}x_{\dot{Q}_{in,Therm}} = \dot{m}_9 ex_9 + \dot{E}x_d$
Quenching cell	$\dot{m}_{11} h_{11} + \dot{m}_{w-in} h_{w-in} = \dot{m}_{12} h_{12} + \dot{m}_{w-out} h_{w-out}$	$\dot{m}_{11} ex_{11} + \dot{m}_{w-in} ex_{w-in} = \dot{m}_{12} ex_{12} + \dot{m}_{w-out} ex_{w-out} + \dot{E}x_d$
Electrolyzer	$\dot{m}_{19} h_{19} + \dot{W}_{elec} = \dot{m}_{20} h_{20}$	$\dot{m}_{19} ex_{19} + \dot{W}_{elec} = \dot{m}_{20} ex_{20} + \dot{E}x_d$
Liquid-gas separator	$\dot{m}_{20} h_{20} = \dot{m}_{21} h_{21} + \dot{m}_{22} h_{22}$	$\dot{m}_{20} ex_{20} = \dot{m}_{21} ex_{21} + \dot{m}_{22} ex_{22} + \dot{E}x_d$
Pump	$\dot{m}_{22} h_{22} + \dot{W}_p = \dot{m}_{23} h_{23}$	$\dot{m}_{22} ex_{22} + \dot{W}_p = \dot{m}_{23} ex_{23} + \dot{E}x_d$
Heat Exchanger	$\dot{m}_{23} h_{23} + \dot{m}_{17} h_{17} = \dot{m}_{24} h_{24} + \dot{m}_{17-1} h_{17-1}$	$\dot{m}_{23} ex_{23} + \dot{m}_{17} ex_{17} = \dot{m}_{24} ex_{24} + \dot{m}_{17-1} ex_{17-1} + \dot{E}x_d$
Expansion valve	$\dot{m}_{24} h_{24} = \dot{m}_{25} h_{25}$	$\dot{m}_{24} ex_{24} = \dot{m}_{25} ex_{25} + \dot{E}x_d$
$CuCl_2$ concentrator	$\dot{m}_{30} h_{30} + \dot{Q}_{in,H5} = \dot{m}_{32} h_{32} + \dot{m}_{33} h_{33}$	$\dot{m}_{30} ex_{30} + \dot{E}x_{\dot{Q}_{in,H5}} = \dot{m}_{32} ex_{32} + \dot{m}_{33} ex_{33} + \dot{E}x_d$
Pressure swing distillation unit	$\dot{m}_{15} h_{15} + \dot{Q}_{in,H4} = \dot{m}_{17} h_{17} + \dot{m}_{18} h_{18}$	$\dot{m}_{15} ex_{15} + \dot{E}x_{\dot{Q}_{in,H4}} = \dot{m}_{17} ex_{17} + \dot{m}_{18} ex_{18} + \dot{E}x_d$
HCl-condenser	$\dot{m}_7 h_7 = \dot{m}_{14} h_{14} + \dot{Q}_{e,HClcond}$	$\dot{m}_7 ex_7 = \dot{m}_{14} ex_{14} + \dot{E}x_{\dot{Q}_{e,HClcond}} + \dot{E}x_d$
Flash chamber	$\dot{m}_{25} h_{25} = \dot{m}_{26} h_{26} + \dot{m}_{27} h_{27}$	$\dot{m}_{25} ex_{25} = \dot{m}_{26} ex_{26} + \dot{m}_{27} ex_{27} + \dot{E}x_d$
Dryer	$\dot{m}_{33} h_{33} + \dot{Q}_{in,H6} = \dot{m}_{35} h_{35} + \dot{m}_{36} h_{36}$	$\dot{m}_{33} ex_{33} + \dot{E}x_{\dot{Q}_{in,H6}} = \dot{m}_{35} ex_{35} + \dot{m}_{36} ex_{36} + \dot{E}x_d$

The energy and exergy efficiencies of the cycle have been evaluated as:

$$\eta = \frac{\dot{m}_{H_2} LHV_{H_2}}{\dot{Q}_{net} + \dot{W}_{net}} \tag{4.53}$$

$$\dot{Q}_{net} = \dot{Q}_{in,H1} + \dot{Q}_{in,H2} + \dot{Q}_{in,H3} + \dot{Q}_{in,H4} + \dot{Q}_{in,H5} + \dot{Q}_{in,H6} + \dot{Q}_{in,Hyd} + \dot{Q}_{in,Therm} \quad (4.54)$$

$$\psi = \frac{\dot{m}_{H_2} ex_{H_2}}{\dot{Ex}_{\dot{Q}_{net}} + \dot{W}_{net}} \quad (4.55)$$

$$\dot{Ex}_{\dot{Q}_{net}} = \dot{Q}_{net}\left(1 - \frac{T_0}{T_c}\right) \quad (4.56)$$

The balanced equations for energy and exergy for each component of the modified integrated cycle are provided in Table 4.7.

4.2.2 Thermal management

The thermal management of the integrated cycle modified with the incorporation of flash vaporization process and hydrocyclone separator has been performed in this study by considering different heat recovery schemes as shown in Table 4.8. The configurations are based on internal heat recovery within the cycle, waste heat recovery from the flue gases of a steel furnace as well as combinations of these two. A flow rate of 9.21 kg/s of flue gases from a steel furnace at a temperature of 810 ºC [82] is considered for waste heat recovery purposes for which a hydrogen production rate of 32.4 kg/h is obtained. The heat recovery is realized for the three most energy-intensive processes/components within the cycle which are hydrolysis, the PSDU, and the $CuCl_2$-concentrator.

Table 4.8. Description of various heat recovery configurations considered

Separation approach	Configuration	Description
Flash vaporization	C-1a	Internal heat recovery within the cycle
	C-1b	Waste heat recovery from steel furnace
	C-1c	Internal and waste heat recovery scheme 1
	C-1d	Internal and waste heat recovery scheme 2
Hydrocyclone separator	C-2a	Internal heat recovery within the cycle
	C-2b	Waste heat recovery from steel furnace
	C-2c	Internal and waste heat recovery

For the cycle with flash vaporization, in configuration C-1a (Figure 4.6a), only the available thermal energy within the cycle is utilized. The heat exchangers 1, 2, and 4 are incorporated in the cycle for this purpose. The excess heat of the steam-HCl mixture exiting the separator-1 at 400ºC is utilized for providing thermal energy to the water stream discharging the quenching cell which consequently transfers this heat in the pressure swing distillation process for azeotropic separation of HCl from the water via heat exchanger-2.

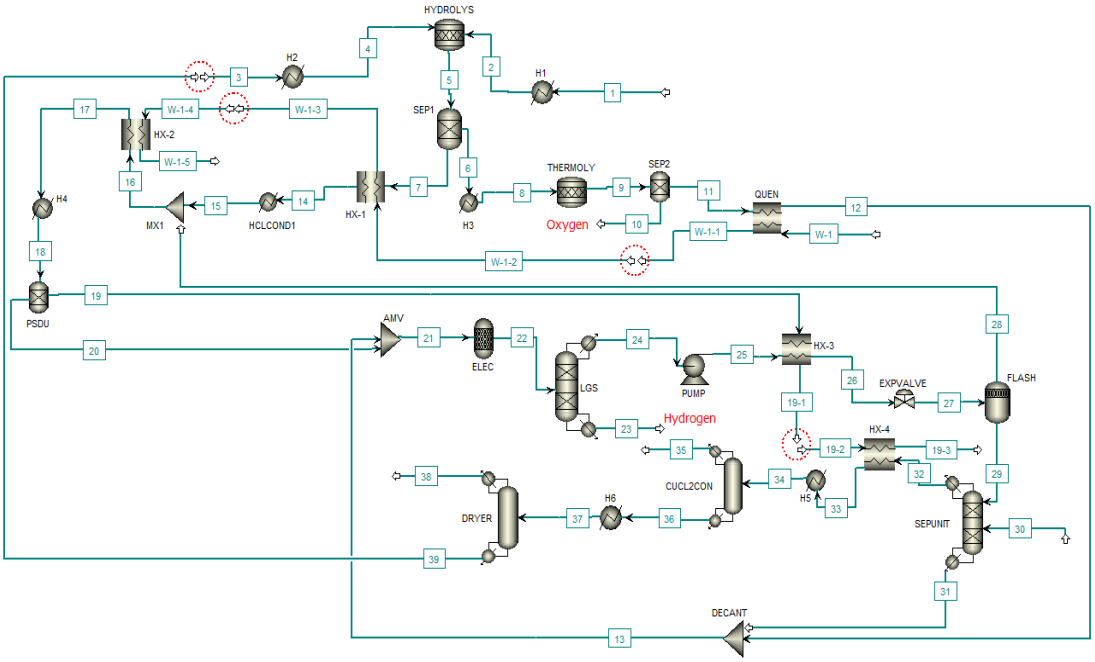
HYDROLYS
H2
H1
SEP1
HX-2
W-1-4
W-1-3
W-1-5
THERMOLY
SEP2
QUEN
H4
MX1
HCLCOND1
HX-1
H3
Oxygen
W-1-1
W-1-2
W-1
PSDU
AMV
ELEC
LGS
PUMP
HX-3
EXPVALVE
FLASH
Hydrogen
HX-4
CUCL2CON
H5
DRYER
H6
SEPUNIT
DECANT

(a)

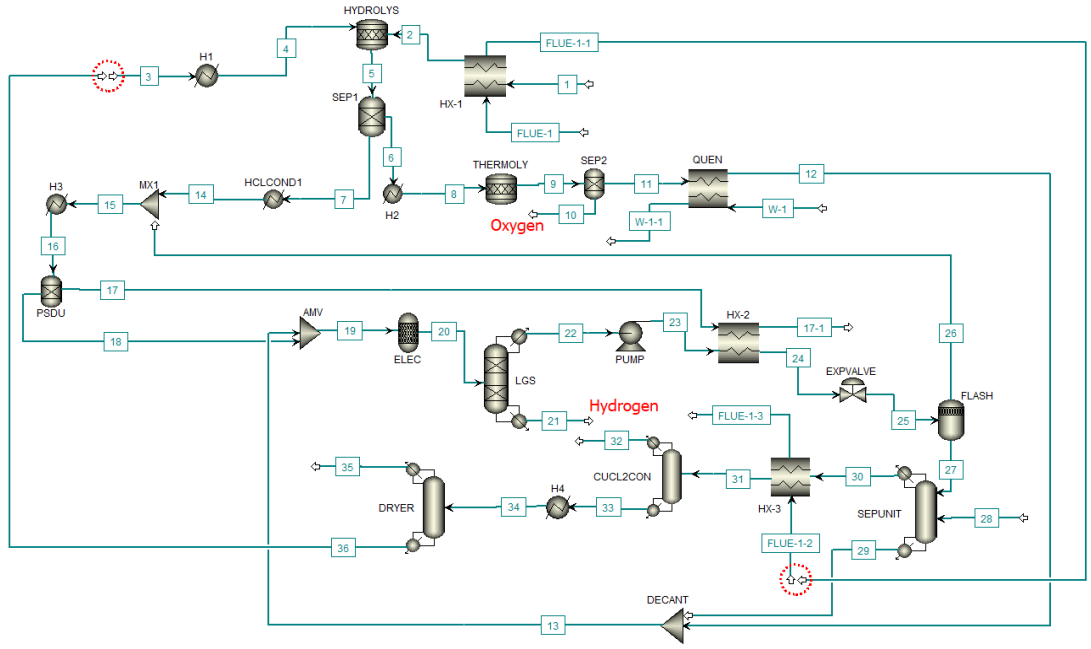
HYDROLYS
H1
FLUE-1-1
HX-1
FLUE-1
SEP1
THERMOLY
SEP2
QUEN
H3
MX1
HCLCOND1
H2
Oxygen
W-1-1
W-1
PSDU
AMV
ELEC
LGS
PUMP
HX-2
EXPVALVE
FLASH
Hydrogen
FLUE-1-3
CUCL2CON
H4
DRYER
HX-3
SEPUNIT
FLUE-1-2
DECANT

(b)

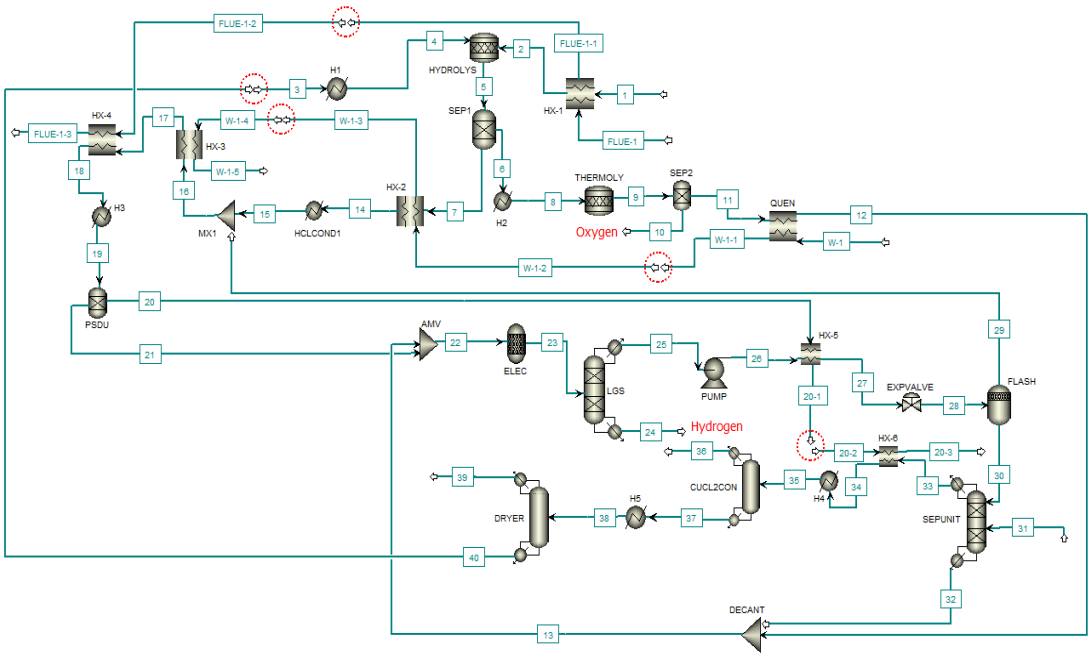

(c)

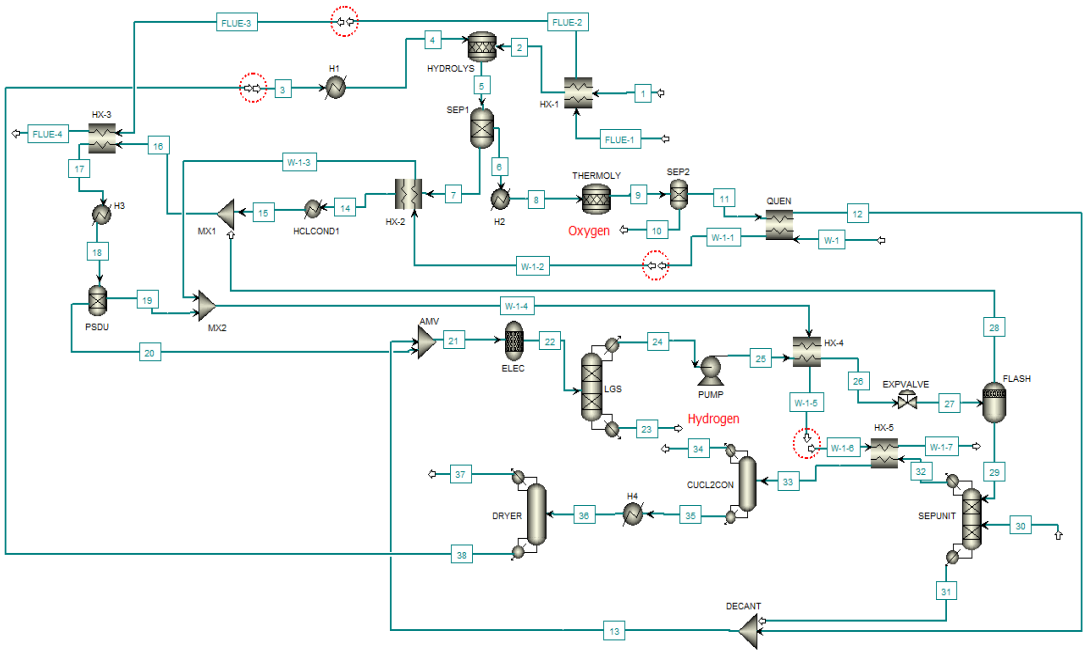

(d)

Fig. 4.6. Process flowsheets of the various heat recovery schemes simulated in Aspen-plus

Further, the steam exiting the heat exchanger-3 (for flash vaporization process) then exchanges its heat with a stream of aqueous $CuCl_2$ mixture for subsequent separation of

water from $CuCl_2$ via heat exchanger-4. In configuration C-1b (Figure 4.6b), the waste heat from a steel furnace is utilized for providing thermal energy within the cycle. The flue gases exchange heat with water at ambient temperature to provide superheated steam at 400ºC for the hydrolysis reaction via heat exchanger-1. The flue gases exiting the heat exchanger-1 then exchange heat with a stream of aqueous $CuCl_2$ mixture similar to configuration C-1a for subsequent separation of water from $CuCl_2$ via heat exchanger-3. However, since the flue gases have sufficient thermal energy after discharging heat exchanger-1, therefore they provide the entire thermal energy for the aqueous $CuCl_2$ mixture to attain the desired temperature thereby eliminating the need for heater-5. In configurations C-1c and C-1d, both internally recovered heat and waste heat from steel a furnace is supplied to the various components/process simultaneously. In configuration C-1c (Figure 4.6c), similar to configuration C-1b, flue gases firstly exchange heat with water for providing steam for the hydrolysis reaction via heat exchanger-1. The steam exiting the quenching cell makes its way to the heat exchanger-2 to gain heat from the steam-HCl mixture exiting the separator-1 which then provides thermal energy to the aqueous HCl mixture (stream 16) via heat exchanger-3. This aqueous HCl mixture further gains thermal energy from the flue gases discharging heat exchanger-1 via heat exchanger-4. The steam exiting heat exchanger-5 (for flash vaporization process), similar to configuration C-1a exchanges heat with a stream of aqueous $CuCl_2$ mixture for subsequent separation of water from $CuCl_2$ via heat exchanger-6. Lastly, in configuration C-1d (Figure 4.6d), the heat exchangers 1, 2, and 3 (heat exchanger-4 in C-1c) work similarly to configuration C-1c. However, the steam exiting the heat exchanger-2 mixes with the steam exiting the PSDU after being azeotropically separated from HCl. This steam, discharging from heat exchanger-4 after providing thermal energy for the flash vaporization process, then exchanges heat with a stream of aqueous $CuCl_2$ mixture for subsequent separation of water from $CuCl_2$ via heat exchanger-5 eliminating the requirement of a heater in this case, unlike configuration C-1c.

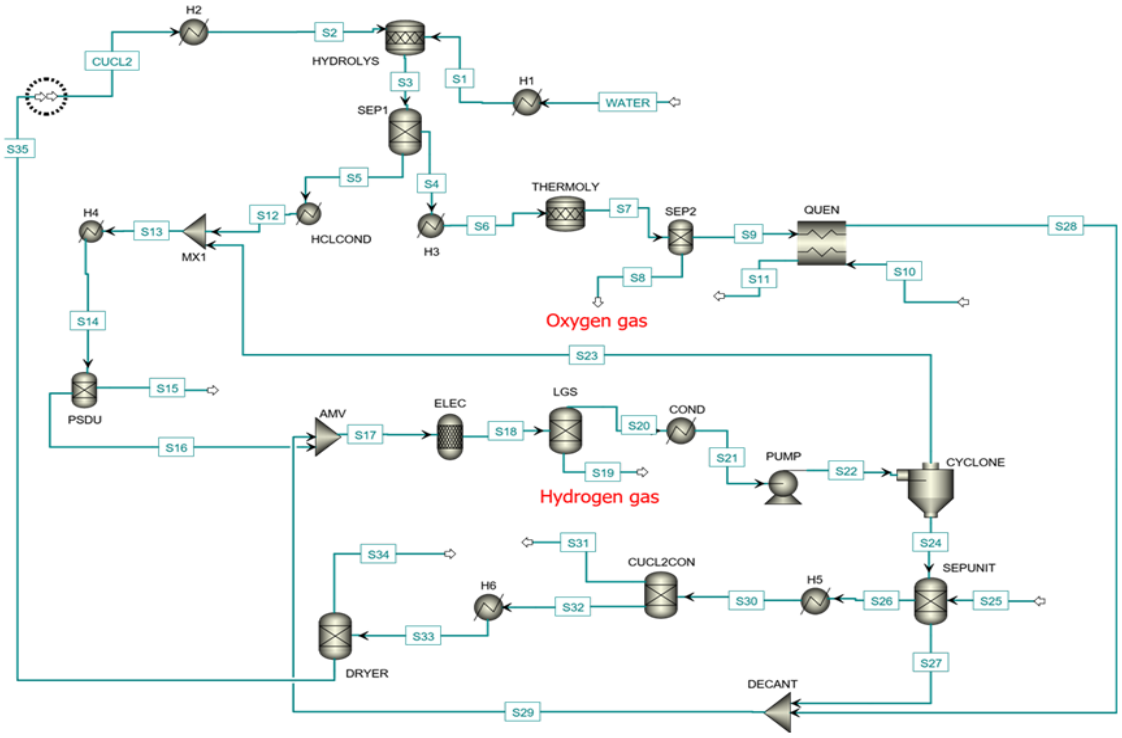
H2
S2
HYDROLYS
CUCL2
S3
S1
H1
WATER
SEP1
S35
S5
S4
THERMOLY
H4
S13
S12
MX1
HCLCOND
H3
S6
S7
SEP2
QUEN
S28
S9
S8
S11
S10
Oxygen gas
S14
S23
S15
PSDU
AMV
ELEC
LGS
COND
S16
S17
S18
S20
S21
PUMP
S22
CYCLONE
S19
Hydrogen gas
S24
S31
S34
CUCL2CON
SEPUNIT
H6
H5
S32
S30
S26
S25
S33
DRYER
S27
DECANT
S29

(a)

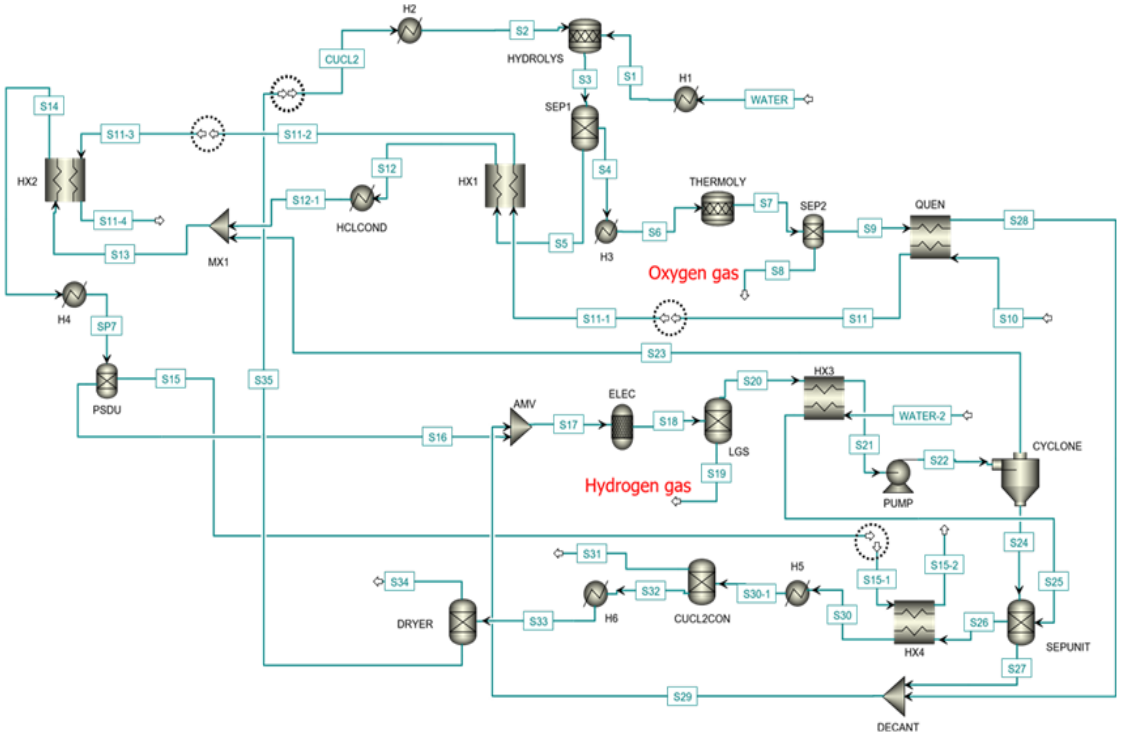
H2
S2
HYDROLYS
CUCL2
S3
S1
H1
WATER
SEP1
S14
S11-3
S11-2
S12
HX2
HX1
S4
THERMOLY
S11-4
S12-1
HCLCOND
S7
SEP2
QUEN
S28
S6
S5
H3
S9
S13
MX1
Oxygen gas
S8
H4
SP7
S11-1
S11
S10
S23
HX3
S20
S15
S35
PSDU
AMV
ELEC
WATER-2
S17
S18
S21
CYCLONE
S16
LGS
S22
S19
Hydrogen gas
PUMP
S31
S24
S15-2
S34
S15-1
S25
H5
S32
S30-1
DRYER
S33
H6
CUCL2CON
S30
S26
HX4
SEPUNIT
S27
S29
DECANT

(b)

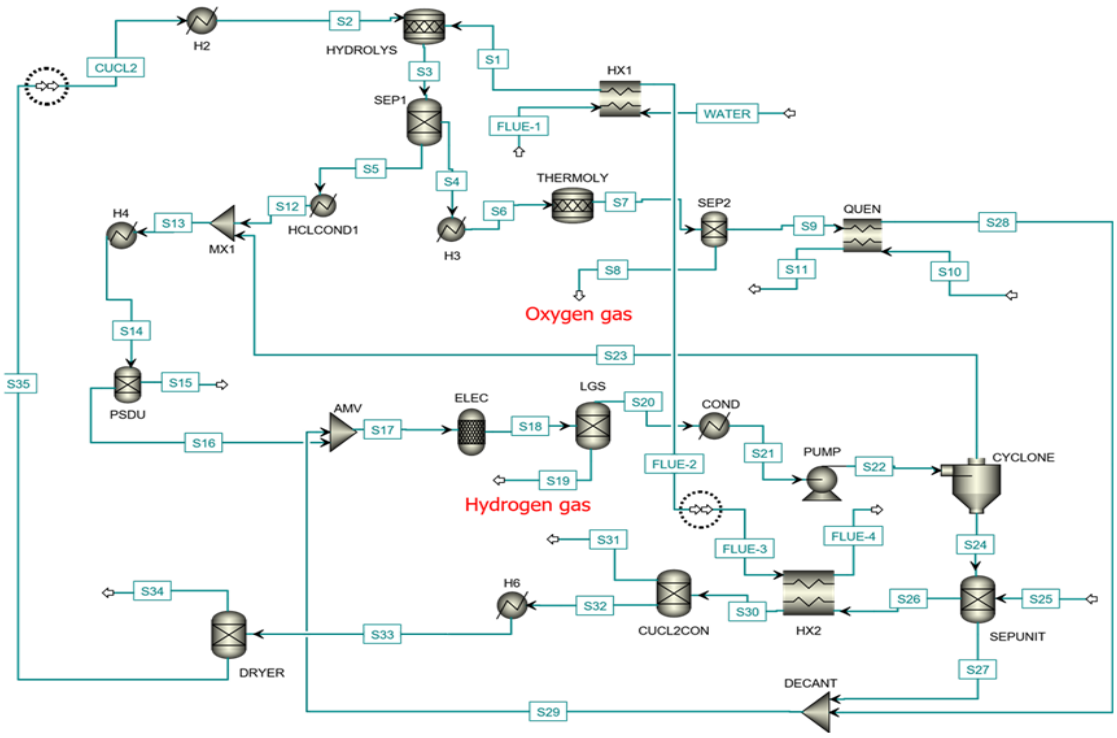

(c)

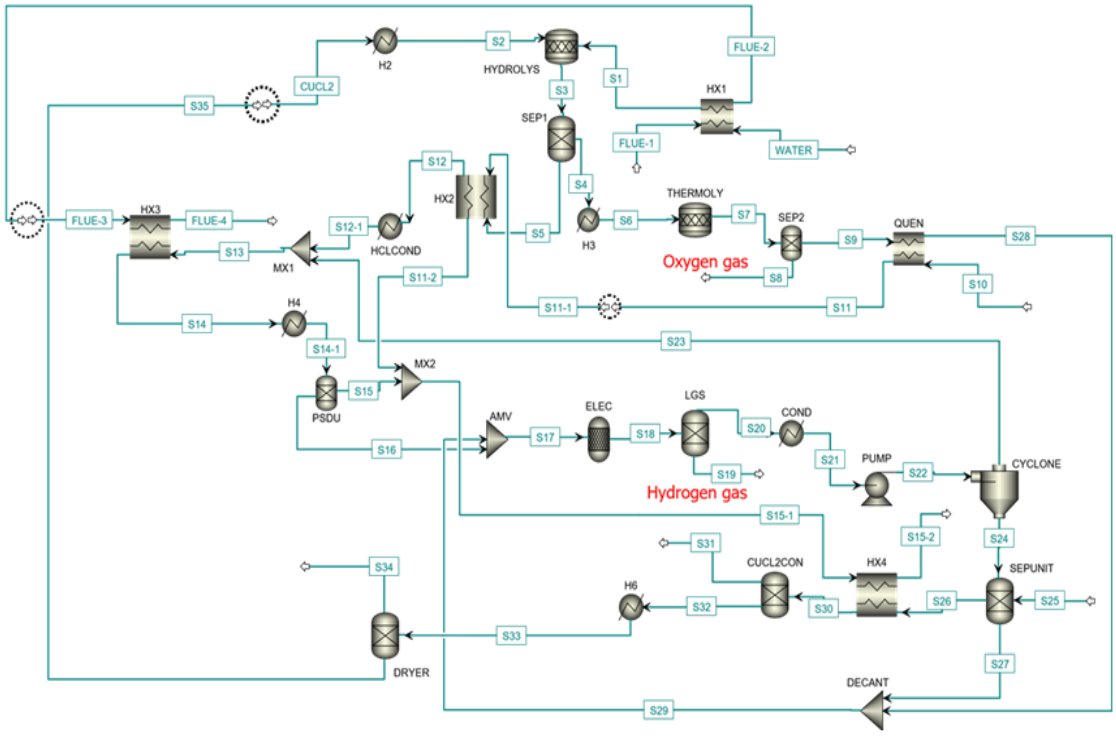

(d)

Fig. 4.7. Process flowsheets of the hydrocyclone separator-based reference cycle and different heat recovery schemes simulated in Aspen-plus

In the cycle with hydrocyclone separator, the anolyte exiting the LGS is first condensed and is then pumped to the hydrocyclone which separates the HCl entirely and water partially from the rest of the constituents of the anolyte (Figure 4.7a). For configuration C-2a (Figure 4.7b), internal heat recovery within the cycle is performed similarly to configuration C-1a through heat exchangers 1 and 2. In configuration C-2b (Figure 4.7c), waste heat recovery from the steel furnace is realized by first providing the thermal energy for the hydrolysis process through the heat exchanger-1 and then supplying the left-over heat in flue gases for the $CuCl_2$-concentrator through the heat exchanger-2. The configuration C-2c (Figure 4.7d) essentially combines the internal and waste heat recovery similar to configuration C-1d.

4.2.3 Exergoeconomic analysis

The exergoeconomic evaluation of the modified integrated cycle is conducted using Aspen-plus. The SPECO approach is used for the exergoeconomic evaluation of the cycle which is based on the same three fundamental steps specified previously in section 4.1.3.2. The exergy of fuel and product for each component of the modified integrated cycle is defined in Table 4.9. The exergetic cost balance for each component of the integrated cycle is performed as defined in equation 4.25.

Table 4.9. Definition of exergy of fuel and product for each component of the modified integrated cycle

Component	Fuel	Product
Hydrolysis	$\dot{E}x_{Q,Hyd}$	$(\dot{E}x_6 + \dot{E}x_7) - (\dot{E}x_2 + \dot{E}x_4)$
Thermolysis	$\dot{E}x_{Q,Therm}$	$(\dot{E}x_{10} + \dot{E}x_{11}) - (\dot{E}x_8)$
HCl-cond-1	$\dot{E}x_{Q,HCl-cond1}$	$\dot{E}x_7 - \dot{E}x_{14}$
PSDU	$\dot{E}x_{Q,H4}$	$(\dot{E}x_{17} + \dot{E}x_{18}) - (\dot{E}x_{15})$
Quench Cell	$\dot{E}x_{w-out} - \dot{E}x_{w-in}$	$\dot{E}x_{11} - \dot{E}x_{12}$
Electrolyzer	$\dot{W}_{elec}$	$(\dot{E}x_{21} + \dot{E}x_{22}) - (\dot{E}x_{19})$
Pump	$\dot{W}_{pump}$	$\dot{E}x_{23} - \dot{E}x_{22}$
Heat exchanger 2	$\dot{E}x_{17} - \dot{E}x_{17-1}$	$\dot{E}x_{24} - \dot{E}x_{23}$
Expansion valve	$\dot{E}x_{24}$	$\dot{E}x_{25}$
Flash chamber	$\dot{E}x_{25}$	$\dot{E}x_{26} + \dot{E}x_{27}$
$CuCl_2$-concentrator	$\dot{E}x_{Q,H5}$	$(\dot{E}x_{32} + \dot{E}x_{33}) - (\dot{E}x_{31})$
Dryer	$\dot{E}x_{Q,H6}$	$(\dot{E}x_{35} + \dot{E}x_{36}) - (\dot{E}x_{33})$
Heater-1 (for standard cycle operation)	$\dot{E}x_{Q,H1}$	$\dot{E}x_2 - \dot{E}x_1$

Heat exchanger 1 (with waste heat recovery)	$\dot{E}x_{Flue-in} - \dot{E}x_{Flue-out}$	$\dot{E}x_2 - \dot{E}x_1$
Heater-2	$\dot{E}x_{Q,H2}$	$\dot{E}x_4 - \dot{E}x_3$
Heater-3	$\dot{E}x_{Q,H3}$	$\dot{E}x_8 - \dot{E}x_6$

The exergoeconomic analysis of the modified integrated cycle is also performed by considering the cycle operation with waste heat recovery (steel furnace) with a hydrogen production capacity of 1.3 T/h (1295 kg/h). The flue gases exiting a steel furnace are assumed to have a mass flow rate of 310 kg/s to provide sufficient thermal energy for the steam to be provided at the required temperature for the hydrolysis step at the desired capacity. Three scenarios are considered in this regard i.e., baseline/average-case scenario, best-case scenario, and worst-case scenario. The unit thermal and electrical energy cost rates for the best, the average, and the worst-case scenarios are considered as 0.08 $/kWh, 0.10 $/kWh, and 0.12 $/kWh, respectively. The methodology for evaluating the hourly levelized cost rate of each cycle component is the same as provided in section 4.1.3.2. Based on the definition of the exergy of fuel and product of each cycle component in Table 4.9, the exergetic balanced cost equations are formulated and shown in Table 4.10.

Table 4.10. Balanced exergetic cost and auxiliary equations for all cycle components

Component	Exergetic cost rate balance equation	Auxiliary equation
Hydrolysis	$\dot{C}_2 + \dot{C}_4 + \dot{Z}_{Hyd,Sep1} + \dot{E}x_{Q,Hyd}c_{th} = \dot{C}_6 + \dot{C}_7$	$\frac{\dot{C}_6}{\dot{E}x_6} = \frac{\dot{C}_7}{\dot{E}x_7}$
Thermolysis	$\dot{C}_8 + \dot{Z}_{Therm,Sep2} + \dot{E}x_{Q,Therm}c_{th} = \dot{C}_{10} + \dot{C}_{11}$	$\frac{\dot{C}_{10}}{\dot{E}x_{10}} = \frac{\dot{C}_{11}}{\dot{E}x_{11}}$
Quench cell	$\dot{C}_{11} + \dot{C}_{w-in} + \dot{Z}_{QC} = \dot{C}_{12} + \dot{C}_{w-out}$	$\frac{\dot{C}_{11}}{\dot{E}x_{11}} = \frac{\dot{C}_{12}}{\dot{E}x_{12}}$ $\frac{\dot{C}_{w-in}}{\dot{E}x_{w-in}} = \frac{\dot{C}_{w-out}}{\dot{E}x_{w-out}}$
PSDU	$\dot{C}_{15} + \dot{Z}_{PSDU,H4} + \dot{E}x_{Q,H4}c_{th} = \dot{C}_{17} + \dot{C}_{18}$	$\frac{\dot{C}_{17}}{\dot{E}x_{17}} = \frac{\dot{C}_{18}}{\dot{E}x_{18}}$
Electrolyzer	$\dot{C}_{19} + \dot{Z}_{Elec,LGS} + \dot{W}_{elec}c_{elec} = \dot{C}_{21} + \dot{C}_{22}$	$\frac{\dot{C}_{21}}{\dot{E}x_{21}} = \frac{\dot{C}_{22}}{\dot{E}x_{22}}$
Pump	$\dot{C}_{22} + \dot{Z}_{Pump} + \dot{W}_{Pump}c_{elec} = \dot{C}_{23}$	-

Heat Exchanger 2	$\dot{C}_{17} + \dot{C}_{23} + \dot{Z}_{HX-2} = \dot{C}_{24} + \dot{C}_{17-1}$	$\frac{\dot{C}_{17}}{\dot{E}x_{17}} = \frac{\dot{C}_{17-1}}{\dot{E}x_{17-1}}$
Expansion valve	$\dot{C}_{24} + \dot{Z}_{exp-valve} = \dot{C}_{25}$	-
Flash chamber	$\dot{C}_{25} + \dot{Z}_{Flash} = \dot{C}_{26} + \dot{C}_{27}$	$\frac{\dot{C}_{26}}{\dot{E}x_{26}} = \frac{\dot{C}_{27}}{\dot{E}x_{27}}$
Separation unit	$\dot{C}_{27} + \dot{C}_{28} + \dot{Z}_{Sep-unit} = \dot{C}_{29} + \dot{C}_{30}$	$\frac{\dot{C}_{29}}{\dot{E}x_{29}} = \frac{\dot{C}_{30}}{\dot{E}x_{30}}$
$CuCl_2$-concentrator	$\dot{C}_{30} + \dot{Z}_{CuCl_2-con,H5} + \dot{E}x_{Q,H5}c_{th} = \dot{C}_{32} + \dot{C}_{33}$	$\frac{\dot{C}_{32}}{\dot{E}x_{32}} = \frac{\dot{C}_{33}}{\dot{E}x_{33}}$
Dryer	$\dot{C}_{33} + \dot{Z}_{Dryer,H6} + \dot{E}x_{Q,H6}c_{th} = \dot{C}_{35} + \dot{C}_{36}$	$\frac{\dot{C}_{35}}{\dot{E}x_{35}} = \frac{\dot{C}_{36}}{\dot{E}x_{36}}$
HCl-condenser	$\dot{C}_{14} + \dot{Z}_{HCl-cond} + \dot{E}x_{Q,HCl-cond}c_w = \dot{C}_7$	-
Heater-1	$\dot{C}_1 + \dot{Z}_{H1} + \dot{E}x_{Q,H1}c_{th} = \dot{C}_2$	-
Heater-2	$\dot{C}_3 + \dot{Z}_{H2} + \dot{E}x_{Q,H2}c_{th} = \dot{C}_4$	-
Heater-3	$\dot{C}_6 + \dot{Z}_{H3} + \dot{E}x_{Q,H3}c_{th} = \dot{C}_8$	-
Heat Exchanger 1	$\dot{C}_1 + \dot{C}_{Flue-in} + \dot{Z}_{HX-1} = \dot{C}_2 + \dot{C}_{Flue-out}$	$\frac{\dot{C}_{Flue-in}}{\dot{E}x_{Flue-in}} = \frac{\dot{C}_{Flue-out}}{\dot{E}x_{Flue-out}}$

4.2.4 Exergoenvironmental analysis

The exergoenvironmental analysis, similar to the exergoeconomic analysis, considers the development of balanced environmental impact and auxiliary equations based on the F and P-rules for obtaining the environmental impact rate at each state point as explained in section 4.1.4. The environmental impact rates of the components of the modified integrated cycle are obtained by normalizing the environmental impact rates for the same components obtained in [47] for a four-step Cu-Cl cycle according to the requirement of the modified cycle at CERL. The environmental impact rate and auxiliary equations for the modified cycle are provided in Table 4.11.

Table 4.11 Balanced environmental impact and auxiliary equations for cycle components

Component	Environmental impact balance equation	Auxiliary equation
Hydrolysis	$\dot{B}_2 + B_4 + \dot{Y}_{Hyd} + \dot{E}x_{Q,Hyd} b_{th} = \dot{B}_6 + \dot{B}_7$	$\frac{\dot{B}_6}{\dot{E}x_6} = \frac{\dot{B}_7}{\dot{E}x_7}$
Thermolysis	$\dot{B}_8 + Y_{Therm} + \dot{E}x_{Q,Therm} b_{th} = \dot{B}_{10} + \dot{B}_{11}$	$\frac{\dot{B}_{10}}{\dot{E}x_{10}} = \frac{\dot{B}_{11}}{\dot{E}x_{11}}$
Quench cell	$\dot{B}_{11} + \dot{B}_{w-in} + \dot{Y}_{QC} = \dot{B}_{12} + \dot{B}_{w-out}$	$\frac{\dot{B}_{11}}{\dot{E}x_{11}} = \frac{\dot{B}_{12}}{\dot{E}x_{12}}$ $\frac{\dot{B}_{w-in}}{\dot{E}x_{w-in}} = \frac{\dot{B}_{w-out}}{\dot{E}x_{w-out}}$
PSDU	$\dot{B}_{15} + \dot{Y}_{H4} + \dot{E}x_{Q,H4} b_{th} = \dot{B}_{17} + \dot{B}_{18}$	$\frac{\dot{B}_{17}}{\dot{E}x_{17}} = \frac{\dot{B}_{18}}{\dot{E}x_{18}}$
Electrolyzer	$\dot{B}_{19} + \dot{Y}_{Elec} + \dot{W}_{elec} b_{elec} = \dot{B}_{21} + \dot{B}_{22}$	$\frac{\dot{B}_{21}}{\dot{E}x_{21}} = \frac{\dot{B}_{22}}{\dot{E}x_{22}}$
Pump	$\dot{B}_{22} + \dot{Y}_{Pump} + \dot{W}_{Pump} b_{elec} = \dot{B}_{23}$	-
Heat Exchanger 2	$\dot{B}_{17} + \dot{B}_{23} + \dot{Y}_{HX-2} = \dot{B}_{24} + \dot{B}_{17-1}$	$\frac{\dot{B}_{17}}{\dot{E}x_{17}} = \frac{\dot{B}_{17-1}}{\dot{E}x_{17-1}}$
Expansion valve	$\dot{B}_{24} + \dot{Y}_{exp-valve} = \dot{B}_{25}$	-
$CuCl_2$-concentrator	$\dot{B}_{30} + \dot{Y}_{H5} + \dot{E}x_{Q,H5} b_{th} = \dot{B}_{32} + \dot{B}_{33}$	$\frac{\dot{B}_{32}}{\dot{E}x_{32}} = \frac{\dot{B}_{33}}{\dot{E}x_{33}}$
Dryer	$\dot{B}_{33} + \dot{Y}_{H6} + \dot{E}x_{Q,H6} b_{th} = \dot{B}_{35} + \dot{B}_{36}$	$\frac{\dot{B}_{35}}{\dot{E}x_{35}} = \frac{\dot{B}_{36}}{\dot{E}x_{36}}$
HCl-condenser	$\dot{B}_{14} + \dot{Y}_{HCl-cond} + \dot{E}x_{Q,HCl-cond} b_w = \dot{B}_7$	-
Heater-1	$\dot{B}_1 + \dot{Y}_{H1} + \dot{E}x_{Q,H1} b_{th} = \dot{B}_2$	-
Heater-2	$\dot{B}_3 + \dot{Y}_{H2} + \dot{E}x_{Q,H2} b_{th} = \dot{B}_4$	-
Heater-3	$\dot{B}_6 + \dot{Y}_{H3} + \dot{E}x_{Q,H3} b_{th} = \dot{B}_8$	-

4.3 Formulation of an empirical model for flash vaporization process

A basic analytical correlation for predicting the mass flow rate of the separated mixture of HCl and H_2O after each experimental run of the flash vaporization process is developed in this thesis. The model is developed based on the mass conversation principle for the flash

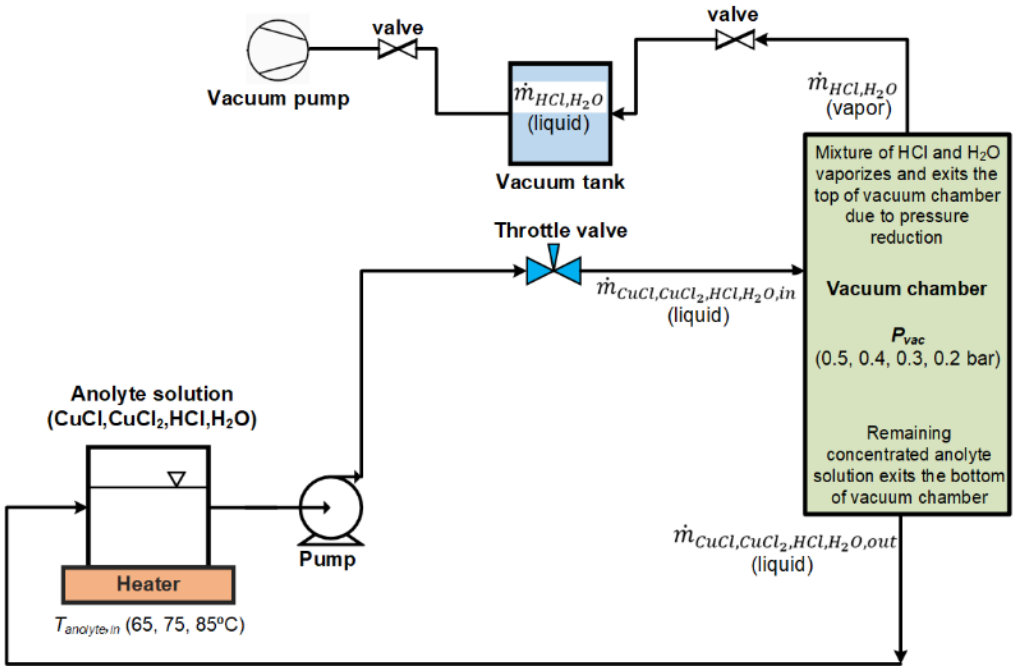

Fig. 4.8. Detailed illustration of the flash vaporization process

vaporization process along with certain experimental variables which influence the separation process. A schematic representation showing the details of flash vaporization process is illustrated in Figure 4.8.

A general representation of the mass balance equation for the flash vaporization process is given as:

$$\dot{m}_{anolyte,in} = \dot{m}_{output1} + \dot{m}_{output2} \tag{4.57}$$

Equation 4.57 in more specific terms can be written as:

$$\dot{m}_{anolyte,in} = \dot{m}_{concentrated\ anolyte,out} + \dot{m}_{separated\ vapor,out} \tag{4.58}$$

or

$$\dot{m}_{CuCl,CuCl_2,HCl,H_2O,in} = \dot{m}_{CuCl,CuCl_2,HCl,H_2O,out} + \dot{m}_{HCl,H_2O} \tag{4.59}$$

Here, $\dot{m}_{CuCl,CuCl_2,HCl,H_2O,in}$ represents the mass flow rate of the anolyte being fed into the flash chamber, $\dot{m}_{HCl,H_2O}$ represents the mass flow rate of the anolyte being vaporized as a separated mixture of HCl and H_2O and $\dot{m}_{CuCl,CuCl_2,HCl,H_2O,out}$ represents the mass flow rate of the concentrated anolyte being recycled through the discharge port of the flash chamber. Equation 4.59 can be rewritten in terms of volume flow rate as:

$$\rho_{CuCl,CuCl_2,HCl,H_2O,in}\dot{V}_{CuCl,CuCl_2,HCl,H_2O,in} = \rho_{CuCl,CuCl_2,HCl,H_2O,out}\dot{V}_{CuCl,CuCl_2,HCl,H_2O,out} + \dot{m}_{HCl,H_2O} \quad (4.60)$$

or

$$\dot{m}_{HCl,H_2O} = \rho_{CuCl,CuCl_2,HCl,H_2O,in}\dot{V}_{CuCl,CuCl_2,HCl,H_2O,in} - \rho_{CuCl,CuCl_2,HCl,H_2O,out}\dot{V}_{CuCl,CuCl_2,HCl,H_2O,out} \quad (4.61)$$

Assuming that the density of the anolyte entering and discharging the flash chamber is almost the same, the above equation can be simplified as:

$$\dot{m}_{HCl,H_2O} = \rho_{CuCl,CuCl_2,HCl,H_2O}(\dot{V}_{CuCl,CuCl_2,HCl,H_2O,in} - \dot{V}_{CuCl,CuCl_2,HCl,H_2O,out}) \quad (4.62)$$

In addition to the density and the volume flow rate of the anolyte entering and discharging the flash chamber, there are a few other variables which influence the rate of vaporization based on the obtained experimental observations. The temperature at which the anolyte enters the flash chamber directly impacts the rate of separation. Moreover, the vacuum pressure inversely influences the rate of separation. The lower the vacuum pressure achieved inside the flash chamber, the higher is the rate of separation. Thus, equation 4.62 is modified as:

$$\dot{m}_{HCl,H_2O} = \frac{\rho_{CuCl,CuCl_2,HCl,H_2O}(\dot{V}_{CuCl,CuCl_2,HCl,H_2O,in} - \dot{V}_{CuCl,CuCl_2,HCl,H_2O,out})\, T_{anolyte,in}}{P_{vacuum,flash\ chamber}} \quad (4.63)$$

Here, $T_{anolyte,in}$ and $P_{vacuum,flash\ chamber}$ represent the inlet temperature of the anolyte solution and the vacuum pressure inside the flash chamber, respectively. In addition, the rate of vaporization is directly influenced by the difference between the pressure achieved by the anolyte solution upstream of the throttling valve and the pressure inside the flash chamber. Another factor which is essential to be considered in this regard is the boiling or vaporization temperature of HCl and H_2O mixture. Hence, the rate of vaporization is inversely impacted by the difference between the vaporization temperature of the HCl and H_2O mixture at ambient pressure and the experimentally considered inlet temperature of the anolyte solution for the HCl and H_2O mixture to be vaporized at the given vacuum conditions achieved inside the flash chamber. Hence, equation 4.63 is further modified to its final form as:

$$\dot{m}_{HCl,H_2O} = \frac{\rho_{CuCl,CuCl_2,HCl,H_2O}(\dot{V}_{CuCl,CuCl_2,HCl,H_2O,in} - \dot{V}_{CuCl,CuCl_2,HCl,H_2O,out})\, T_{anolyte,in}\Delta P}{P_{vacuum,flash\ chamber}\Delta T} \quad (4.64)$$

Equation 4.64 is a simplified empirical correlation obtained to predict the mass flow rate of the vaporization fraction of anolyte. For the different experimental cases, the input conditions are provided in Tables 4.12, 4.13, and 4.14 for the variation in operating temperature, vacuum pressure, and volume flow rate, respectively. The quantity of the separated fraction in terms of percentage in a single run is obtained by considering the ratio of the mass flow rate of the separated HCl and H_2O mixture to the mass flow rate of the feed anolyte solution entering the flash chamber which is mathematically defined as:

$$Percentage\ separation = \frac{\dot{m}_{HCl,H_2O,out}}{\dot{m}_{CuCl,CuCl_2,HCl,H_2O,in}} \times 100 \quad (4.65)$$

Table 4.12 Input conditions for variation in operating temperature of anolyte

$T_{anolyte,in}$ (ºC)	ΔT (ºC)	P_{vac} (bar)	ΔP (bar)	$\rho_{anolyte}$ (kg/m^3)	$\dot{V}_{anolyte,in}$ (l/s)	$\dot{V}_{anolyte,out}$ (l/s)
65	43.6	0.15	1.1	1586.5	0.0042	0.004150
70	38.6					0.004143
75	33.6					0.004133
80	28.6					0.004122
85	23.6					0.004112

Table 4.13 Input conditions for variation in vacuum pressure of flash chamber

$T_{anolyte,in}$ (ºC)	ΔT (ºC)	P_{vac} (bar)	ΔP (bar)	$\rho_{anolyte}$ (kg/m^3)	$\dot{V}_{anolyte,in}$ (l/s)	$\dot{V}_{anolyte,out}$ (l/s)
65	43.6	0.5	0.75	1586.5	0.0042	0.004158
		0.45	0.8			0.004154
		0.4	0.85			0.004153
		0.35	0.9			0.004148
		0.3	0.95			0.004142
		0.25	1			0.004136
		0.2	1.05			0.004133

Table 4.14 Input conditions for variation in volume flow rate of anolyte

$T_{anolyte,in}$ (ºC)	ΔT (ºC)	P_{vac} (bar)	ΔP (bar)	$\rho_{anolyte}$ (kg/m^3)	$\dot{V}_{anolyte,in}$ (l/s)	$\dot{V}_{anolyte,out}$ (l/s)
65	43.6	0.15	1.1	1586.5	0.00250	0.002495
					0.00333	0.00332
					0.00417	0.00415
					0.0050	0.0049
					0.0058	0.0057
					0.0067	0.0066

The anolyte inlet temperature is considered in the range of 65 to 85ºC for which ΔT is in the range of 43.6 to 23.6ºC. The vacuum pressure inside flash chamber is considered in the range of 0.5 to 0.2 bar for which ΔP is in the range of 0.75 to 1.05 bar. For the case with constant vacuum pressure and flow rate, the ratio $\frac{T_{anolyte,in}\Delta P}{P_{vacuum,flash\ chamber}\Delta T}$ is found to be in the range of 10.9 to 26.4. On the other hand, for the case with constant anolyte inlet temperature and flow rate, this ratio is found to be in the range of 2.2 to 7.8.

In closing, this chapter provides the details of the modeling and simulation of the existing and the modified integrated cycles. The various analyses conducted such as energy and exergy, thermal management, exergoeconomic, exergoenvironmental, and multi-objective optimization are also provided in detail. The formulation of an empirical model for theoretical prediction of the mass flow rate of the separated anolyte fraction through the flash vaporization process is also discussed. The following chapter provides the various experimental and modeling results for the integrated cycle.

CHAPTER 5 : RESULTS AND DISCUSSION

This chapter presents the modeling as well as the experimental results. The modeling results correspond to the actual integrated cycle at CERL along with the cycle conceptually modified with the flash vaporization process. The experimental results correspond to the separation process for a standalone flash vaporization set-up. Comparative assessments are also performed and presented for both modeling and experimental results.

5.1 Modeling results of the actual integrated cycle at CERL

This section presents the modeling results for the actual integrated Cu-Cl cycle at CERL. The modeling results of the integrated cycle correspond to the energy and exergy analyses, thermal management, exergoeconomic analysis through EXCEM and SPECO approaches, exergoenvironmental analysis, and multi-objective optimization. The results are discussed in terms of the performance assessment of the overall cycle, sensitivity analysis, and comparative assessment of the cycle through the data reported in the open literature.

5.1.1 Energy and exergy analyses results

The results of the energy and exergy analyses of the integrated cycle at CERL are obtained through the evaluation of the thermodynamic properties at each state point of the cycle through Aspen-plus and Engineering equation solver (EES). The various thermodynamic properties of the integrated cycle at each state point and the operating conditions are provided in Table 5.1. The heat input and discharge rates of the numerous components of the integrated cycle are shown in Figures 5.1 and 5.2, respectively. When water input at 25ºC is considered for the hydrolysis reaction, the hydrolysis step (which includes the hydrolysis reactor and heaters 1 and 8) of the cycle, the PSDU, and the $CuCl_2$-concentrator are evaluated to have the maximum heat input rates. The hydrolysis step is extremely energy-intensive since plenty of thermal energy is expended for the process of water conversion into superheated steam. Moreover, the PSDU and the $CuCl_2$-concentrator process higher mass flows and operate at higher operating temperatures for the separation of different chemicals within the cycle. However, with waste heat recovery, the heat input rate for the hydrolysis step significantly reduces while altogether eliminates for the PSDU and the $CuCl_2$ concentrator (Figure 5.1). On the contrary, The HCl-condenser-1 and the steam condenser are evaluated to have the maximum heat rejection rates. The HCl-

condenser-1 processes the incoming mixture of HCl and H_2O at a high temperature of 400ºC and condenses it to 50ºC which is why it has the highest heat discharge rate in the integrated cycle while the steam condenser also condenses the incoming water at higher temperatures. The exergy destruction rates of the numerous components of the integrated cycle are shown in Figure 5.3. According to the thermodynamic properties obtained as a result of Aspen-plus simulations, the thermolysis step (constituting the thermolysis reactor and the heater-2) and the HCl-condenser-1 results in the highest exergy destruction rates within the integrated cycle. The cycle's overall exergy and energy efficiencies are obtained as 6.6 and 10.2%, respectively.

Table 5.1. Thermodynamic properties at each state point of the integrated cycle

Stream	Species	Mass flow rate (kg/s)	Temperature (°C)	Specific enthalpy (kJ/kg)	Specific exergy (kJ/kg)
S1	H_2O	0.10	400	-12690.9	785.7
S2	$CuCl_2$	0.06	400	-1318.3	686.5
S3	$H_2O/HCl/Cu_2Ocl_2$	0.16	400	-8303.0	658.3
S4	Cu_2Ocl_2	0.05	400	-1681.5	126.8
S5	H_2O/HCl	0.11	400	-11155.3	838.6
S6	Cu2Ocl2	0.05	530	-1653.7	143.3
S7	$O_2/CuCl$	0.05	530	-981.6	772.9
S8	O_2	0.0036	530	498.0	333.2
S9	CuCl	0.04	530	-1101.2	895.8
S10	H_2O	0.02	5	-15948.3	52.8
S11	H_2O	0.02	100	-15255.7	144.4
S12	H_2O/HCl	0.11	50	-13798.3	232.8
S13	H_2O/HCl	0.12	50	-13540.8	258.2
S14	H_2O/HCl	0.12	106	-11477.8	629.1
S15	H_2O	0.09	106	-13271.0	541.8
S16	H_2O/HCl	0.03	106	-6080.4	1282.2
S17	$H_2O/HCl/CuCl$	0.11	74	-4118.9	1064.7
S18	$H_2O/HCl/H_2/CuCl/CuCl_2$	0.11	45	-4242.9	11338.4
S19	H_2	0.00045	45	286.1	117159.3
S20	$H_2O/HCl/CuCl/CuCl_2$	0.11	45	-4271.7	752.4
S21	$H_2O/HCl/CuCl/CuCl_2$	0.11	104	-3805.2	822.4
S22	$H_2O/HCl/CuCl/CuCl_2$	0.08	104	-2923.5	573.5
S23	H_2O/HCl	0.03	104	-6689.8	1169.9
S24	H_2O/HCl	0.03	45	-7624.9	1040.0

S25	$H_2O/HCl/CuCl/CuCl_2$	0.08	107	-2921.4	574.0
S26	$H_2O/CuCl/CuCl_2$	0.07	107	-1951.6	529.7
S27	H_2O/HCl	0.01	107	-9403.8	801.8
S28	H_2O/HCl	0.01	50	-10966.2	544.8
S29	$H_2O/CuCl/CuCl_2$	0.07	85	-2059.6	508.2
S30	H_2O	0.04	30	-15843.4	50.2
S31	CuCl	0.01	32	-1386.5	770.0
S32	$H_2O/CuCl_2$	0.10	32	-6927.0	151.9
S33	$H_2O/CuCl_2$	0.10	110	-5944.9	253.7
S34	H_2O	0.03	110	-13263.4	543.5
S35	$H_2O/CuCl_2$	0.07	110	-3305.3	368.1
S36	$H_2O/CuCl_2$	0.07	130	-3290.1	176.9
S37	CuCl	0.04	45	-1384.8	770.1
S38	CuCl	0.05	42	-1385.1	770.1
S39	$CuCl_2$	0.06	130	-1473.6	618.9
S40	H_2O	0.01	130	-13225.4	552.7
S41	H_2O	0.03	45	-15780.7	52.8

The influence of the flow rate of $CuCl_2$ on the flow rates of the products of the hydrolysis reaction (H_2O, Cu_2Ocl_2, and HCl) is shown in Figure 5.4. Upon increasing the flow rate of $CuCl_2$, the flow rates of the products of the hydrolysis reaction increase as well. Nonetheless, the quantity of excess H_2O as part of the output of the hydrolysis reaction decrease since it reacts with the $CuCl_2$ feed of the reaction.

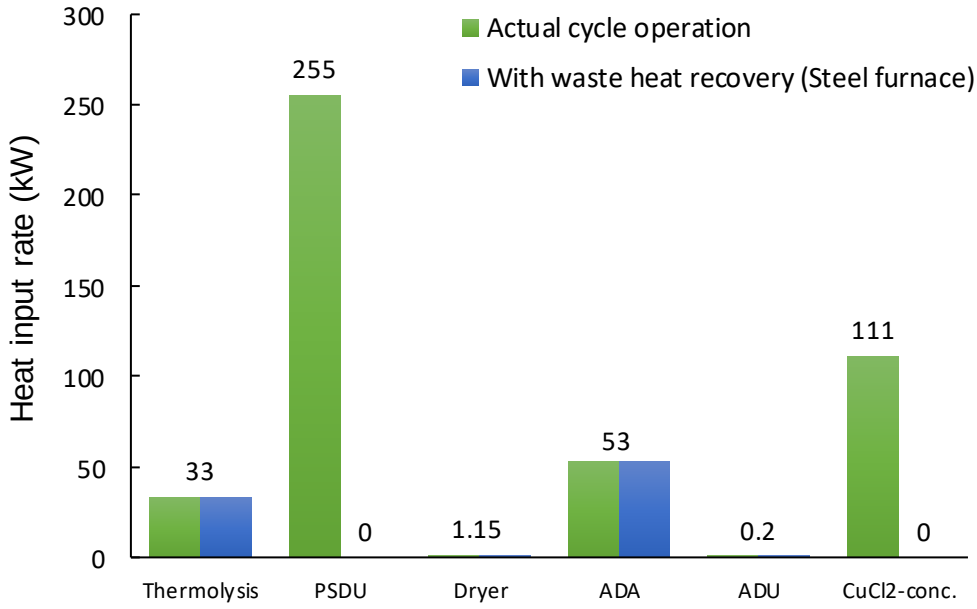

(a)

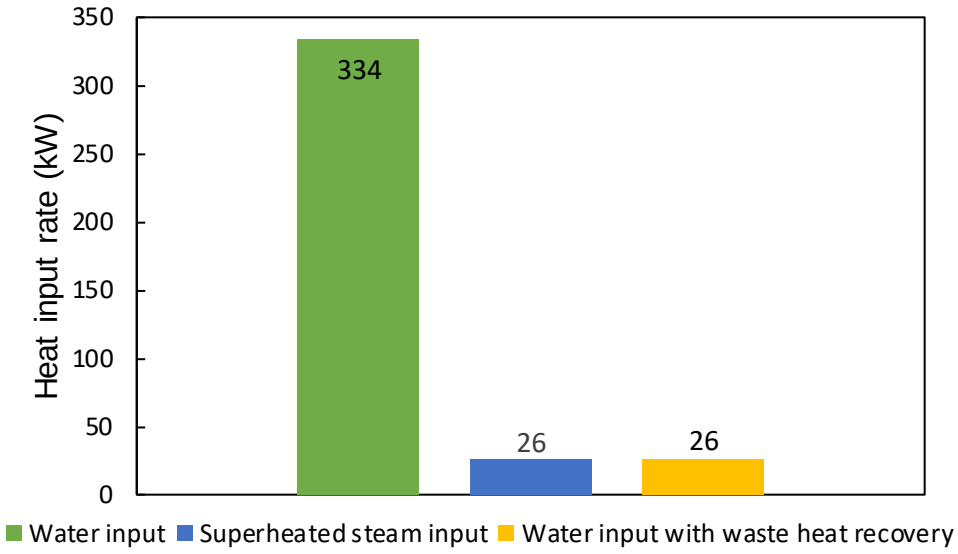

(b)

Fig. 5.1. Heat input rate of (a) various components of the integrated cycle and (b) hydrolysis step of the integrated cycle with water and superheated steam inputs

Figure 5.5 shows the influence of the flow rate of $CuCl_2$ on the flow rates of the oxygen produced during the thermolysis step and the hydrogen generated during the electrolysis step of the integrated cycle. The figure shows that the flow rate of the oxygen and hydrogen products directly increases as the input rate of the $CuCl_2$ feed increases. However, between hydrogen and oxygen, the input feed rate of $CuCl_2$ more profoundly influences the production rate of hydrogen.

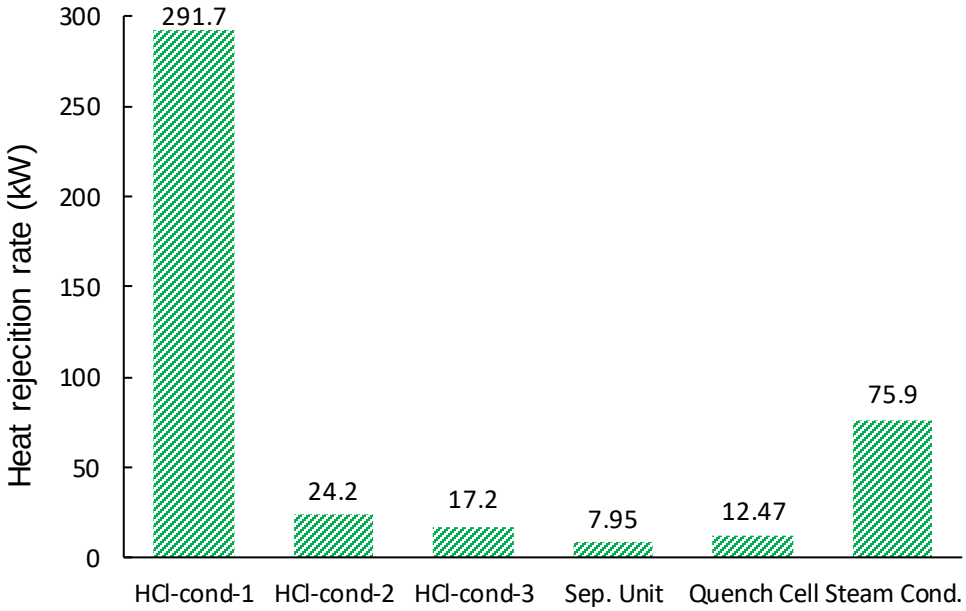

Fig. 5.2. Heat discharge rates of several components of the Cu-Cl cycle

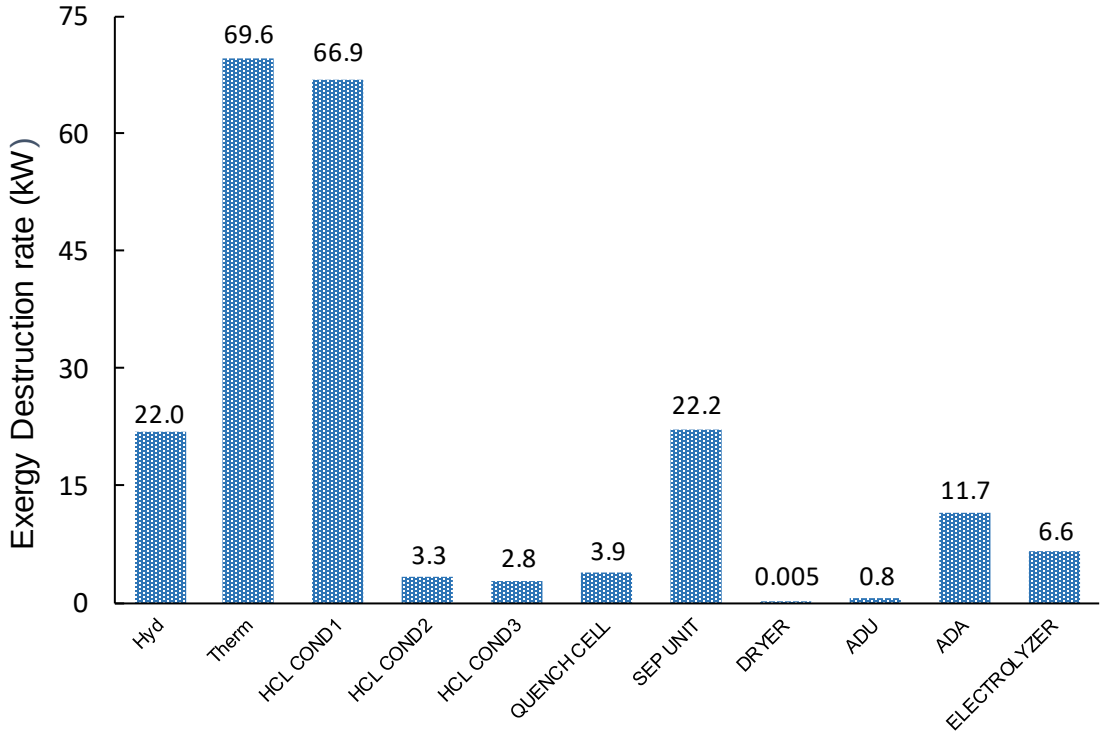

Fig. 5.3. Rates of exergy destructions for different components of the Cu-Cl cycle

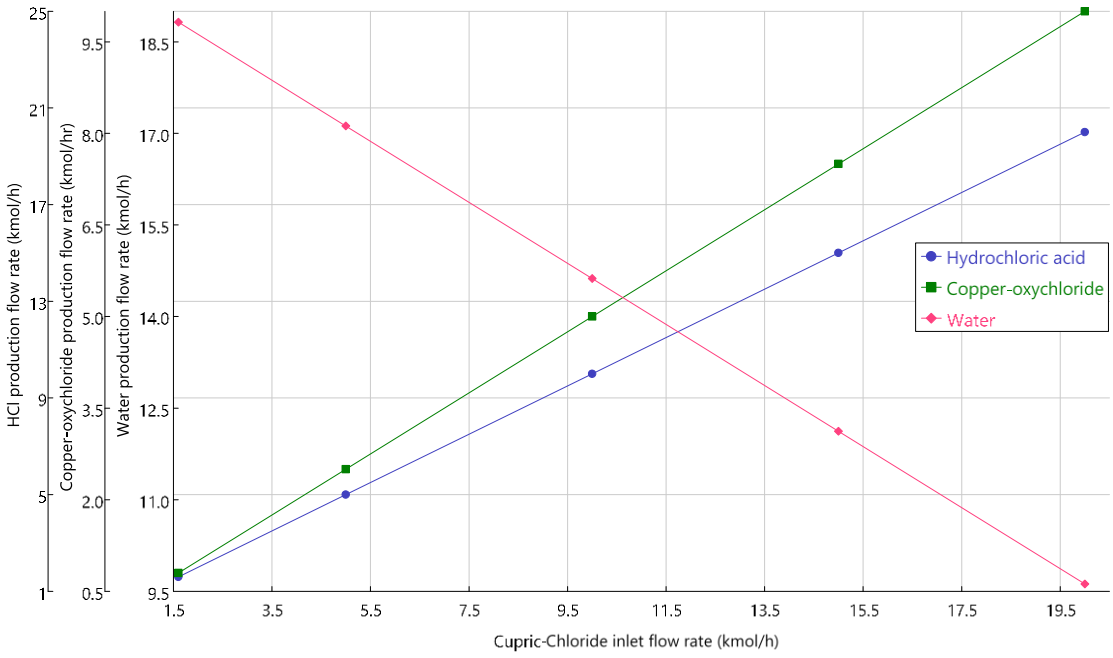

Fig. 5.4. Effect of the mass flow rate of $CuCl_2$ on the flow rates of H_2O, HCl, and Cu_2Ocl_2

Figure 5.6 shows the influence of the mass flow rate of Cu_2Ocl_2 on the heat input rates of the thermolysis reactor and the heater-2 of the integrated cycle. It is seen from the figure

that as the Cu_2Ocl_2 flow rate, acting as the feed for the thermolysis reaction, increases, the amount of heat input rate required by the thermolysis reactor and heater-2 consequently increases as well to achieve the required temperatures. Also, the mass flow rate of the produced oxygen increases.

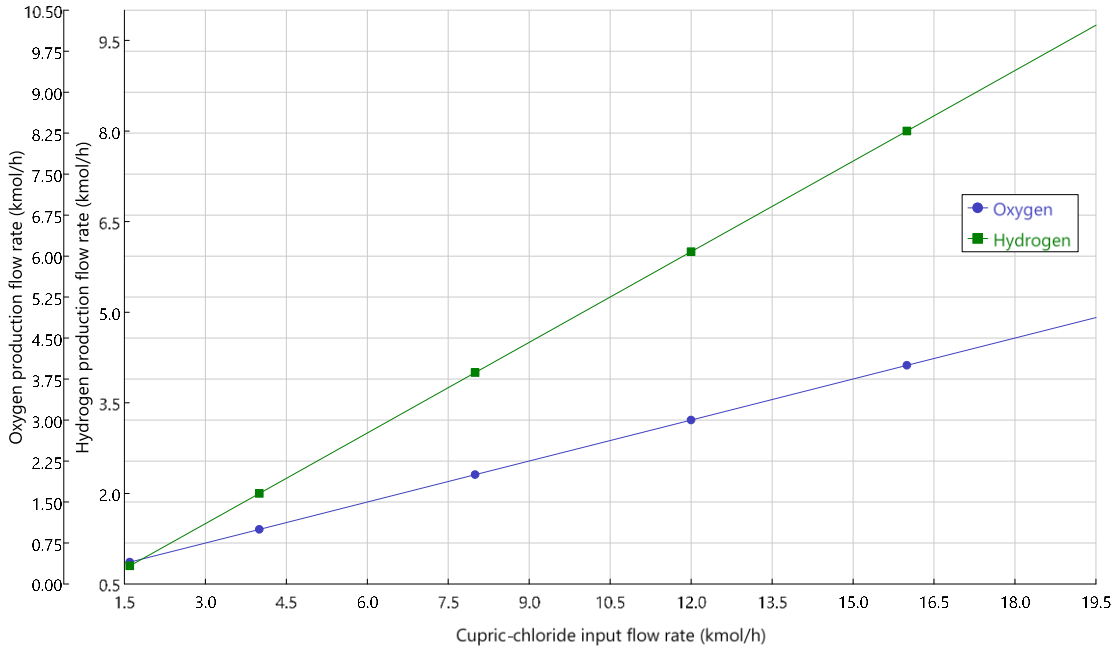

Fig. 5.5. Effect of the mass flow rate of $CuCl_2$ on the mass flow rates of oxygen and hydrogen

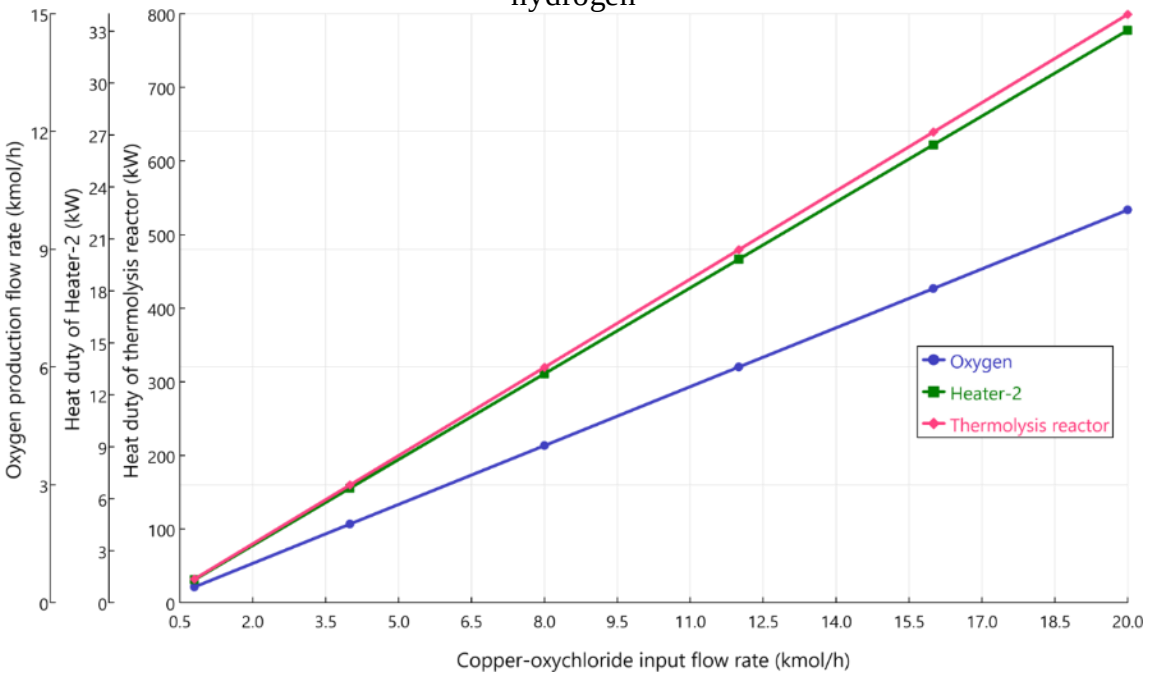

Fig. 5.6. Effect of the mass flow rate of Cu_2Ocl_2 on the mass flow rate of oxygen and heat input rates of the thermolysis reactor and the heater-2

The impact of the mass flow rate of $CuCl_2$ on the mass flow rate of the resulting Cu_2Ocl_2 produced and the heat input rate of the hydrolysis reactor is shown in Figure 5.7. For the hydrolysis reaction to occur, the temperature needed for the hydrolysis process is to be achieved inside the reactor. Thus, excess thermal energy needs to be provided to the hydrolysis reactor to process the increased incoming flow rate of the $CuCl_2$ feed which causes the heat input rate of the hydrolysis reactor to increase. Moreover, as a consequence, it directly influences the rate at which the Cu_2Ocl_2 product is formed.

The impact of the mass flow rate of the anolyte on the heat input rates of the ADA and the ADU is shown in Figure 5.8. According to the obtained thermodynamic results, there is a linear increase in the heat input rates of both the ADA and the ADU. Further, this increase is relatively gradual up until the mass flow rate of 15 kmol/h in contrast to a relatively more sudden increase beyond this flow rate indicating a varying influence of the flow rate of the anolyte on the heat input rates of the two components.

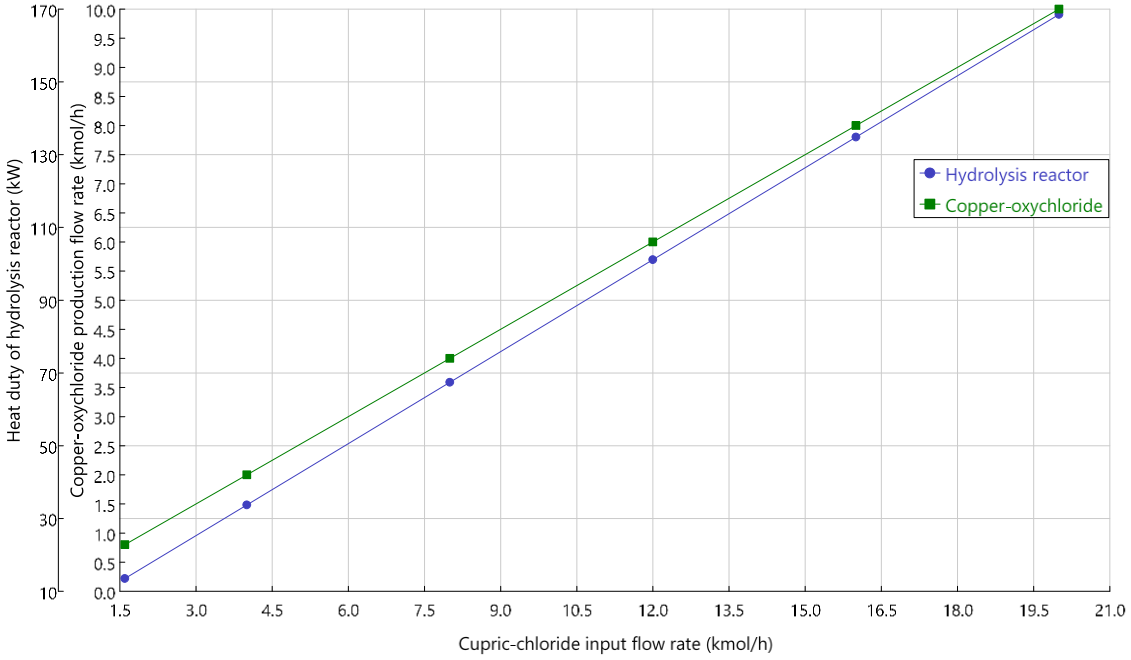

Fig. 5.7. Effect of the mass flow rate of $CuCl_2$ on the mass flow rate of Cu_2Ocl_2 and heat input rate of the hydrolysis reactor

Figure 5.9 shows the influence of the mass flow rate of H_2O provided to the separation unit for separation of CuCl and $CuCl_2$ on the rate of heat input of the dryer and the $CuCl_2$-concentrator and the rate of heat rejection from the steam condenser of the integrated cycle. The H_2O input is provided for the separation process due to the inability of the CuCl to get

dissolved in H_2O thereby allowing convenient separation of $CuCl_2$ from CuCl. Thus, an increase in the feed H_2O flow rate to the separation unit causes the heat input rate of the dryer and the $CuCl_2$-concentrator to increase as well. This also results in a subsequent increase in the amount of thermal energy to be discharged through the steam condenser.

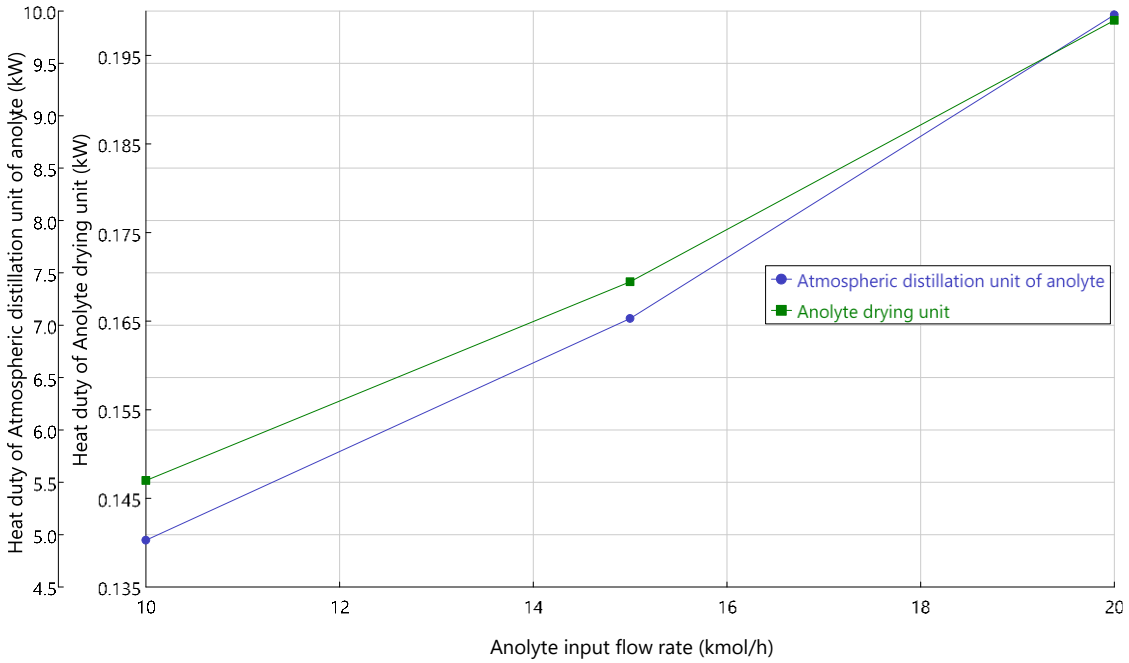

Fig. 5.8. Effect of the mass flow rate of the anolyte on the heat input rates of the ADA and the ADU

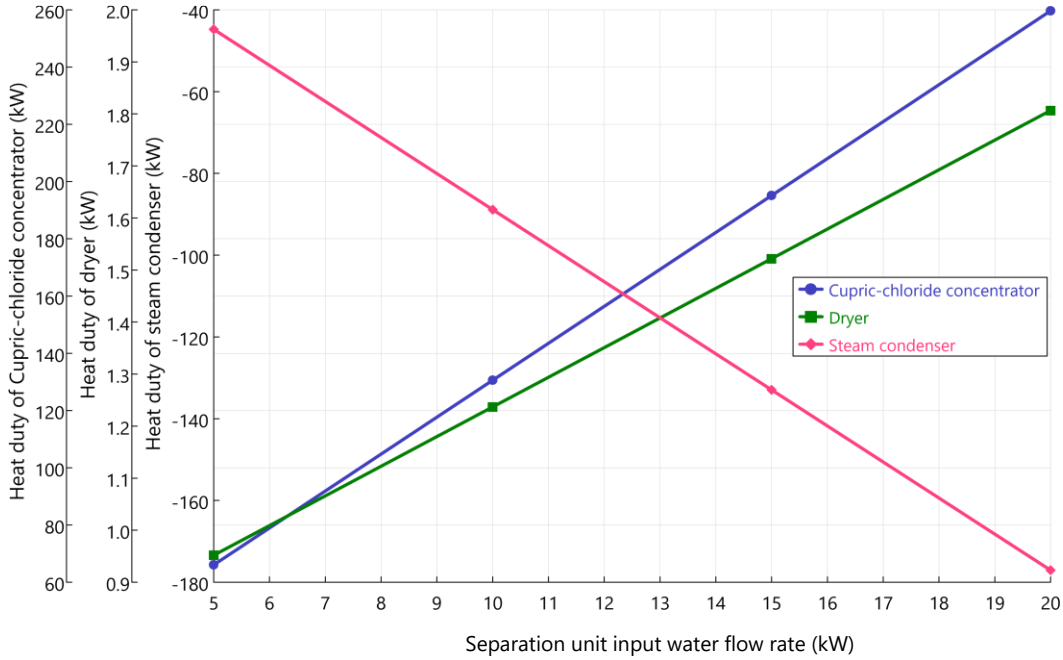

Fig. 5.9. Effect of the mass flow rate of the separation unit on the heat input rates of the dryer unit, the $CuCl_2$ concentrator, and the steam condenser

Figures 5.10 and 5.11 show the impact of the ambient and the maximum temperatures of the cycle, respectively on the overall efficiencies of the integrated cycle. It is seen from the figures that the energy efficiency of the cycle remains completely independent of both these temperatures by virtue of its definition which does not include temperatures. However, these temperatures have a significant impact on the exergy efficiency of the cycle since the definition of exergy efficiency incorporates both the reference and the cycle temperatures. Moreover, the exergy efficiency is found to increase and decrease respectively with an increase in the ambient and the maximum cycle temperatures.

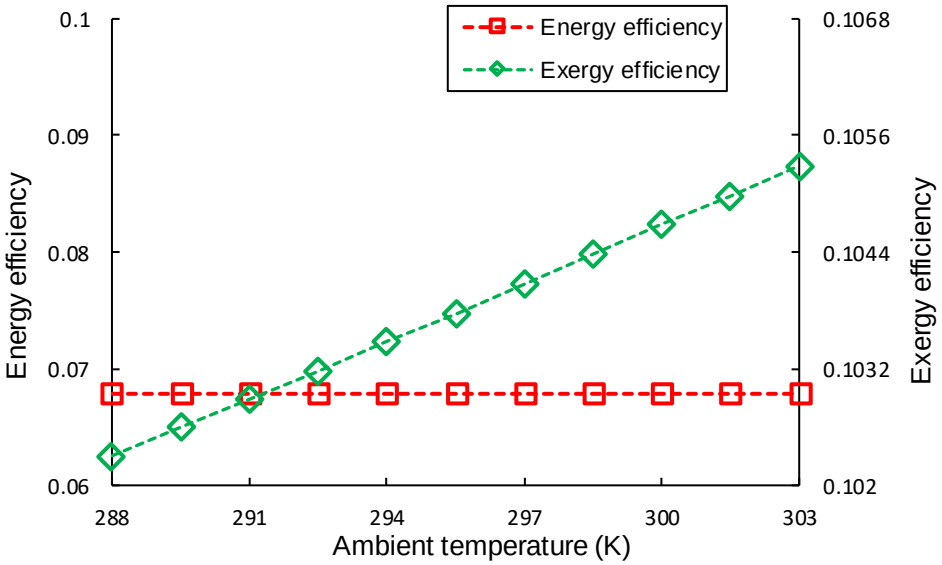

Fig. 5.10. Influence of the reference temperature on the overall efficiencies of the cycle

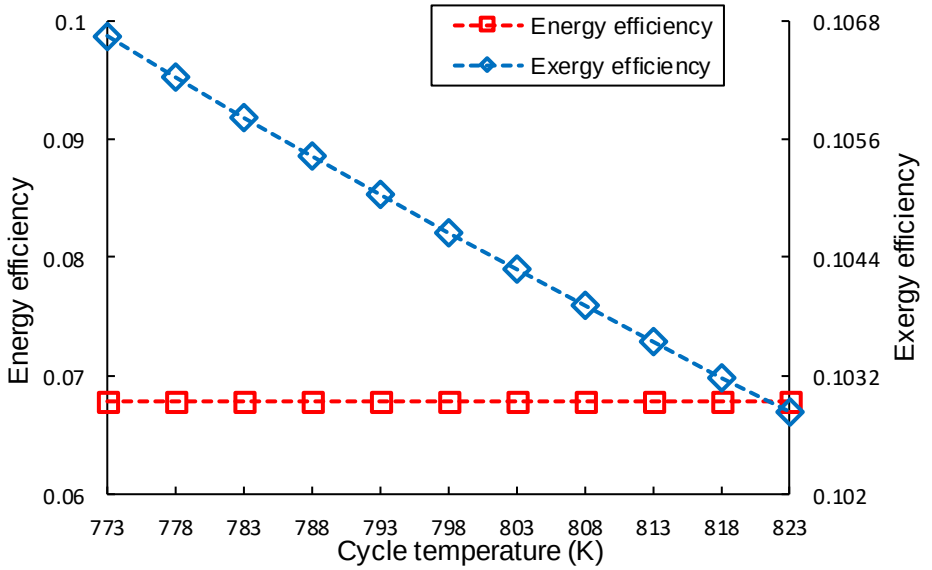

Fig. 5.11. Influence of the cycle temperature on the overall efficiencies of the cycle

5.1.2 Thermal management results

The various heat recovery schemes considered for the thermal management of the integrated Cu-Cl cycle are evaluated in terms of the rate of exergy destruction, rate of net thermal exergy, overall cycle efficiencies, net heat input rate, heat input rate of the hydrolysis process, and steam temperatures after recovery of steam and heat.

Figure 5.12 compares the various heat recovery schemes and the reference case (with no heat recovery) in terms of the rate of exergy destruction of the heater-1 of the cycle. The reference case results in the maximum exergy destruction rate of heater-1 (364 kW). Among the heat recovery schemes, configuration C-4 results in the lowest (273 kW) and configuration C-3 in the second-lowest (285 kW) exergy destruction rates. On the contrary, configuration C-1 results in the highest (342 kW) and the configuration C-6 in the second-highest (329 kW) exergy destruction rates.

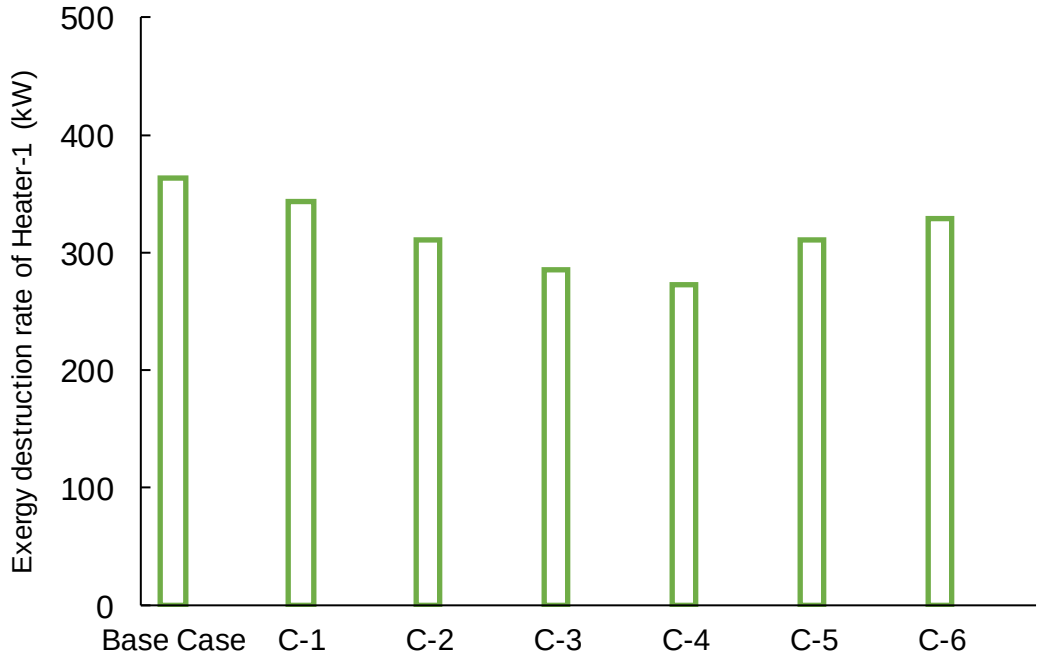

Fig. 5.12. Comparison of rates of exergy destructions of heater-1 of the various heat recovery configurations with the base case

Figure 5.13 compares the various heat recovery schemes and the reference case in terms of the net thermal exergy rate of the cycle. The reference case results in the maximum net thermal exergy rate (492 kW) of the cycle. Among the heat recovery schemes, configuration C-4 results in the lowest (309 kW) and configuration C-3 in the second-

lowest (343 kW) net thermal exergy rates. On the contrary, configuration C-1 results in the highest (417 kW) and the configuration C-6 in the second-highest (383 kW) net thermal exergy rates.

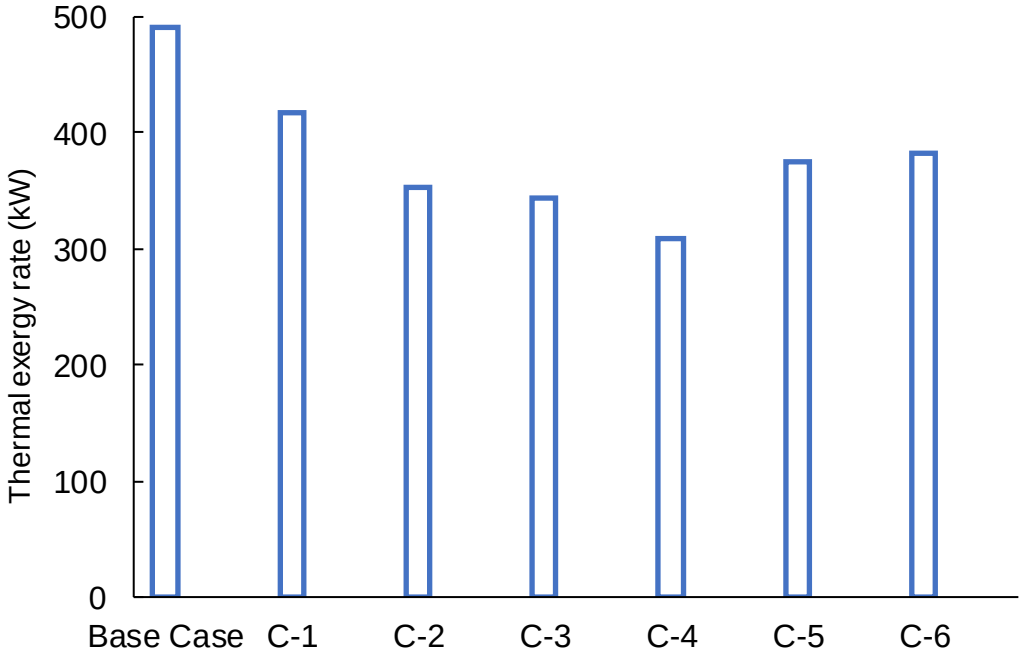

Fig. 5.13. Comparison of thermal exergies of the various heat recovery configurations with the base case

Figure 5.14 compares the various heat recovery schemes and the reference case in terms of the overall cycle efficiencies of the cycle. The reference case results in the lowest overall energy and exergy efficiencies of 6.6 and 10.2%, respectively. Among the heat recovery schemes, configuration C-4 results in the highest energy efficiency of 10.7% and exergy efficiency of 16.3%, and the configuration C-3 in the second-highest energy efficiency of 9.6% and exergy efficiency of 14.8%. On the contrary, the configuration C-1 results in the lowest energy efficiency of 8% and exergy efficiency of 12.2%.

Figure 5.15 compares the various heat recovery schemes in terms of the temperature of the steam after steam and heat recovery. Among the six heat recovery schemes, the configuration C-4 results in the highest steam recovery temperature of 109°C and heat recovery temperature of 391.3°C and the configuration C-2 in the second-highest steam recovery temperature of 107°C and heat recovery temperature of 342.3°C. On the contrary,

configuration C-1 results in the lowest steam recovery temperature of 100°C and heat recovery temperature of 196.4°C.

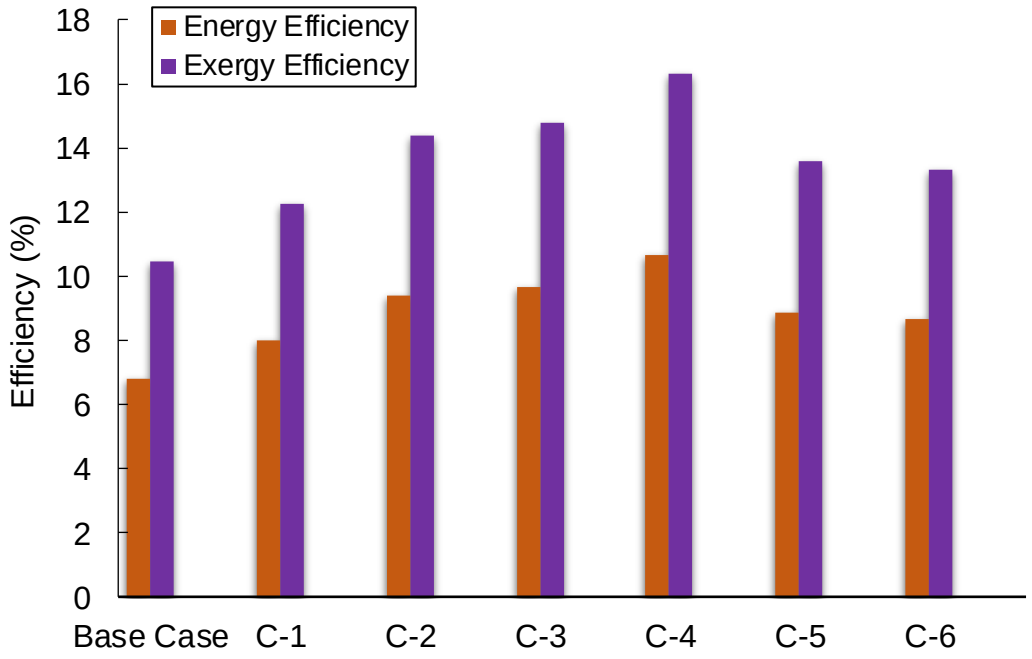

Fig. 5.14. Comparison of the overall cycle efficiencies of the various heat recovery configurations with the base case

Figure 5.16 compares the various heat recovery schemes and the reference case in terms of the net heat input rate of the cycle and the heat input rate of the hydrolysis process. The reference case results in the highest net heat input rate (782 kW) and heat input rate of the hydrolysis process (334 kW). Among the heat recovery schemes, the configuration C-4 results in the lowest net heat input rate (492 kW) and the configuration C-3 in the second-lowest net heat input (546 kW) rates. Moreover, the configuration C-4 results in the lowest heat input rate of the hydrolysis process (25 kW) and the configuration C-2 in the second-lowest heat input rate of the hydrolysis process (37 kW).

Figure 5.17 compares the various heat recovery schemes in terms of the percentage difference of net heat input rate, heat input rate of the hydrolysis process, and rate of exergy destruction of heater-1 with respect to the reference scenario. The configuration C-4 has the highest percentage difference in all specified categories with the values of 37, 93, and 25% respectively for the net heat input rate, heat input rate of the hydrolysis process, and the rate of exergy destruction for heater-1. On the contrary, the configuration C-1 has the

lowest percentage difference in two categories with the values of 76 and 6% respectively for the heat input rate of the hydrolysis process and the rate of exergy destruction for heater-1. In terms of the percentage difference of the net heat input rate, the configuration C-6 results in the lowest value of 15%.

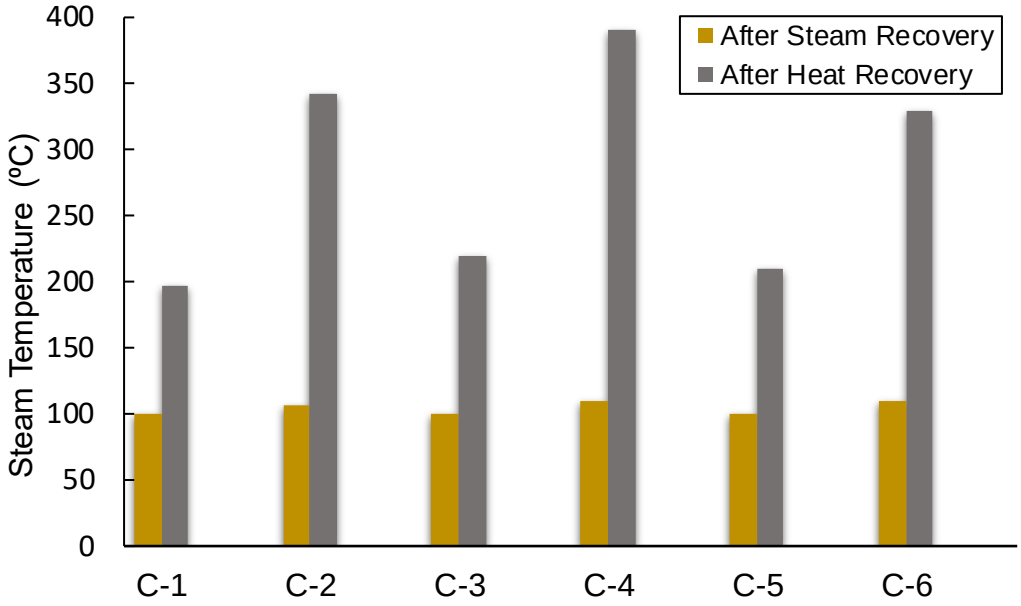

Fig. 5.15. Comparison of the temperatures achieved after recovering steam and heat between the various configurations

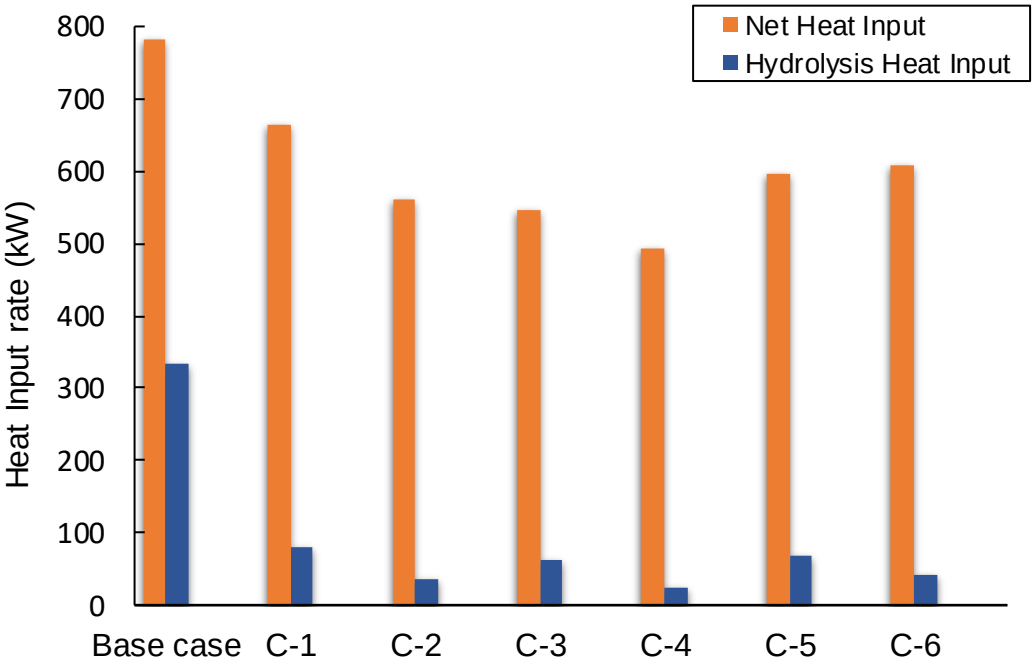

Fig. 5.16. Comparison of the net heat input rates and heat input rates of the hydrolysis unit of the various heat recovery schemes with the base case

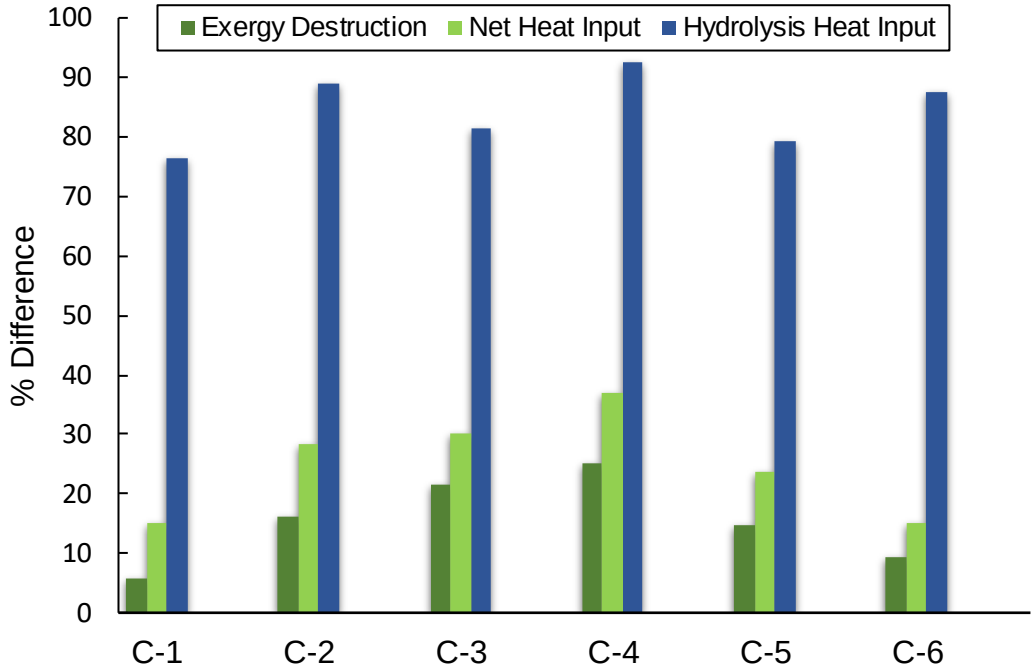

Fig. 5.17. Comparison of percentage difference of the net heat input rates, heat input rates of the hydrolysis unit, and the rates of exergy destructions with respect to the reference case for the various heat recovery schemes

Based on the results shown in all the above figures, the configuration C-4 exhibits the best performance in every aspect due to the two main reasons of maximum heat recovery temperature and lowest value of the S/Cu ratio. With configuration C-4 employed in the integrated cycle, steam at an extremely high temperature can be provided for the hydrolysis step thereby resulting in much reduced net heat input rate, heat input rate of the hydrolysis process, rate of exergy destruction, and net thermal exergy rate. As a consequence, higher overall cycle efficiencies are achieved.

Figure 5.18 shows the influence of the inlet temperature of steam on the rate of heat input of heater-1 of the integrated cycle for all the considered heat recovery schemes. The temperatures at which the steam, after heat recovery, is inputted in heater-1 for each configuration are shown with a dotted line in red. According to the figure, between 25 and 85°C, the heater-1 results in much higher heat input rates ranging from 300 to 450 kW in comparison to when steam input is considered at temperatures ranging from 100 to 390°C for which this heat input rate range reduces to 2 and 80 kW. In the figure, the region of such a drastic reduction in the heat input rate of heater-1 is labeled as the “dipping zone”. A plausible explanation for this sudden reduction in the heat input rate of heater-1 during

this dipping region is that water undergoes a phase change from liquid to gas approximately between the temperature range of 85 and 100°C. In the context of Figure 5.18, when liquid water is considered as the feed for heater-1, it is more energy-intensive to be converted into superheated steam compared with when water in the form of steam is allowed to enter the heater-1. As a consequence, the heat input rate of the hydrolysis process reduces considerably with the incorporation of heat recovery compared with regular cycle operation without heat recovery.

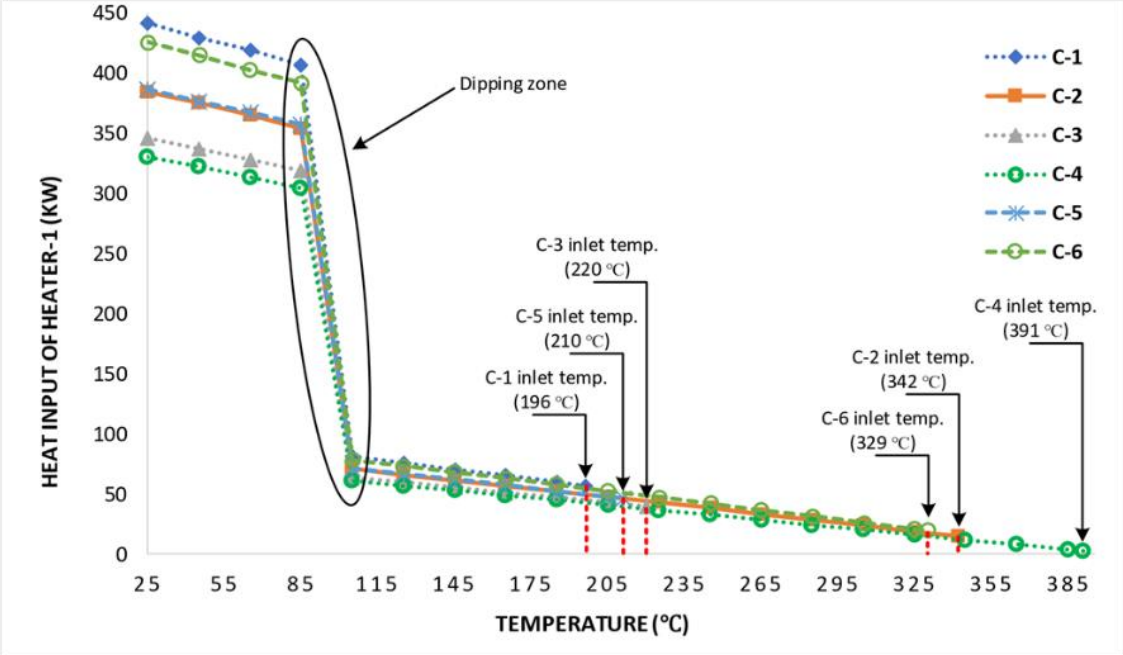

Fig. 5.18. Influence of the steam inlet temperature on the heat input rates of heater-1 for the various schemes

A comparative evaluation of the total thermal energy needed for the hydrolysis step and the remaining processes within the integrated cycle among the regular cycle operation and the different heat recovery schemes is presented in Figure 5.19. From the figure, it is quite obvious that for the reference case, the hydrolysis process accounts for 43% of the heat input of the entire integrated cycle. However, with consideration of internal heat recovery within the integrated cycle, this percentage substantially reduces. Among the various heat recovery schemes, the configuration C-4 takes up only 5% of the total rate of heat input for the hydrolysis process, the configuration C-2 and C-6 account for only 7% and the configurations C-1 and C-6 account for only 12%. Nevertheless, the net heat input rate of

the entire integrated cycle for every heat recovery scheme is different but much less than the reference case.

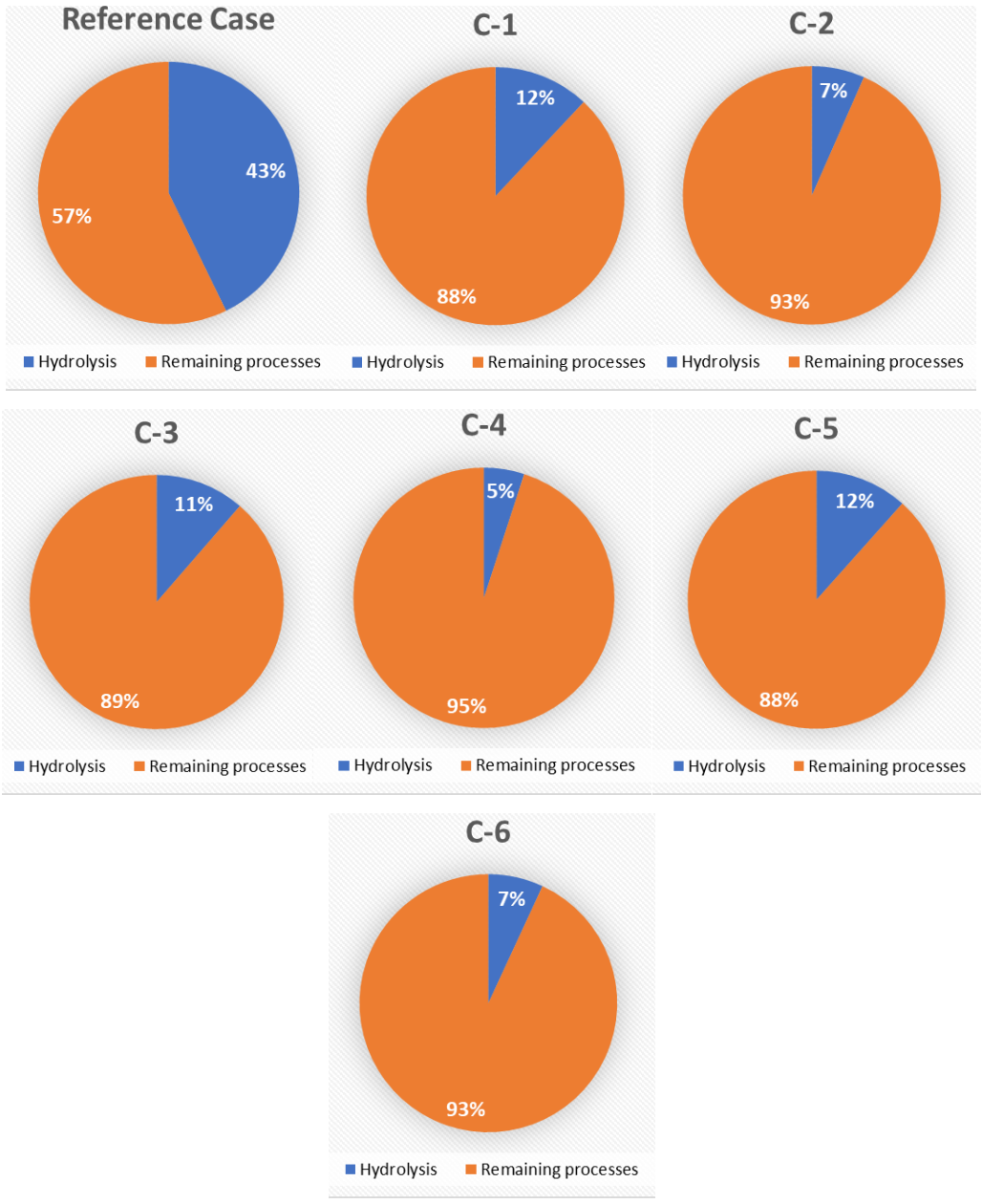

Fig. 5.19. Comparison of the rates of heat input for the hydrolysis step and the remaining processes of the cycle for the reference case and the several schemes

5.1.3 Exergoeconomic analysis results (EXCEM)

This section discusses the results of the exergoeconomic assessment of the integrated cycle at CERL through the application of the EXCEM approach. According to the modeling and simulation of the integrated cycle, the exergoeconomic evaluation is carried out in terms

of the capital costs, thermodynamic loss rates, and the ratio of these two quantities the details of which are provided in Table 5.2. The integrated cycle is simulated for a hydrogen production capacity of 1.6 T/h operating at overall exergy and energy efficiencies of 10.2 and 6.6%, respectively. The relevant statistical data obtained in the context of the thermodynamic loss rate to the capital cost ratio for the integrated cycle is provided in Table 5.3. To evaluate the cost of various process equipment of a given system, various mathematical relations and expressions are developed and reported in the literature. Moreover, various software packages are also used for the cost analysis purposes such as *Capcost*. For the present exergoeconomic assessment of the integrated cycle, the Aspen-plus software package is used for cost analysis in addition to thermodynamic modeling and simulation purposes. Aspen-plus considers the input flow rate and operating conditions (pressure and temperature) for certain equipment based on which it assesses the costs of certain equipment of a given system.

Table 5.2. Capital cost and thermodynamic loss data for the different cycle components

Components	K **(10^3 \$)**	$\dot{L}_{ex}$ **(MW)**	$\dot{R}_{ex}$ **(Kw/\$)**	$\dot{L}_{en}$ **(MW)**	$\dot{R}_{en}$ **(Kw/\$)**
Hydrolysis	970.3	21.56	0.0222	27.08	0.0279
Thermolysis	382.4	74.34	0.1944	64.18	0.1678
Dryer	53.5	0.48	0.0090	2.31	0.0432
ADU	46.7	0.88	0.0189	0.35	0.0076
ADA	111.0	16.87	0.1520	107.59	0.9693
HCl-cond-1	574.1	68.73	0.1197	594.58	1.0357
HCl-cond-2	141.9	0.77	0.0054	51.30	0.3615
HCl-cond-3	98.1	0.70	0.0072	35.88	0.3657
Quench Cell	232.4	3.99	0.0172	0	0
Electrolyzer	154.8	6.57	0.0424	0.012	0.0001
Other equipment	3746.6	-	-	-	-
Total	6511.8	194.90	0.5884	883.29	2.9788

Table 5.3. Statistical data for the ratio of thermodynamic loss rate to capital cost

Parameter	**Based on exergy loss**	**Based on energy loss**
$\dot{R}_{min}$(Kw/\$)	5E-03	0
$\dot{R}_{max}$(Kw/\$)	0.1944	1.036
Mean $\dot{R}$ (Kw/\$)	0.059	0.298
Standard deviation	0.070	0.397
Co-efficient of variation (%)	118.42	133.35

Figure 5.20 shows the rate balances for cost, energy, exergy, and mass of the integrated cycle at CERL. In the context of mass conservation, upon the thermochemical dissociation of water into oxygen and hydrogen, water exits as steam (97.5%) while 2.2% of feed water is converted to oxygen and 0.28% to hydrogen thereby conserving the mass within the cycle. Every chemical used within the cycle is eventually recycled. In the context of energy conservation, the thermal and electrical energies entering the cycle are distributed as 99.36 and 0.64%, respectively. Whereas 97.5% of this input energy is lost to the environment, 2.41% is utilized as hydrogen and 0.08% is utilized in the form of oxygen. In the context of exergy, as mentioned before, it either remains the same or reduces. Thus, the exergy provided as input to the integrated cycle is much higher than the exergies of hydrogen and oxygen. Moreover, there is a significant difference between the content of exergies between oxygen and hydrogen such that the chemical exergy of hydrogen (117166.3 kJ/kg) greatly exceeds that of oxygen (124.1 kJ/kg). In Figure 5.20c, the waste exergy emitted and exergy destroyed within the cycle is shown in grey color. In the context of cost, as mentioned previously, it either remains the same or increases. Thus, the total cost required for the generation of hydrogen through the integrated cycle is the sum of the various costs including the input cost of thermal and electrical energies, capital cost, and operating and maintenance cost of the cycle. The unit electrical energy is considered to be 6.3 $/GJ based on [83] while the unit cost of steam is estimated to be 19.9 $/T. For the considered capacity of hydrogen production, the evaluated cost rate of hydrogen is 8978 $/h for which the unit cost of hydrogen is obtained to be 5.54 $/kg with a cost generation rate of 665.7 $/h as shown through the grey color in Figure 5.20d accounting for the entire cost of the equipment as well as the operation and maintenance of the system.

Comparing the unit cost of hydrogen obtained through a four-step Cu-Cl, a cost of 3.3 $/kg is reported in [19] by Lewis et al. and 3.36 $/kg in [47] by Ozbilen et al. for hydrogen production capacities of 125 MT/day and 5.2 T/h, respectively. The evaluation of the hourly levelized capital cost rates is carried out as stated in the guidelines provided in [84]. The several cost-related parameters and their values needed for exergoeconomic evaluation of the integrated cycle are provided in Table 5.4.

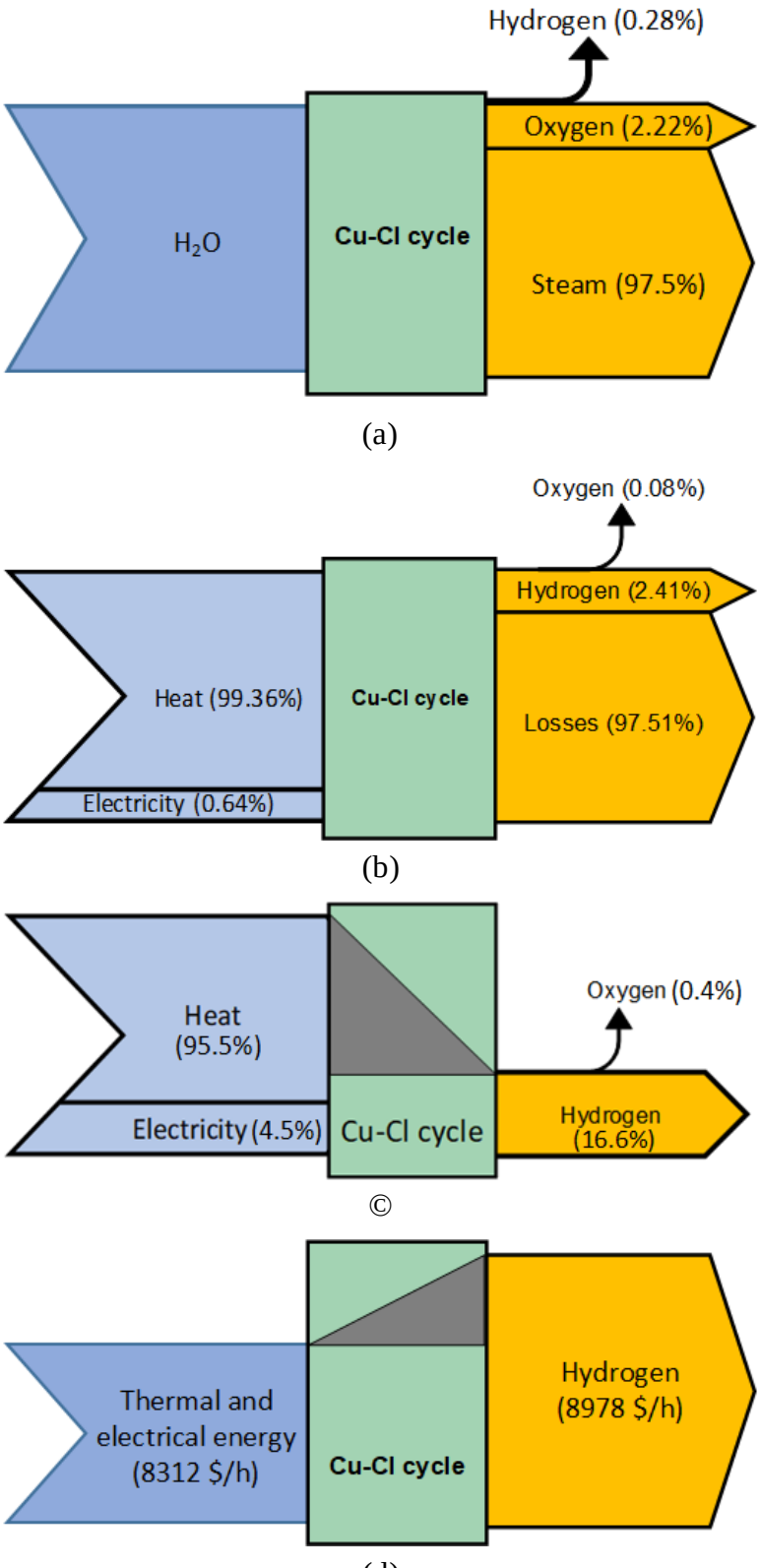

Fig. 5.20. (a) Mass, (b) energy, (c) exergy, and (d) cost rate balances in the Cu-Cl cycle

Table 5.4. Values of several operating parameters and input costs for evaluating the hourly levelized costs in the Cu-Cl cycle

Parameter	Value
Total capital cost (10^7 $)	2.39
Total operating cost (10^3 $/year)	657.45
Total maintenance cost (10^3 $/year)	126.01
Lifetime of the system (years)	10
Interest rate (%)	20
Salvage value ratio (%)	20
Capital recovery factor	0.24
Present value factor	0.16
Operating hours per year (hours)	8766
Operating and maintenance cost factor	1.06 [84]

The influence of the production capacity of hydrogen on the cost rate and the unit hydrogen cost is shown in Figure 5.21. The production capacities considered range between 162 and 1620 kg/h. From the figure, it is seen that the unit cost of hydrogen reduces with an increase in the production capacity. However, this decrease is more abrupt at lower capacities and rather gradual at higher capacities. The unit cost of hydrogen is evaluated to be 7.1 $/kg for the lowest capacity considered which reduces to 5.5 $/kg at a capacity of 1.6 T/h. Conversely, the cost rate of hydrogen linearly increases upon increasing the production capacity of hydrogen from a minimum of 1147 $/h to 8978 $/h for the lowest and the highest considered capacities, respectively.

The influence of the annual operating time of the integrated cycle on the hourly levelized total equipment cost is shown in Figure 5.22. The annual operating time of the integrated cycle is varied from 8000 to 9000 hours per year for the same range of production capacities considered. For all capacities, the hourly levelized cost decreases as the annual operating time increase. Nevertheless, this behavior is more noticeable at higher capacities compared with lower ones. For the minimum annual operating time considered, the hourly levelized cost remains in the range of 345 to 730 $/h while for the maximum operating time, the hourly levelized cost remains in the range of 306 to 648 $/h.

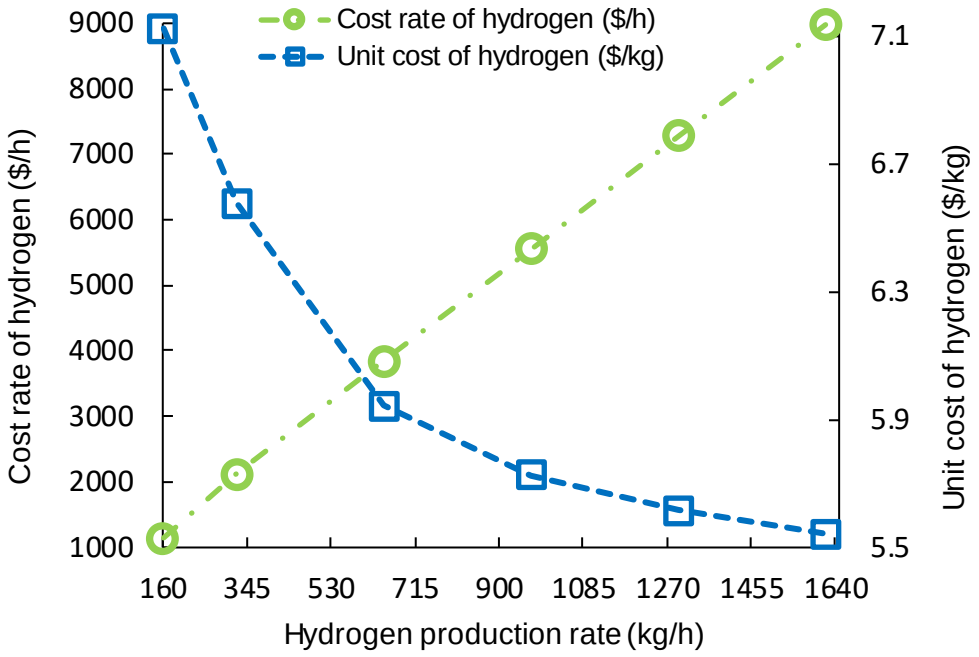

Fig. 5.21. Influence of the rate of hydrogen production on the cost rate and the unit hydrogen cost

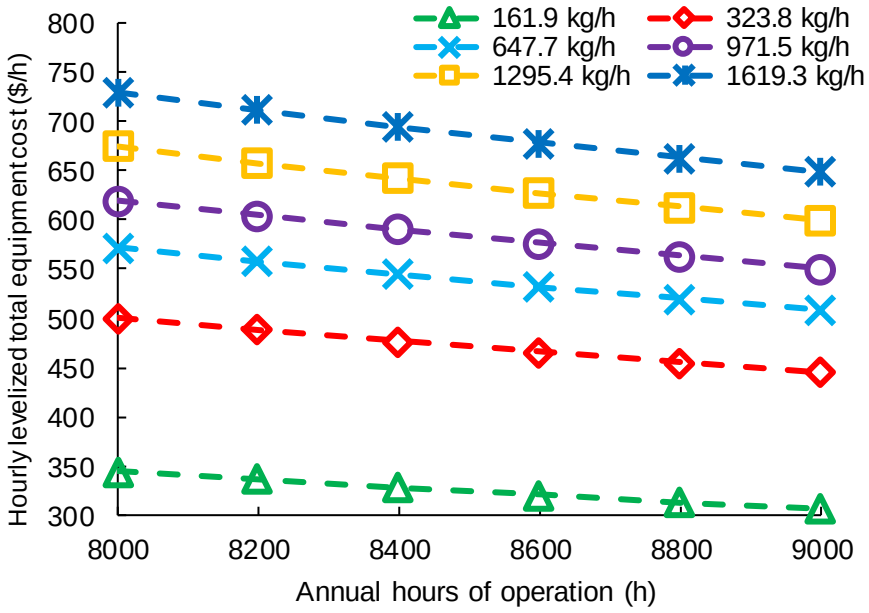

Fig. 5.22. Influence of annual operating time on hourly levelized total equipment cost

The influence of the operating and maintenance cost factor on the hourly levelized cost is shown in Figure 5.23. The operating and maintenance cost factors for the integrated cycle are varied from 1 to 1.5 for the same range of production capacities considered. For all capacities, the hourly levelized cost increases as the operating and maintenance cost factor increase eventhough this behavior is more distinct at higher capacities compared with

lower ones. For the minimum operating and maintenance cost factor considered, the hourly levelized cost remains in the range of 297 to 581 $/h while for the maximum operating and maintenance cost factor, the hourly levelized cost remains in the range of 445 to 942 $/h.

The influence of the temperature of the feed steam provided to heater-1 of the integrated cycle on the cost rate of hydrogen is shown in Figure 5.24. The feed temperature of steam impacts the unit steam cost. Under normal mode of operation of the integrated cycle, the feed provided to heater-1 is in the form of liquid water at ambient temperature however, with the incorporation of internal heat recovery, the feed to heater-1 can be supplied as steam or superheated steam. Thus, it is evident from the figure that an increase in the temperature of steam causes a reduction in the cost rate of hydrogen for all capacities considered. Nonetheless, this change is more obvious at higher capacities than the lower ones. For the minimum feed steam temperature considered, the cost rate remains in the range of 1076 to 8265 $/h while for the maximum feed steam temperature, the cost rate remains in the range of 886 to 5185 $/h.

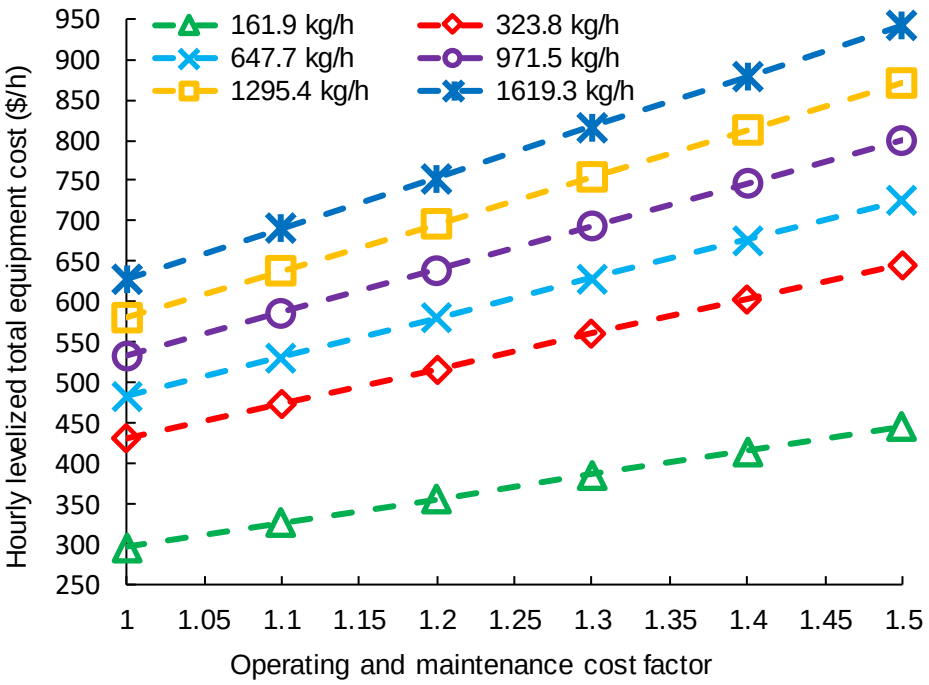

Fig. 5.23. Effect of the operating and maintenance cost factor on the hourly levelized total equipment cost

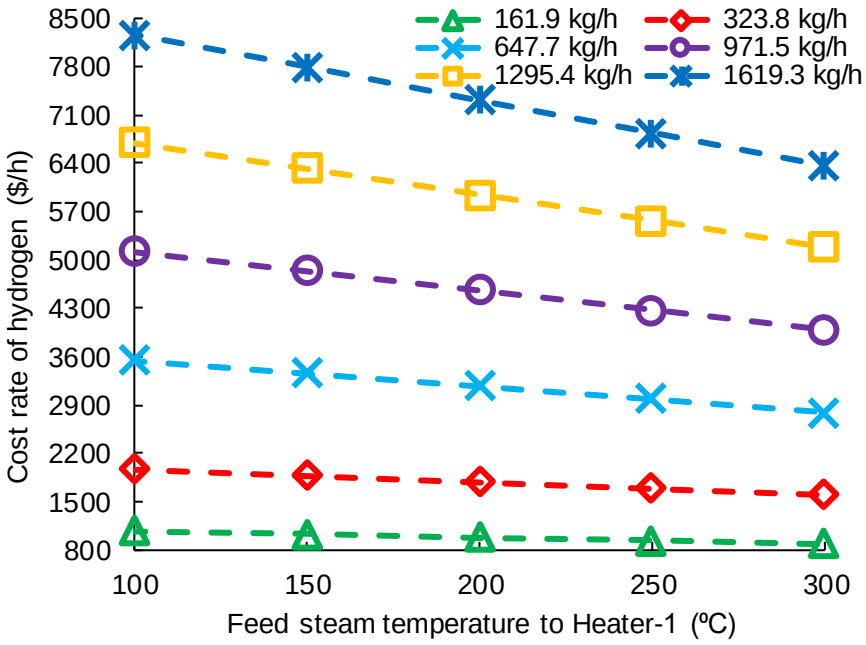

Fig. 5.24. Impact of the temperature of the feed steam to Heater-1 on the cost rate of hydrogen

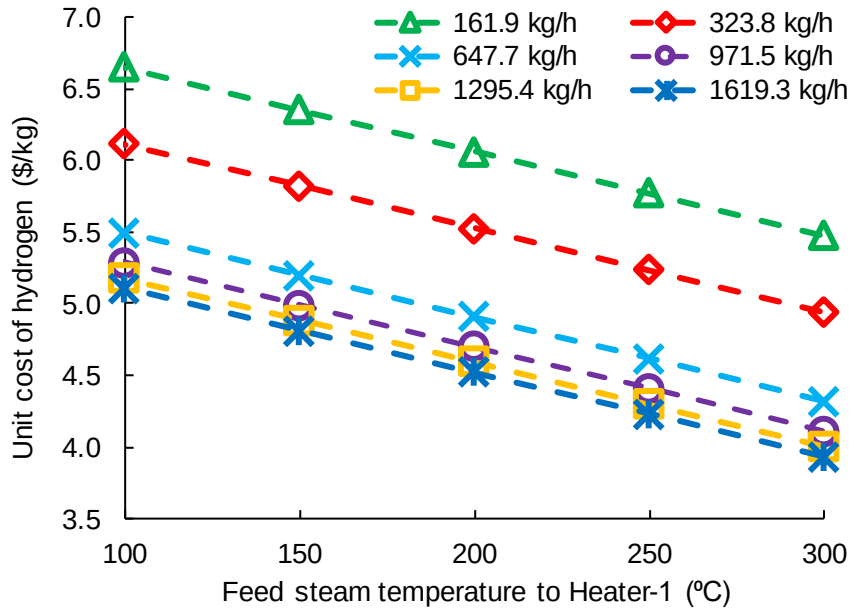

Fig. 5.25. Impact of the temperature of the feed steam to Heater-1 on the unit hydrogen cost

The influence of the temperature of the feed steam provided to heater-1 of the integrated cycle on the unit cost of hydrogen is shown in Figure 5.25. Thus, it is seen from the figure that an increase in the temperature of steam causes a reduction in the unit hydrogen cost for all capacities considered. Further, a decrease in the unit hydrogen cost between the

considered feed steam temperatures (100 to 300ºC) is evaluated as 1.17 $/kg for all considered capacities. For the minimum feed steam temperature considered, the unit hydrogen cost remains in the range of 6.6 to 5.1 $/kg while for the maximum feed steam temperature, the unit hydrogen cost remains in the range of 5.5 to 3.9 $/kg.

The decrease in the unit cost of hydrogen in terms of percentage change for the various steam input temperatures with respect to the feed input at ambient temperature at a capacity of 1.6 T/h is shown in Figure 5.26. According to the figure, a significant reduction in the unit hydrogen cost is achievable by employing heat recovery in the integrated cycle. When the feed steam input at the minimum considered temperature is realized, a percentage decrease of about 8% is achieved in the unit cost of hydrogen while this percentage reduction increases up to 29% at the highest feed steam temperature.

A comparison of the cost of the purchased components of some of the main components of the integrated cycle (the thermolysis and hydrolysis reactors, the electrolyzer, the HCl-condenser-1, and the PSDU) at various capacities is presented in Figure 5.27. Based on the obtained results, it is concluded that the cost of the purchased equipment is influenced by the capacity of hydrogen production however, this influence is relatively higher for some equipment than the others. Also, this influence is considerably less at lower capacities compared with higher ones.

The influence of the production capacity on the distribution of the cost of the purchased components for anolyte separation and hydrogen production purposes is shown in Figure 5.28. Processes/components such as electrolysis, thermolysis, hydrolysis, the PSDU, and the HCl-condenser-1 of the cycle are used during the hydrogen production phase of the cycle whereas components like the ADU, the ADA, the other HCl-condensers, the dryer, and the $CuCl_2$-concentrator are used for the anolyte separation phase of the cycle. The cost of the purchased equipment of several components increases with an increase in the capacity of the cycle. As per the figure, the share of the total cost of the components for hydrogen production purposes in the cycle initially increases up to a certain capacity before reducing. Conversely, the share of the total cost of the components for anolyte separation purposes in the cycle initially reduces up to a certain capacity before increasing. For the minimum and the maximum capacities considered, the share of the cost of the components

for hydrogen production is 83 and 80%, respectively. On the other hand, for the minimum and the maximum capacities considered, the share of the cost of the components for anolyte separation is 17 and 20%, respectively.

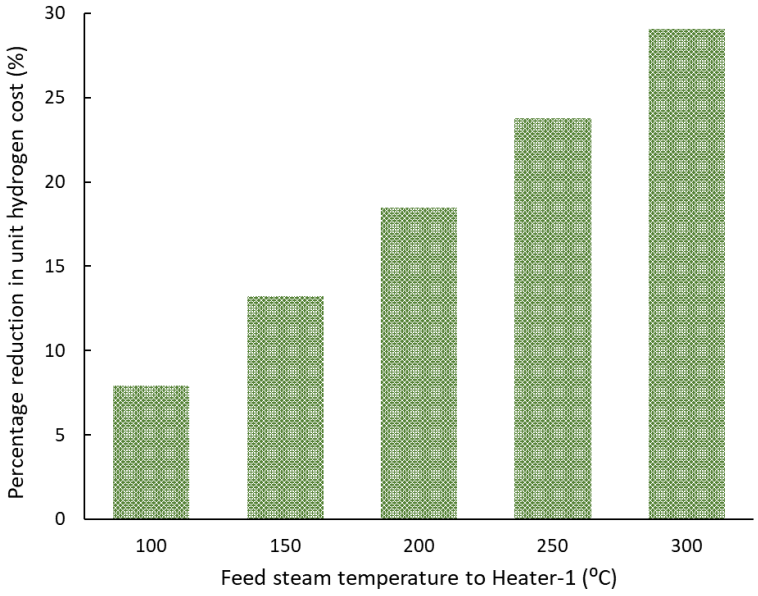

Fig. 5.26. Percentage reduction in the unit cost of hydrogen at different temperatures of the feed steam with respect to the reference case (25 °C)

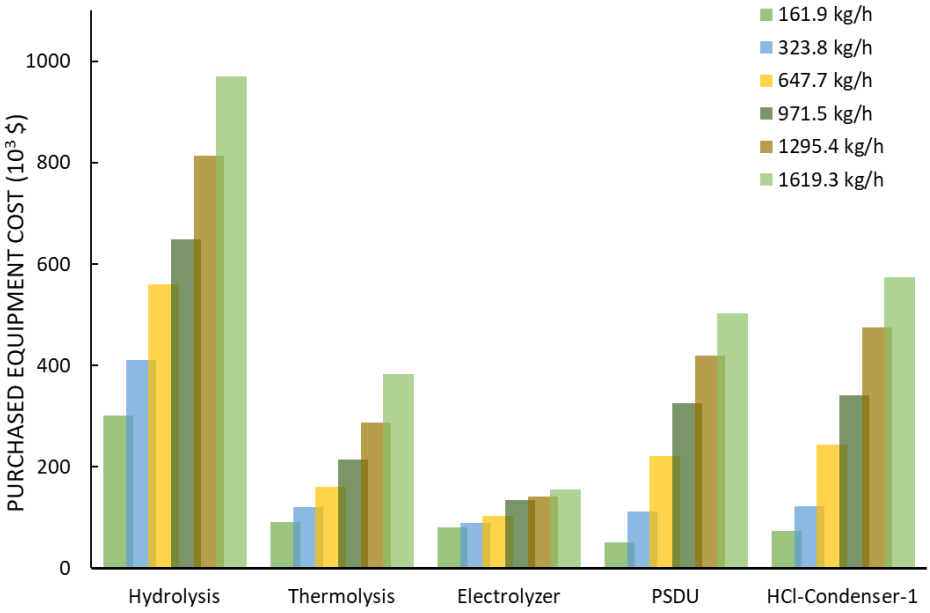

Fig. 5.27. Effect of the capacity of hydrogen production on the cost of the purchased equipment of major system components

The ratio of the rate of the exergetic loss to capital cost ($\dot{R}_{ex}$) for every process and component of the integrated cycle is shown presented in Figure 5.29. According to the

obtained data, the dryer, the quench cell, the ADU, and the HCl-condensers 2 and 3 have the lowest values. On the contrary, the ADA, the HCl-condenser-1, and the thermolysis reactor result in the maximum values.

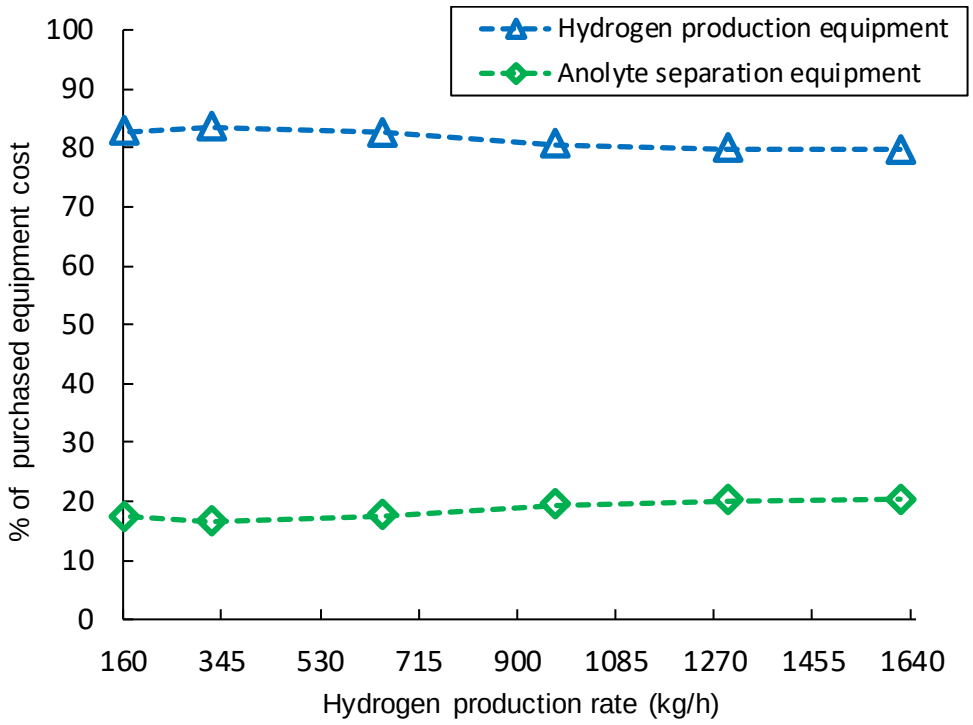

Fig. 5.28. Effect of hydrogen production capacity on the percentage of purchased equipment cost for hydrogen production and anolyte separation

Figure 5.30 compares the unit cost of hydrogen for different capacities (2, 10, and 50 tons) of hydrogen production between the integrated cycle at CERL and a four-step Cu-Cl cycle studied in [83]. Similar to Figure 5.21, the unit cost reduces with an increase in the production capacities with the reduction more sudden at lower and more gradual at higher capacities. The difference in the unit cost is higher for the capacities in the range of 2 and 10 tons compared with the capacities in the range of 10 and 50 tons for both the present analysis and [83]. This similarity in the reduction behavior in both studies serves as a validation of the results obtained in the current analysis. The considerably higher unit cost in the current analysis compared with [83] is due to the reason that more equipment is considered for the integrated cycle at CERL which profoundly influences the unit cost.

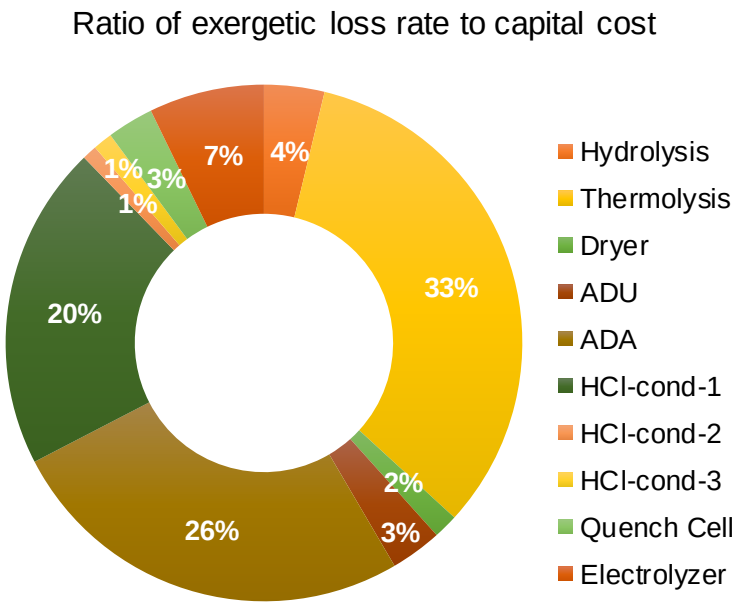

Fig. 5.29. Percentage distribution of the exergetic loss rate to the capital cost ratio for different components of the Cu-Cl cycle

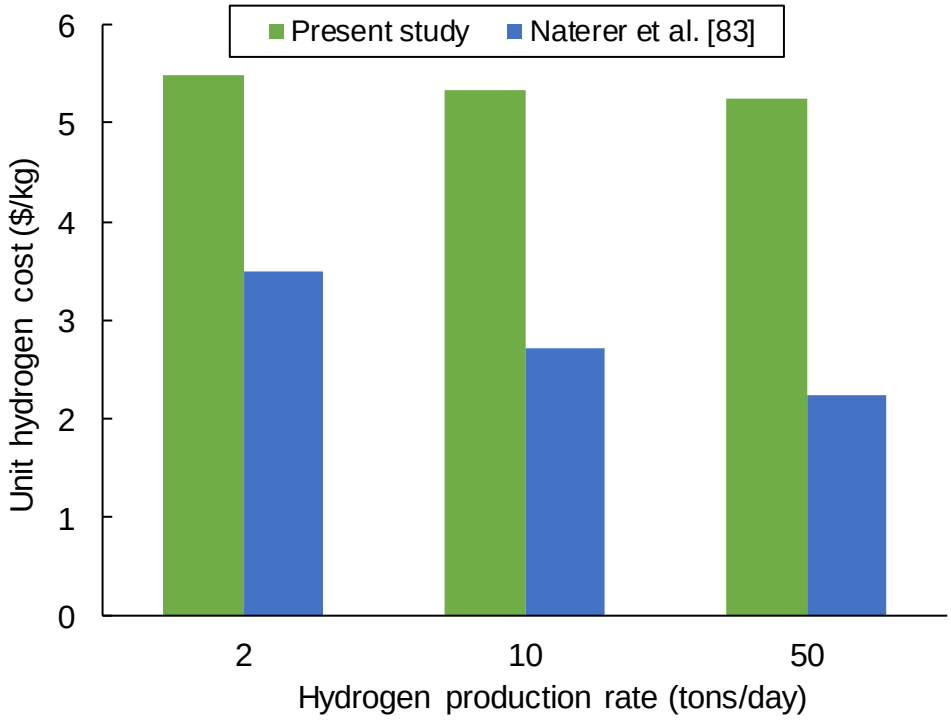

Fig. 5.30. Comparison of reduction trend in the unit cost of hydrogen at various production capacities between the present study and Naterer et al. [83]

5.1.4 Exergoeconomic analysis results (SPECO)

The cost rate, unit or specific cost rate, and the rate of exergy at each state point of the integrated cycle are provided in Table 5.5 which are evaluated based on the exergetic cost balance and auxiliary equations formulated and presented in Table 4.4. The exergy rate at each state point is evaluated according to the thermodynamic analysis of the cycle in Aspen-plus. At a capacity of 1.3 T/h, the exergy cost at state point 19, at which hydrogen is generated, is evaluated as 6407.5 $/h for which the unit cost of hydrogen is evaluated as 4.94 $/kg. Table 5.6 provides the capital cost rate of all equipment and the cost of the numerous purchased components of the integrated cycle. The relative difference of cost and the exergoeconomic factor of a few main equipment of the integrated cycle are obtained and provided in Table 5.7. A value of the exergoeconomic factor for a given component close to 1 is interpreted as high capital cost while a value close to 0 is interpreted as extremely high exergy destruction associated cost rate. According to the evaluated results, the thermolysis step results in the lowest, and the HCl condensers 2 and 3 results in the maximum values of the exergoeconomic factor. Moreover, the dryer unit and the HCl condenser 1 result in the lowest and the highest values of the relative cost difference, respectively. The exergy destruction associated and the hourly levelized total cost rates of a few main equipment of the integrated cycle are presented in Figure 5.31. Based on the evaluated results, the exergy destruction associated cost rates are much higher compared to the hourly levelized total cost rates of the numerous equipment. Thus, there is a dominant share of the process irreversibilities of several equipment towards the overall cost of the cycle. Hence, there is a need to significantly decrease the rate of exergy destruction within the cycle.

Table 5.5. Exergy and specific exergy costs at all state points of the Cu-Cl cycle

Stream	$\dot{E}x$ (MW)	$\dot{C}$ ($/h)	c ($/MJ)	Stream	$\dot{E}x$ (MW)	$\dot{C}$ ($/h)	c ($/MJ)
$CuCl_2$	131897.36	0	0	S21	204282.48	8518.53	0.042
Water	17990.01	0	0	S22	125275.39	6680.15	0.053
S1	282838.66	17723.64	0.063	S23	34692.19	1849.73	0.053
S2	148291.18	736.97	0.005	S24	27719.87	1873.53	0.068
S3	380673.02	19314.37	0.051	S25	125368.83	6683.92	0.053
S4	21791.00	1169.57	0.016	S26	109447.14	5966.18	0.055
S5	339489.57	18210.62	0.016	S27	13256.56	722.51	0.055

S6	24633.80	1271.95	0.052	S28	7862.73	739.22	0.094
S7	132859.82	3329.27	0.025	S29	106544.60	5973.10	0.056
S8	4282.78	97.14	0.008	S30	7196.00	0	0
S9	142477.58	3238.32	0.008	S31	24488.64	1998.20	0.0816
S10	3802.94	318.95	0.084	S32	48770.92	3979.59	0.0816
S11	9444.85	797.38	0.084	S33	94992.73	6408.89	0.0675
S12	94076.67	18925.91	0.201	S34	56756.11	2565.15	0.0452
S13	94076.67	18925.91	0.201	S35	85511.72	3864.78	0.0452
S14	249431.69	24052.92	0.096	S36	43995.13	3893.72	0.0885
S15	168501.32	14014.15	0.083	S37	122478.96	2783.65	0.0227
S16	120933.15	10090.19	0.083	S38	122478.96	2783.65	0.0227
S17	273349.15	12873.84	0.047	S39	106947.47	3166.80	0.0296
S18	2859142.28	14367.02	0.005	S40	24734.27	732.38	0.0296
S19	151771.32	6407.55	0.042	S41	5511.37	2664.71	0.4835
S20	188632.21	7963.31	0.042				

While evaluating the capital costs of certain processes and equipment like the electrolyzer, the thermolysis, and the hydrolysis, it is to be noted that the cost rates associated with those processes include the heaters, reactors, and separators as well. The lowest exergy destruction associated cost rates are evaluated for the HCl condensers 2 and 3 and the thermolysis step accounts for the maximum value. Moreover, the lowest capital cost rate is evaluated for the ADU while the hydrolysis step accounts for the highest value. The percentage distribution of the numerous equipment of the cycle in the context of the capital cost rate is presented in Figure 5.32. Based on the evaluated results, the HCl condenser 3, the dryer unit, and the ADU are among the equipment with the lowest shares of capital cost rates while the hydrolysis step has the highest contribution in the cycle in this regard.

Table 5.6. Capital cost rate and cost of purchased equipment for all cycle components

Component	**PEC (10^3 \$)**	Z_k^T **(\$/h)**
Hydrolysis reactor	970.3	99.2
Thermolysis reactor	382.4	39.1
Electrolyzer	154.8	15.8
Steam Condenser	385.5	39.4
Dryer	53.5	5.5
PSDU	503.1	51.4
Quench Cell	232.4	23.8
HCl-condenser-1	574.1	58.7

HCl-condenser-2	141.9	14.5
HCl-condenser-3	98.1	10.0
$CuCl_2$-Concentrator	205.8	21.0
ADU	46.7	4.8
Preheater	27.2	2.8
Separation Unit	45.9	4.7
Separator-1	643.9	65.8
Separator-2	66.0	6.7
Separator-3	37.6	3.8
ADA	111.0	11.3
Heater-1	400.5	40.9
Heater-2	185.5	18.9
Heater-3	447.5	45.7
Heater-4	163.2	16.7
Heater-5	11.2	1.1
Heater-7	347.3	35.5
Heater-8	250.7	25.6
Condenser	25.7	2.6
Total	**6511.8**	**665.7**

The impact of the total lifetime of the cycle on the total cost rate at different interest rate values is shown in Figure 5.33. The interest rates are varied between 5 and 20% while the lifetime is varied between 10 and 20 years. From the figure, it is seen that the cost rate reduces as the lifetime is increased for all interest rates. The cost rate at the minimum considered lifetime at the minimum interest rate is 15100 $/h reducing to 14986 $/h at the maximum considered lifetime. Conversely, the cost rate at the minimum considered lifetime at the maximum interest rate is 15438 $/h reducing to 15362 $/h at the maximum considered lifetime.

Table 5.7. Exergoeconomic factor and relative cost difference values for different components of the cycle

Component	**f (%)**	**r**
Hydrolysis	9.70	0.41
Thermolysis	0.86	0.73
Dryer	14.56	0.07
ADU	6.27	0.96
ADA	1.63	0.92
HCl-cond-1	3.77	35.58

HCl-cond-2	46.41	11.29
HCl-cond-3	39.60	16.09
Quench Cell	1.65	0.73
Electrolyzer	2.91	0.52

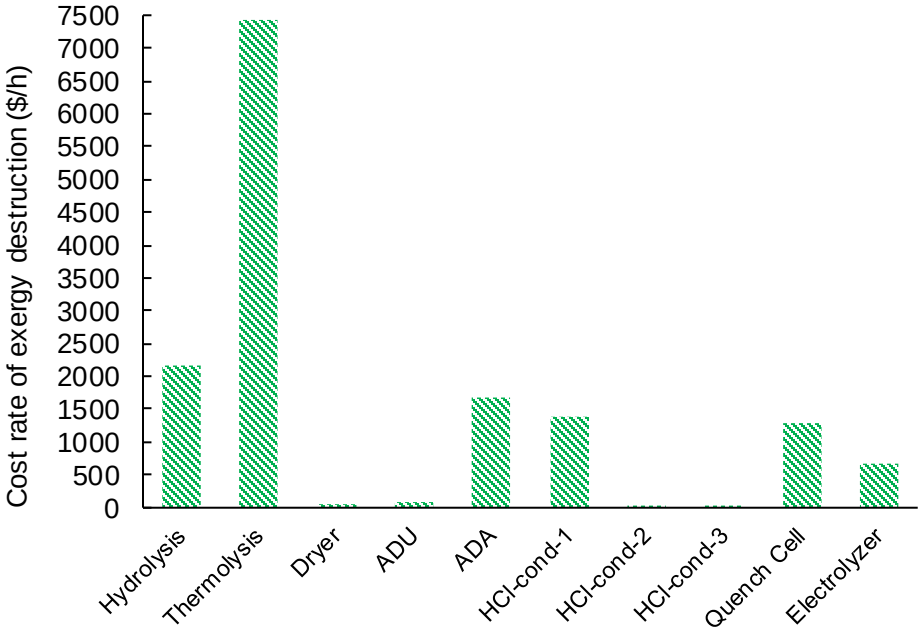

(a)

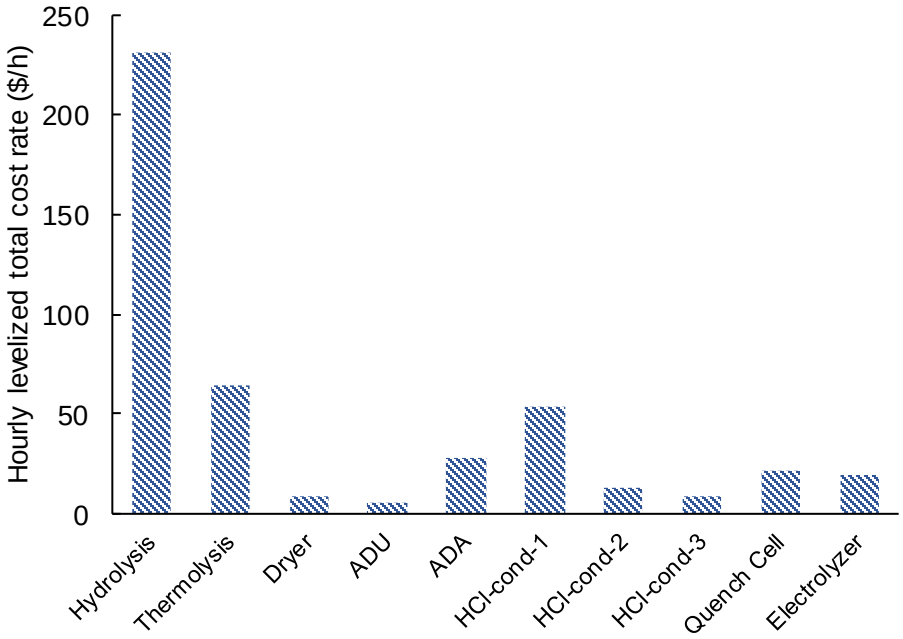

(b)

Fig. 5.31. (a) Exergy destruction cost rates and (b) total cost rates of various components

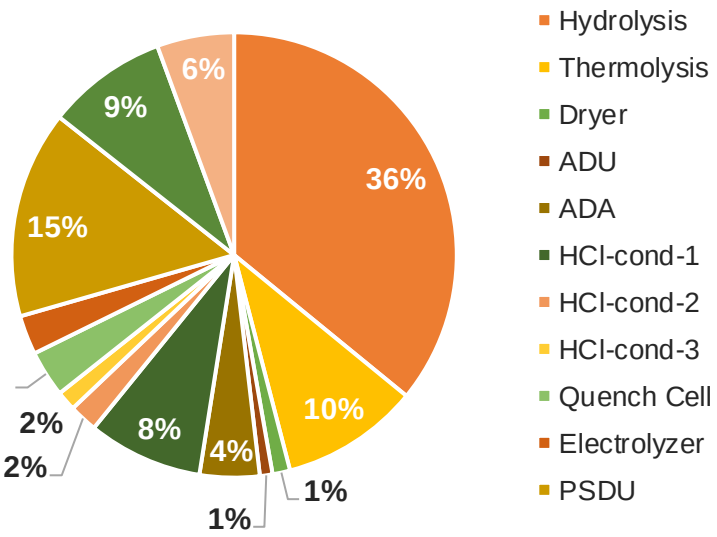

Fig. 5.32. Percentage distribution of the hourly levelized total cost rates among several processes

The impact of the total lifetime of the cycle on the total cost rate at different operating and maintenance cost factor values is shown in Figure 5.34. The operating and maintenance cost factor is varied between 1.0 and 1.4 while the lifetime is varied between 10 and 20 years. From the figure, it is seen that the cost rate reduces as the lifetime is increased for all operating and maintenance cost factors. The cost rate at the minimum considered lifetime at the minimum operating and maintenance cost factor is 15401 $/h reducing to 15328 $/h at the maximum considered lifetime. Conversely, the cost rate at the minimum considered lifetime at the maximum operating and maintenance cost factor is 15652 $/h reducing to 15551 $/h at the maximum considered lifetime.

The impact of the total lifetime of the cycle on the total cost rate at different annual operating times is shown in Figure 5.35. The annual operating times are varied between 8000 and 9000 while the lifetime is varied between 10 and 20 years. From the figure, it is seen that the cost rate reduces as the lifetime is increased for all annual operating times. The cost rate at the minimum considered lifetime at the minimum annual operating time is 15502 $/h reducing to 15418 $/h at the maximum considered lifetime. Conversely, the cost rate at the minimum considered lifetime at the maximum annual operating time is 15421 $/h reducing to 15346 $/h at the maximum considered lifetime.

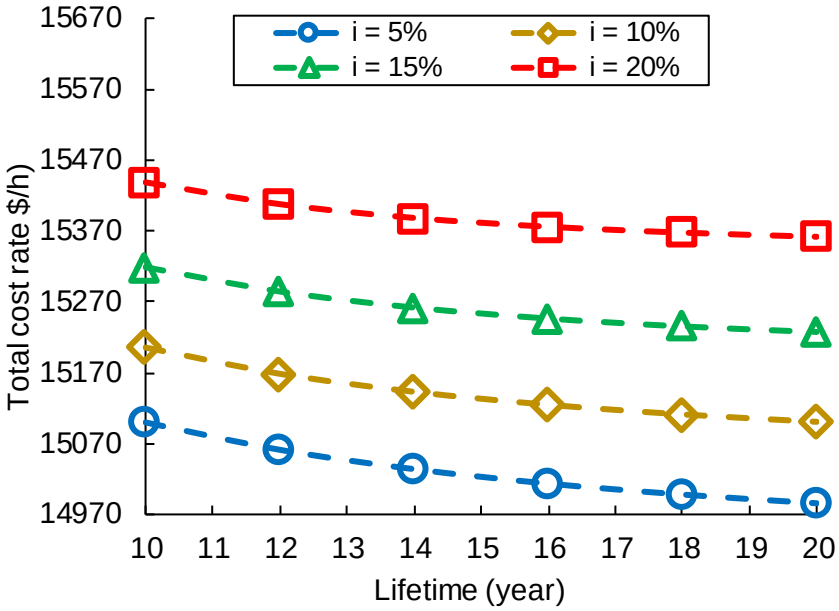

Fig. 5.33. Effect of the lifetime of the cycle on the total cost rate at different interest rates

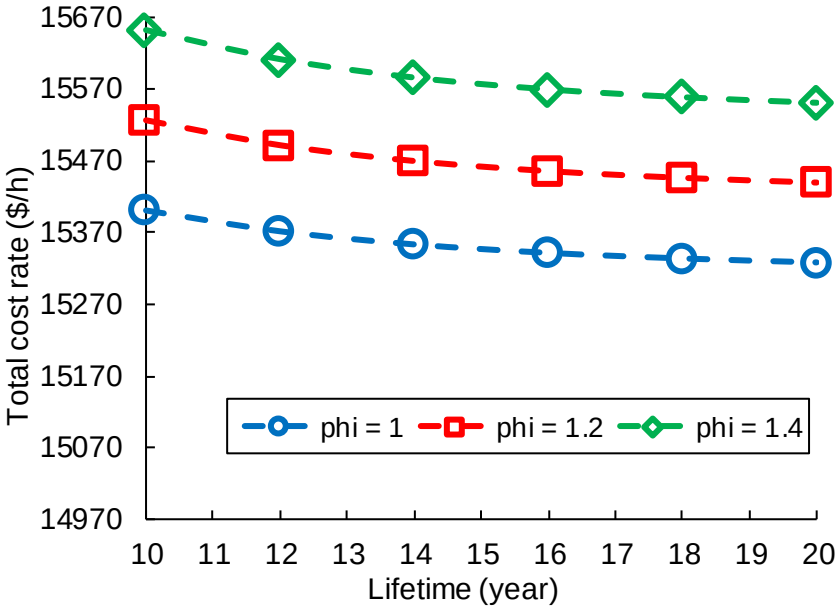

Fig. 5.34. Effect of the lifetime of the cycle on the total cost rate at different operating and maintenance factor values

Figure 5.36 shows the influence of the annual operating time on the hourly levelized capital cost rate of the integrated cycle at different interest rates. The interest rates are varied between 5 and 20% while the annual operating times are varied between 8000 and 9000 hours per year. From the figure, it is seen that the hourly levelized cost reduces as the annual operating time is increased for all interest rate values. The hourly levelized cost at

the minimum considered annual operating time at the minimum interest rate is 360 $/h reducing to 320 $/h at the maximum considered annual operating time. Conversely, the hourly levelized cost at the minimum considered annual operating time at the maximum interest rate is 731 $/h reducing to 650 $/h at the maximum considered annual operating time.

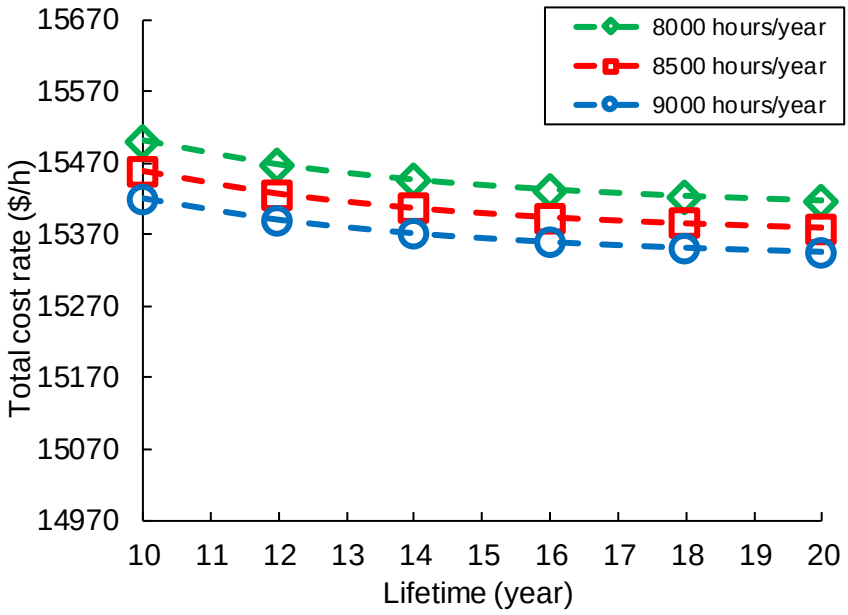

Fig. 5.35. Effect of the lifetime of the cycle on the total cost rate at different annual operating times

Figure 5.37 shows the influence of the operating and maintenance cost factor on the hourly levelized capital cost rate of the integrated cycle at different interest rates. The interest rates are varied between 5 and 20% while the operating and maintenance cost factor is varied between 1.0 and 1.5. From the figure, it is seen that the hourly levelized cost increases as the operating and maintenance cost factor is increased for all interest rate values. The hourly levelized cost at the minimum considered operating and maintenance cost factor at the minimum interest rate is 310 $/h increasing to 465 $/h at the maximum considered operating and maintenance cost factor. Conversely, the hourly levelized cost at the minimum considered operating and maintenance cost factor at the maximum interest rate is 629 $/h increasing to 944 $/h at the maximum considered operating and maintenance cost factor.

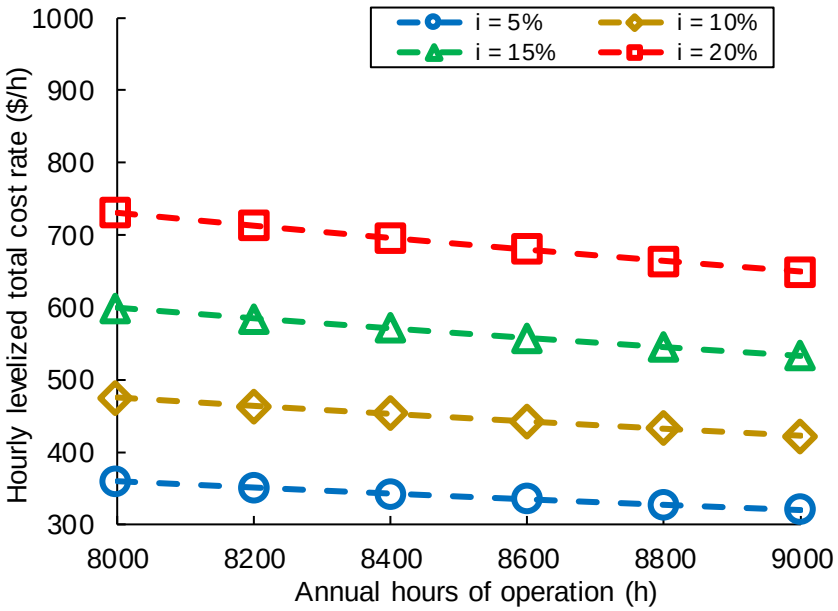

Fig. 5.36. Effect of the annual operating time of the cycle on the hourly levelized total cost rate at different interest rate values

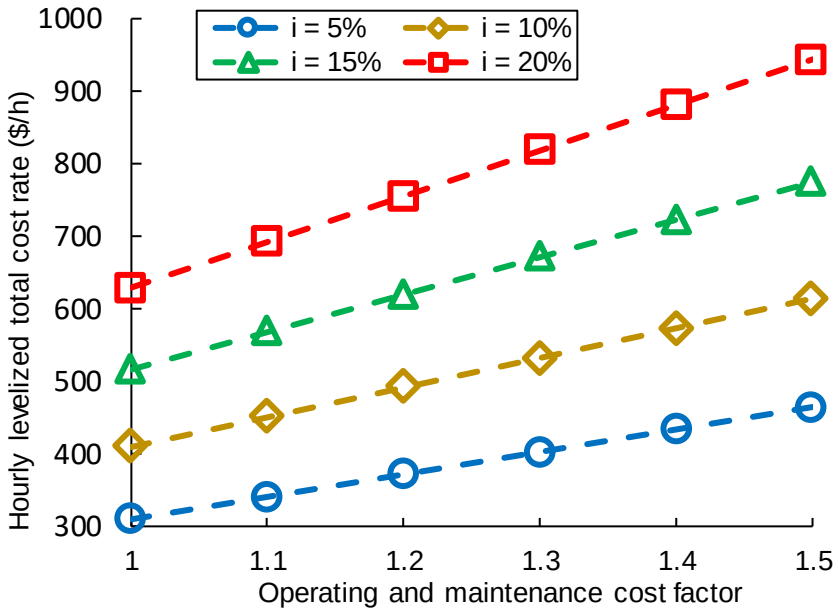

Fig. 5.37. Impact of the operating and maintenance cost factor on the hourly levelized capital cost rate at different interest rate values

Figure 5.38 presents the influence of the decrease in the capital cost of different equipment on their respective total cost rates. The capital cost rate reduction is varied between 10 and 20%. For different equipment, the corresponding percentage decrease in the total cost rate is based on their cost rates of exergy destruction. Among the several equipment, the components for which the total cost rates impact the most are the HCl condensers 2 and 3

due to their low-cost rates of exergy destruction. At the lowest capital cost rate reduction considered, the decrease in the total cost rate is evaluated to be 5 and 4%, respectively for the HCl condensers 2 and 3 while at the maximum capital cost rate reduction considered, the decrease in the total cost rate is evaluated to be 9 and 8% for the respective components.

A comparison of the obtained results in the current analysis with the results of an exergoeconomic study considering a conceptual four-step cycle in [47] is carried out for comparative evaluation purposes. Figure 5.39 shows the variation in the exergoeconomic factor and the total cost rate with respect to the unit cost of electrical energy for both the current analysis and reference [47]. The unit cost of electrical energy is varied between 0.06 and 0.16 $/kWh. For both cases, the total cost rate linearly increases and the exergoeconomic factor non-linearly decreases when the unit cost of electrical energy is increased thereby validating the trends obtained in the current analysis.

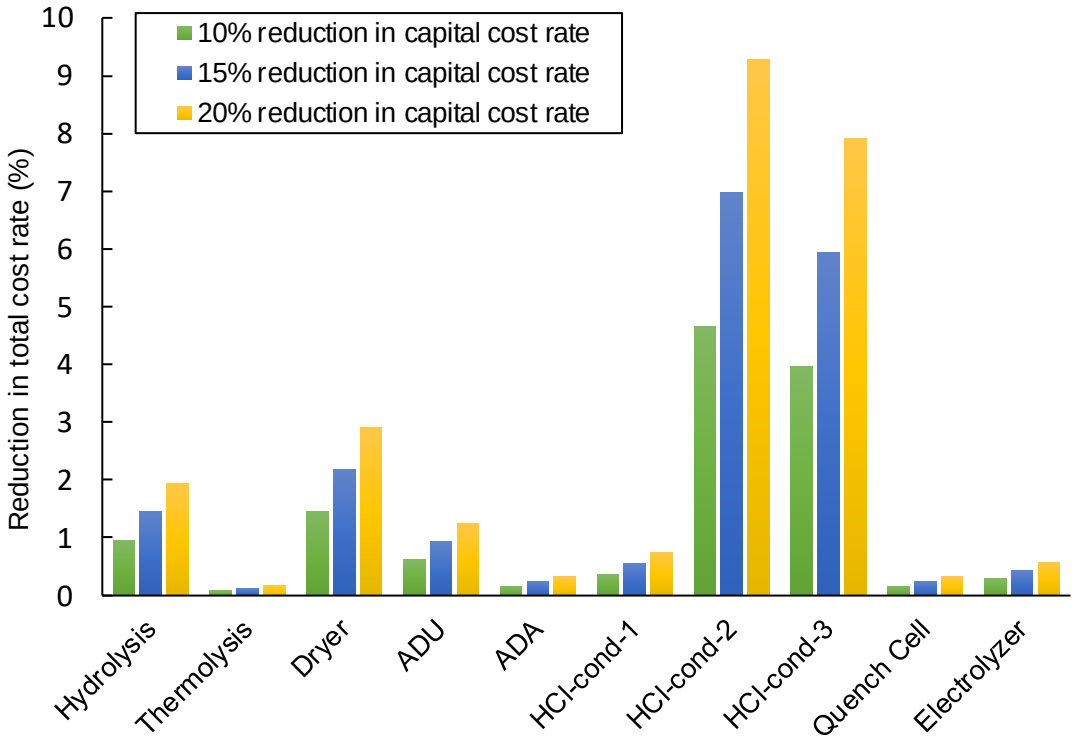

Fig. 5.38. Percentage reduction in the total cost rates of various components due to a decrease in capital cost rates

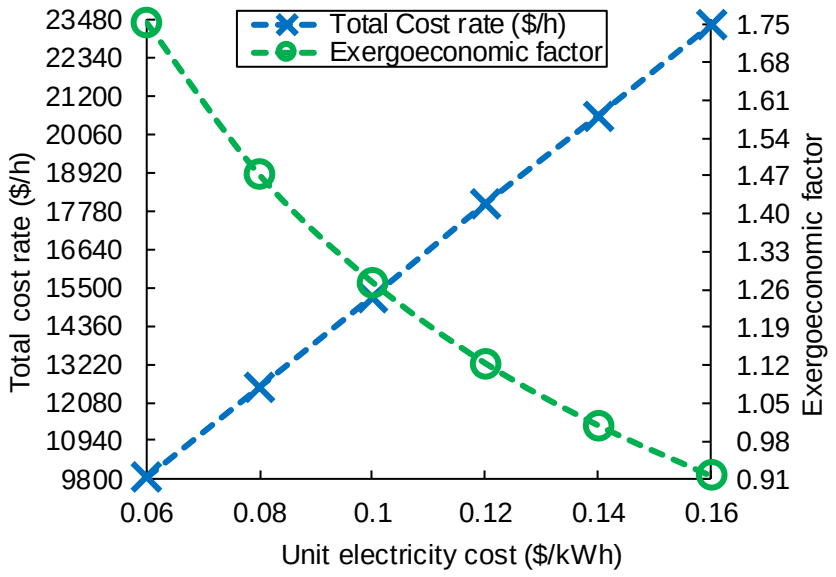

(a)

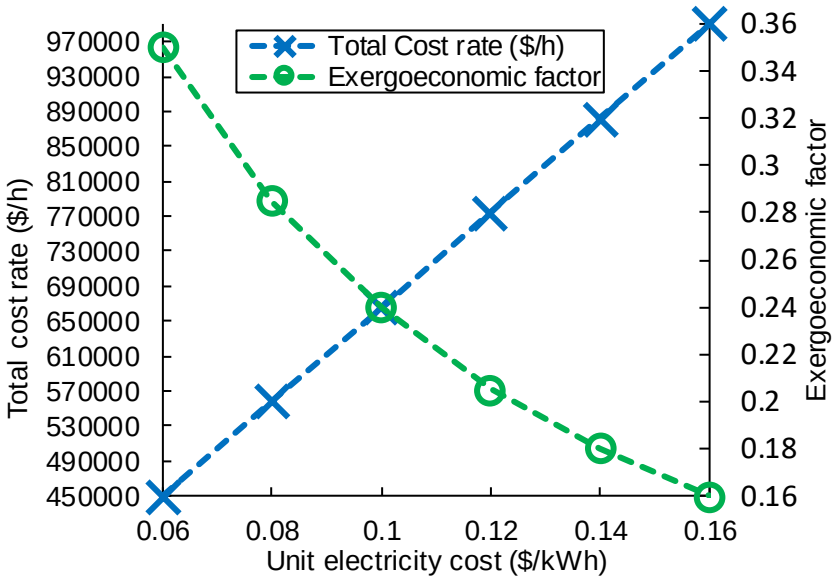

(b)

Fig. 5.39. Effect of the unit cost of electricity on the exergoeconomic factor and the total cost rate in (a) present study and (b) Ozbilen et al. [47]

5.1.5 Exergoenvironmental analysis results

The evaluation of the rate of exergy at each state point for each stream is carried out based on the simulation results of the integrated cycle modeled in Aspen-plus. Three cases are considered in this exergoenvironmental assessment of the integrated Cu-Cl cycle. These cases are termed as the best case, the reference case, and the worst-case scenarios. The criteria for each of these cases are based on the unit environmental impact of thermal and

electrical energies. The unit environmental impact rate of thermal energy is taken as 6 mPt/kWh and the unit environmental impact rate of electrical energy is taken as 22 mPt/kWh for the baseline case from reference [47]. The unit environmental impact rates of thermal and electrical energies for the best-case scenario are assumed as 5 mPt/kWh and 16 mPt/kWh, respectively and for the worst-case scenario as 7 mPt/kWh and 28 mPt/kWh, respectively. The specific and the rate of environmental impact for each exergy stream of the cycle is estimated by applying the environmental impact balance equations given in Table 4.11 and are shown in Table 5.8 for all the three considered cases.

Table 5.8. Environmental and specific environmental impact at each state point of Cu-Cl cycle for the reference, best-case, and worst-case scenarios

Stream	Best case		Reference case		Worst case	
	$\dot{B}$ (Pt/s)	b (mPt/kJ)	$\dot{B}$ (Pt/s)	b (mPt/kJ)	$\dot{B}$ (Pt/s)	b (mPt/kJ)
$CuCl_2$	0	0	0	0	0	0
Water	0	0	0	0	0	0
S1	0.2455	0.0031	0.2947	0.0037	0.3438	0.0044
S2	0.00987	0.0002	0.0118	0.0003	0.0138	0.0003
S3	0.26592	0.0025	0.3182	0.0030	0.3723	0.0035
S4	0.01602	0.0026	0.0192	0.0032	0.0224	0.0037
S5	0.2499	0.0026	0.2990	0.0032	0.3499	0.0037
S6	0.01717	0.0025	0.0206	0.0030	0.0240	0.0035
S7	0.045206	0.0012	0.0542	0.0015	0.0633	0.0017
S8	0.001316	0.0011	0.0016	0.0013	0.0018	0.0015
S9	0.04389	0.0011	0.0526	0.0013	0.0614	0.0016
S10	0.00422	0.0040	0.0049	0.0047	0.00591	0.0056
S11	0.01048	0.0040	0.0124	0.0047	0.0147	0.0056
S12	0.3301	0.0126	0.3801	0.0145	0.4301	0.0165
S13	0.3301	0.0126	0.3801	0.0145	0.4301	0.0165
S14	0.4007	0.0058	0.4648	0.0067	0.5289	0.0076
S15	0.2333	0.0050	0.2706	0.0058	0.3079	0.0066
S16	0.1674	0.0050	0.1942	0.0058	0.221	0.0066
S17	0.2051	0.0027	0.2395	0.0031	0.2738	0.0036
S18	0.2688	0.0003	0.3272	0.0004	0.3853	0.0005
S19	0.1198	0.0028	0.1459	0.0035	0.1718	0.0041
S20	0.149	0.0028	0.1813	0.0035	0.2135	0.0041
S21	0.1564	0.0028	0.1903	0.0033	0.2239	0.0039
S22	0.1225	0.0035	0.1490	0.0043	0.1754	0.0050

S23	0.0339	0.0035	0.0413	0.0043	0.0485	0.0050
S24	0.035	0.0045	0.0424	0.0055	0.0497	0.0065
S25	0.12255	0.0035	0.1491	0.0043	0.1755	0.0050
S26	0.1093	0.0036	0.1329	0.0044	0.1565	0.0051
S27	0.01325	0.0036	0.0161	0.0044	0.0189	0.0052
S28	0.01406	0.0064	0.0169	0.0077	0.0198	0.0091
S29	0.1098	0.0037	0.1334	0.0045	0.157	0.0053
S30	0	0	0	0	0	0
S31	0.03656	0.0054	0.0446	0.0066	0.0525	0.0077
S32	0.07313	0.0054	0.0888	0.0066	0.1045	0.0077
S33	0.10637	0.0040	0.1287	0.0049	0.1511	0.0057
S34	0.04243	0.0027	0.0514	0.0033	0.0603	0.0038
S35	0.06394	0.0027	0.0774	0.0033	0.0908	0.0038
S36	0.06429	0.0053	0.0082	0.0007	0.0913	0.0075
S37	0.0377	0.0011	0.0453	0.0013	0.0528	0.0016
S38	0.0377	0.0011	0.0453	0.0013	0.0528	0.0016
S39	0.05222	0.0018	0.0066	0.0002	0.0741	0.0025
S40	0.01207	0.0018	0.0015	0.0002	0.0172	0.0025
S41	0.04979	0.0325	0.0587	0.0384	0.0676	0.0442

Table 5.9. Environmental impact rate of different components and the associated criteria for different equipment

Equipment	$\dot{Y}$ **(mPt/h)**	**Criteria**
Hydrolysis	0.256	$\dot{m}_{steam}$
Thermolysis	0.0028	$\dot{m}_{Cu2OCl2}$
Dryer (Preheater)	0.00057	A_{PH}
ADU (H5)	0.000094	A_{H5}
ADA (H4)	0.003	A_{H4}
HCl-condenser-1	0.028	$A_{HCl-cond-1}$
HCl-condenser-2	0.0034	$A_{HCl-cond-2}$
HCl-condenser-3	0.0021	$A_{HCl-cond-3}$
Quench cell	0.0053	A_{QC}
Electrolyzer	0.1004	$\dot{W}_{elec}$
$CuCl_2$-concentrator (H7)	0.0125	A_{H7}
PSDU (H3)	0.0164	A_{H3}
Steam condenser	0.0204	A_{SC}
H1	0.023	A_{H1}
H2	0.0014	A_{H2}
H8	0.0105	A_{H8}
Condenser	0.00039	A_{Cond}

Table 5.9 provides the environmental impact rates of numerous equipment of the integrated cycle and the related criteria defined for each of that equipment. The cycle is modeled with a total operational lifetime of 10 years and a total annual operating time of 8766 years according to the economic assessment of the integrated cycle in Aspen-plus. The exergoenvironmental factor and the relative specific environmental impact difference are evaluated and presented in Table 5.10.

Table 5.10. The relative differences of the unit environmental impact and the exergoenvironmental factor for different components for the considered cases

Equipment	Best case		Reference case		Worst case	
	$f_{b,k}$ (%)	$r_{b,k}$	$f_{b,k}$ (%)	$r_{b,k}$	$f_{b,k}$ (%)	$r_{b,k}$
Electrolyzer	9.55E-05	0.361	6.95E-05	0.434	5.46E-05	0.476
HCl-cond-1	1.68E-05	17.79	1.68E-05	20.637	1.68E-05	23.484
HCl-cond-2	0.00018	5.76	0.00018	7.192	0.00018	8.606
HCl-cond-3	0.00012	8.57	0.00012	10.531	0.00012	12.479
Thermolysis	1.13E-06	0.204	9.42E-07	0.203	8.07E-07	0.205
Hydrolysis	0.000269	0.811	0.000224	0.806	0.000192	0.811
ADU	2.13E-06	1.59	1.77E-06	1.625	1.52E-06	1.649
Dryer	2.36E-05	0.266	1.96E-05	0.277	1.68E-05	0.283
Quench Cell	9.24E-06	0.723	7.83E-06	0.718	6.60E-06	0.723
ADA	3.56E-06	1.53	2.96E-06	1.570	2.54E-06	1.592

The equipment-associated and exergy destruction-associated environmental impact rates for the numerous components of the integrated cycle at CERL are presented in Figure 5.40. The exergy destruction associated environmental impact rates are obtained for the three cases considered in this analysis. Since the thermolysis step results in the maximum exergy destruction rate (from the thermodynamic analysis), it also has the highest exergy destruction associated environmental impact rate by virtue of the irreversibilities related to the process. Moreover, there is a considerable impact of the unit thermal and electrical energies on the thermolysis step compared with the other steps/processes of the integrated cycle. In terms of the equipment-associated environmental impact rate, the hydrolysis step results in the highest value since the hydrolysis step involves several equipment, processes the highest flow rates, and operates under high temperatures.

The percentage distribution of the equipment-associated environmental impact rates for all equipment of the integrated cycle is shown in Figure 5.41. Based on the analysis, the steps accounting for the highest shares of the equipment associated environmental impact rates are hydrolysis and electrolysis whereas the processes accounting for the lowest corresponding values include HCl condensers 2 and 3, the ADA, the ADU, the dryer, and the thermolysis step.

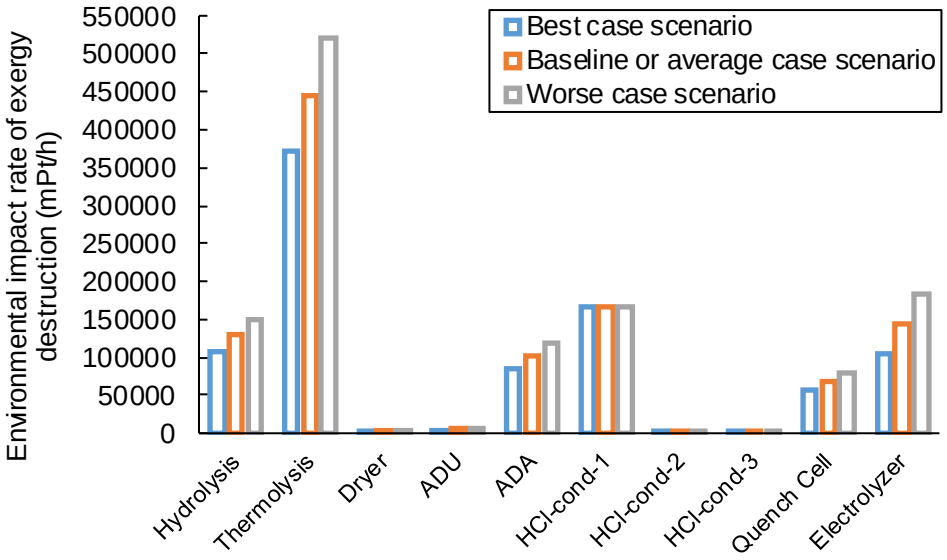

(a)

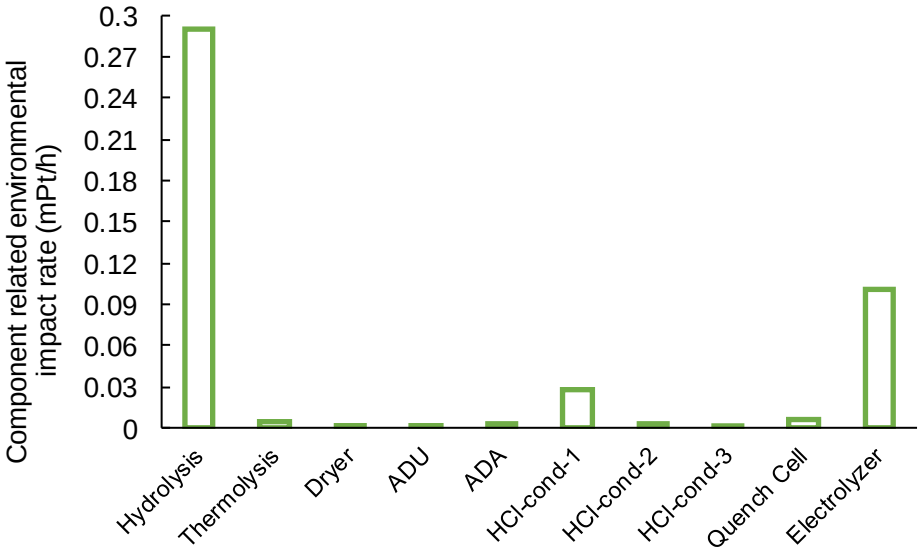

(b)

Fig. 5.40. (a) Environmental impact rates due to exergy destructions for the considered cases and (b) component-associated environmental impact rates for different components

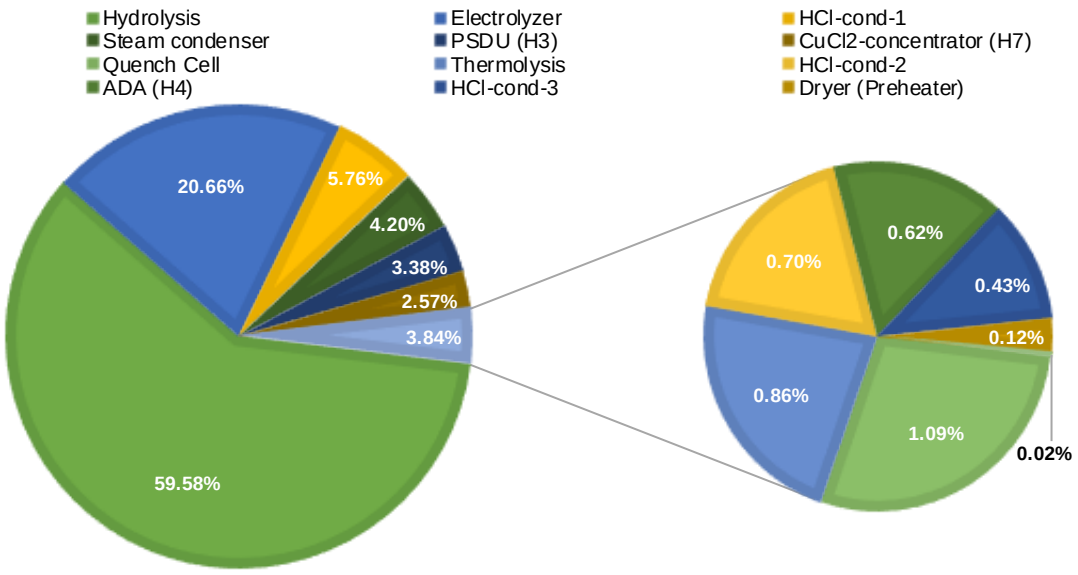

Fig. 5.41. Component-related environmental impact rates in terms of percentages for different components/processes

The percentage distribution of the exergy destruction associated environmental impact rate for all equipment of the integrated cycle for the different cases considered is shown in Figure 5.42. The thermolysis step has the maximum share of the exergy destruction associated environmental impact rate for all the cases (best case: 41.1%, baseline case: 41.8%, worst case: 42.2%). The second-highest share for the best case and the baseline case is of the HCl condenser 1 while the electrolysis step has the second-highest share for only the worst-case scenario.

The influence of the unit environmental impact rate of thermal energy on the exergoenvironmental factor and the cumulative or total environmental impact rate is presented in Figure 5.43. Based on the analysis, the exergoenvironmental factor and the total or cumulative environmental impact rate decreases and increases respectively when the unit thermal energy environmental impact rate is increased from 4 to 12 mPt/kWh. However, the cumulative environmental impact rate increases linearly whereas the exergoenvironmental factor decreases non-linearly. For the minimum unit environmental impact rate of thermal energy, the exergoenvironmental factor and the cumulative environmental impact rate are evaluated to be 0.0008 and 838615 mPt/h, respectively while for the maximum unit environmental impact rate of thermal energy, the

exergoenvironmental factor and the cumulative environmental impact rate are evaluated to be 0.0005 and 1751752 mPt/h, respectively.

The variation in the exergoenvironmental factor due to an increase in the lifetime of the cycle for all considered cases is presented in Figure 5.44. Based on the analysis, the exergoenvironmental factor nonlinearly decreases with an increase in the lifetime of the cycle between 10 and 60 years for every case. For the minimum lifetime of the cycle, the exergoenvironmental factor lies in the range of 0.0006 and 0.00073 for all considered cases while for the maximum lifetime of the cycle, the exergoenvironmental factor lies in the range of 0.00010 and 0.00012.

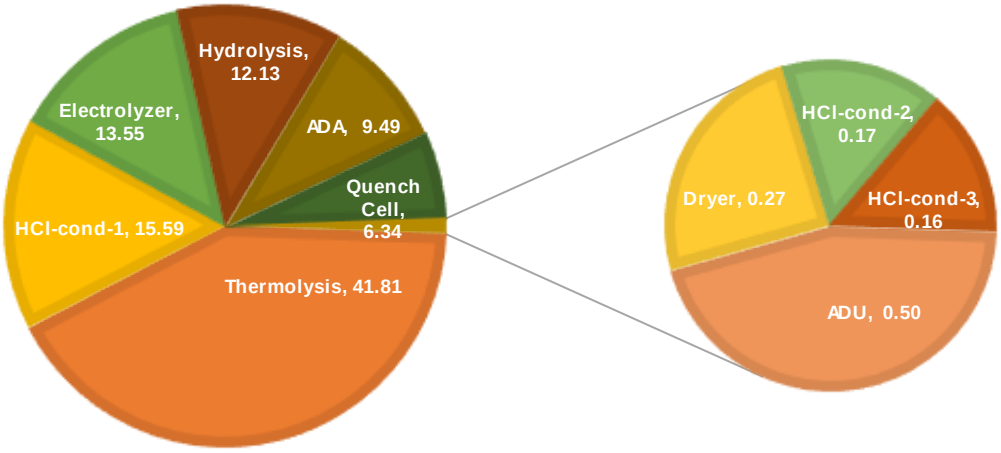

(a)

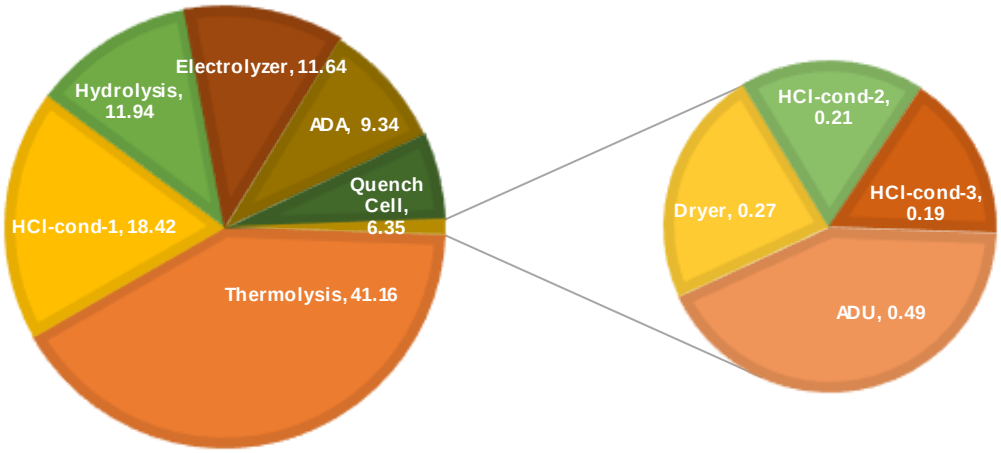

(b)

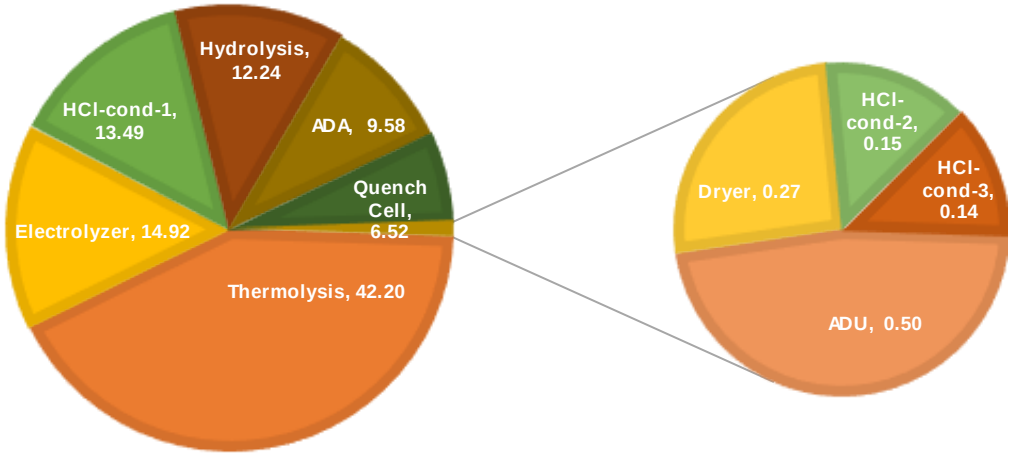

(c)

Fig. 5.42. Percentage distribution of the environmental impact rates associated with the rates of exergy destructions for different components/processes for (a) reference, (b) best-case, and (c) worst-case scenarios

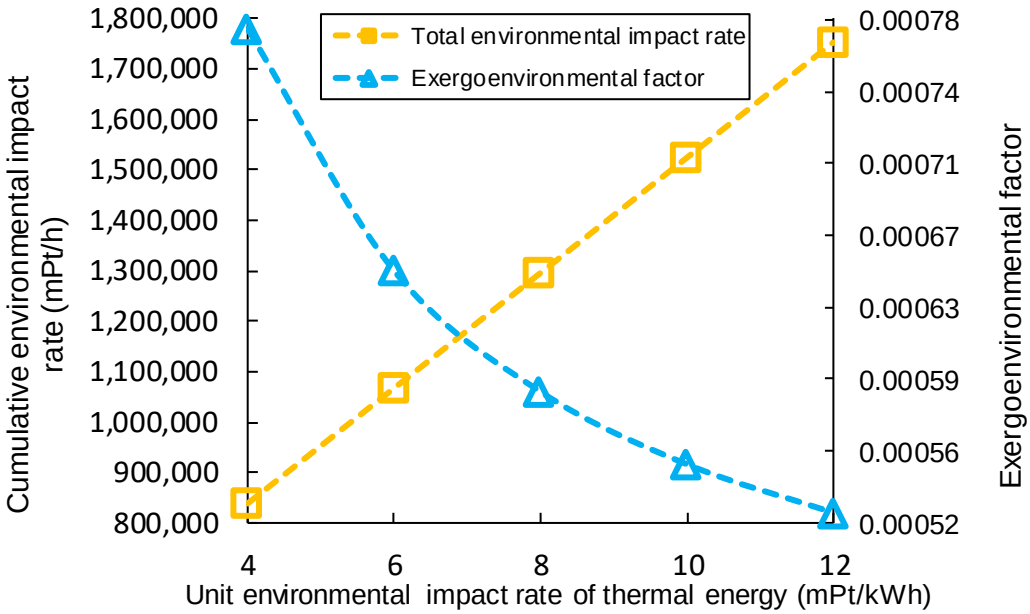

Fig. 5.43. Variation in the exergoenvironmental factor and cumulative environmental impact rates with unit thermal energy environmental impact rates

The impact of the annual operating time of the cycle on the exergoenvironmental factor for all considered cases is shown in Figure 5.45. Similar to Figure 5.44, the exergoenvironmental factor nonlinearly decreases with an increase in the annual operating time of the cycle between 5000 and 9000 hours per year for every case. For the minimum annual operating time of the cycle, the exergoenvironmental factor lies in the range of

0.0010 and 0.0013 for all considered cases while for the maximum annual operating time of the cycle, the exergoenvironmental factor lies in the range of 0.00057 and 0.00071.

The variation in the equipment-associated environmental impact rate due to an increase in the lifetime of the cycle is presented in Figure 5.46. The lifetime of the cycle is varied between 10 and 60 years. Based on the analysis, the equipment-associated environmental impact rate has a nonlinear inverse relationship with the lifetime of the cycle. The equipment-associated environmental impact rate is evaluated to be 0.44 mPt/h at the minimum and 0.07 mPt/h at the maximum lifetime of the cycle.

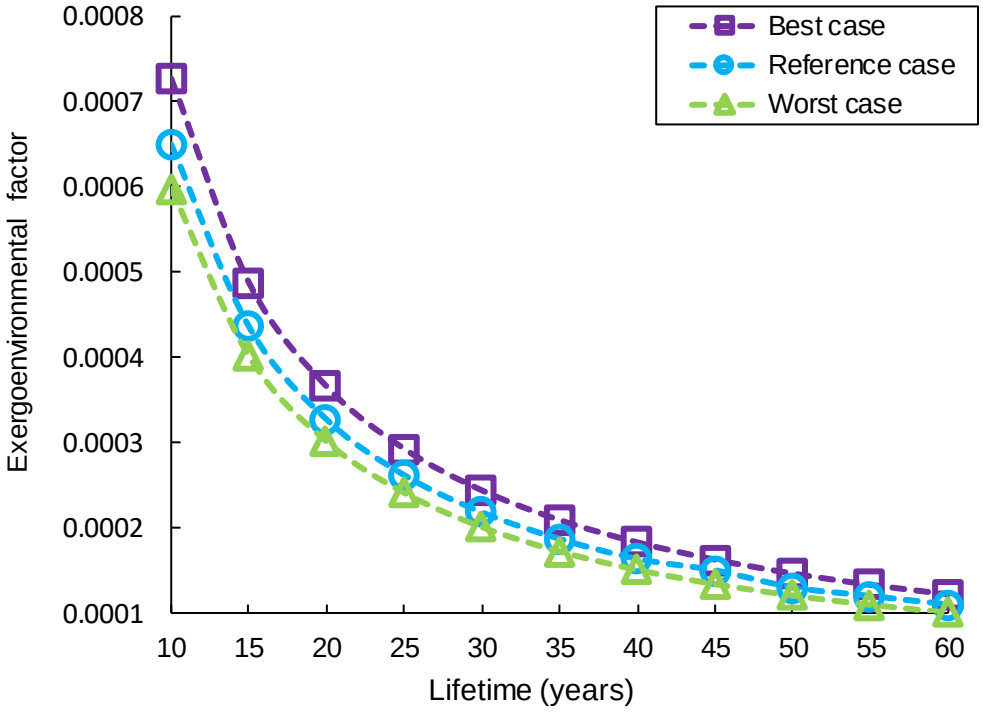

Fig. 5.44. Variation in the exergoenvironmental factor with lifetime for the considered cases

The variation in the equipment-associated environmental impact rate due to an increase in the annual operating time of the cycle is presented in Figure 5.47. The annual operating time of the cycle is varied between 5000 and 9000 hours per year. Based on the analysis, the equipment-associated environmental impact rate has an almost linearly inverse relationship with the annual operating time of the cycle. The equipment-associated environmental impact rate is evaluated to be 0.77 mPt/h at the minimum and 0.43 mPt/h at the maximum annual operating times of the cycle.

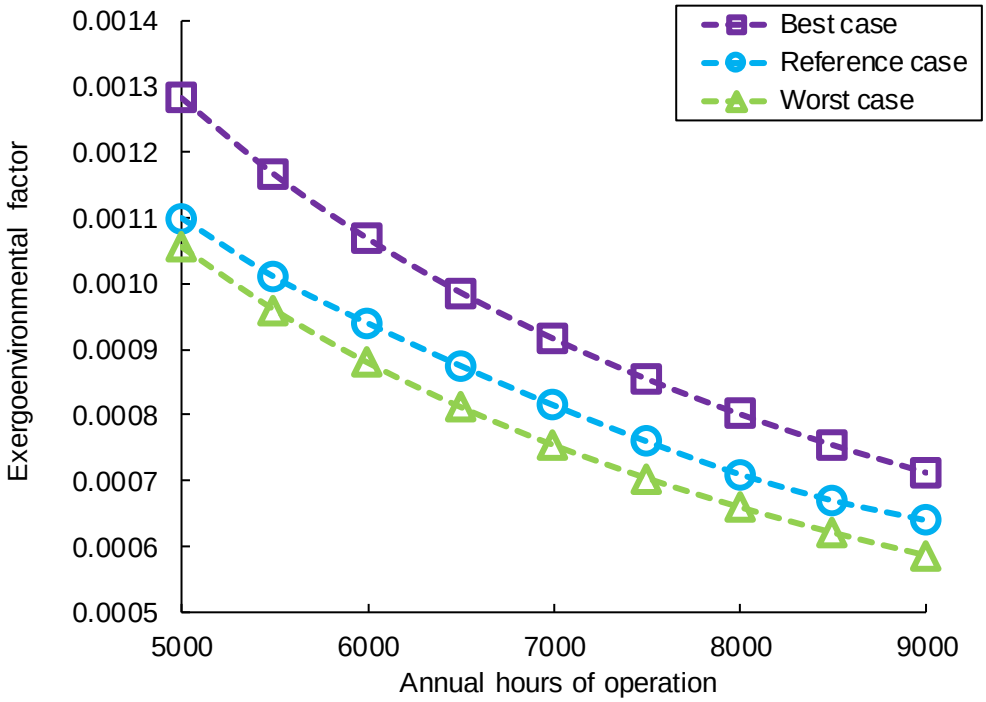

Fig. 5.45. Variation in the exergoenvironmental factor with annual operating time for the considered cases

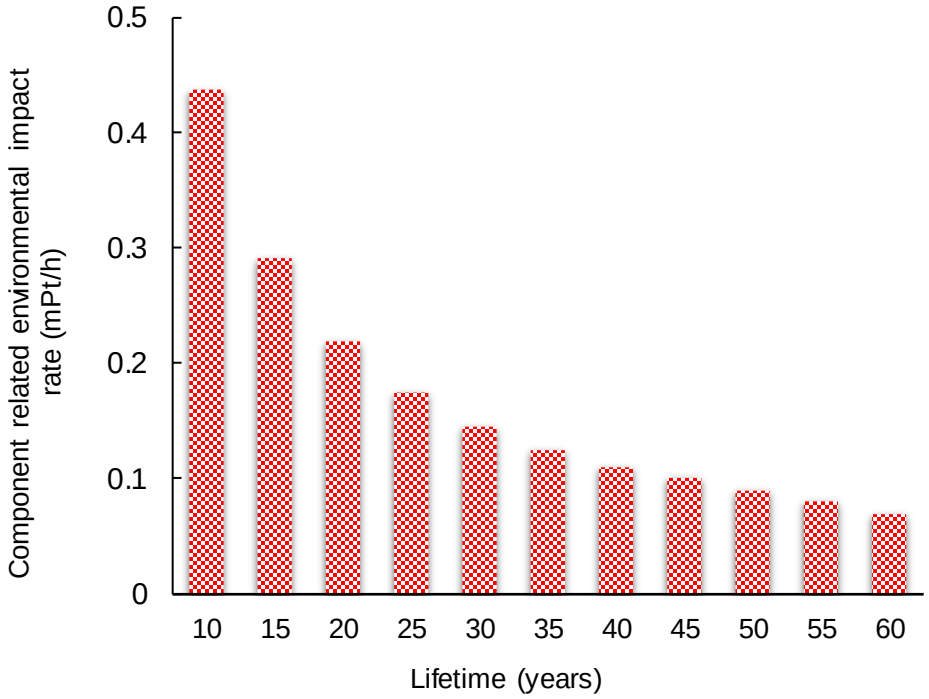

Fig. 5.46. Variation in the component-related environmental impact rates with lifetime

The cumulative or total environmental impact rate and the exergoenvironmental factor for the considered cases for the integrated cycle are shown in Figure 5.48. The cumulative or total environmental impact rate and the exergoenvironmental factor increase and decrease respectively with an increase in the unit thermal and electrical energy environmental impact rates. Between the best and the worst-case scenarios, the exergoenvironmental factor lies in the range of 0.00073 and 0.0006 while the cumulative or total environmental impact rate lies in the range of 903067 and 1233202 mPt/h.

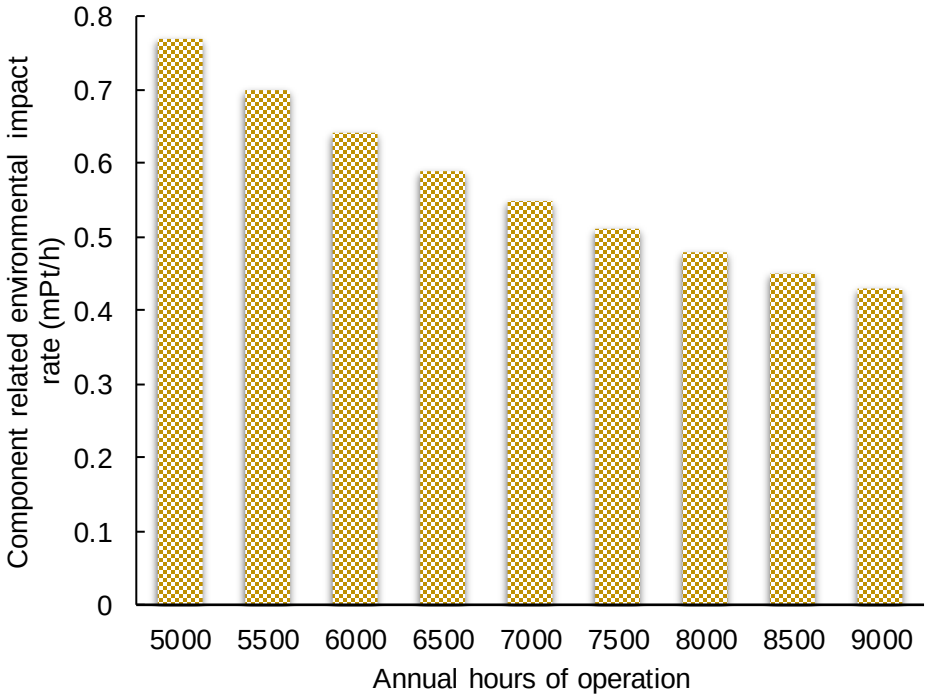

Fig. 5.47. Variation in the component-related environmental impact rates with annual operating time

The impact of the lifetime of the cycle on the cumulative or total environmental impact rate at various annual operating times for all the considered cases in this analysis is presented in Figure 5.49. The lifetime is varied between 10 and 60 years and the annual operating time is varied from 7000 to 9000 hours per year. Increasing both the lifetime and the annual operating time causes a reduction in the cumulative or total environmental impact rate for all cases. The cumulative or total environmental impact rate for the best case at the minimum annual operating time lies in the range of 903067.52 to 903057.40 mPt/h whereas, at the maximum annual operating time, this range lies between 903067.06

and 903067.04 mPt/h. The cumulative or total environmental impact rate for the baseline case at the minimum annual operating time lies in the range of 1066899.24 to 1066899.12 mPt/h whereas, at the maximum annual operating time, this range lies between 1066898.78 and 1066898.76 mPt/h. The cumulative or total environmental impact rate for the worst case at the minimum annual operating time lies in the range of 1233202.39 to 1233202.27 mPt/h whereas, at the maximum annual operating time, this range lies between 1233201.94 and 1233201.91 mPt/h.

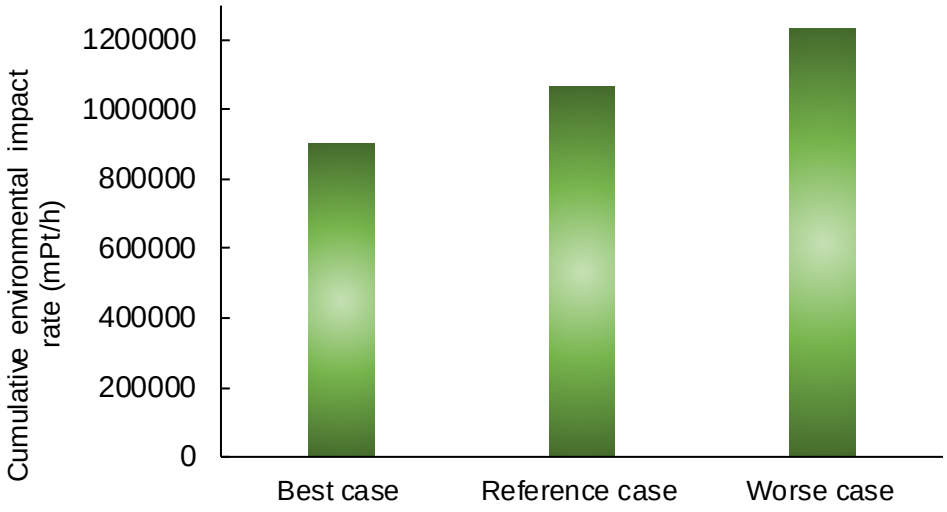

(a)

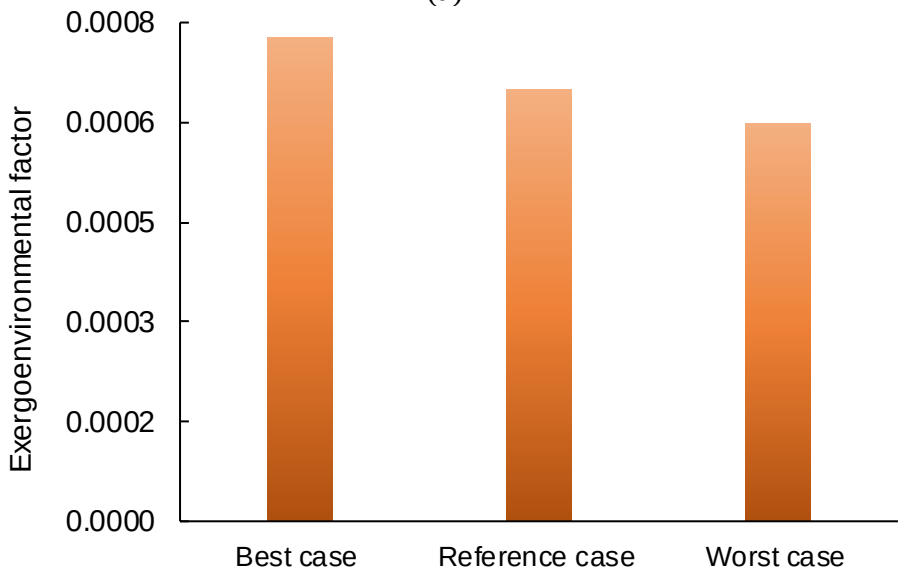

(b)

Fig. 5.48. Variation in the (a) cumulative environmental impact rates and (b) exergoenvironmental factors for the reference, the best-case, and the worst-case scenarios

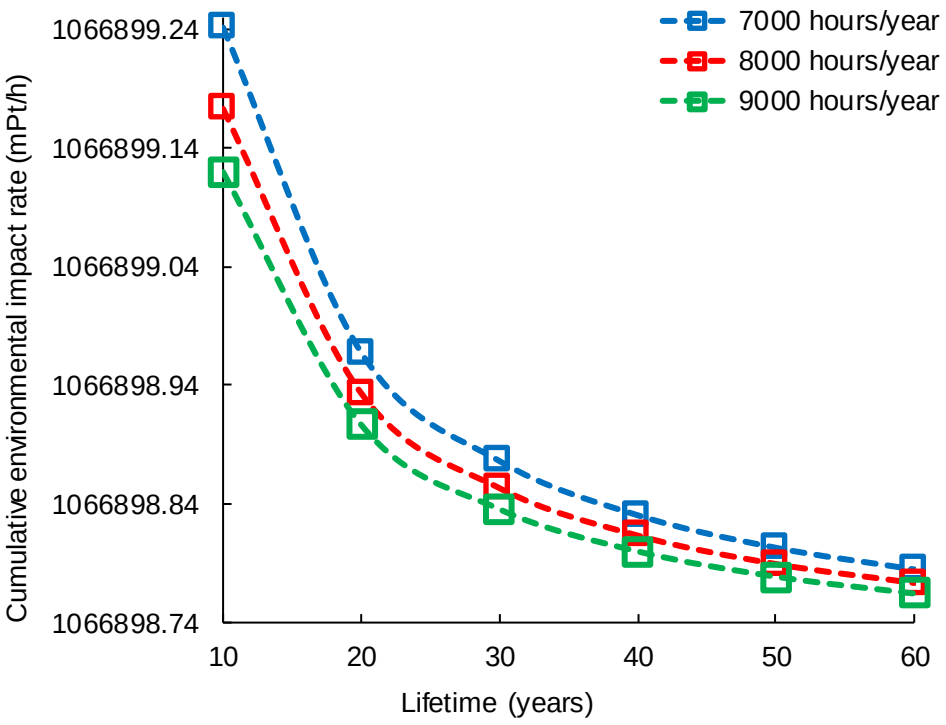
7000 hours/year
8000 hours/year
9000 hours/year
Cumulative environmental impact rate (mPt/h)
1066899.24
1066899.14
1066899.04
1066898.94
1066898.84
1066898.74
10
20
30
40
50
60
Lifetime (years)

(a)

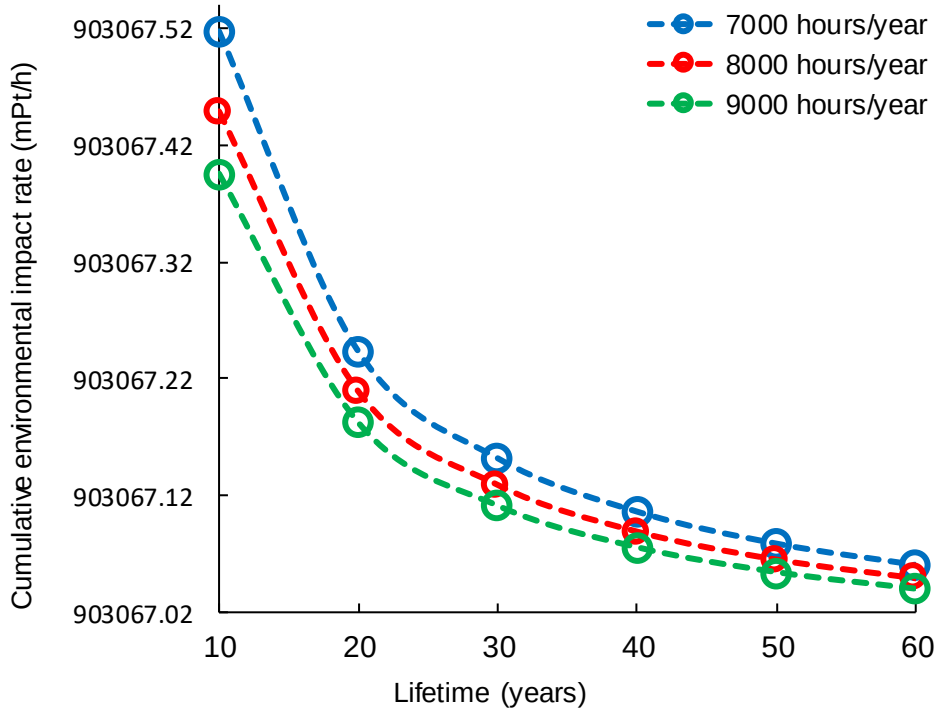
7000 hours/year
8000 hours/year
9000 hours/year
Cumulative environmental impact rate (mPt/h)
903067.52
903067.42
903067.32
903067.22
903067.12
903067.02
10
20
30
40
50
60
Lifetime (years)

(b)

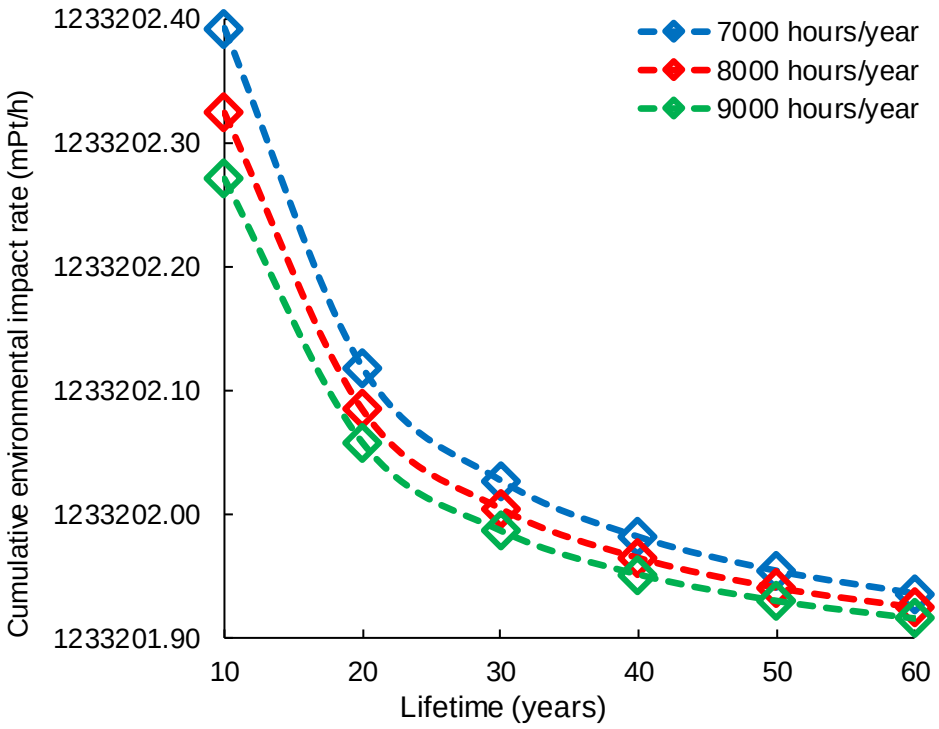

(c)

Fig. 5.49. Variation in the cumulative environmental impact rates with lifetime for the (a) reference, (b) best-case, and (c) worst-case scenarios

The influence of the choice of the electrical energy source on the GWP of the integrated cycle is presented in Figure 5.50. The data for the various sources of electrical energy is taken from [85]. The sources of electricity include both conventional (fossil fuel) and renewable. Between the several electrical energy sources, coal accounts for the highest GWP while wind and nuclear results in the lowest GWP values. Moreover, the conventional sources considering utilizing fossil fuels generally result in higher GWP compared with renewable sources. Fossil fuels assume the leading role in the context of global energy generation and among the different sources, natural gas is the third most exploited choice for power production [86]. Hence, although the Cu-Cl cycle is one of the cleaner ways of thermochemical hydrogen generation, however, the pathway taken to provide the required electricity greatly influences its overall environmental impact.

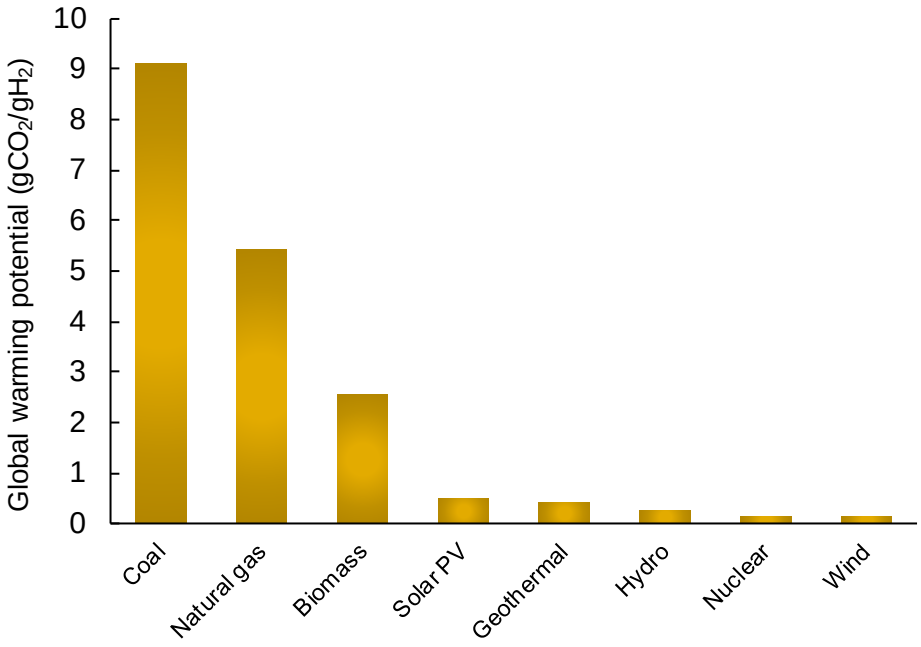

Fig. 5.50. GWP values of hydrogen obtained through different electricity sources via the Cu-Cl cycle

5.1.6 Multi-objective optimization results

The mean square error (MSE) is obtained according to the averaged difference between the squared values of the actual and the ANN outputs in the neural net fitting application. For the better operation of the ANN, low values of MSE are desirable. Moreover, the regression values, ranging between 1 and 0, are extremely essential for the performance of ANN. In this context, values nearer to 0 are undesirable as they are interpreted as random correlation while the values nearer to 1 are most desirable as they are interpreted as closer correlation to the original simulation or experimental data. Figure 5.51 shows the regression graphs obtained for the multi-objective optimization analysis of the integrated cycle exhibiting an extremely good correlation between the predicted and the original data ensured through a gradual increment in the number of hidden layers during the training process via a trial-and-error method. 50 hidden layers are selected as the optimum number for the present multi-objective optimization analysis. The results for the different considered optimization cases are discussed as follows.

Figure 5.52 shows the *Pareto Frontier* solution of all the optimized points and the trade-off values for case 1 of the multi-objective optimization analysis of the integrated cycle.

The point showing the minimum values of heat cost rate and hydrogen generation rate and the maximum value of exergy efficiency is referred to as point "A" while point "B" refers to the point showing the maximum heat cost rate and hydrogen generation rate and the minimum exergy efficiency value. Point A is considered the best solution when heat cost rate and exergy efficiency are the only optimization objectives. On the contrary, point B is considered the best solution when hydrogen generation rate is the only optimization objective. The trade-off point labeled as point "C" is the point where all objective functions intersect with each other which is the foundation of a multi-objective optimization problem. Table 5.11 provides the values of the decision variables and objective functions for points A, B, and the trade-off point C provided in Figure 5.52. The objective function values for point C pertaining to case 1 are 8.1%, 223 $/h, and 3.4 kg/h respectively for exergy efficiency, heat cost rate, and hydrogen generation rate at a S/Cu ratio of 16.3 and a feed steam input temperature of 25ºC.

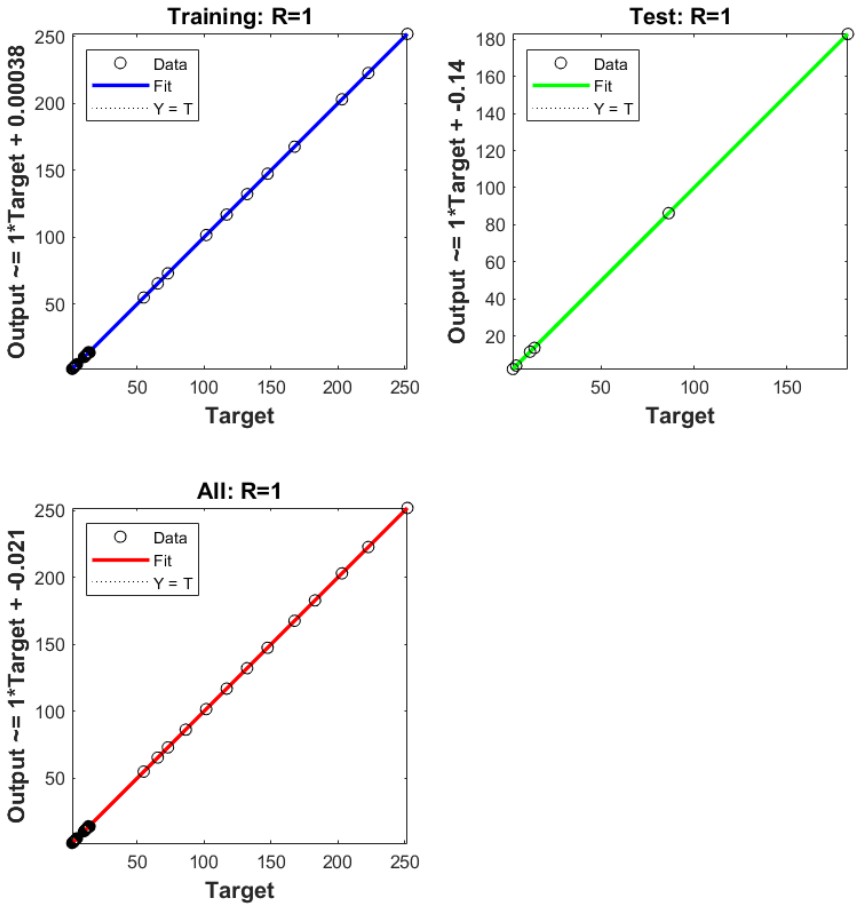

Fig. 5.51. Neural Network training regression graphs using 50 hidden layers

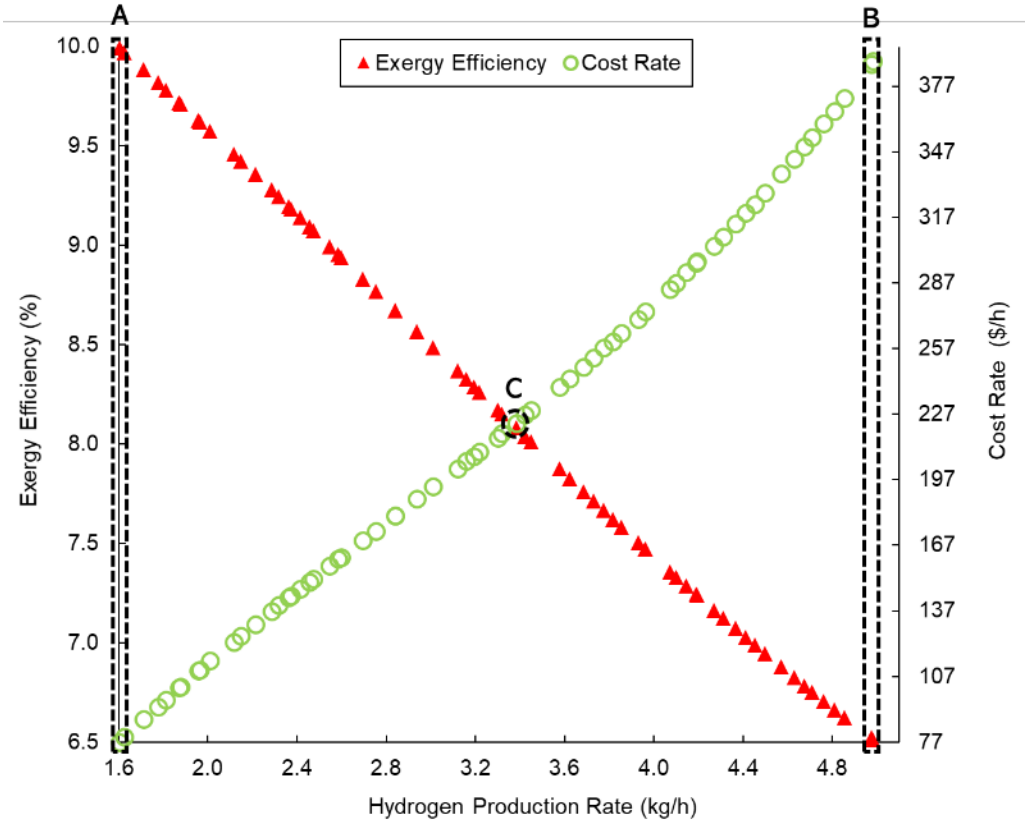

Fig. 5.52. Case 1: Trade-off values of objective functions shown through the Pareto frontier solution

Table 5.11. Case 1: Values of decision variables and objective functions for points A, B, and C

Points		**A**	**B**	**C**
Objective functions	$\dot{m}_{H_2}$(kg/h)	1.6	5	3.4
	ψ (%)	10	6.5	8.1
	$\dot{C}$ ($/h)	77.1	387.1	223
Decision variables	S/Cu	10.7	22.9	16.3
	T_{steam}(°C)	25	25	25
	$\dot{Q}_{net,in}$(kW)	771.3	3848.1	2188.5

Figure 5.53 shows the *Pareto Frontier* solution of all the optimized points and the trade-off values for case 2 of the multi-objective optimization analysis of the integrated cycle. Table 5.12 provides the values of the decision variables and objective functions for points A, B, and the trade-off point C provided in Figure 5.53. The objective function values for point C pertaining to case 2 are 12.1%, 149 $/h, and 3.4 kg/h respectively for exergy

efficiency, heat cost rate, and hydrogen generation rate at a S/Cu ratio of 16.7 and a feed steam input temperature of 100ºC.

Figure 5.54 shows the *Pareto Frontier* solution of all the optimized points and the trade-off values for case 3 of the multi-objective optimization analysis of the integrated cycle. Table 5.13 provides the values of the decision variables and objective functions for points A, B, and the trade-off points C_1 and C_2 provided in Figure 5.54. The objective function values for point C_1 pertaining to case 3 are 12.5%, 148 $/h, and 3.5 kg/h respectively for exergy efficiency, heat cost rate, and hydrogen generation rate at a S/Cu ratio of 16.5 and a feed steam input temperature of 200ºC. The objective function values for point C_2 pertaining to case 3 are 12.3%, 157 $/h, and 3.6 kg/h respectively for exergy efficiency, heat cost rate, and hydrogen generation rate at a S/Cu ratio of 16.9 and a feed steam input temperature of 200ºC.

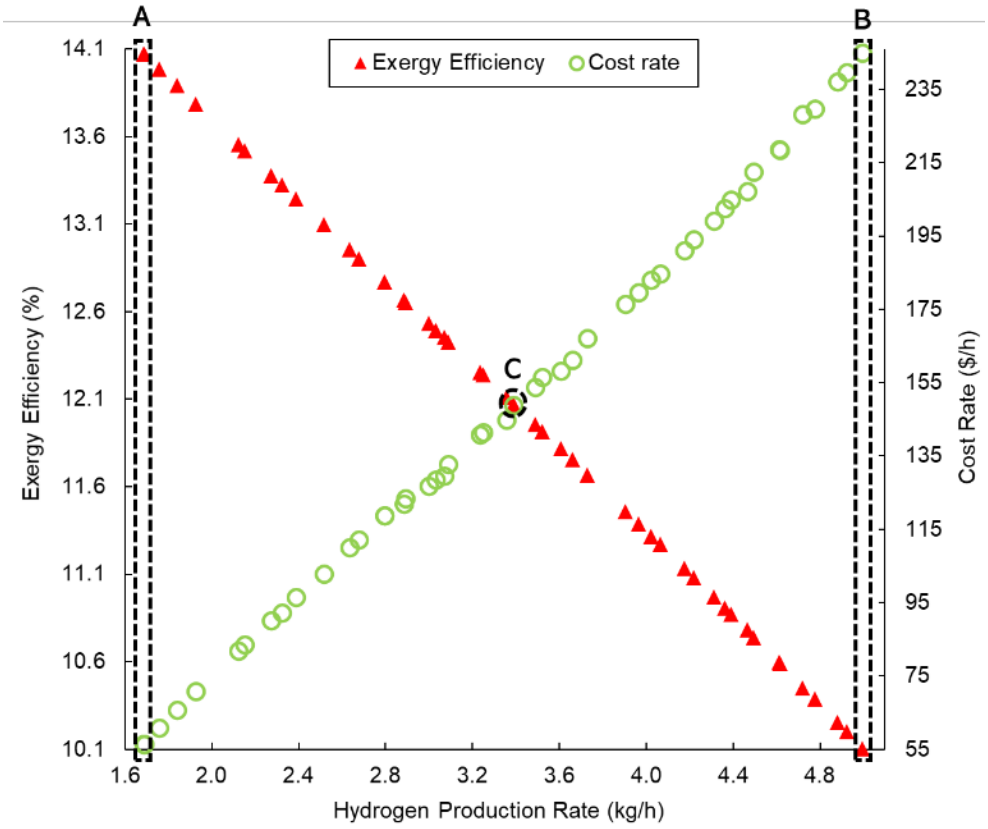

Fig. 5.53. Case 2: Trade-off values of objective functions shown through the Pareto frontier solution

Table 5.12. Case 2: Values of decision variables and objective functions for points A, B, and C

Points		A	B	C
Objective functions	$\dot{m}_{H_2}$(kg/h)	1.7	5.0	3.4
	ψ (%)	14.1	10.1	12.1
	$\dot{C}$ ($/h)	56.4	245	148.8
Decision variables	S/Cu	10.7	22.9	16.7
	T_{steam}(°C)	100	100	100
	$\dot{Q}_{net,in}$(kW)	564.6	2485.1	1506.9

Figure 5.55 shows the *Pareto Frontier* solution of all the optimized points and the trade-off values for case 4 of the multi-objective optimization analysis of the integrated cycle. Table 5.14 provides the values of the decision variables and objective functions for points A, B, and the trade-off point C provided in Figure 5.55. The objective function values for point C pertaining to case 4 are 14.7%, 122 $/h, and 3.3 kg/h respectively for exergy efficiency, heat cost rate, and hydrogen generation rate at a S/Cu ratio of 15.7 and a feed steam input temperature of 300°C.

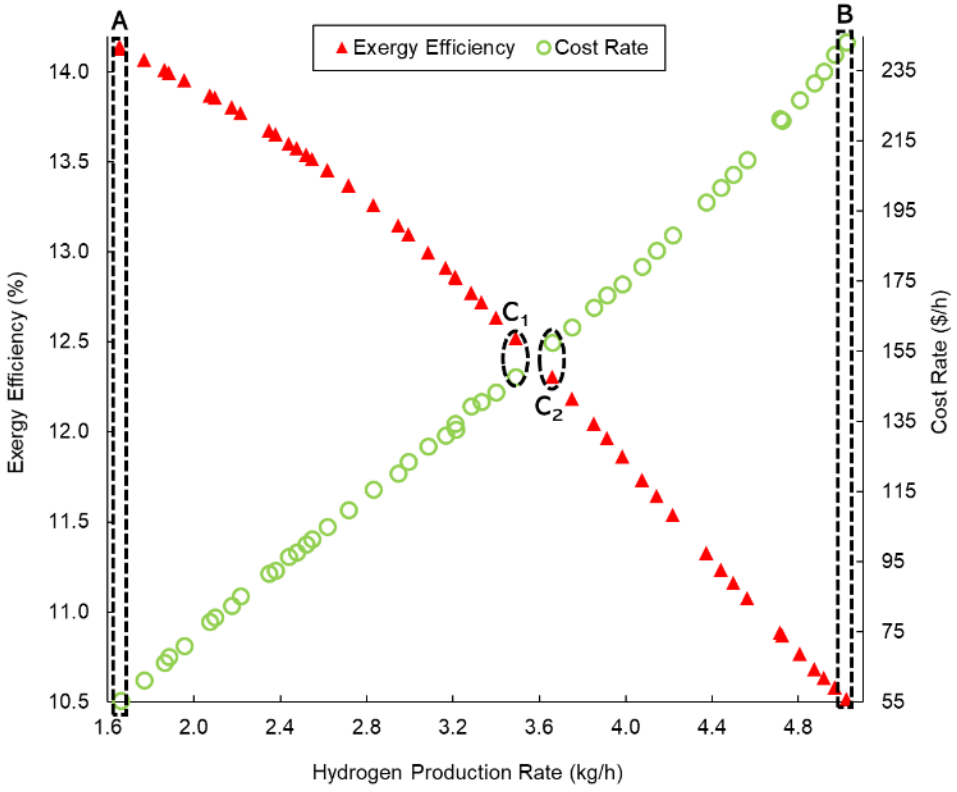

Fig. 5.54. Case 3: Trade-off values of objective functions shown through the Pareto frontier solution

Table 5.13. Case 3: Values of decision variables and objective functions for points A, B, C_1, and C_2

Points		A	B	C_1	C_2
Objective functions	$\dot{m}_{H_2}$(kg/h)	1.6	5.02	3.49	3.66
	ψ (%)	14.1	10.5	12.5	12.3
	$\dot{C}$ ($/h)	54.9	243.2	147.8	157.5
Decision variables	S/Cu	10.7	22.9	16.5	16.9
	T_{steam}(°C)	200	200	200	200
	$\dot{Q}_{net,in}$(kW)	549.3	2468.6	1497.7	1596

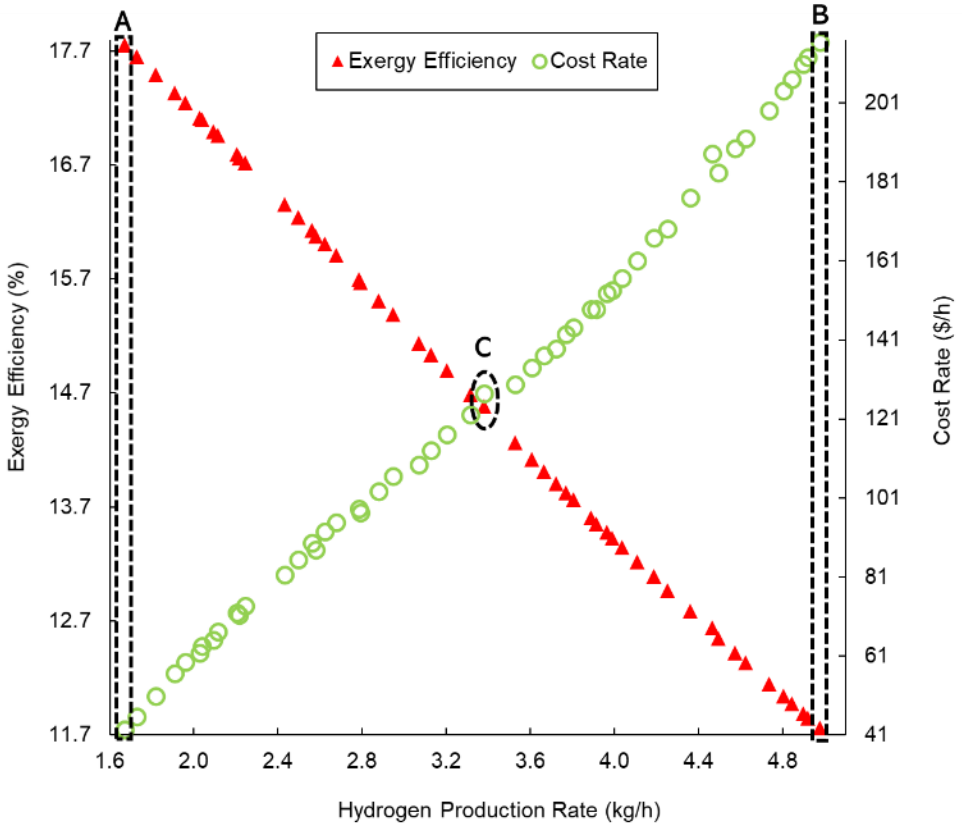

Fig. 5.55. Case 4: Trade-off values of objective functions shown through the Pareto frontier solution

For the various optimization cases considered and their obtained results as shown in Table 5.11 through 5.14 and Figures 5.52 through 5.55, the S/Cu ratios of the optimized points for all cases range from 15.7 to 16.9. The rate of hydrogen generation does not vary considerably for all cases. The feed steam temperature substantially influences the heat cost rates and exergy efficiencies. When feed for the cycle is considered at ambient temperature, the exergy efficiency lies between 6.5 and 10%. However, these ranges significantly change with consideration of feed steam at higher temperatures. When the

feed steam temperature is considered between 100 and 300ºC, the exergy efficiency is found to lie between 10.1 and 17.8%. The range for heat cost rate is also influenced by the feed stream temperature. When feed for the cycle is considered at ambient temperature, the heat cost rate lies between 77 and 387 $/h. However, when the feed steam temperature is considered between 100 and 300ºC, the heat cost rate is found to lie between 42 and 216 $/h.

Table 5.14. Case 4: Values of decision variables and objective functions for points A, B, and C

Points		**A**	**B**	**C**
Objective functions	$\dot{m}_{H_2}$(kg/h)	1.67	4.98	3.32
	ψ (%)	17.8	11.8	14.7
	$\dot{C}$ ($/h)	42.4	216.4	122
Decision variables	S/Cu	10.7	22.8	15.7
	T_{steam}(ºC)	300	300	300
	$\dot{Q}_{net,in}$(kW)	424.1	2117.3	1203.1

A comparison of the current multi-objective optimization analysis with reference [67] is carried out in terms of percentage decrease or increase for the reference scenarios considered in each study and the results are provided in Table 5.15. In the context of single-objective optimization in [67], a reduction in total heat cost rate and an increase in the exergy efficiency of 33 and 3.3%, respectively is attained. Conversely, in the context of multi-objective optimization in [67], a reduction in total heat cost rate and a simultaneous increase in the exergy efficiency of 4.5 and 0.8%, respectively is achieved. In the present multi-objective optimization analysis, case 1, where feed is provided at ambient temperature, is considered the baseline case. Therefore, for case 2, a reduction in total cost rate and a simultaneous increase in the exergy efficiency of 33.2 and 49.3%, respectively is attained. For case 3, a reduction in total heat cost rate and a simultaneous increase in the exergy efficiency of 33.7 and 54.3%, respectively is realized. For case 4, a reduction in total heat cost rate and a simultaneous increase in the exergy efficiency of 45.3 and 81.4%, respectively is realized. There is no noticeable change in the rate of hydrogen generation for all cases. Among the four optimization scenarios, realizing steam input at the highest temperature of 300ºC significantly optimizes the overall performance of the cycle.

Table 5.15. Comparison of optimization results between the present study and ref. [67]

O. F.	Reference [67]			Present study		
	Exergy-based opt.	**Cost-based opt.**	**Exergoeconomic multi-objective opt.**	**Case 2**	**Case 3**	**Case 4**
ψ (%)	3.3% ↑ w.r.t base case	-	0.8% ↑ w.r.t base case	49.3% ↑ w.r.t case 1	54.3% ↑ w.r.t case 1	81.4% ↑ w.r.t case 1
$\dot{C}$ ($/h)	-	33% ↓ w.r.t base case	4.5% ↓ w.r.t base case	33.2% ↓ w.r.t case 1	33.7% ↓ w.r.t case 1	45.3% ↓ w.r.t case 1

Figure 5.56 provides a comparison of the rate of hydrogen generation, exergy efficiency, and heat cost rate against the S/Cu ratio between the optimization data achieved from MATLAB and the simulation data of Aspen-plus. The comparison is carried out only for case 1 where feed is provided to the cycle at ambient temperature for validation purposes. The proximity between the data sets of the Aspen-plus and the MATLAB suggests a close and acceptable correlation with each other. The heat cost rate, exergy efficiency, and hydrogen generation rate for the S/Cu ratios of 10.7, 16.3, and 22.9 achieved through the MATLAB optimization and the Aspen-plus simulation data are compared and shown in Table 5.16. The highest percentage difference between the compared data are 2.3, 6.5, and 14.5% corresponding to the exergy efficiency, the rate of hydrogen generation, and the heat cost rate.

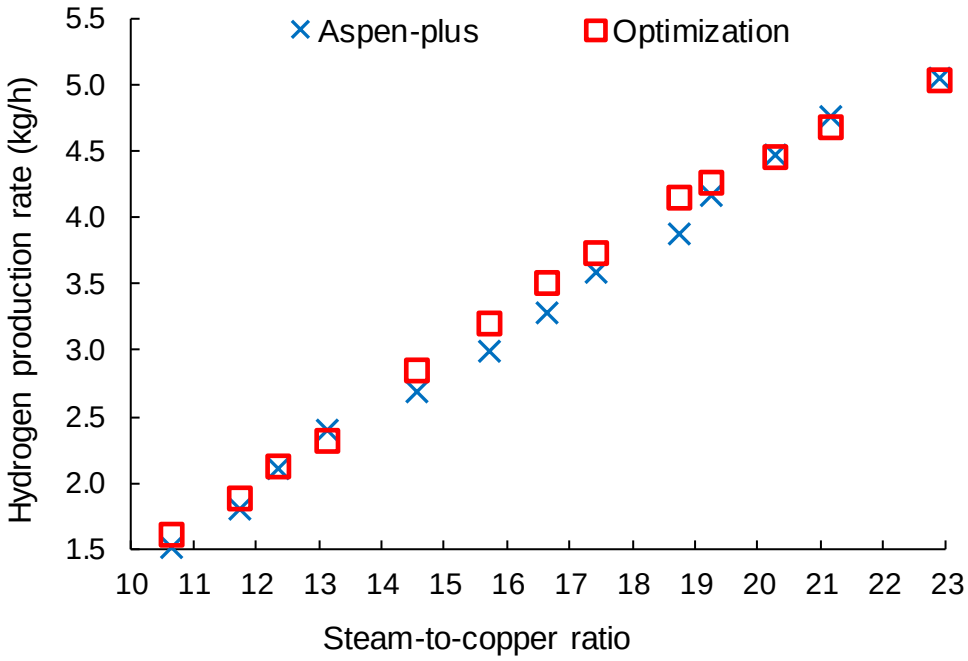

(a)

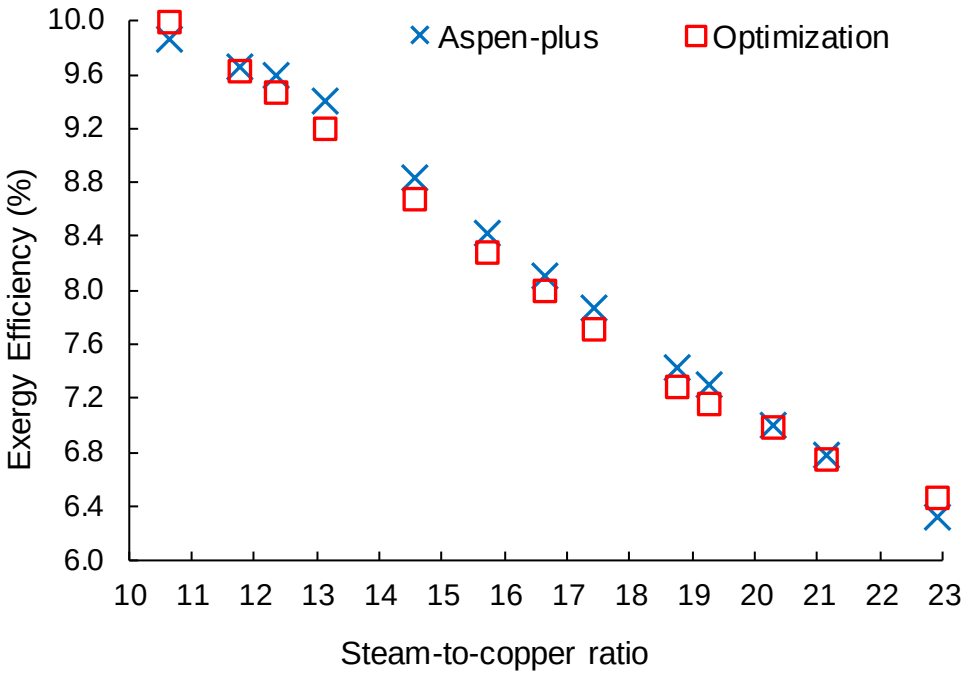

(b)

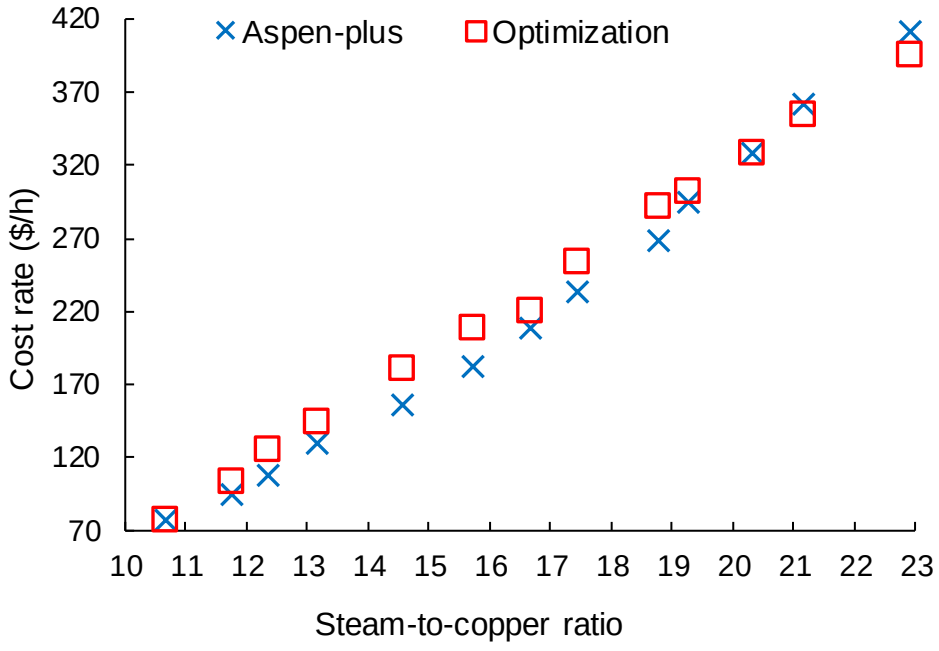

(c)

Fig. 5.56. Comparison of optimization results obtained through MATLAB and Aspen-plus simulations for variation in (a) rate of hydrogen production, (b) exergy efficiency, and (c) heat cost rate with respect to S/Cu

Table 5.16. Comparison between the MATLAB and the Aspen-plus simulation results for the objective function values

S/Cu	$\dot{m}_{H_2}$(kg/h)		ψ (%)		$\dot{C}$ ($/h)	
	Aspen-plus	MATLAB	Aspen-plus	MATLAB	Aspen-plus	MATLAB
10.7	1.5	1.6	9.9	10	77.1	77.1
16.3	3.2	3.4	8.0	8.1	205	223
22.9	5.1	5.0	6.3	6.5	411	395

5.2 Modeling results of the cycle conceptually modified with flash vaporization

This section presents the modeling results for the cycle conceptually modified such that the anolyte separation step is realized through the flash vaporization process. The modeling results of the modified cycle correspond to the energy and exergy analyses, thermal management, exergoeconomic analysis, exergoenvironmental analysis, and the comparative assessment of the modified cycle with respect to the actual integrated cycle at CERL.

5.2.1 Energy and exergy analyses results

The energy and exergy analyses results obtained through the modeling of the integrated cycle conceptually modified with the flash vaporization process simulated in Aspen-plus are discussed in this section. A comparison of the energy and exergy analyses results for the modified integrated cycle is carried out with the actual integrated cycle at CERL for cycle efficiencies, the overall rate of exergy destruction, the net rate of heat input and discharge, and rates of exergy destruction and heat input pertaining to the anolyte separation step. In this context, the various performance parameters are evaluated based on the state properties obtained at all state points of the modified integrated cycle which are presented in Table 5.17.

Based on the thermodynamic evaluation, the rates of exergy destructions for the numerous components of the modified integrated cycle is presented in Figure 5.57. According to the obtained data, the components with the minimum rates of exergy destructions are the heat exchanger-2 and the dryer unit while the components with the maximum rates of exergy destructions include the thermolysis and hydrolysis steps and the HCl-condenser.

The net rate of heat input and discharge for the modified and the actual integrated cycles are compared in Figure 5.58. Based on the obtained results, between the two cycles, the modified cycle is evaluated to have lower net heat input and discharge rates due to the substitution of the two energy-intensive components of the actual integrated cycle (the ADA and the ADU) with relatively less energy-intensive components including the pump, the heat exchanger, the flash chamber, and the expansion or throttling valve. The modified cycle also results in a lower net heat discharge rate since some of the condensers of the actual integrated cycle are removed.

The rate of the overall exergy destruction in the modified and the actual integrated cycles are compared in Figure 5.59. Based on the evaluated data, between the two cycles, the modified cycle accounts for the lower rate of the overall exergy destruction since some of the components of the actual cycle result in higher exergy destruction rates including the HCl-condensers 2 and 3, the steam condenser, the ADA, and the ADU are removed and substituted with certain components with lower process irreversibilities.

Table 5.17. Thermodynamic data at all state points of the modified cycle

Stream	$\dot{m}$ **(kg/s)**	T **(°C)**	P **(bar)**	h **(kJ/kg)**	ex **(kJ/kg)**
1	100	25	1	-15864.3	50.0
2	100	400	1	-12690.9	785.7
3	60	25	1	-1531.0	610.6
4	60	400	1	-1318.3	686.5
5	160	400	1	-8341.5	660.9
6	48	400	1	-1681.5	126.8
7	112	400	1	-11174.5	840.1
8	48	530	1	-1653.7	143.3
9	48	530	1	-981.6	772.9
10	4	530	1	498.0	333.2
11	44	530	1	-1101.2	895.8
12	44	45	1	-15948.3	52.8
13	44	45	1	-15321.9	131.2
W-in	20	5	1	-13823.0	232.8
W-out	20	100	1	-13859.2	258.1
14	112	50	1	-11734.1	644.3
15	112	50	1	-13271.0	541.8
16	112	106	1	-6531.0	1300.9
17	86	106	1	-4428.3	1072.9
18	26	106	1	-4577.1	11338.3

19	70	83	1	286.1	117159.3
20	70	45	1	-4613.9	752.1
21	0.4	45	1	-8341.5	660.9
22	69.6	45	1	-1681.5	126.8
23	69.6	51	2	-3504.9	636.7
24	69.6	102	2	-3393.3	655.0
25	69.6	52	0.2	-3393.3	635.6
26	6.7	52	0.2	-8106.2	1165.3
27	62.9	52	0.2	-2887.4	579.5
28	40	25	1	-15864.3	50.0
29	8.8	32	1	-1391.3	769.8
30	94.1	32	1	-8540.5	336.2
31	94.1	110	1	-7257.8	580.7
32	32.3	110	1	-13260.3	543.9
33	61.8	110	1	-4121.5	599.9
34	61.8	130	1	-4104.4	604.1
35	13.8	130	1	-13225.4	552.7
36	48	130	1	-1473.6	618.9
17-1	86	100	1	-13361.0	523.7

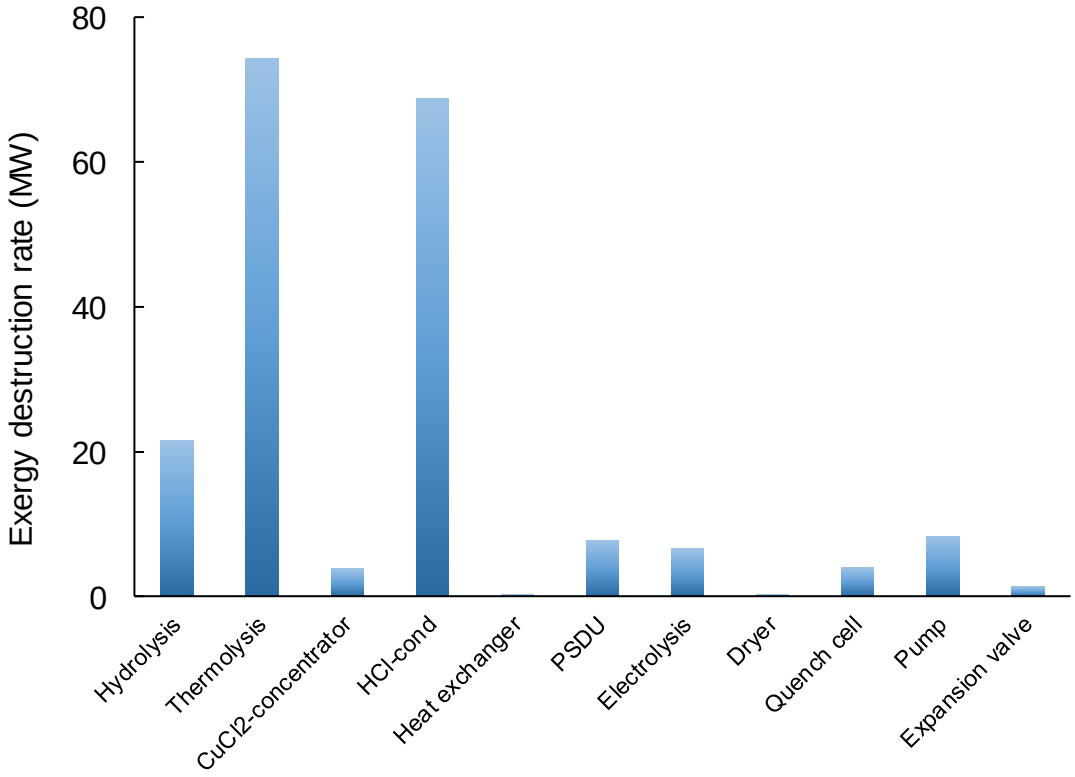

Fig. 5.57. Rates of exergy destructions for several components of the modified cycle

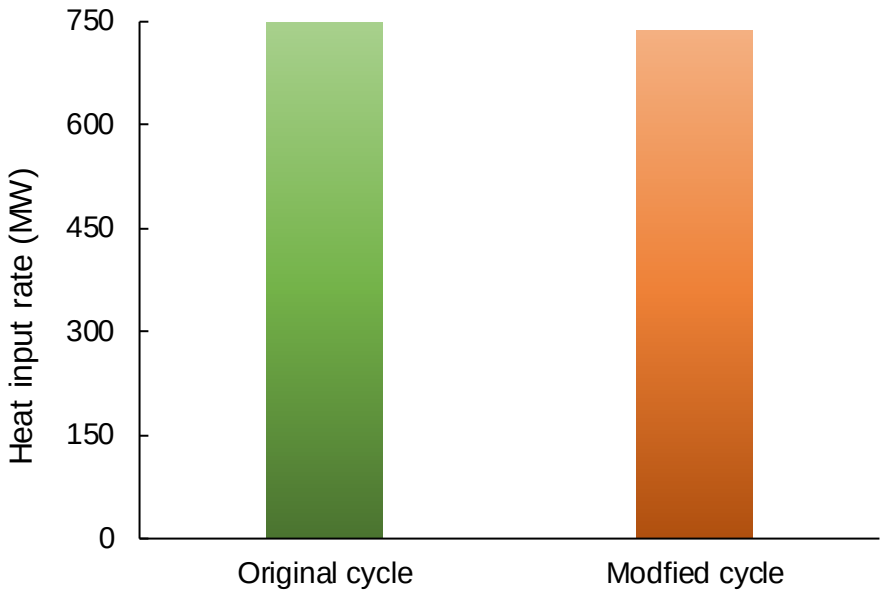

(a)

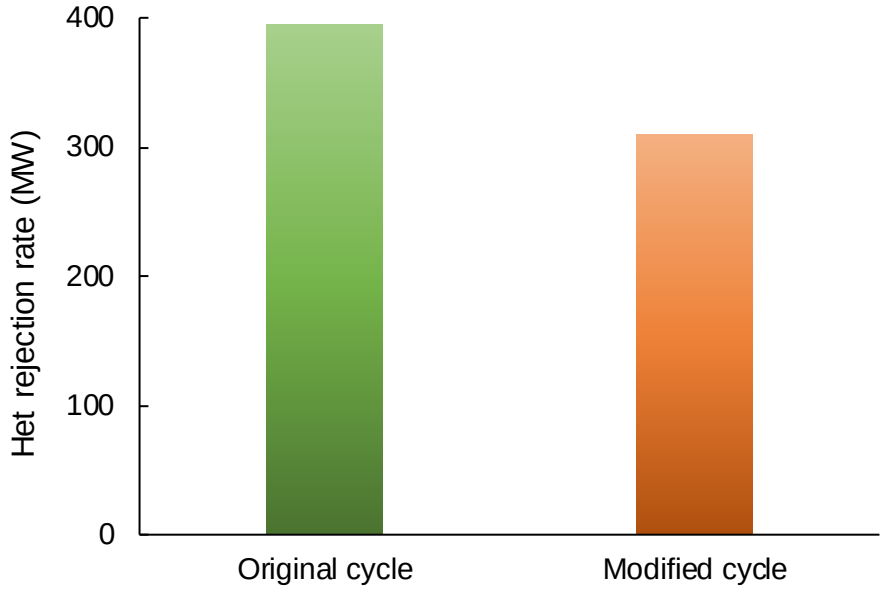

(b)

Fig. 5.58. Comparison of (a) net heat input rates and (b) net heat rejection rates between the original and modified cycles

The modified and the actual integrated cycles are compared for the overall cycle efficiencies in Figure 5.60. The actual integrated cycle operates at an energy efficiency of 6.6% compared with 7.2% of the cycle modified with the flash vaporization process. Moreover, the actual integrated cycle operates at an exergy efficiency of 10.2% compared with 11% of the cycle modified with the flash vaporization process.

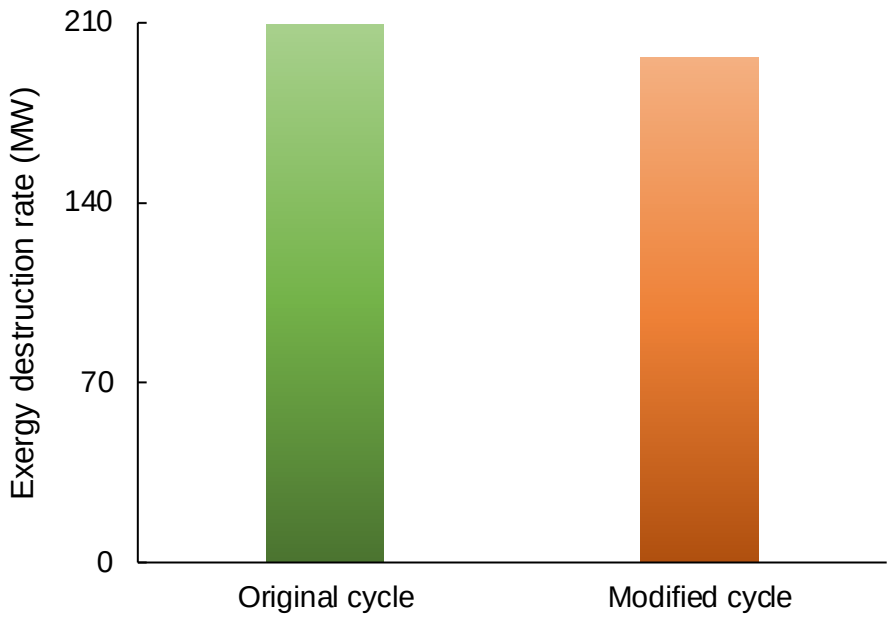

Fig. 5.59. Comparison of net exergy destruction rates between the original and modified cycles

The percentage distribution for the numerous components of the modified cycle for the heat input rate is presented in Figure 5.61. Based on the evaluated data, the process/component with the maximum share of heat input is found to be the hydrolysis step while the PSDU has the second-highest share of heat input among the numerous other components of the cycle. Consequently, these processes need to have thermal management via either waste or internal heat recovery for the enhancement of the cycle efficiencies.

The rates of heat input and exergy destruction associated with the anolyte separation step are compared for the modified and the actual integrated cycle in Figures 5.62 and 5.63. An approximate decrease of 10% in the rate of heat input for the anolyte separation step of the modified cycle is observed with reference to the actual integrated cycle. Moreover, an approximate decrease of 40% in the rate of exergy destruction for the anolyte separation step of the modified cycle is observed with reference to the actual integrated cycle.

A comparison of the obtained energy and exergy efficiencies of the modified integrated cycle in this study with various conceptual four-step cycle layouts reported in the literature is provided in Table 5.18. In the context of the four-step Cu-Cl cycle, the energy

efficiencies generally reported in the literature lie in the range of 40 and 55% [19] that are quite high compared with those reported in [17] and in this thesis section 5.1.1.

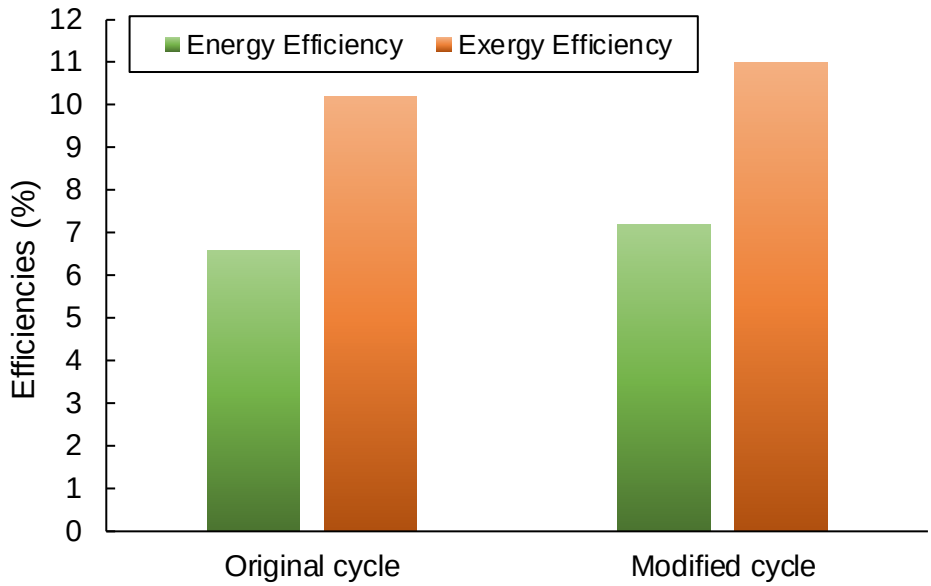

Fig. 5.60. Comparison of overall efficiencies between the original and modified cycles

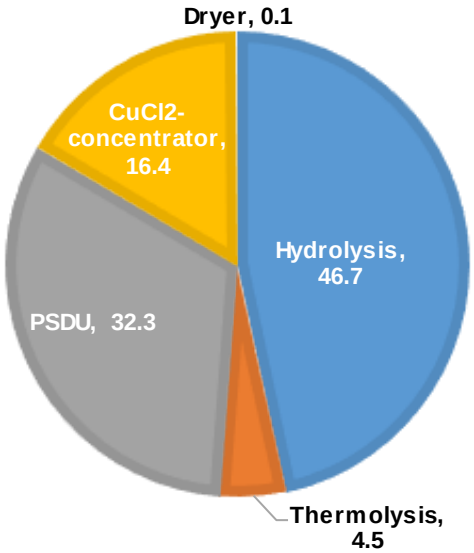

Fig. 5.61. Percentage distribution of the rates of heat input for the different steps/ processes of the modified cycle

In this context, a major factor for those high efficiencies is the considered designs of the cycle in the literature which are too basic and only consider the main steps of the cycle. However, a more practical and comprehensive design is considered for the integrated cycle

at CERL for which numerous secondary components for the realization of various auxiliary processes in the cycle are incorporated. The $CuCl_2$-concentrator, the ADU, the PSDU, and the ADA are a few of those components. Also, the numerous conceptual designs of the cycle reported in the literature do not include the azeotropic separation of the H_2O and HCl mixture that is very essential for the electrolysis reaction of the cycle. Further, the anolyte separation step of the cycle is mostly carried out via a single step in numerous investigations. However, the same process is realized in multiple steps in the cycle at CERL through a more practical approach incorporating several processes that are quite energy-intensive which is one of factors towards reducing the cycle efficiencies. Some of the cycle designs in the literature also consider heat recovery for different processes in the cycle (hydrolysis in particular) whereas the cycle at CERL operates without heat recovery adding to lower cycle efficiencies. Other than the results reported in this thesis in sections 5.1.1 and 5.2.1, the only assessment of the integrated cycle at CERL is reported in [17] that also suggested such low efficiencies. A couple of reasons for the difference in the results between [17] and sections 5.1.1 and 5.2.1 of this thesis are the slightly different operating conditions and the efficiency definitions.

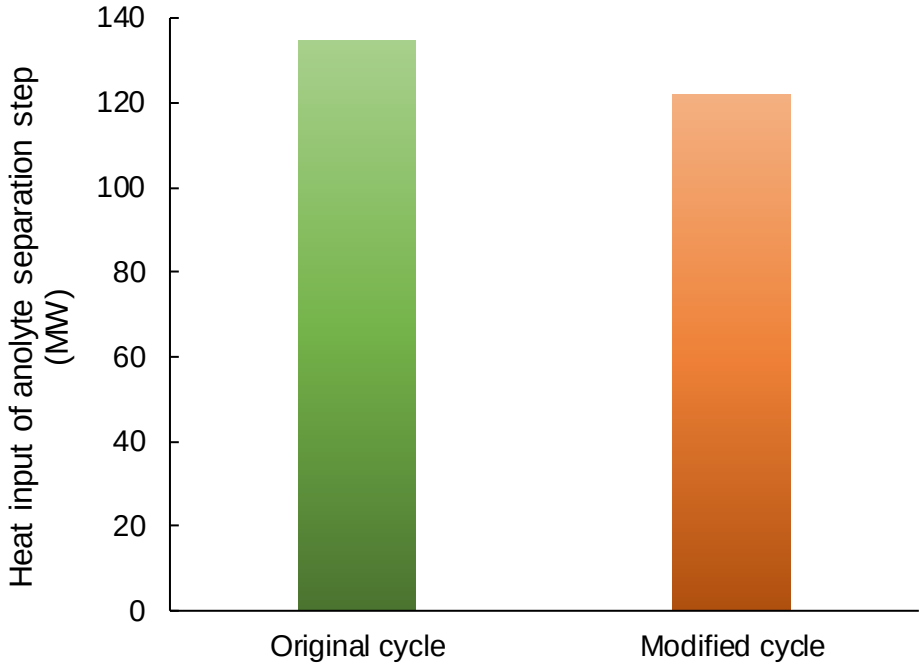

Fig. 5.62. Comparison between the original and modified cycles in terms of the rates of heat input of the anolyte separation step

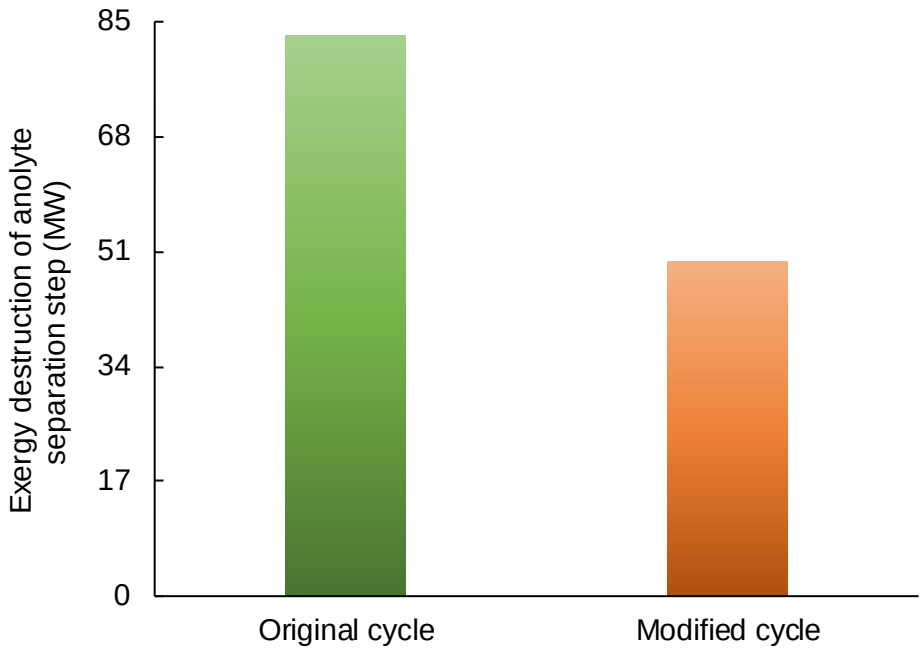

Fig. 5.63. Comparison between the original and modified cycles in terms of the rates of exergy destructions of the anolyte separation step

Table 5.18 Comparison between the present study and the literature for the overall cycle efficiencies

Reference	Energy efficiency	Exergy efficiency
[19]	40.4%	-
[14]	43%	-
[17]	11.6%	35%
Section 6.1.1	6.6%	10.2%
Section 6.2.1	7.2%	11%

5.2.2 Thermal management results

The obtained results based on the Aspen-plus simulations conducted for the various heat recovery configurations for the cycle operating with flash vaporization and hydrocyclone separator are presented and compared in this section. The comparisons are made in terms of the overall energy and exergy efficiencies, the overall heat input rate, heat input rates of the most energy-intensive components, percentage difference of the various configurations with respect to the reference case for net heat input rate and efficiencies and heat recovery ratio.

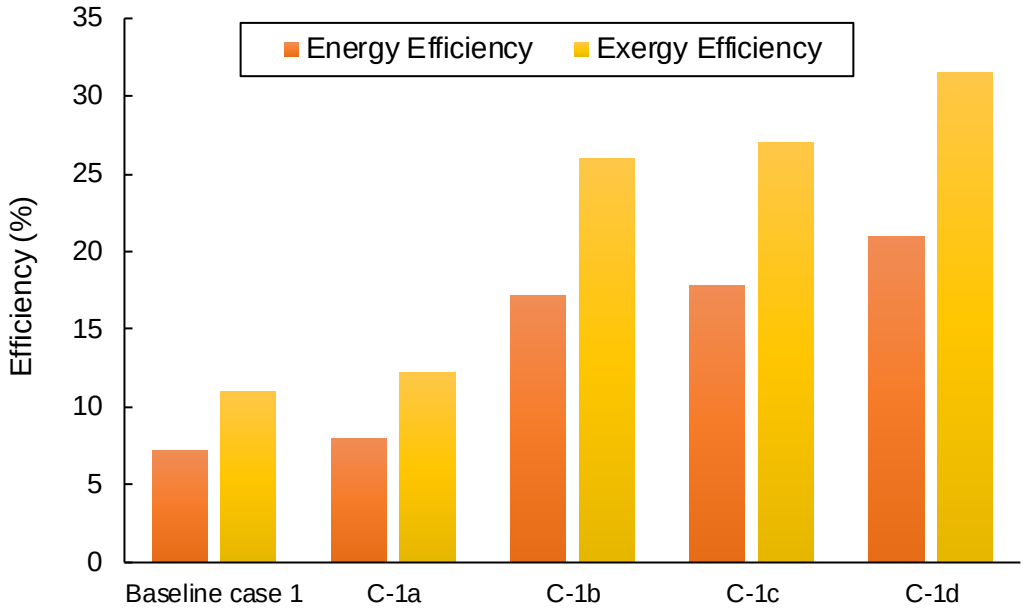

(a)

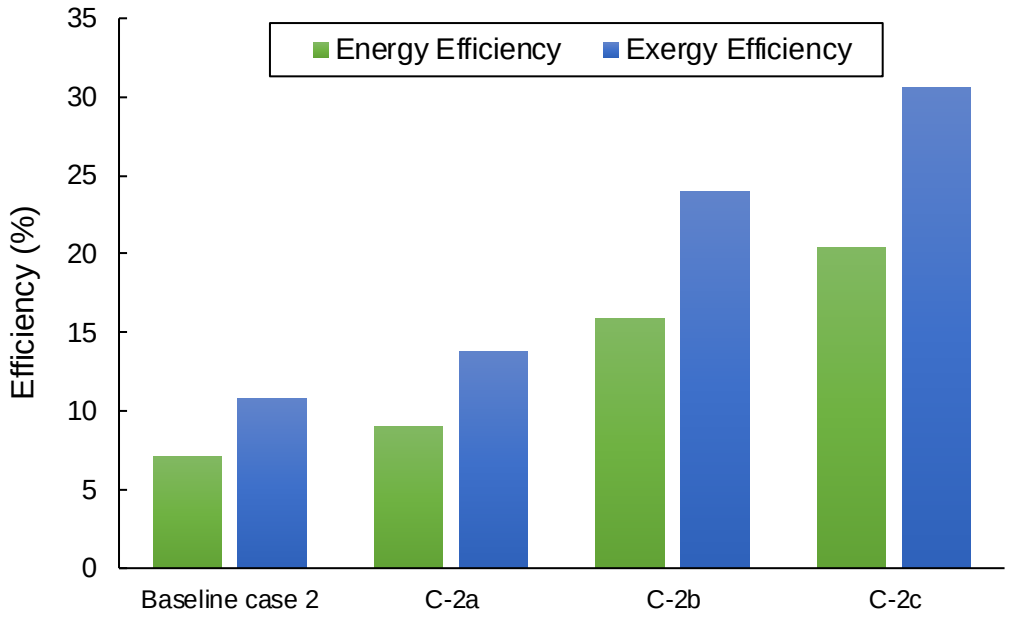

(b)

Fig. 5.64. Comparison of efficiencies among the several configurations considered for the cycle operating with (a) flash vaporization and (b) hydrocyclone separator

Figures 5.64a and 5.64b show the energy and exergy efficiencies for the baseline case and various heat recovery schemes considered for the cycles equipped with flash vaporization and hydrocyclone separator, respectively. Among the various heat recovery schemes considered, the combination of waste and internal heat recovery yields the highest efficiencies in comparison with the stand-alone internal and waste heat recovery schemes.

In the context of flash vaporization, the configuration C-1d results in the highest efficiencies with the values of 21% and 31.5% for energy and exergy efficiencies, respectively. The increase in efficiencies for configurations C-1b and C-1c does not vary considerably. The energy and exergy efficiencies for configuration C-1b are obtained to be 17.2% and 26%, respectively whereas these corresponding values increase to 17.8% and 27% for the configuration C-1c. In contrast, the configuration C-1a results in the lowest values of exergy and energy efficiencies of 12.2% and 8% respectively among all considered heat recovery schemes. The baseline case of the integrated cycle modified with the flash vaporization process results in an energy efficiency of 7.2% and an exergy efficiency of 11%. For the cycle operating with hydrocyclone separator, the configuration C-2c results in the highest energy and exergy efficiency values of 20.4% and 30.6% respectively while C-2a results in the lowest energy and exergy efficiency values of 9% and 14% respectively. The baseline case, in this case, yields values almost similar to flash vaporization with an energy efficiency of 7.1% and an exergy efficiency of 10.8%.

Figures 5.65a and 5.65b show the overall heat input for the baseline case and various heat recovery schemes considered for the cycles equipped with flash vaporization and hydrocyclone separator, respectively. It can be seen from the figure that incorporation of heat recovery within the cycle causes the total heat input to significantly drop for both separation approaches. The overall heat input values for the standard cycle operation are evaluated to be 14733 kW for flash vaporization and 14480 kW for the hydrocyclone separator. Among the different configurations for flash vaporization, the highest reduction in the heat input is obtained for C-1d with a value of 4831 kW while for the hydrocyclone separator, the highest reduction in the heat input is obtained for C-2c having a value of 5195 kW.

Figures 5.66a and 5.66b show the heat input rates for the hydrolysis process, the PSDU, and the $CuCl_2$-concentrator for the baseline case as well as for the various heat recovery schemes considered for the cycles equipped with flash vaporization and hydrocyclone separator, respectively. For both flash vaporization and hydrocyclone separator, the hydrolysis process experiences a significant reduction in heat input.

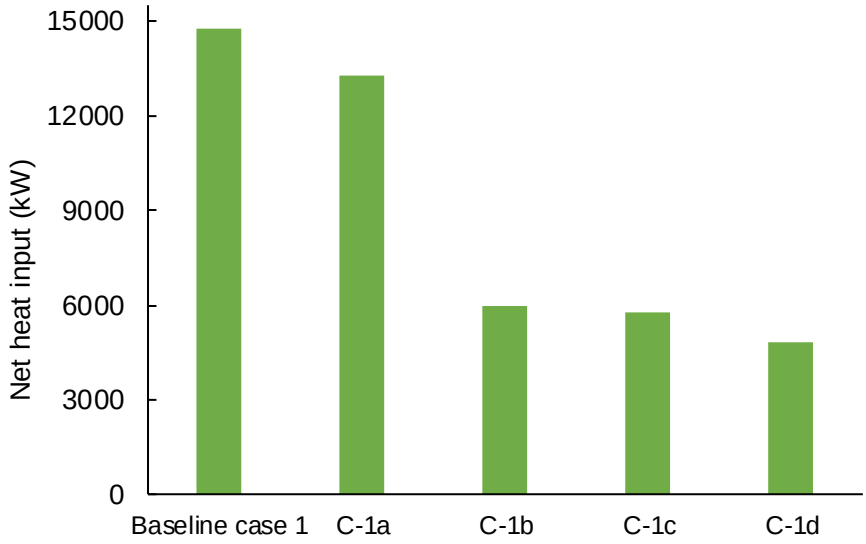

(a)

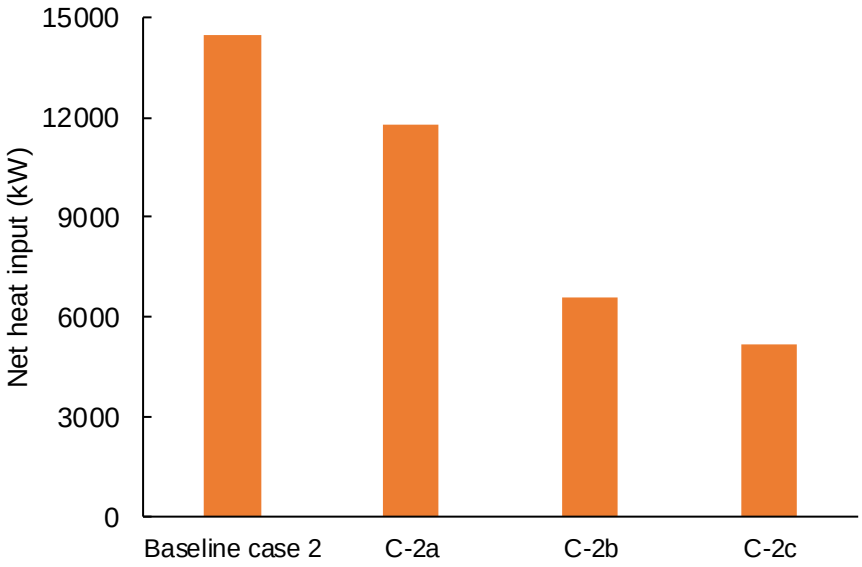

(b)

Fig. 5.65. Comparison of heat input rates among the several configurations considered for the cycle operating with (a) flash vaporization and (b) hydrocyclone separator

With regards to flash vaporization, for the baseline case and C-1a, the required heat input rate of the cycle is evaluated to be 6873 kW while this value is substantially reduced to 526 kW for the other three heat recovery schemes. For the PSDU, the heat input rate remains the same for the standard cycle operation and C-1b with a value of 4755 kW. These values reduce to 3615 kW for both C-1a and C-1d. However, the lowest heat input rate for the PSDU is obtained for C-1c with a value of 2434 kW. For the $CuCl_2$-concentrator, the heat

input rate for the baseline case is evaluated as 2416 kW while this value drops to 2091 kW for both C-1a and C-1c. However, this value becomes zero while considering C-1b and C-1d. Similar trends are observed for the hydrolysis process and the PSDU for the cycle with the hydrocyclone separator. However, for the $CuCl_2$-concentrator, the configuration C-2a significantly reduces the heat input rate to 22 kW while this value becomes zero for both C-2b and C-2c. These trends signify the influence of waste heat recovery on reducing the required heat input rates for various components within the cycle.

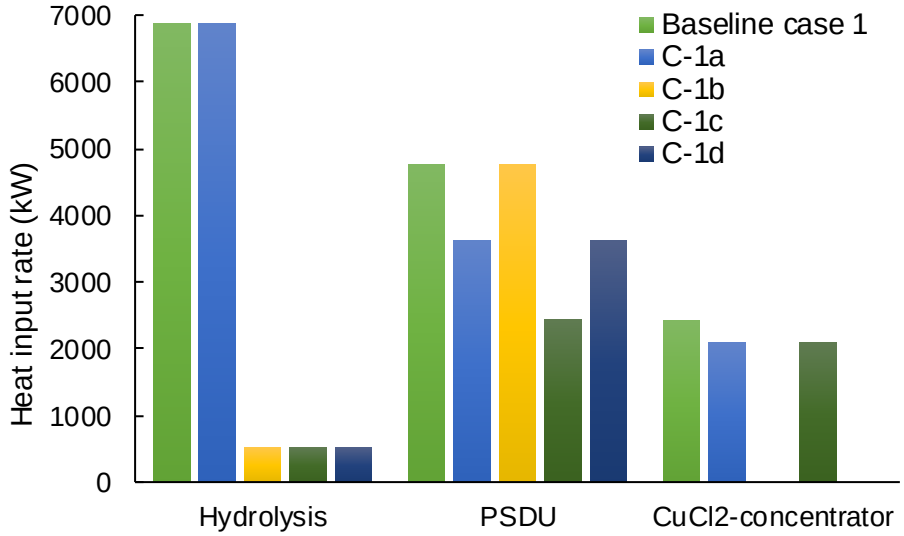

(a)

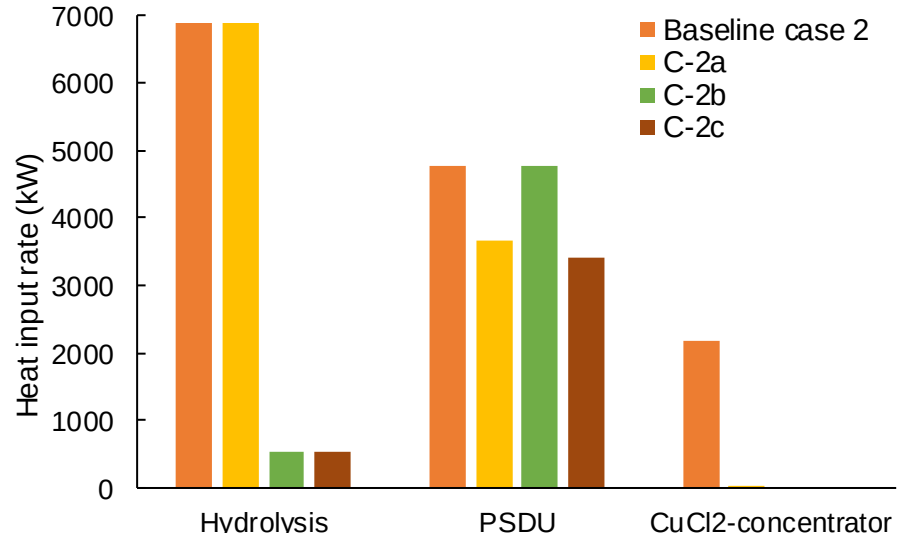

(b)

Fig. 5.66. Comparison of heat input rates of hydrolysis, PSDU, and $CuCl_2$-concentrator among the several configurations considered for the cycle operating with (a) flash vaporization and (b) hydrocyclone separator

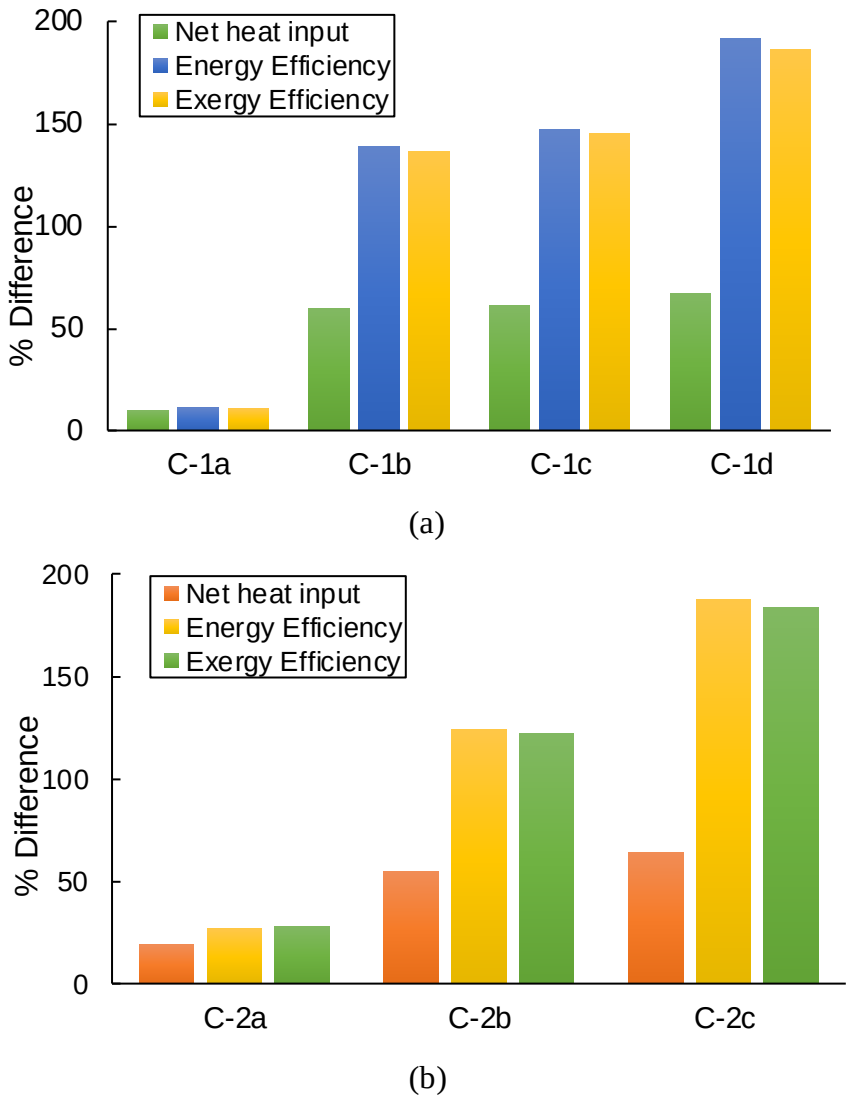

Fig. 5.67. Percentage decrease in heat input rates and increase in efficiencies with respect to the reference case for various heat recovery schemes for the cycle operating with (a) flash vaporization and (b) hydrocyclone separator

Figures 5.67a and 5.67b represent the percentage difference of the several heat recovery schemes considered in terms of the net heat input rate, energy efficiency, and exergy efficiency with respect to the baseline case for the cycles equipped with flash vaporization and hydrocyclone separator, respectively. With respect to the cycle with flash vaporization, the highest percentage increase in efficiencies and decrease in the heat input is obtained for the configuration C-1d with a 192% increase in energy efficiency, 186% increase in exergy efficiency, and 67% reduction in the heat input of the cycle. C-1b and C-1c also show a considerable difference in this regard with a corresponding reduction in the net heat input rates of 59% and 61%, an increase in energy efficiencies of 139% and 147%, and an

increase in exergy efficiencies of 136% and 145%. C-1a results in the lowest increase and decrease in efficiencies and net heat input rate, respectively.

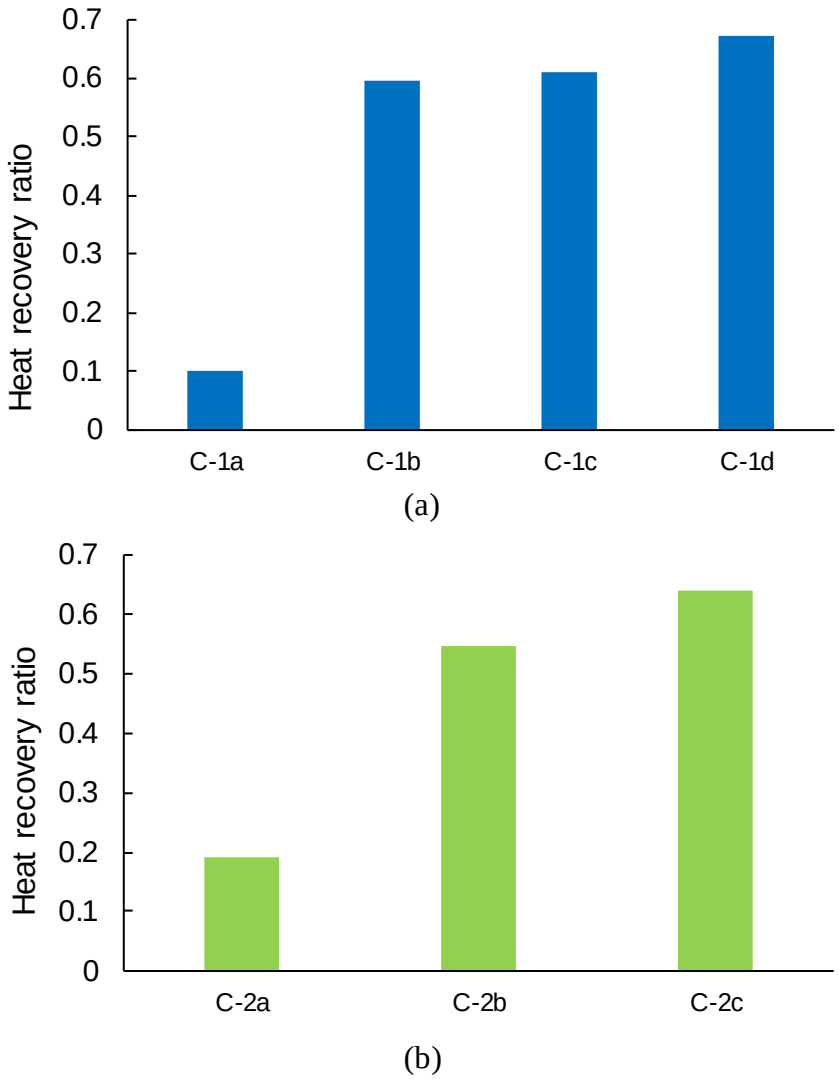

Fig. 5.68. Comparison of heat recovery ratio of various heat recovery schemes for the cycle operating with (a) flash vaporization and (b) hydrocyclone separator

Figures 5.68a and 5.68b show the comparison between the cycles with flash vaporization and hydrocyclone separator respectively in terms of the heat recovery ratio. The heat recovery ratio in this study is defined as the ratio of the difference of the heat input rate between the baseline case and the heat recovery configuration to the heat input rate of the baseline case. For flash vaporization, the highest value of heat recovery ratio is evaluated as 0.67 for the configuration C-1d while the lowest heat recovery ratio of 0.10 is obtained for C-1a. For the hydrocyclone separator, the highest heat recovery ratio of 0.64 is obtained for the configuration C-2c while the lowest value in this regard is obtained for C-2a. Thus,

in both scenarios, the combination of internal and waste heat recovery results in the highest heat recovery ratios.

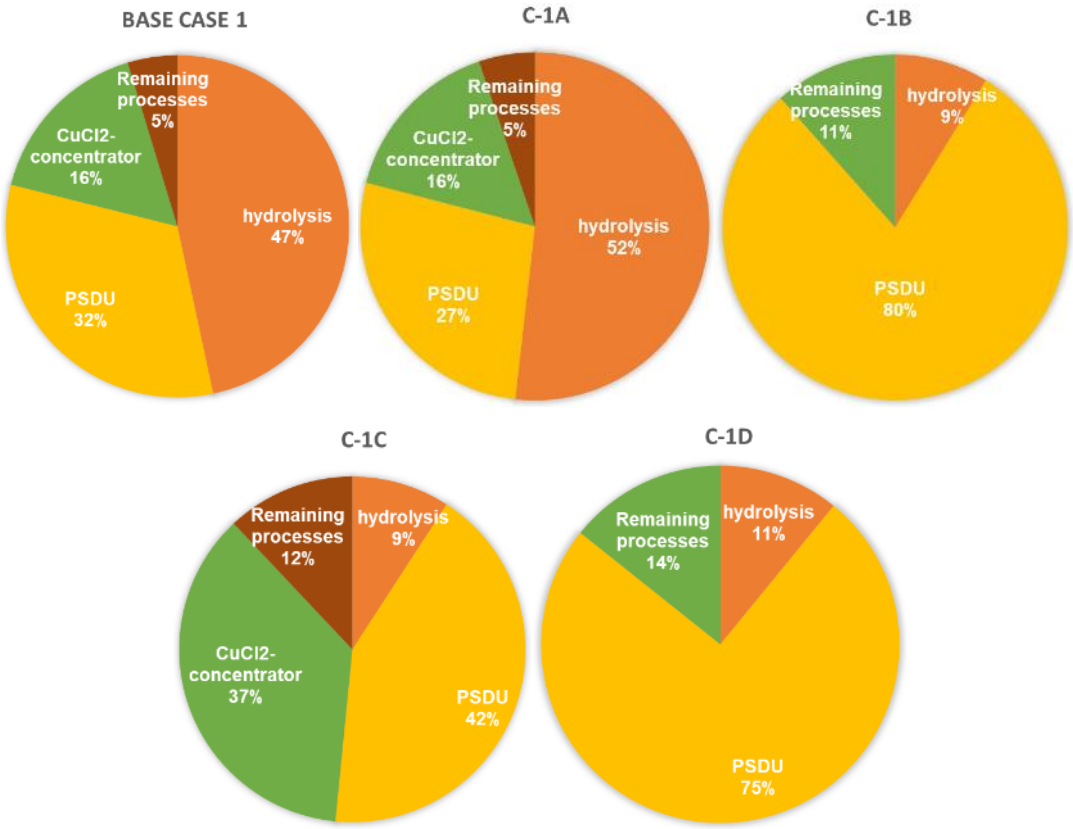

Fig. 5.69. Comparison of heat input rates for hydrolysis, PSDU, $CuCl_2$-concentrator, and the remaining processes within the cycle between the reference case and heat recovery schemes

Figure 5.69 shows the percentage distribution of the heat input rates for the hydrolysis process, the PSDU, the $CuCl_2$-concentrator, and the remaining processes in the cycle for the baseline case and the several heat recovery schemes considered with respect to the heat input rate of each configuration for the cycle with flash vaporization. The hydrolysis process accounts for 47% and 52% heat input rate for the reference case and C-1a respectively being the most energy-intensive process. While the same process accounts for 9% for both C-1b and C-1c and 11% for C-1d. The reason for this behavior is that the heat input rate supplied to provide superheated steam for the hydrolysis process in the reference case and C-1a does not involve any contribution from sources of heat recovery. The $CuCl_2$-concentrator accounts for 16% of the heat input rate for the reference case and C-1a. While this value relatively increases to 37% for configuration C-1c due to a reduction in the heat

input rate. For configurations C-1b and C-1d, the heat input rate of the $CuCl_2$-concentrator becomes zero since all the required thermal energy is supplied through heat recovery. This is also the reason for the consequent increase in the share of heat input rate of the PSDU for C-1b and C-1d. Due to the decrease in the heat input rates of the three most energy-intensive processes within the cycle, the share of the required heat input rate for the remaining processes in the cycle relatively increases due to a decrease in the net heat input rate of the cycle.

From Figures 5.64 through 5.67, the heat recovery schemes for the cycle incorporated with hydrocyclone separator yield relatively higher overall efficiencies and lower overall heat input rates. However, the feasibility of the flash vaporization process in terms of the practical implementation for the anolyte separation is much higher than hydrocyclone separators since hydrocyclone separators are more effective for separating heterogeneous mixtures while the flash vaporization process is more suitable for separating homogenous mixtures.

5.2.3 Exergoeconomic analysis results

The results for the exergoeconomic analysis of the modified integrated cycle are obtained for the unit thermal and electrical energy cost rates of 0.10 $/kWh. The exergy rate, cost rate, and specific cost at each state point of the modified cycle are provided in Table 5.19.

Figure 5.70 shows the total capital cost rates and exergy destruction cost rates of different components of the modified integrated cycle. The components with higher exergy destruction rates do not necessarily have the higher cost rates of exergy destructions since the unit thermal and electrical energy cost rates are much higher than that of the cold water used in condensers of the cycle. This is why the exergy destruction cost rate of the HCl condenser is much lower even having a higher exergy destruction rate. Moreover, the exergy destruction cost rates dominate the capital cost rates for all components. The highest capital cost rate is obtained for the hydrolysis step since there are various components associated with the hydrolysis process.

Figure 5.71 provides a comparison of the overall cost rate of exergy destruction between the original and modified integrated cycles. The original cycle has a higher exergy

destruction cost rate as a result of the higher overall exergy destruction. Figure 5.72 provides a comparison of the unit hydrogen cost between the original and modified cycles. The unit hydrogen cost for the original cycle is evaluated as 4.9 $/kg while for the modified cycle, this value is reduced to 4.7 $/kg for the considered capacity.

Table 5.19. Details of exergy cost and exergy rate of the modified cycle

State point	$\dot{E}x$ (MW)	$\dot{C}$ ($/h)	c ($/MJ)	State point	$\dot{E}x$ (MW)	$\dot{C}$ ($/h)	c ($/MJ)
1	4.997	0	0	19	75.93	12175.2	0.045
2	78.56	17716.7	0.063	20	794.21	13659.4	0.005
3	36.64	0	0	21	42.16	6090.94	0.040
4	41.19	732.6	0.005	22	52.40	7571.08	0.040
5	105.74	19286.2	0.051	23	44.37	7600.5	0.048
6	6.05	1160.4	0.053	24	45.64	8145.4	0.050
7	94.30	18130.8	0.053	25	44.29	8146.3	0.051
8	6.84	1259.6	0.051	26	7.79	1434.4	0.051
9	36.90	3310.3	0.025	27	36.51	6715.5	0.051
10	1.19	96.5	0.023	28	1.99	0	0
11	39.58	3217.6	0.023	29	6.80	1188.5	0.049
12	34.02	2754.3	0.022	30	31.66	5531.1	0.049
13	34.02	2754.3	0.022	31	54.68	8241.8	0.042
W-in	1.06	312.5	0.082	32	17.57	5722.8	0.090
W-out	2.62	781.2	0.083	33	7.79	2537.8	0.090
14	26.13	17425.4	0.185	34	37.36	2567.6	0.019
15	26.13	17425.4	0.185	35	7.65	525.9	0.019
16	69.29	22511.8	0.090	36	29.71	2046.5	0.019
17	46.80	13095.1	0.078	17-1	45.24	12571.3	0.08
18	33.59	9421.0	0.078				

The results based on the application of the SPECO approach are also obtained for the best, average, and worst-case scenarios for the modified cycle operation with and without heat recovery. The exergy rate, exergy cost, and specific exergy cost rate at each state point in the cycle are evaluated as shown in Table 5.20 for the cycle operation without heat recovery and in Table 5.21 for the cycle operation with waste heat recovery. The several parameters used for evaluation of the total cost rate of each component of the modified cycle are provided in Table 5.22.

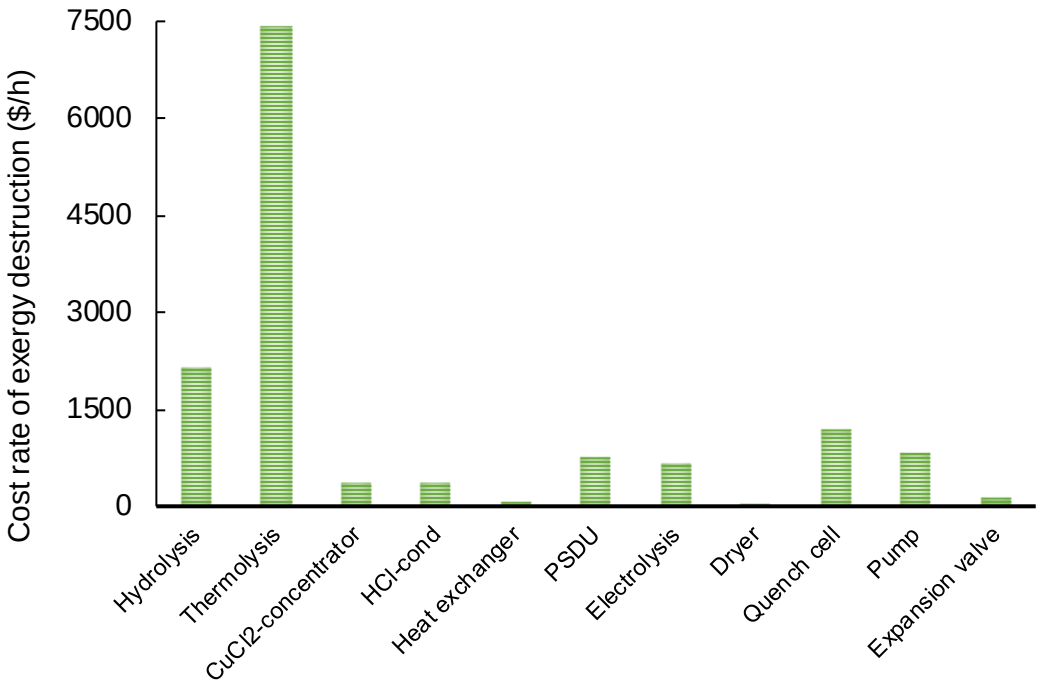

(a)

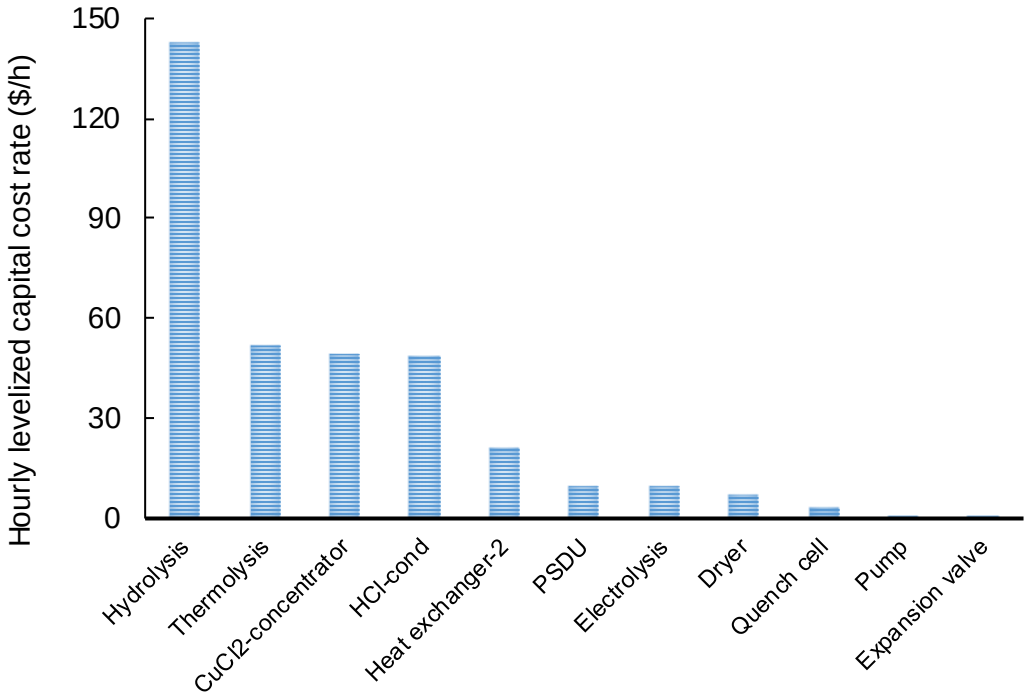

(b)

Fig. 5.70. (a) Cost rates of exergy destructions and (b) capital cost rates of various components

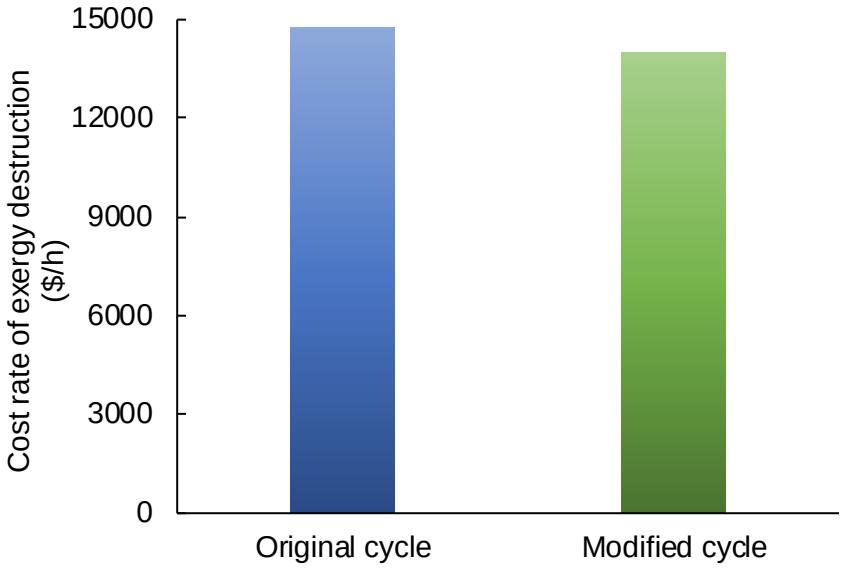

Fig. 5.71. Comparison between the original and modified cycle in terms of cost rates of exergy destructions

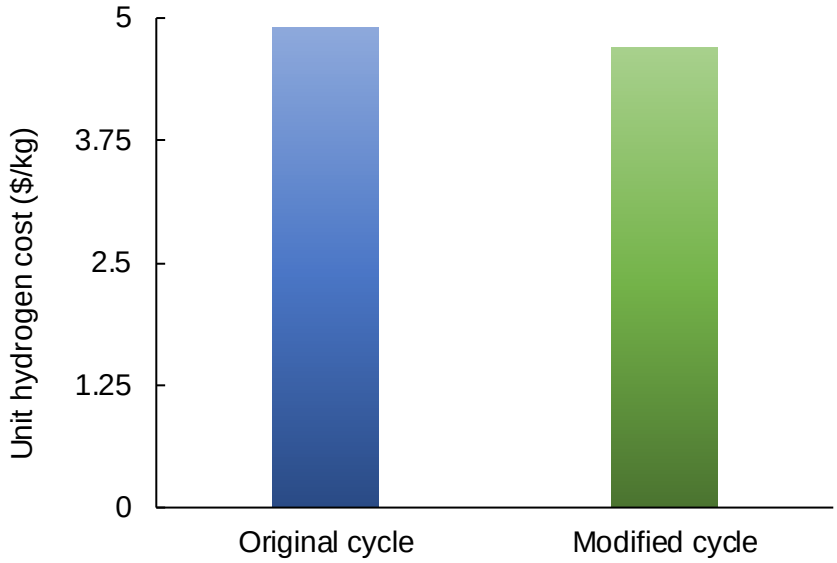

Fig. 5.72. Comparison between the original and modified cycle in terms of unit hydrogen cost

The cost of the purchased equipment and the hourly levelized total cost rate of the several cycle components are provided in Table 5.23. Figure 5.73 provides a comparison of the unit hydrogen for the best, the average, and the worst-case scenarios between the cycle operation with and without heat recovery. For the best-case scenario, the unit hydrogen cost is evaluated to be 3.75 $/kg for the actual cycle operation whereas this value decreases to 1.6 $/kg for the cycle operation with waste heat recovery.

Table 5.20 Exergy rate, exergy cost, and specific exergy cost rate for the three cases for cycle operation without waste heat recovery

State point	$\dot{E}x$ (MW)	Best case		Average case		Worst case	
		$\dot{C}$ ($/h)	c ($/MJ)	$\dot{C}$ ($/h)	c ($/MJ)	$\dot{C}$ ($/h)	c ($/MJ)
1	4.99	0	0	0	0	0	0
2	78.56	14180.4	0.050	17716.7	0.063	20893.2	0.074
3	36.64	0	0	0	0	0	0
4	41.191	590.3	0.004	732.6	0.005	874.9	0.006
5	105.74	15456.7	0.041	19286.2	0.051	22755.9	0.060
6	6.053	930.1	0.043	1160.4	0.053	1369.2	0.063
7	94.303	14531.6	0.043	18130.8	0.053	21391.7	0.063
8	6.84	1012.6	0.041	1259.6	0.051	1485.1	0.060
9	36.90	2659.6	0.020	3310.3	0.025	3939.4	0.030
10	1.19	77.5	0.018	96.5	0.023	114.8	0.027
11	39.58	2585.9	0.018	3217.6	0.023	3828.4	0.027
12	34.02	2221.3	0.018	2754.3	0.022	3288.6	0.027
13	34.02	2221.3	0.018	2754.3	0.022	3288.6	0.027
W-in	1.06	246.4	0.065	312.5	0.082	363.7	0.096
W-out	2.623	615.9	0.065	781.2	0.083	909.2	0.096
14	26.13	13826.2	0.147	17425.4	0.185	20686.3	0.220
15	26.13	13826.2	0.147	17425.4	0.185	20686.3	0.220
16	69.29	17896.3	0.072	22511.8	0.090	26788.9	0.107
17	46.80	10410.8	0.062	13095.1	0.078	15582.7	0.093
18	33.59	7489.8	0.062	9421.0	0.078	11210.5	0.093
19	75.93	9711.1	0.036	12175.2	0.045	14499.1	0.053
20	794.21	10899.8	0.004	13659.4	0.005	16278.8	0.006
21	42.15	4860.62	0.032	6090.94	0.040	7258.74	0.048
22	52.39	6041.8	0.032	7571.08	0.040	9022.7	0.048
23	44.37	6065.5	0.038	7600.5	0.048	9057.8	0.057
24	45.64	6503.0	0.040	8145.4	0.050	9702.2	0.059
25	44.29	6503.9	0.041	8146.3	0.051	9703.1	0.061
26	7.79	1145.4	0.041	1434.4	0.051	1708.4	0.061
27	36.51	5362.3	0.041	6715.5	0.051	7998.4	0.061
28	1.99	0	0	0	0	0	0
29	6.80	949.1	0.039	1188.5	0.049	1415.3	0.058
30	31.66	4413.3	0.039	5531.1	0.049	6587.0	0.058
31	54.68	6588.0	0.033	8241.8	0.042	9833.8	0.050
32	17.58	4577.1	0.072	5722.8	0.090	6825.7	0.108
33	7.79	2029.7	0.072	2537.8	0.090	3026.9	0.108
34	37.36	2054.0	0.015	2567.6	0.019	3062.2	0.023
35	7.65	420.9	0.015	525.9	0.019	627.1	0.023
36	29.71	1637.9	0.015	2046.5	0.019	2440.0	0.023
17-1	45.24	9994.4	0.06	12571.3	0.08	14959.4	0.09

Table 5.21 Exergy rate, exergy cost, and specific exergy cost rate for the three cases for cycle operation with waste heat recovery

State point	$\dot{E}x$ (MW)	Best case		Average case		Worst case	
		$\dot{C}$ ($/h)	c ($/MJ)	$\dot{C}$ ($/h)	c ($/MJ)	$\dot{C}$ ($/h)	c ($/MJ)
1	4.99	0	0	0	0	0	0
2	78.56	37.73	0.00013	37.73	0.00013	37.73	0.00013
3	36.64	0	0	0	0	0	0
4	41.191	590.3	0.004	732.6	0.005	874.9	0.006
5	105.74	1313.1	0.003	1606.3	0.004	1899.5	0.005
6	6.053	79.3	0.004	96.9	0.004	114.5	0.005
7	94.303	1238.7	0.004	1514.3	0.004	1789.8	0.005
8	6.84	161.6	0.007	195.9	0.008	230.2	0.009
9	36.90	1808.2	0.014	2246.2	0.017	2684.1	0.020
10	1.19	52.8	0.012	65.5	0.015	78.3	0.018
11	39.58	1759.2	0.012	2184.5	0.015	2609.6	0.018
12	34.02	1511.2	0.012	1876.5	0.015	2241.6	0.018
13	34.02	1511.2	0.012	1876.5	0.015	2241.6	0.018
W-in	1.06	166.1	0.044	207.6	0.055	248.0	0.065
W-out	2.623	415.2	0.044	515.7	0.055	616.1	0.065
14	26.13	533.9	0.006	809.5	0.009	1085.0	0.012
15	26.13	533.9	0.006	809.5	0.009	1085.0	0.012
16	69.29	4604.0	0.018	5895.8	0.024	7187.6	0.029
17	46.80	2680.7	0.016	3431.4	0.020	4182.7	0.025
18	33.59	1928.5	0.016	2468.6	0.020	3009.1	0.025
19	75.93	3439.7	0.013	4345.1	0.016	5250.8	0.019
20	794.21	4628.3	0.002	5829.2	0.002	7030.4	0.002
21	42.15	2064.6	0.014	2600.0	0.017	3135.5	0.021
22	52.39	2566.3	0.014	3231.8	0.017	3897.5	0.021
23	44.37	2590.0	0.016	3261.2	0.020	3932.6	0.025
24	45.64	2718.1	0.017	3419.2	0.021	4120.7	0.025
25	44.29	2718.98	0.017	3420.1	0.021	4121.6	0.026
26	7.79	479.2	0.017	602.6	0.021	726.1	0.026
27	36.51	2243.5	0.017	2821.2	0.021	3399.2	0.026
28	1.99	0	0	0	0	0	0
29	6.80	397.5	0.016	499.7	0.020	601.9	0.025
30	31.66	1850.0	0.016	2325.5	0.020	2801.1	0.025
31	54.68	4024.3	0.020	5035.9	0.026	6047.6	0.031
32	17.58	2800.8	0.044	3501.7	0.055	4202.6	0.066
33	7.79	1242.1	0.044	1552.8	0.055	1863.7	0.066
34	37.36	1266.3	0.009	1582.5	0.012	1899.0	0.014
35	7.65	259.9	0.009	324.5	0.012	389.2	0.014
36	29.71	1011.2	0.009	1262.8	0.012	1514.5	0.014
17-1	45.24	2573.47	0.016	3294.14	0.020	4015.39	0.025

Table 5.22 Operating parameters of the cycle with their values

Parameter	Value
Capital cost (10^7 \$)	1.53
Capital recovery factor	0.24
Present value factor	0.16
Cycle's lifetime (years)	10
Number of annual operating hours	8766
Salvage value ratio (%)	20
Interest rate (%)	20
Operating and maintenance cost factor	1.06

Table 5.23 Purchased equipment cost and hourly levelized total cost rate of several components

Component	PEC (10^3 \$)	$\dot{Z}_k^T$	
		Without waste heat recovery	With waste heat recovery
Hydrolysis reactor	970.3	82.33	81.36
Thermolysis reactor	382.4	32.45	32.06
Electrolyzer	80.5	6.83	6.75
Dryer	57.0	4.84	4.78
Pressure swing distillation unit	50.7	4.30	4.25
Quench Cell	38.4	3.26	3.22
HCl-condenser	574.1	48.71	48.14
$CuCl_2$-Concentrator	222.0	18.84	18.61
Separation Unit	47.1	4.00	3.95
Separator-1	58.3	4.95	4.89
Separator-2	45.2	3.84	3.79
Liquid gas separator	31.0	2.63	2.60
H1	400.5	33.98	21.02
H2	250.7	21.27	15.55
H3	185.5	15.74	5.06
H4	60.3	5.12	-
H5	356.8	30.27	29.92
H6	26.0	2.21	2.18
Heat exchanger 1	450.0	-	37.73
Heat exchanger 2	248.4	21.08	20.83
Pump	11.8	1.00	0.99
Flash chamber	43.9	3.72	3.68
Expansion valve	10.5	0.89	0.88

For the baseline or average case scenario, the unit cost of hydrogen is obtained to be 4.7 $/kg for the actual cycle operation which decreases to 2 $/kg with incorporating waste heat recovery. Finally, for the worst-case scenario, the unit hydrogen costs for the cycle without and with waste heat recovery are evaluated to be 5.6 $/kg and 2.4 $/kg, respectively. For each of these scenarios, the unit hydrogen cost experiences a reduction of approximately 57%. These trends show the significant impact of waste heat recovery on reducing the unit cost of hydrogen. Moreover, with realizing internal heat recovery within the integrated cycle, these values are subject to a further reduction which may potentially improve the commercialization potential of the cycle.

The share of the total cost rates of various components of the cycle with and without waste heat recovery is demonstrated in Figure 5.74. According to the obtained data, the hydrolysis step takes up the maximum cost rate within the cycle having shares of 40.5% and 41.2% for the cycle operation without and with waste heat recovery, respectively. On the contrary, separation unit, flash chamber, quench cell, pump, and expansion valve are amongst the components with the lowest contribution towards the total cost rate of the cycle with values as high as 1.1% and as low as 0.2% for both modes of cycle operation.

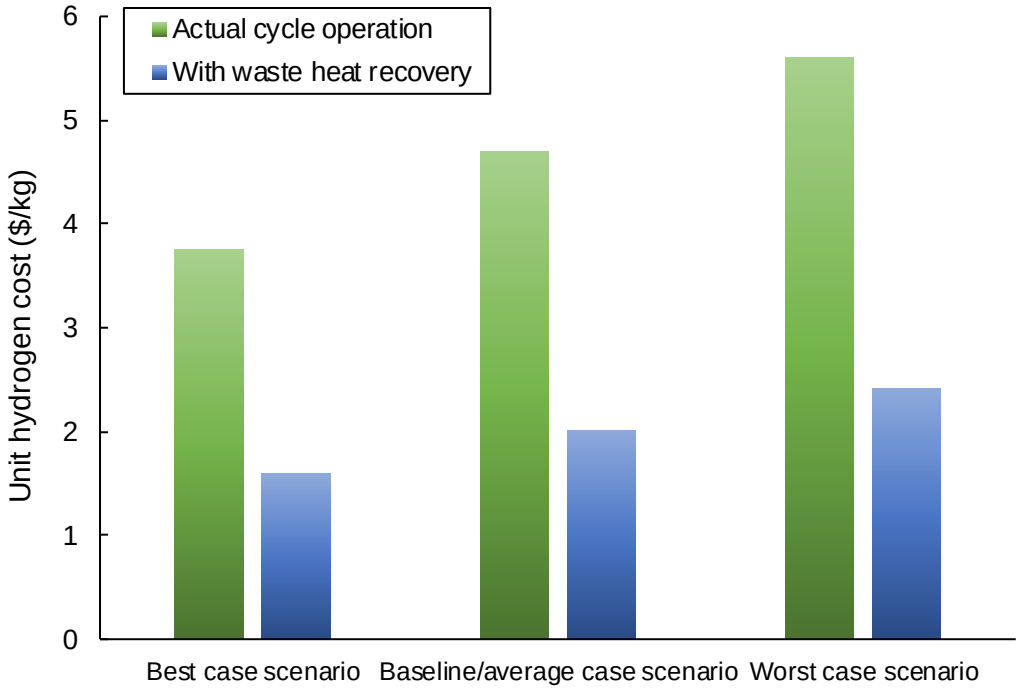

Fig. 5.73. Comparison of unit hydrogen cost for the three scenarios between cycle operation with and without waste heat recovery

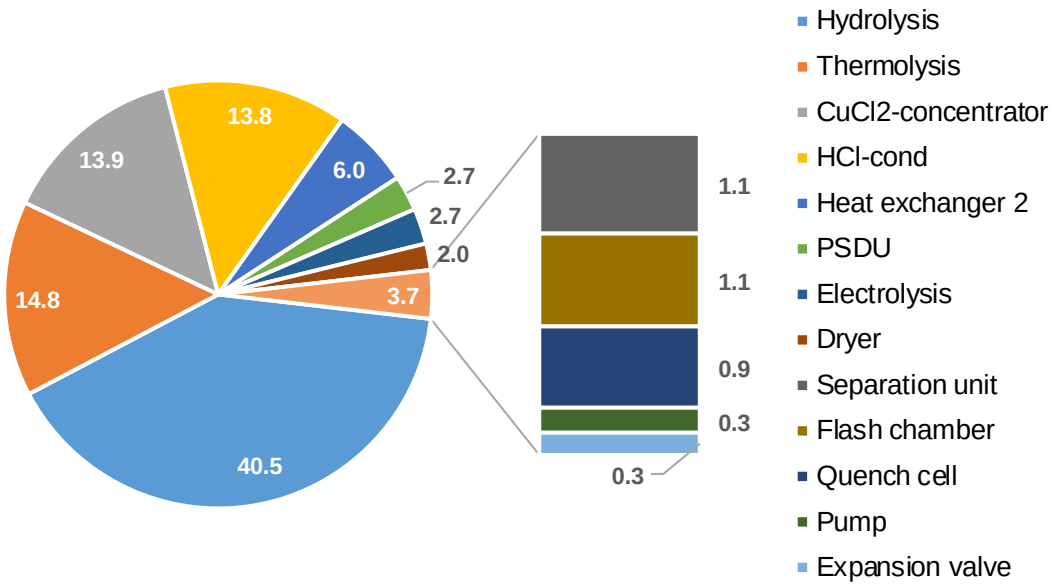

(a)

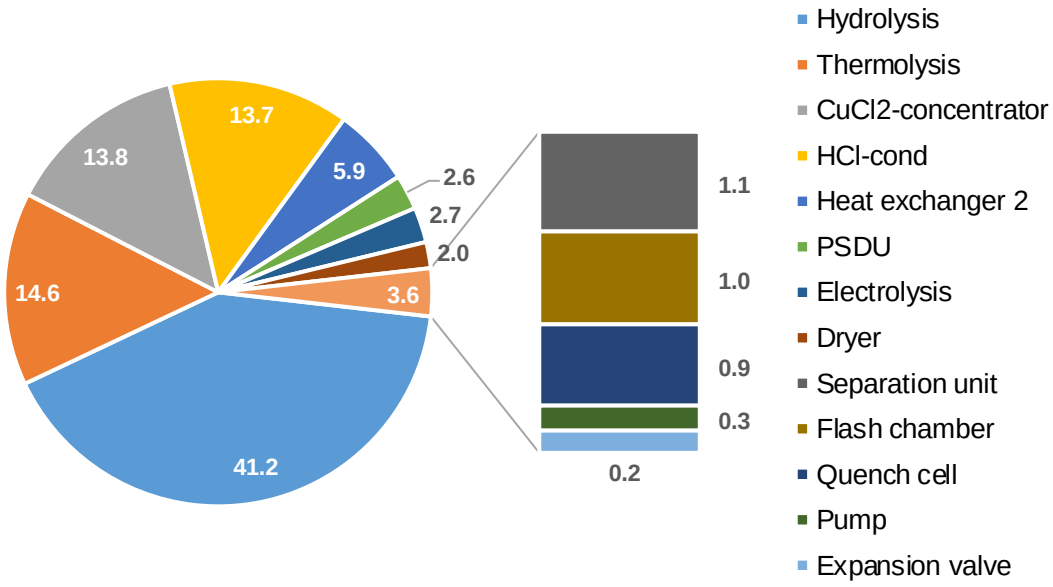

(b)

Fig. 5.74. Distribution of the total cost rates for several components of the cycle (a) without waste heat recovery and (b) with waste heat recovery

5.2.4 Exergoenvironmental analysis results

The results of the exergoenvironmental analysis of the modified integrated cycle are obtained by considering the environmental impact rate of thermal and electrical energies of 6 mPt/h and 22 mPt/h, respectively. The environmental impact and the corresponding criteria for the several components of the modified cycle are provided in Table 5.24. The environmental and specific environmental impact rate at each state point of the cycle is provided in Table 5.25. Figure 5.75 shows the environmental impact rate of exergy destruction and component-related environmental impact rate for various components of the modified cycle. The thermolysis step is evaluated to have the highest value of environmental impact rate of exergy destruction while the heat exchanger-2 and the dryer show the lowest corresponding values. Even though the exergy destruction rates of electrolyzer and pump are not that high, their environmental impact rate of exergy destruction is on the higher side due to the relatively higher environmental impact rate of electrical energy compared with thermal energy. On the contrary, the hydrolysis step accounts for the highest value in terms of the component-related environmental impact rate.

Table 5.24 Environmental impact rate and criteria for various cycle components

Component	$\dot{Y}$ (mPt/h)	Criteria
Hydrolysis	0.256	$\dot{m}_{steam}$
Thermolysis	0.0028	$\dot{m}_{Cu2OCl2}$
Dryer (H6)	0.00057	A_{H6}
HCl-condenser	0.028	$A_{HCl-cond}$
Quench cell	0.0053	A_{QC}
Electrolyzer	0.1004	$\dot{W}_{elec}$
$CuCl_2$-concentrator (H5)	0.0125	A_{H5}
PSDU (H4)	0.0164	A_{H4}
H1	0.023	A_{H1}
H3	0.0014	A_{H3}
H2	0.0105	A_{H2}
Pump	0.000034	$\dot{W}_{pump}$
Heat exchanger 2	0.00204	A_{HX-2}
Exp valve	6.05E-08	$\dot{m}_{anolyte}$

Figures 5.76 and 5.77 provide a comparison between the original and modified integrated cycles in terms of the overall environmental impact rate of exergy destruction and

component-related environmental impact rate, respectively. The original cycle is evaluated to have a higher component-related environmental impact rate while the modified cycle accounts for the higher environmental impact rate of exergy destruction. The lower component-related environmental impact rate of the modified cycle is due to a reduction in the overall number of components of the cycle and replacement with components having lower component-related environmental impact rates. On the other hand, the modified cycle results in a higher environmental impact rate of exergy destruction. This is due to the reason that some of the components of the original cycle (which are replaced in the modified cycle) are thermal energy-driven while the modified cycle includes a circulation pump which requires electrical energy and the value of the environmental impact rate of thermal energy is much lower than that of electrical energy.

Table 5.25 Exergy rate, environmental impact, and specific environmental impact at each state point of the modified integrated cycle

State point	$\dot{E}x$ (MW)	$\dot{B}$ (Pt/s)	b (mPt/kJ)	State point	$\dot{E}x$ (MW)	$\dot{B}$ (Pt/s)	b (mPt/kJ)
1	4.99	0	0	19	75.93	0.172	0.0023
2	78.56	0.295	0.0038	20	794.21	0.157	0.0002
3	36.64	0	0	21	42.15	0.117	0.0028
4	41.191	0.012	0.0003	22	52.39	0.146	0.0028
5	105.74	0.318	0.0030	23	44.37	0.147	0.0033
6	6.053	0.019	0.0032	24	45.64	0.154	0.0034
7	94.303	0.300	0.0032	25	44.29	0.154	0.0035
8	6.84	0.021	0.0030	26	7.79	0.027	0.0035
9	36.90	0.054	0.0015	27	36.51	0.127	0.0035
10	1.19	0.002	0.0013	28	1.99	0	0
11	39.58	0.053	0.0013	29	6.80	0.022	0.0033
12	34.02	0.045	0.0013	30	31.66	0.105	0.0033
13	34.02	0.045	0.0013	31	54.68	0.149	0.0027
W-in	1.06	0.005	0.0047	32	17.58	0.048	0.0027
W-out	2.623	0.012	0.0047	33	7.79	0.101	0.0027
14	26.13	0.220	0.0084	34	37.36	0.102	0.0027
15	26.13	0.220	0.0084	35	7.65	0.021	0.0027
16	69.29	0.304	0.0044	36	29.71	0.081	0.0027
17	46.80	0.177	0.0038	17-1	45.24	0.17	0.0038
18	33.59	0.127	0.0038				

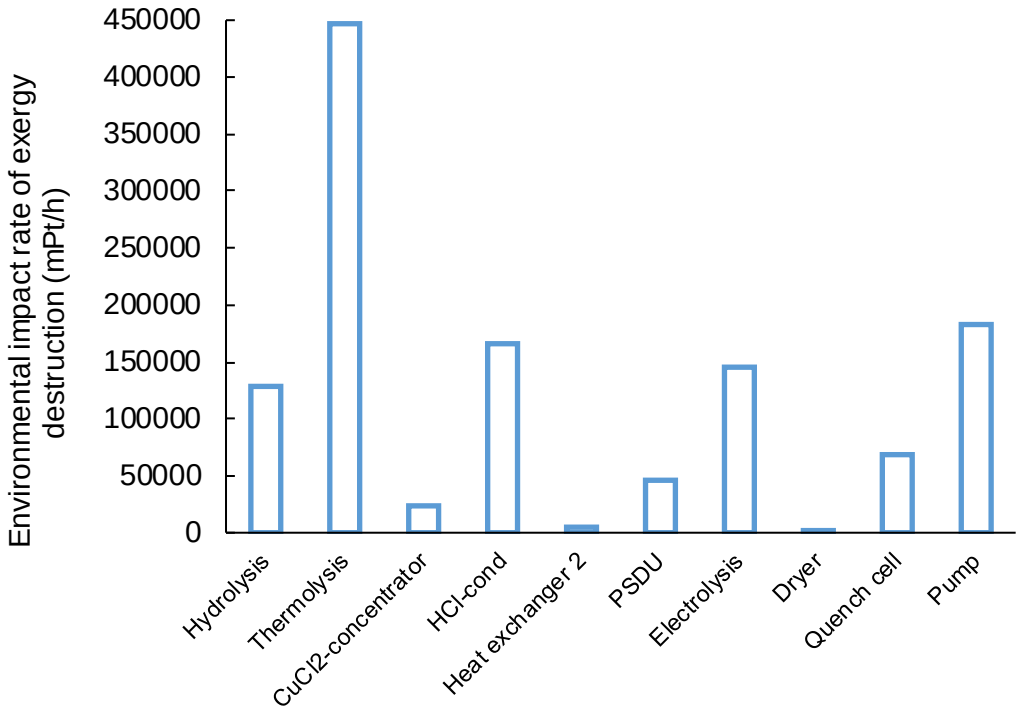

(a)

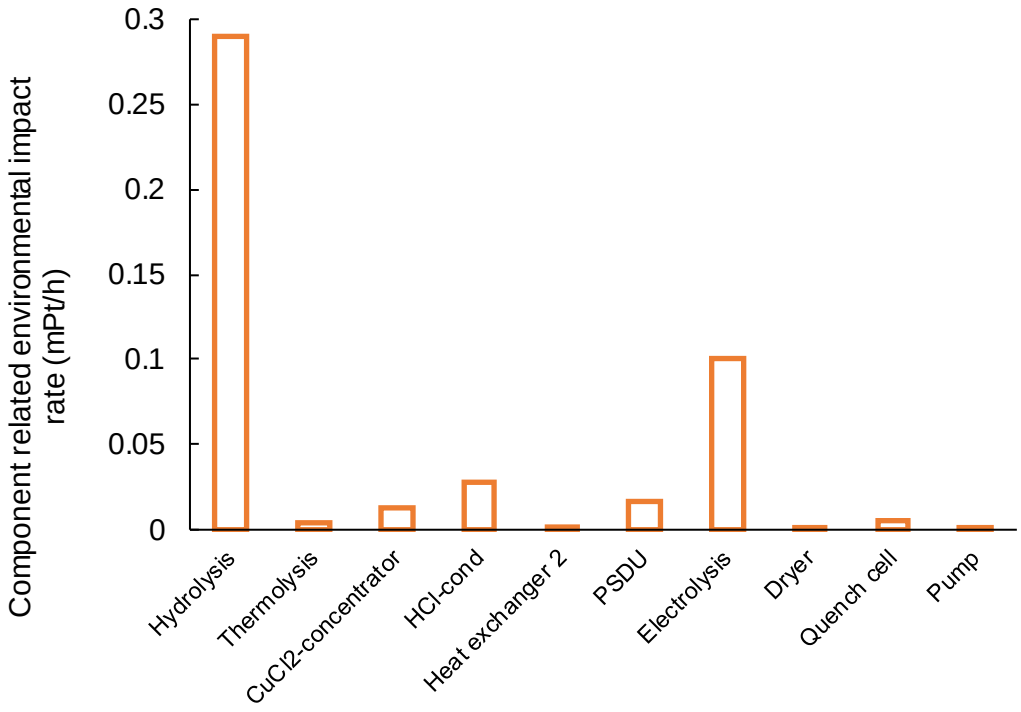

(b)

Fig. 5.75. (a) Environmental impact rates of exergy destructions and (b) component-related environmental impact rates of various components

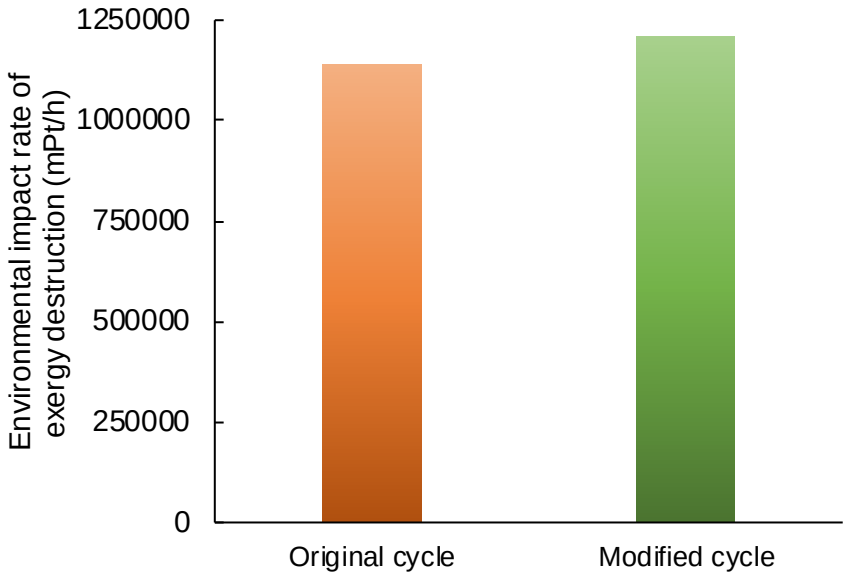

Fig. 5.76. Comparison between the original and modified cycle in terms of environmental impact rates of exergy destructions

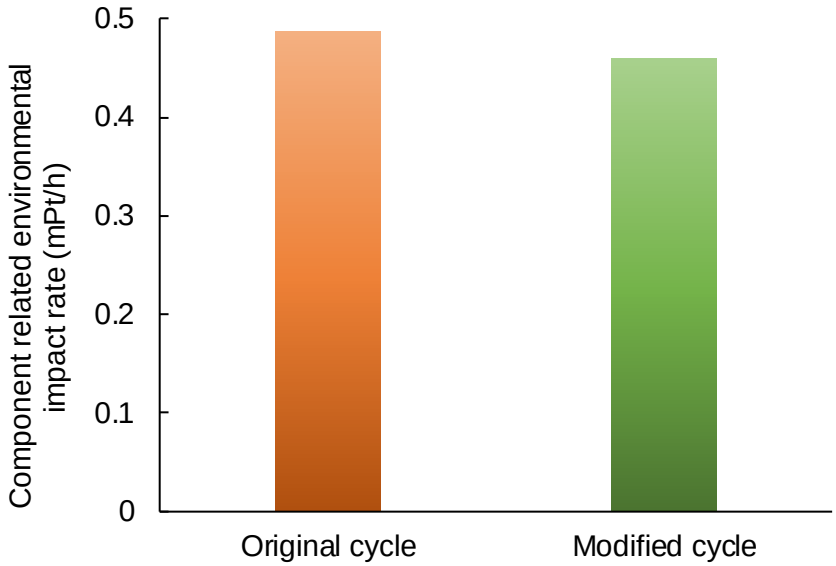

Fig. 5.77. Comparison between the original and modified cycle in terms of component-related environmental impact rates

5.3 Experimental results of the standalone flash vaporization process

The results obtained through the experiments performed on a stand-alone experimental set-up for the flash vaporization process are presented and discussed in this section. The results are obtained in terms of the volume of the HCl and H_2O mixture separated from the anolyte mixture at various operating conditions. Moreover, the molarity and percentage

concentration of HCl in the separated mixture is also obtained and discussed. Further, a comparative evaluation of the obtained results is also carried out experimentally.

Figure 5.78 shows the effect of the operating temperature of the anolyte on the volume of the separated mixture of HCl and H_2O for the two flash chamber configurations considered at a constant vacuum pressure of 0.15 bar and a flow rate of 0.004 l/s. Three different temperatures i.e., 65, 75, and 85ºC are considered in this regard. According to the performed experiments, the volume of separated HCl and H_2O mixture increases with an increase in the operating temperature of the anolyte. However, the separated volume through flash chamber 1 is much higher than flash chamber 2. The minimum and the maximum separated volumes in flash chamber 1 range between 15 and 26 ml respectively after 10 experimental runs while for flash chamber 2, these values range between 4.5 and 11 ml.

Figure 5.79 shows the effect of vacuum pressure of the anolyte on the volume of the separated mixture of HCl and H_2O for the two flash chamber configurations considered at a constant operating temperature of 65ºC and a flow rate of 0.004 l/s. The vacuum pressure is varied from 0.5 bar to 0.2 bar in this regard. The experimental observations show that a decrease in the vacuum pressure of the anolyte causes an increase in the separated volume of the HCl and H_2O mixture for both flash chambers. However, similar to Figure 1, flash chamber 1 yields a higher volume of the separated mixture compared with flash chamber 2. The minimum and the maximum separated volumes in flash chamber 1 range between 1.6 and 2.5 ml respectively after 3 experimental runs while for flash chamber 2, these values range between 0.5 and 0.95 ml.

Figure 5.80 shows the effect of the flow rate of the anolyte on the volume of the separated mixture of HCl and H_2O for the two flash chamber configurations considered at a constant operating temperature of 65ºC and a vacuum pressure of 0.15 bar. The flow rates are varied from 0.003 l/s to 0.005 l/s. According to the performed experiments, the volume of separated HCl and H_2O mixture increases with an increase in the flow rate of the anolyte. However, following the same trends of Figures 5.78 and 5.79, the separated volume in flash chamber 1 is much higher than flash chamber 2. The minimum and the maximum

separated volumes in flash chamber 1 range between 1.8 and 2.7 ml respectively after 3 experimental runs while for flash chamber 2, these values range between 0.6 and 1.2 ml.

Based on these experimental results, the separation performance of flash chamber 1 is observed to be much better than that of flash chamber 2 for all operating conditions. This better performance of flash chamber 1 may be attributed to its geometrical specifications such as the inlet location which is at the top reducing its distance from the outlet port compared with the bottom inlet of flash chamber 2. Moreover, it has a higher L/D ratio in comparison with flash chamber 2.

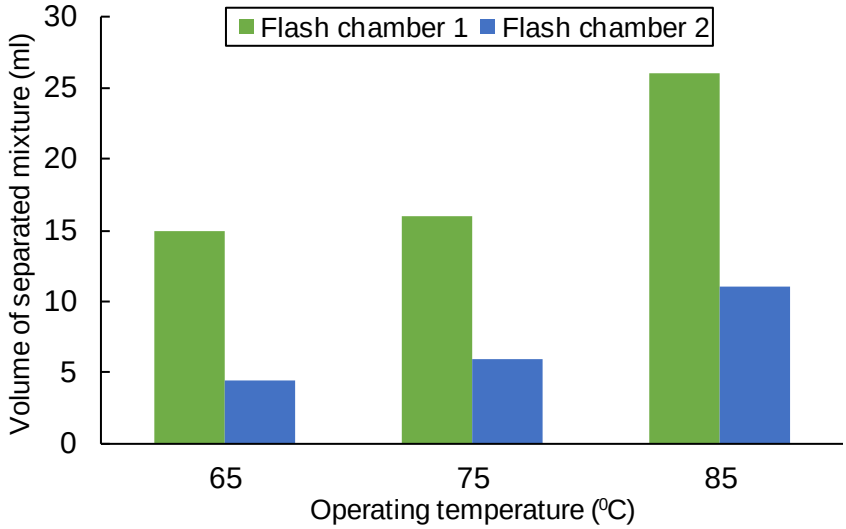

Fig. 5.78. Variation in volume of separated mixture of HCl and H_2O with temperature for flash chambers 1 and 2 at constant pressure and flow rate

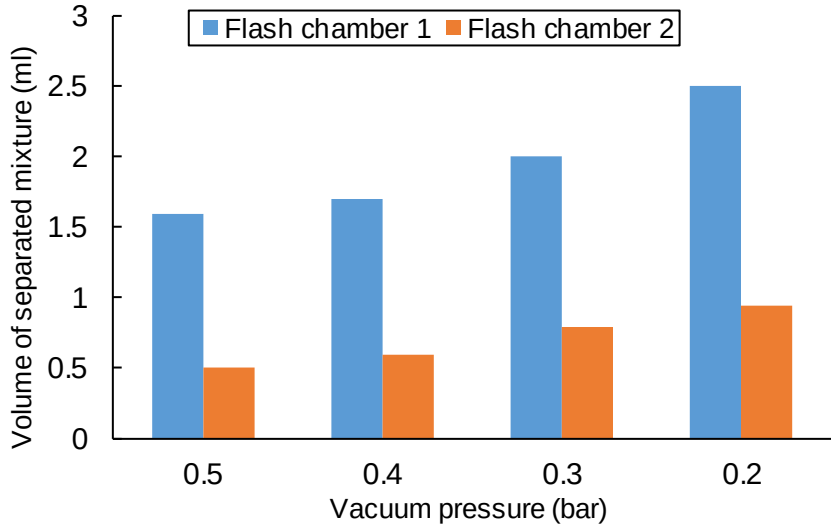

Fig. 5.79. Variation in volume of separated mixture of HCl and H_2O with vacuum pressure for flash chambers 1 and 2 at constant operating temperature and flow rate

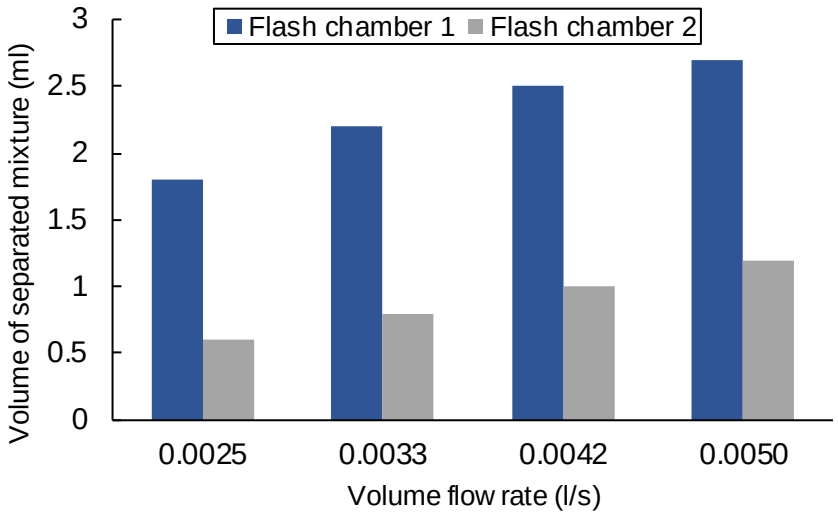

Fig. 5.80. Variation in volume of separated mixture of HCl and H_2O with flow rate for flash chambers 1 and 2 at constant operating temperature and vacuum pressure

Figure 5.81 shows the mass of the separated mixture of HCl and H_2O in grams after one experimental run at the three considered operating temperatures for both flash chamber designs at a constant flow rate of 250 ml/min and a constant vacuum pressure of 0.15 bar. The obtained separated mass per run for flash chamber 1 is higher than flash chamber 2 at all operating temperatures. The separated mass for flash chamber 1 ranges between 2.4 and 4.1 g while ranges between 0.7 and 1.7 g for flash chamber 2 between the minimum and the maximum operating temperatures considered.

Figure 5.82 shows the mass of the separated mixture of HCl and H_2O in grams after one experimental run at various vacuum pressures for both flash chamber designs at a constant flow rate of 250 ml/min and a constant operating temperature of 65ºC. The obtained separated mass per run for flash chamber 1 is higher than flash chamber 2 at all vacuum pressures. The separated mass for flash chamber 1 ranges between 0.84 and 1.32 g while ranges between 0.25 and 0.51 g for flash chamber 2 between the minimum and the maximum vacuum pressures considered.

Figure 5.83 shows the mass of the separated mixture of HCl and H_2O in grams after one experimental run at various Reynolds numbers for both flash chamber designs at a constant vacuum pressure of 0.15 bar and a constant operating temperature of 65ºC. The obtained separated mass per run for flash chamber 1 is higher than flash chamber 2 at all flow rates.

The separated mass for flash chamber 1 ranges between 1.11 and 1.43 g while ranges between 0.32 and 0.63 g for flash chamber 2 between the minimum and the maximum Reynolds numbers considered.

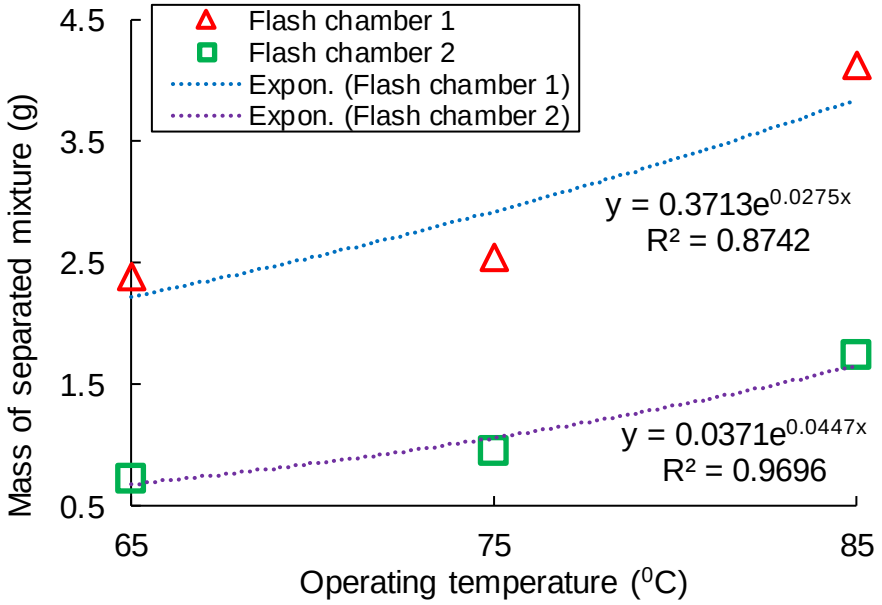

Fig. 5.81. Variation in mass of separated mixture of HCl and H_2O with temperature for flash chambers 1 and 2 at constant pressure and flow rate

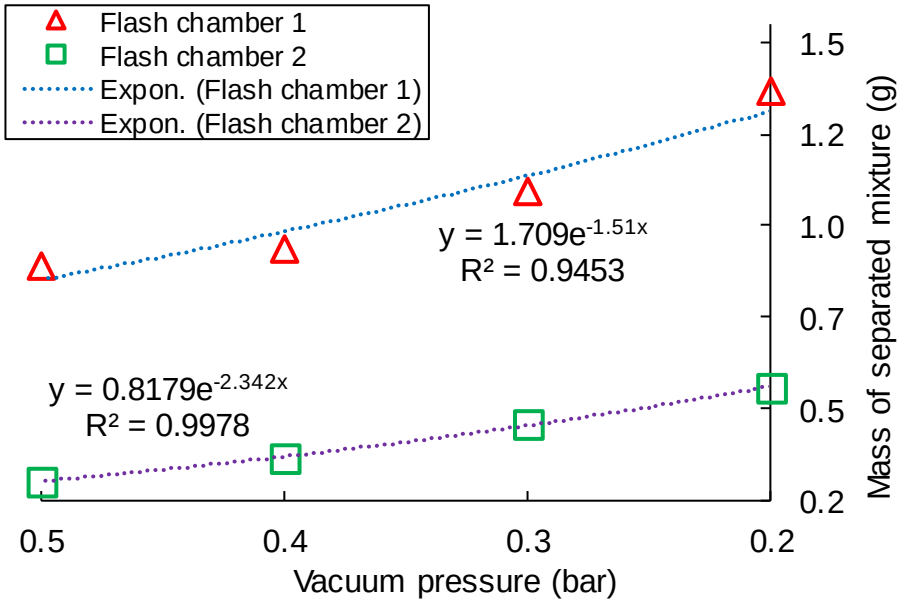

Fig. 5.82. Variation in mass of separated mixture of HCl and H_2O with vacuum pressure for flash chambers 1 and 2 at constant operating temperature and flow rate

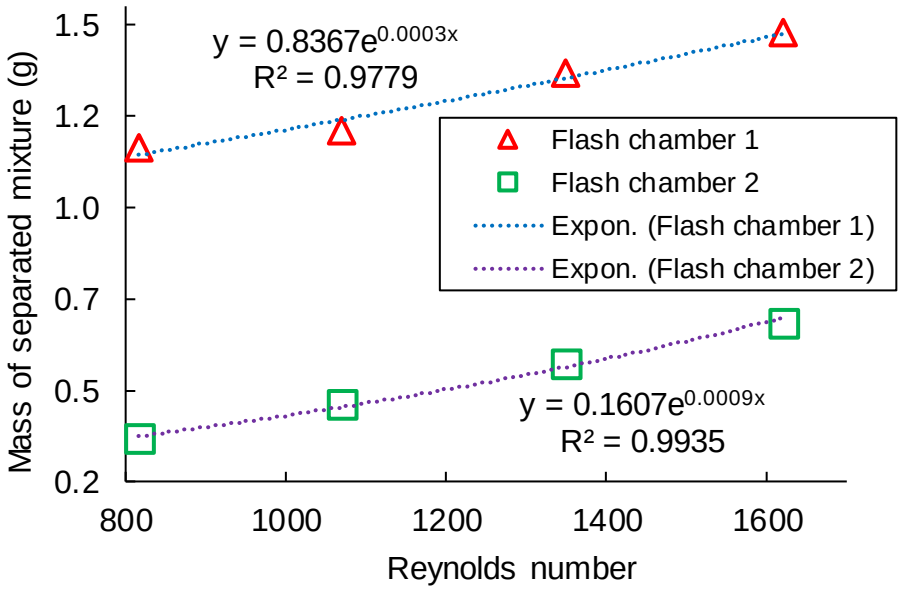

Fig. 5.83. Variation in mass of separated mixture of HCl and H_2O with Reynolds number for flash chambers 1 and 2 at constant vacuum pressure and operating temperature

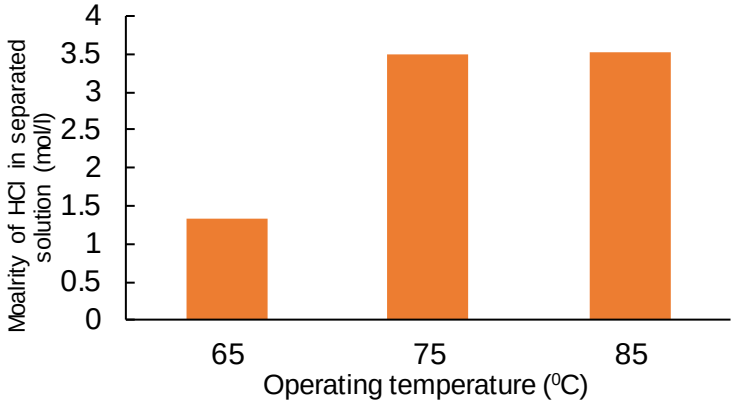

(a)

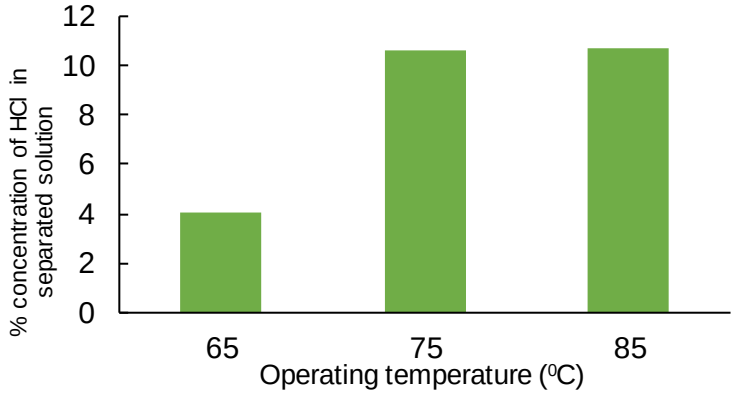

(b)

Fig. 5.84. Variation in (a) molarity and (b) % concentration of HCl in separated solution with temperature

Figures 5.84a and 5.84b show the effect of operating temperature on molarity and % concentration of HCl in the separated solution, respectively. An increase in operating temperature from 65 to 85ºC causes the molarity and the % concentration of HCl to increase in the separated mixture. However, this increase is substantial when the temperature is increased from 65 to 75ºC while insignificant when the temperature is increased from 75 to 85ºC. The molarity of HCl in the separated mixture increases from 1.33 to 3.50 mol/l when the operating temperature increases from 65 to 75ºC however it experiences a minor increase from 3.50 to 3.52 mol/l upon increasing the temperature from 75 to 85ºC. Similarly, the % concentration of HCl in the separated mixture increases from 4.04% to 10.64% when the operating temperature increases from 65 to 75ºC whereas it only increases up to 10.71% when the temperature increases from 75 to 85ºC.

Figure 5.85 shows the separated mixture samples of HCl and H_2O at 65, 75, and 85ºC at a constant operating vacuum pressure of 0.15 bar and a flow rate of 300 ml/min. As the operating temperature increases, the separated mixture gets bluer in color for both flash chamber designs. An increase in density of blue color of the HCl and H_2O mixture suggests an increase in concentration of the dissolved $CuCl_2$ when the flash vaporization process is realized at higher temperatures. This has been experimentally observed and verified since the $CuCl_2$ dissolved in water produces a clear blue colored solution.

Table 5.26 shows the optimal operating conditions of the anolyte including operating temperatures, vacuum pressures, and flow rate for various objectives. For scenario 1 when the objectives include high separation volume and HCl concentration in the separated mixture, a temperature of 85ºC, a vacuum pressure of 0.15 bar, and a flow rate of 0.005 l/s is observed as the optimal conditions. For scenario 2 when the objectives include moderate separation volume as well as operating temperature and high concentration of HCl in the separated mixture, a temperature of 75ºC, a vacuum pressure of 0.15 bar, and a flow rate of 0.005 l/s are found to be the optimal conditions. For scenario 3 when the objectives include moderate separation volume, low HCl concentration in the separated mixture and minimum operating temperature, a temperature of 65ºC, a vacuum pressure of 0.15 bar, and a flow rate of 0.005 l/s are observed as the optimal conditions.

(a) (b) (c)

Fig. 5.85. Samples of the separated HCl and H_2O mixture at (a) 65ºC, (b) 75ºC, and (c) 85ºC

Figure 5.86 provides a comparison between the flash vaporization process and atmospheric distillation process of anolyte at the same operating temperature as well as at a temperature of 85ºC. A total of 10 experimental runs for each case are conducted and it is concluded that the volume separated after each run at 104ºC at a vacuum pressure of 0.15 bar is much higher than that at ambient pressure. Further, the separated volume at 85ºC and a vacuum pressure of 0.15 bar is also much higher compared with the volume separated at 104ºC at ambient pressure. This increase in volume with respect to the reference conditions (104ºC at ambient pressure) is evaluated to be 225% for 104ºC and 0.15 bar vacuum pressure and 112.5% for 85ºC and 0.15 bar vacuum pressure.

Table 5.26 Optimal operating conditions for various process objectives

Scenario	**Objective**	**Operating conditions**		
		T (ºC)	**P_{vac} (bar)**	**$\dot{V}$ (l/s)**
1	High volume separation High HCl concentration in the separated mixture	85	0.15	0.005
2	Moderate volume separation High HCl concentration in the separated mixture Moderate operating temperature	75		
3	Moderate volume separation Low HCl concentration in the separated mixture Lowest operating temperature	65		

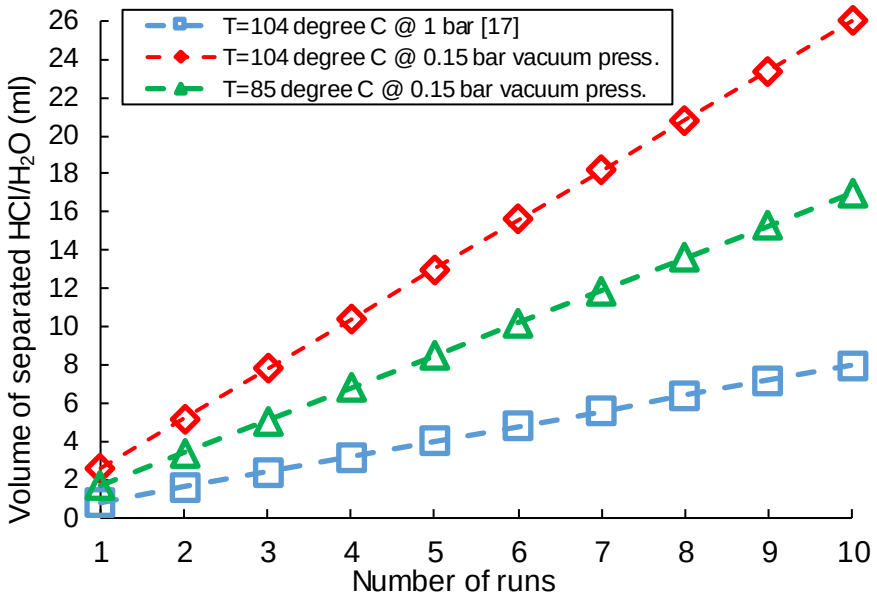

Fig. 5.86. Comparison of separated mixture volume between flash vaporization process and the atmospheric distillation process of anolyte in the actual integrated cycle

The main reason for selecting a modeling-based study for comparison of experimental results for flash vaporization is that there are no studies in literature that experimentally considers the anolyte separation process in a Cu-Cl cycle at atmospheric pressure. However, the operating conditions considered in [17] are the suggested conditions for the atmospheric distillation process to take place in the actual integrated Cu-Cl cycle at CERL by the authors.

5.4 Empirical correlation results

This section presents the obtained results for the empirical correlation developed for predicting the theoretical mass flow rate of the separated mixture of the HCl and H_2O mixture as a consequence of the flash vaporization process. Figures 5.87, 5.88 and 5.89 provide a comparison between the theoretically calculated and experimentally obtained mass flow rates of the separated fraction of the mixture of HCl and H_2O for the variation in operating temperature, vacuum pressure, and volume flow rate, respectively. Figures 5.90, 5.91, and 5.92 provide a comparison between the theoretically calculated and experimentally obtained percentage separation for the variation in operating temperature, vacuum pressure, and volume flow rate, respectively. Based on the comparison between the theoretical and experimental data, it is observed that the empirical model over predicts the mass flow rate of the vaporization fraction of the anolyte.

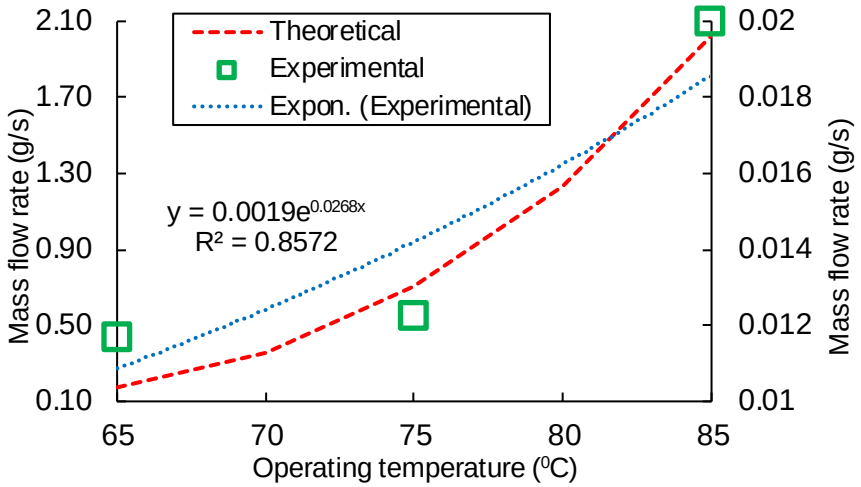

Fig. 5.87. Comparison of variation in mass flow rate of the separated mixture of HCl and H_2O with operating temperature between the model and experimental data

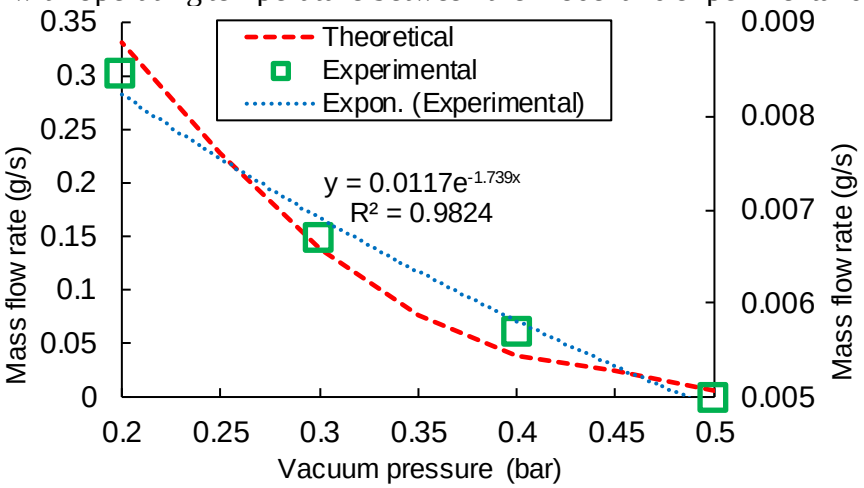

Fig. 5.88. Comparison of variation in mass flow rate of the separated mixture of HCl and H_2O with vacuum pressure between the model and experimental data

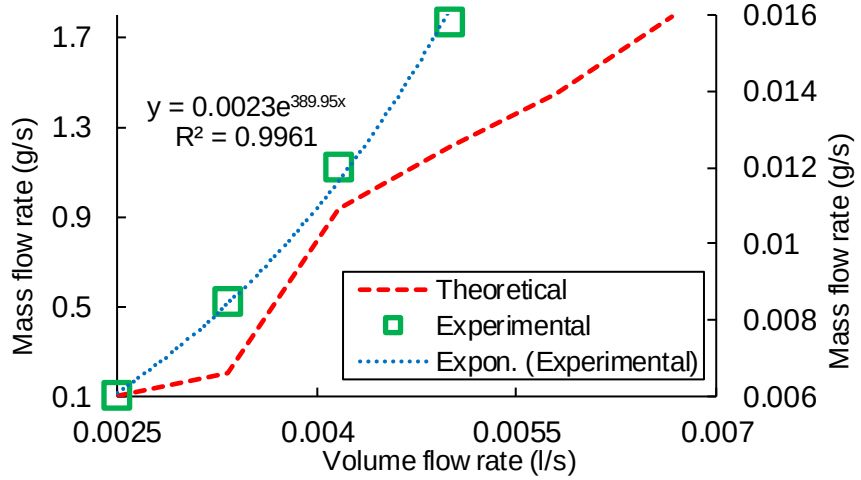

Fig. 5.89. Comparison of variation in mass flow rate of the separated mixture of HCl and H_2O with volume flow rate between the model and experimental data

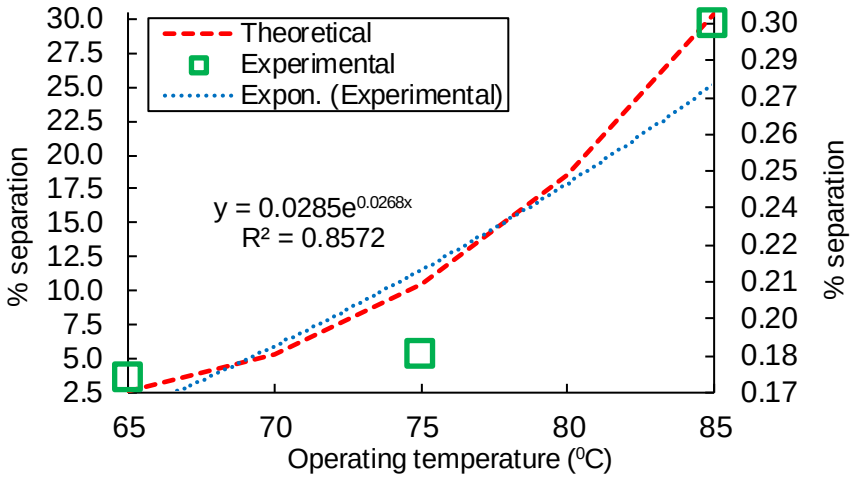

Fig. 5.90. Comparison of variation in percentage separation with operating temperature between the model and experimental data

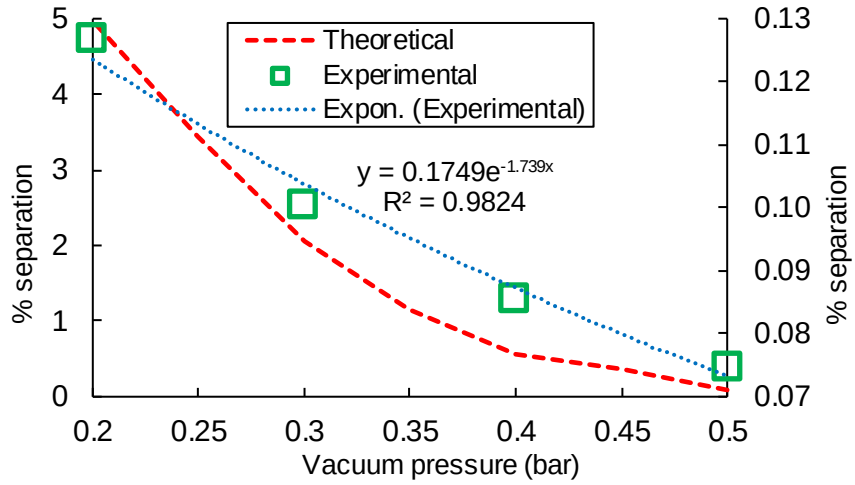

Fig. 5.91. Comparison of variation in percentage separation with vacuum pressure between the model and experimental data

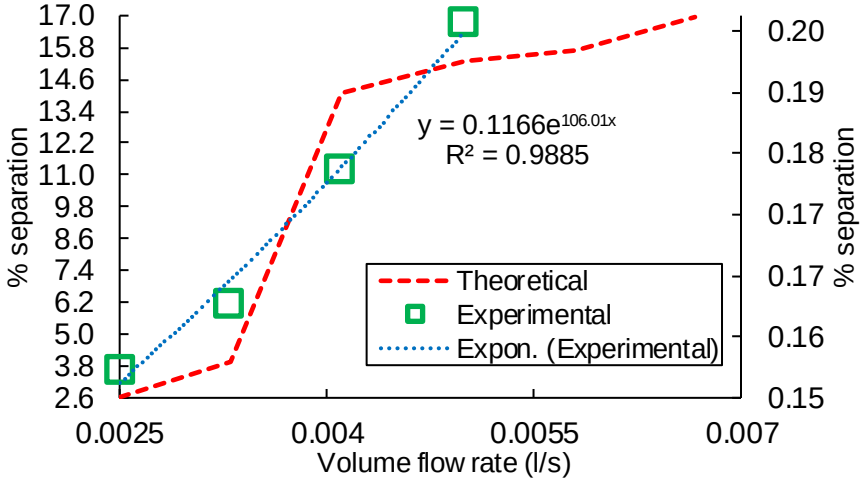

Fig. 5.92. Comparison of variation in percentage separation with volume flow rate between the model and experimental data

However, the variation trends obtained for each case are quite similar for both the theoretical and experimental data. Thus, modifications in this empirical model are needed which require further extensive experimental work for identification of certain factors, the inclusion of which, may further improve the accuracy of the model's prediction. This could be achieved as part of a future work since the scope of this thesis study includes the development of a basic and a novel empirical correlation for theoretical prediction of the flash vaporization phenomenon. In this regard, the developed model has the potential to serve as a benchmark for future studies.

5.5 Potential process improvements

There are four-steps in the Cu-Cl cycle and each of them possess a certain margin of improvement. The first step of the cycle i.e., the hydrolysis step needs considerable reduction in its heat input rate by considering thermal management through internal and/or waste heat recovery thereby increasing overall efficiencies. Various thermal management schemes have been conceptually suggested in this thesis. However, a big challenge lies in its experimental realization at the lab-scale due to the design complexity and fabrication cost of heat exchangers. Similarly, the highest rate of exergy destruction in the cycle is associated with the thermolysis step (Figure 5.93) which is a consequence of the high irreversibilities affiliated with the process. An improvement in thermolysis step is essential however, the design complexity and fabrication cost of the thermolysis reactor at lab-scale is a big challenge for its experimental implementation. The same goes for the electrolysis step where design optimization of the electrolyzer may improve the overall cycle performance.

Based on the thermodynamic and exergoeconomic analyses of the Cu-Cl cycle carried out in this thesis, it is concluded that an improvement in the anolyte separation step of the cycle can potentially improve the overall cycle performance. An essential requirement of achieving such potential improvement is implementation of a process which is less energy intensive and more cost effective. Flash vaporization process is found to meet both these criteria through modeling and simulation of the cycle incorporated with this approach in Aspen-plus. The experimental implementation of this approach at lab-scale is also practically feasible based on the relatively fewer design complexities associated.

Moreover, the development of a stand-alone experimental set up for flash vaporization is much more financially viable compared with other steps of the cycle. It is because of these reasons that the anolyte separation step of the cycle has been selected for an overall improvement in the cycle performance.

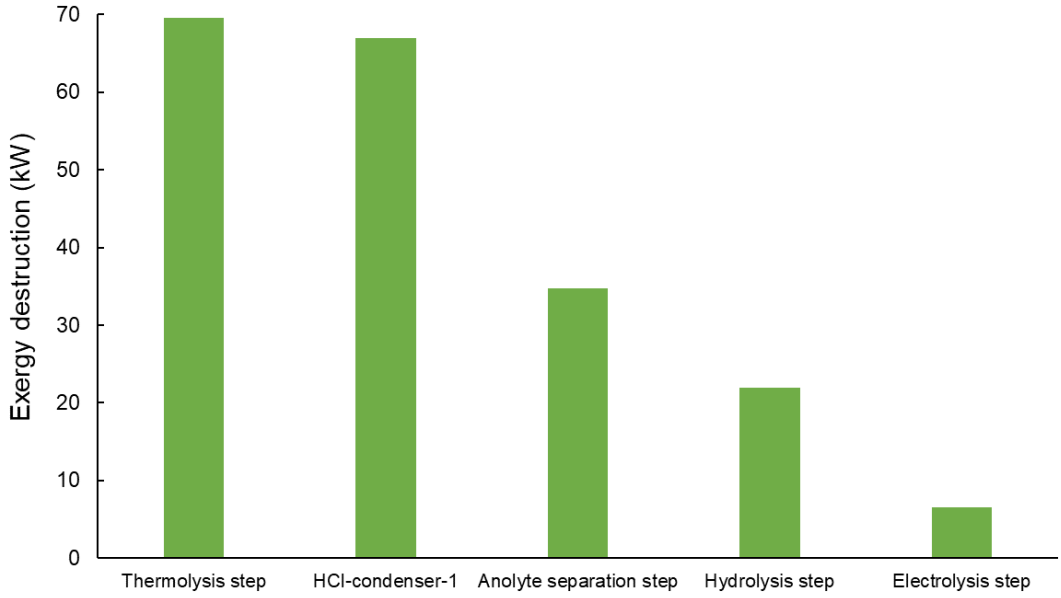

Fig. 5.93. Exergy destruction rates of some of the main processes in the cycle

In closing, this chapter provides comprehensive modeling results for the existing and the modified integrated cycles based on energy and exergy, thermal management, exergoeconomic, exergoenvironmental, and multi-objective optimization analyses. Moreover, the experimental results for the flash vaporization process, the empirical modeling results and the potential improvements in various steps of the cycle are discussed. The following chapter provides the main conclusions and recommendations of this thesis.

CHAPTER 6 : CONCLUSIONS AND RECOMMENDATIONS

In this chapter, the major outcomes, results, and findings obtained from this thesis are briefly described. Based on these findings, recommendations for future studies are provided.

6.1 Conclusions

In this thesis, a four-step integrated thermochemical Cu-Cl cycle for hydrogen production is investigated through numerical modeling in Aspen-plus. The investigated system is based on the actual lab-scale Cu-Cl cycle setup developed at CERL at the Ontario Tech University. This thesis studies the integrated cycle through various analyses such as energy and exergy, thermal management, exergoeconomic, exergoenvironmental and multi-objective optimization. This thesis also considers the development of a new and alternate approach for the anolyte separation step of the cycle through the flash vaporization process. In this regard, the integrated cycle is first conceptually modified with the flash vaporization process, modeled in Aspen-plus and investigated through energy and exergy, thermal management, exergoeconomic, and exergoenvironmental approaches. The modeling results of the actual and the modified integrated cycles are also compared for comparative evaluation of both systems. The flash vaporization process is also experimentally investigated through a standalone experimental set-up specifically developed as part of this thesis for assessing the practical feasibility of the approach for the anolyte separation step of the cycle.

The main findings obtained as a result of the modeling of the integrated Cu-Cl cycle at CERL are summarized as follows:

- The thermolysis step (second step) of the cycle results in the highest exergy destruction rate, the hydrolysis step (first step) of the cycle results in the highest heat input rate, and the HCl-condenser-1 of the cycle results in the highest heat discharge rate.
- The cycle operates at an energy efficiency of 6.6% and an exergy efficiency of 10.2%.

- Among the several internal heat recovery schemes considered for thermal management of the cycle, the maximum energy and exergy efficiencies of the cycle are obtained as 10.7% and 16.3% respectively at a S/Cu ratio of 12.9 due to the highest heat recovery temperature of 391.3ºC.
- The unit cost of hydrogen obtained as a result of the application of the EXCEM approach is obtained as 5.5 $/kg at a production capacity of 1.6 T/h with a cost generation rate of 665.7 $/h.
- The unit cost of hydrogen obtained as a result of the application of the SPECO approach is obtained as 4.9 $/kg at a production capacity of 1.3 T/h with an exergy cost of hydrogen of 6407.5 $/h and a specific exergy cost of hydrogen of 0.042 $/MJ.
- According to the exergoenvironmental assessment of the cycle, the hydrolysis step results in the maximum component-related environmental impact rate whereas the thermolysis step results in the maximum environmental impact rate of exergy destruction.
- According to the multi-objective optimization of the cycle, an increase in the cost rate and hydrogen production capacity while a reduction in the exergy efficiency of the cycle occurs upon increasing the S/Cu ratio.
- The trade-off or the optimal point of all objective functions for all the considered cases occurs at S/Cu ratios ranging from 15.7 to 16.9.

The main findings obtained as a result of the modeling of the integrated Cu-Cl cycle conceptually modified with flash vaporization process are summarized as follows:

- The cycle operates at an energy efficiency of 7.2% and an exergy efficiency of 11% which are relatively higher than those of the actual integrated cycle at CERL.
- The modified cycle results in lower net heat input rate and overall exergy destruction rate compared with the actual integrated cycle at CERL.
- The incorporation of the flash vaporization process also reduces the heat input rate and exergy destruction rate associated with the anolyte separation step of the cycle.
- Among the several internal/waste heat recovery schemes considered for the thermal management of the modified cycle, the highest energy and exergy efficiencies of

21% and 31.5%, respectively are obtained when both internal and waste heat recovery from a steel plant are considered.

- The unit hydrogen cost for the modified cycle is also lower than the actual cycle.
- Moreover, the unit hydrogen cost for the modified cycle operating without heat recovery is obtained to be between 3.75 $/kg (best case scenario) and 5.6 $/kg (worst case scenario) with an average unit hydrogen cost of 4.7 $/kg while this value is evaluated to be between 1.6 $/kg (best case scenario) and 2.4 $/kg (worst case scenario) with an average unit hydrogen cost of 2 $/kg for the cycle operating with waste heat recovery for a plant producing hydrogen at a rate of 1.3 T/h.

The primary findings obtained from the experiments performed via a standalone flash vaporization setup are summarized below:

- An increase in operating temperature results in a higher volume of the separated mixture of HCl and H_2O at a fixed vacuum pressure and flow rate.
- An increase in vacuum pressure results in a higher volume of the separated mixture of HCl and H_2O at a fixed operating temperature and flow rate.
- An increase in flow rate results in a higher volume of the separated mixture of HCl and H_2O at a fixed operating temperature and vacuum pressure.
- The separated mixture of HCl and H_2O turns bluer in color with an increase in operating temperature.
- Flash chamber 1, which has a higher L/D ratio compared with flash chamber 2, results in higher volume separation at all operating conditions.
- At both 75^0C and 85^0C, the separated solution results in a much higher and nearly the same HCl concentration than at 65^0C.
- At both 65^0C and 75^0C, the separated volume is nearly the same and much less than the volume at 85 ^{0}C.

6.2 Recommendations

Considering findings obtained from this thesis, the following recommendations are provided for future studies:

- There is a need to perform further modeling studies and validation with experimental results for the individual steps and the complete integrated Cu-Cl cycle at CERL.
- There is a need to perform further optimization studies for each step of the integrated cycle by considering different objective functions and decision variables.
- Internal heat recovery, as suggested in this thesis, should be experimentally realized for improvement in cycle efficiencies.
- The flash vaporization process should be performed at higher flow rates and higher vacuum pressures for the separation to occur at lower operating temperatures.
- The samples of the separated mixture of HCl and H_2O should be further characterized through the Fourier-transform infrared spectroscopy and thermogravimetric analysis for more accurate and detailed sample assessment.
- Different flash chamber designs should be investigated and various geometric parameters should be examined for optimal flashing performance.
- Life cycle assessment and scale-up studies of the integrated cycle should be performed.
- Various integrated systems based on the four-step Cu-Cl cycle should be developed and studied.

REFERENCES

[1] N. Bauer, J. Hilaire, R. Brecha, J. Edmonds, K. Jiang, E. Kriegler, H. Rogner, and F. Sferra, "Assessing global fossil fuel availability in a scenario framework," *Energy*, vol. 111, pp. 580–592, 2016.

[2] J. Andrews, "Designing a sustainable hydrogen energy economy," *Int. J. Sustain. Des.*, vol. 1, no. 4, p. 361, 2011.

[3] O. Ellabban, H. Abu-Rub, and F. Blaabjerg, "Renewable energy resources: Current status, future prospects and their enabling technology," *Renew. Sustain. Energy Rev.*, vol. 39, pp. 748–764, 2014.

[4] N. Z. Muradov and T. N. Veziroğlu, "From hydrocarbon to hydrogen-carbon to hydrogen economy," *Int. J. Hydrogen Energy*, vol. 30, no. 3, pp. 225–237, 2005.

[5] I. Dincer and C. Zamfirescu, "Sustainable hydrogen production options and the role of IAHE," *Int. J. Hydrogen Energy*, vol. 37, no. 21, pp. 16266–16286, 2012.

[6] I. Staffell, D. Scamman, A. Velazquez, P. Balcombe, P. Dodds, P. Ekins, N. Shah, and K. Ward, "The role of hydrogen and fuel cells in the global energy system," *Energy Environ. Sci.*, vol. 12, no. 2, pp. 463–491, 2019.

[7] Ö. F. Dilmaç and S. K. Özkan, "Energy and exergy analyses of a steam reforming process for hydrogen production," *Int. J. Exergy*, vol. 5, no. 2, pp. 241–248, 2008.

[8] A. Moumen, G. Azizi, K. Ben Chekroun, and M. Baghour, "The effects of livestock methane emission on the global warming: A review," *Int. J. Glob. Warm.*, vol. 9, no. 2, pp. 229–253, 2016.

[9] A. T-Raissi, "Water splitting: Thermochemical," *Encyclopedia of Inorganic and Bioinorganic Chemistry*. John Wiley & Sons, 2012.

[10] F. Safari and I. Dincer, "A review and comparative evaluation of thermochemical water splitting cycles for hydrogen production," *Energy Convers. Manag.*, vol. 205, p. 112182, 2020.

[11] J. R. Schuster, "Status of thermochemical water-splitting development at general atomics. Gen Atom GA report GA-A14666," 1977.

[12] M. A. Lewis, M. Serban, and J. K. Basco, "Hydrogen production at <550°C using a low temperature thermochemical cycle," Argonne National Laboratory, 9700 S. Cass Avenue, Argonne, IL 60439, 2003.

[13] M. A. Lewis, J. G. Masin, and R. B. Vilim, "Development of the low temperature Cu-Cl thermochemical cycle," in *International Congress on Advances in Nuclear Power Plants*, Seoul, Korea, May 15-19, 2005.

[14] Z. L. Wang, K. S. Gabriel, and G. F. Naterer, "Thermochemical process heat requirements of the copper-chlorine cycle for nuclear-based hydrogen production," in *29th Conference of the Canadian Nuclear Society*, Toronto, Ontario, June 1-4, 2008.

[15] Z. L. Wang, G. F. Naterer, K. S. Gabriel, R. Gravelsins, and V. N. Daggupati, "New Cu-Cl thermochemical cycle for hydrogen production with reduced excess steam requirements," *Int. J. Green Energy*, vol. 6, no. 6, pp. 616–626, 2009.

[16] H. Ishaq and I. Dincer, "A comparative evaluation of three Cu-Cl cycles for hydrogen production," *Int. J. Hydrogen Energy*, vol. 44, no. 16, pp. 7958–7968, 2019.

[17] A. Farsi, C. Zamfirescu, I. Dincer, and G. F. Naterer, "Thermodynamic assessment

of a lab-scale experimental copper-chlorine cycle for sustainable hydrogen production," *Int. J. Hydrogen Energy*, vol. 44, no. 33, pp. 17595–17610, 2019.

[18] M. S. Ferrandon, M. A. Lewis, D. F. Tatterson, A. Gross, D. Doizi, L. Croize, V. Dauvois, J. L. Roujou, Y. Zanella, and P. Carles, "Hydrogen production by the Cu-Cl thermochemical cycle: Investigation of the key step of hydrolysing $CuCl_2$ to Cu_2OCl_2 and HCl using a spray reactor," *Int. J. Hydrogen Energy*, vol. 35, no. 3, pp. 992–1000, 2010.

[19] M. A. Lewis, M. S. Ferrandon, D. F. Tatterson, and P. Mathias, "Evaluation of alternative thermochemical cycles - Part III further development of the Cu-Cl cycle," *Int. J. Hydrogen Energy*, vol. 34, no. 9, pp. 4136–4145, 2009.

[20] R. V. Singh, M. R. Pai, A. M. Banerjee, G. R. Patkare, R. V. Pai, A. Kumar, A. K. Yadav, S. Phaphale, and A. Tripathi, "Investigations on the hydrolysis step of copper-chlorine thermochemical cycle for hydrogen production," *Int. J. Energy Res.*, vol. 44, no. 4, pp. 2845–2863, 2020.

[21] R. S. Schatz, S. Kim, S. Khurana, M. V. Fedkin, and S. N. Lvov, "High efficiency CuCl electrolyzer for Cu-Cl thermochemical cycle," in *ECS Transactions*, 2012, vol. 50, no. 49, pp. 153–164.

[22] D. M. Hall, N. N. Akinfiev, E. G. Larow, R. S. Schatz, and S. N. Lvov, "Thermodynamics and Efficiency of a CuCl(aq)/HCl(aq) Electrolyzer," *Electrochim. Acta*, vol. 143, pp. 70–82, 2014.

[23] Y. Gong, E. Chalkova, N. N. Akinfiev, V. N. Balashov, M. V. Fedkin, and S. N. Lvov, "CuCl-HCl electrolyzer for hydrogen production via Cu-Cl thermochemical cycle," in *ECS Transactions*, 2009, vol. 19, no. 10, pp. 21–32.

[24] G. F. Naterer, S. Suppiah, M. Lewis, K. Gabriel, I. Dincer, M. A. Rosen, M. Fowler *et al.*, "Recent Canadian advances in nuclear-based hydrogen production and the thermochemical Cu-Cl cycle," *Int. J. Hydrogen Energy*, vol. 34, no. 7, pp. 2901–2917, 2009.

[25] G. F. Naterer, V. N. Daggupati, G. Marin, K. S. Gabriel, and Z. L. Wang, "Thermochemical hydrogen production with a copper-chlorine cycle, II: Flashing and drying of aqueous cupric chloride," *Int. J. Hydrogen Energy*, vol. 33, no. 20, pp. 5451–5459, 2008.

[26] G. F. Naterer, S. Suppiah, M. A. Rosen, K. S. Gabriel, I. Dincer, O. Jianu *et al.*, "Advances in unit operations and materials for the Cu–Cl cycle of hydrogen production," *Int. J. Hydrogen Energy*, vol. 42, no. 24, pp. 15708–15723, 2017.

[27] Z. Wang, V. Daggupati, G. Marin, K. Pope, Y. Xiong, E. Secnik, G. F. Naterer, and K. S. Gabriel, "Towards integration of hydrolysis, decomposition and electrolysis processes of the Cu-Cl thermochemical water splitting cycle," *Int. J. Hydrogen Energy*, vol. 37, no. 21, pp. 16557–16569, 2012.

[28] H. Ishaq and I. Dincer, "Design and performance evaluation of a new biomass and solar based combined system with thermochemical hydrogen production," *Energy Convers. Manag.*, vol. 196, no. March, pp. 395–409, 2019.

[29] W. Wu, F. T. Hsu, and H. Y. Chen, "Design and energy evaluation of a stand-alone copper-chlorine (Cu-Cl) thermochemical cycle system for trigeneration of electricity, hydrogen, and oxygen," *Int. J. Energy Res.*, vol. 42, no. 2, pp. 830–842, 2018.

[30] W. Wu, H. Yu, and J. Hwang, "'Energy analysis of a class of copper-chlorine (Cu-

Cl) thermochemical cycles,'" *Int. J. Hydrogen Energy*, vol. 42, pp. 15990–16002, 2017.
[31] H. Sayyaadi and M. Saeedi Boroujeni, "Conceptual design, process integration, and optimization of a solar Cu-Cl thermochemical hydrogen production plant," *Int. J. Hydrogen Energy*, vol. 42, no. 5, pp. 2771–2789, 2017.
[32] F. Khalid, I. Dincer, and M. A. Rosen, "Thermodynamic viability of a new three step high temperature Cu-Cl cycle for hydrogen production," *Int. J. Hydrogen Energy*, vol. 43, no. 41, pp. 18783–18789, 2018.
[33] H. Ishaq, I. Dincer, and G. F. Naterer, "Industrial heat recovery from a steel furnace for the cogeneration of electricity and hydrogen with the copper-chlorine cycle," *Energy Convers. Manag.*, vol. 171, pp. 384–397, 2018.
[34] G. F. Naterer, K. Gabriel, Z. L. Wang, V. N. Daggupati, and R. Gravelsins, "Thermochemical hydrogen production with a copper-chlorine cycle. I: oxygen release from copper oxychloride decomposition," *Int. J. Hydrogen Energy*, vol. 33, no. 20, pp. 5439–5450, 2008.
[35] S. Ghandehariun, M. A. Rosen, and G. F. Naterer, "Comparison of molten salt heat recovery options in the Cu-Cl cycle of hydrogen production," *Int. J. Hydrogen Energy*, vol. 36, pp. 11328–11337, 2011.
[36] A. Ozbilen, I. Dincer, and M. A. Rosen, "Development of new heat exchanger network designs for a four-step Cu-Cl cycle for hydrogen production," *Energy*, vol. 77. pp. 338–351, 2014.
[37] M. A. Rosen and I. Dincer, "Exergy-cost-energy-mass analysis of thermal systems and processes," *Energy Convers. Manag.*, vol. 44, no. 10, pp. 1633–1651, 2003.
[38] M. Ozturk and I. Dincer, "Exergoeconomic analysis of a solar assisted tea drying system," *Dry. Technol.*, vol. 38, no. 5–6, pp. 655–662, 2020.
[39] A. N. Anozie and O. J. Odejobi, "Influence of reference temperature on exergy and exergoeconomic performance of a natural gas fired thermal power plant," *Int. J. Exergy*, vol. 13, no. 1, pp. 102–123, 2013.
[40] A. Lazzaretto and G. Tsatsaronis, "SPECO: A systematic and general methodology for calculating efficiencies and costs in thermal systems," *Energy*, vol. 31, no. 8–9, pp. 1257–1289, 2006.
[41] J. Oyekale, M. Petrollese, F. Heberle, D. Brüggemann, and G. Cau, "Exergetic and integrated exergoeconomic assessments of a hybrid solar-biomass organic Rankine cycle cogeneration plant," *Energy Convers. Manag.*, vol. 215. 2020.
[42] T. Nakyai, S. Authayanun, Y. Patcharavorachot, A. Arpornwichanop, S. Assabumrungrat, and D. Saebea, "Exergoeconomics of hydrogen production from biomass air-steam gasification with methane co-feeding," *Energy Convers. Manag.*, vol. 140. pp. 228–239, 2017.
[43] O. K. Singh and S. C. Kaushik, "Exergoeconomic analysis of a Kalina cycle coupled coal-fired steam power plant," *Int. J. Exergy*, vol. 14, no. 1, pp. 38–59, 2014.
[44] E. J. C. Cavalcanti, G. F. De Souza, and M. S. R. Lima, "Evaluation of cogeneration plant with steam and electricity production based on thermoeconomic and exergoenvironmental analyses," *Int. J. Exergy*, vol. 25, no. 3, pp. 203–223, 2018.
[45] A. Baghernejad and M. Yaghoubi, "Exergoeconomic analysis and optimization of an Integrated Solar Combined Cycle System (ISCCS) using genetic algorithm," *Energy Convers. Manag.*, vol. 52, no. 5. pp. 2193–2203, 2011.

[46] A. Chitsaz, A. S. Mehr, and S. M. S. Mahmoudi, "Exergoeconomic analysis of a trigeneration system driven by a solid oxide fuel cell," *Energy Convers. Manag.*, vol. 106. pp. 921–931, 2015.
[47] A. Ozbilen, I. Dincer, and M. A. Rosen, "Development of a four-step Cu-Cl cycle for hydrogen production - Part I: Exergoeconomic and exergoenvironmental analyses," *Int. J. Hydrogen Energy*, vol. 41, no. 19, pp. 7814–7825, 2016.
[48] L. Meyer, G. Tsatsaronis, J. Buchgeister, and L. Schebek, "Exergoenvironmental analysis for evaluation of the environmental impact of energy conversion systems," *Energy*, vol. 34, no. 1, pp. 75–89, 2009.
[49] A. Boyano, A. M. Blanco-Marigorta, T. Morosuk, and G. Tsatsaronis, "Exergoenvironmental analysis of a steam methane reforming process for hydrogen production," *Energy*, vol. 36, no. 4, pp. 2202–2214, 2011.
[50] E. J. C. Cavalcanti, "Exergoeconomic and exergoenvironmental analyses of an integrated solar combined cycle system," *Renew. Sustain. Energy Rev.*, vol. 67, pp. 507–519, 2017.
[51] F. Petrakopoulou, A. Boyano, M. Cabrera, and G. Tsatsaronis, "Exergoeconomic and exergoenvironmental analyses of a combined cycle power plant with chemical looping technology," *Int. J. Greenh. Gas Control*, vol. 5, no. 3, pp. 475–482, 2011.
[52] G. Bonforte, J. Buchgeister, G. Manfrida, and K. Petela, "Exergoeconomic and exergoenvironmental analysis of an integrated solar gas turbine/combined cycle power plant," *Energy*, vol. 156, pp. 352–359, 2018.
[53] Y. Casas-Ledón, F. Spaudo, and L. E. Arteaga-Pérez, "Exergoenvironmental analysis of a waste-based Integrated Combined Cycle (WICC) for heat and power production," *J. Clean. Prod.*, vol. 164, pp. 187–197, 2017.
[54] D. H. D. Rocha and R. J. Silva, "Exergoenvironmental analysis of a ultra-supercritical coal-fired power plant," *J. Clean. Prod.*, vol. 231, pp. 671–682, 2019.
[55] T. Blumberg, Y. D. Lee, T. Morosuk, and G. Tsatsaronis, "Exergoenvironmental analysis of methanol production by steam reforming and autothermal reforming of natural gas," *Energy*, vol. 181, pp. 1273–1284, 2019.
[56] A. M. Blanco-Marigorta, M. Masi, and G. Manfrida, "Exergo-environmental analysis of a reverse osmosis desalination plant in Gran Canaria," *Energy*, vol. 76, pp. 223–232, 2014.
[57] S. Ghorbani, M. H. Khoshgoftar-Manesh, M. Nourpour, and A. M. Blanco-Marigorta, "Exergoeconomic and exergoenvironmental analyses of an integrated SOFC-GT-ORC hybrid system," *Energy*, vol. 206, p. 118151, 2020.
[58] A. Ahmadi, D. H. Jamali, M. A. Ehyaei, and M. El Haj Assad, "Energy, exergy, economic and exergoenvironmental analyses of gas and air bottoming cycles for production of electricity and hydrogen with gas reformer," *J. Clean. Prod.*, vol. 259, p. 120915, 2020.
[59] W. Wang, J. Wang, Z. Lu, and S. Wang, "Exergoeconomic and exergoenvironmental analysis of a combined heating and power system driven by geothermal source," *Energy Convers. Manag.*, vol. 211, p. 112765, 2020.
[60] P. Ahmadi, I. Dincer, and M. A. Rosen, "Exergy, exergoeconomic and environmental analyses and evolutionary algorithm based multi-objective optimization of combined cycle power plants," *Energy*, vol. 36, no. 10, pp. 5886–5898, 2011.

[61] S. Khanmohammadi, P. Heidarnejad, N. Javani, and H. Ganjehsarabi, "Exergoeconomic analysis and multi objective optimization of a solar based integrated energy system for hydrogen production," *Int. J. Hydrogen Energy*, vol. 42, no. 33, pp. 21443–21453, 2017.
[62] S. Papari, M. Kazemeini, and M. Fattahi, "Modelling-based optimisation of the direct synthesis of dimethyl ether from syngas in a commercial slurry reactor," *Chinese J. Chem. Eng.*, vol. 21, no. 6, pp. 611–621, 2013.
[63] A. Mian, A. V. Ensinas, and F. Marechal, "Multi-objective optimization of SNG production from microalgae through hydrothermal gasification," *Comput. Chem. Eng.*, vol. 76, pp. 170–183, 2015.
[64] S. Mohanty, "Multiobjective optimization of synthesis gas production using non-dominated sorting genetic algorithm," *Comput. Chem. Eng.*, vol. 30, no. 6–7, pp. 1019–1025, 2006.
[65] M. A. Deslauriers, M. Sorin, B. Marcos, and M. A. Richard, "Retrofit of low-temperature heat recovery industrial systems using multiobjective exergoeconomic optimization," *Energy Convers. Manag.*, vol. 130, pp. 207–218, 2016.
[66] D. H. Muhsen, A. B. Ghazali, T. Khatib, I. A. Abed, and E. M. Natsheh, "Multiobjective differential evolution algorithm-based sizing of a standalone photovoltaic water pumping system," *Energy Convers. Manag.*, vol. 118, pp. 32–43, 2016.
[67] A. Ozbilen, I. Dincer, and M. A. Rosen, "Development of a four-step Cu-Cl cycle for hydrogen production - Part II: Multi-objective optimization," *Int. J. Hydrogen Energy*, vol. 41, no. 19, pp. 7826–7834, 2016.
[68] D. Saury, S. Harmand, and M. Siroux, "Flash evaporation from a water pool: Influence of the liquid height and of the depressurization rate," *Int. J. Therm. Sci.*, vol. 44, pp. 953–965, 2005.
[69] D. Zhang, D. Chong, J. Yan, and Y. Zhang, "Study on steam-carrying effect in static flash evaporation," *Int. J. Heat Mass Transf.*, vol. 55, no. 17–18, pp. 4487–4497, 2012.
[70] Y. Liao, D. Lucas, E. Krepper, and R. Rzehak, "Flashing evaporation under different pressure levels," *Nucl. Eng. Des.*, vol. 265, pp. 801–813, 2013.
[71] S. Mutair and Y. Ikegami, "Experimental investigation on the characteristics of flash evaporation from superheated water jets for desalination," *Desalination*, vol. 251, no. 1–3, pp. 103–111, 2010.
[72] Y. Zhang, J. Wang, J. Yan, D. Chong, and J. Liu, "Experimental study on energy transformation and separation characteristic of circulatory flash evaporation," *Int. J. Heat Mass Transf.*, vol. 99. pp. 862–871, 2016.
[73] J. Stengler, K. Schaber, and S. Mall-Gleissle, "Experimental study on low temperature desalination by flash evaporation in a novel compact chamber design," *Desalination*, vol. 448, pp. 103–112, 2018.
[74] C. Wang, R. Xu, X. Chen, P. Jiang, and B. Liu, "Study on water flash evaporation under reduced pressure," *Int. J. Heat Mass Transf.*, vol. 131, pp. 31–40, 2019.
[75] G. Tsatsaronis, "A Review of Exergoeconomic Methodologies," in *Moran MJ, Sciubba E, editors. Second law analysis of thermal systems. New York: American Society of Mechanical Engineers*, 1987, pp. 81–87.
[76] M. A. Rosen and I. Dincer, "Exergoeconomic analysis of power plants operating on

various fuels," *Appl. Therm. Eng.*, vol. 23, no. 6, pp. 643–658, 2003.
[77] O. Jolliet, "Life cycle impact assessment definition.Study of the SETAC-UNEP life cycle initiative," 2003.
[78] A. Bejan, G. Tsatsaronis, and M. Moran, *Thermal design and optimization*. New York: Wiley, 1996.
[79] K. Deb, A. Pratap, S. Agarwal, and T. Meyarivan, "A fast and elitist multiobjective genetic algorithm: NSGA-II," *IEEE Trans. Evol. Comput.*, vol. 6, no. 2, pp. 182–197, 2002.
[80] I. Dincer, M. A. Rosen, and P. Ahmadi, *Optimization of energy systems*. John Wiley & Sons, 2017.
[81] A. Toffolo and A. Lazzaretto, "Evolutionary algorithms for multi-objective energetic and economic optimization in thermal system design," *Energy*, vol. 27, no. 6, pp. 549–567, 2002.
[82] M. Si, "The feasibility of waste heat recovery and energy efficiency assessment in a steel plant," Ph.D dissertation, University of Manitoba, 2011. Available: http://hdl.handle.net/1993/4746.
[83] G. F. Naterer, M. Fowler, J. Cotton, and K. Gabriel, "Synergistic roles of off-peak electrolysis and thermochemical production of hydrogen from nuclear energy in Canada," *Int. J. Hydrogen Energy*, vol. 33, no. 23, pp. 6849–6857, 2008.
[84] H. Y. Kwak, D. J. Kim, and J. S. Jeon, "Exergetic and thermoeconomic analyses of power plants," *Energy*, vol. 28, no. 4. pp. 343–360, 2003.
[85] J. Rogelj, D. Shindell, K. Jiang, S. Fifita, P. Forster, V. Ginzburg, C. Handa, H. Kheshgi, S. Kobayashi, E. Kriegler, L. Mundaca, R. Seferian, and M. V. Vilarino, "Mitigation Pathways Compatible with 1.5°C in the Context of Sustainable Development. In: *Global Warming of 1.5°C. An IPCC Special Report on the impacts of global warming of 1.5°C above pre-industrial levels and related global greenhouse gas emission pathways, in the context of strengthening the global response to the threat of climate change, sustainable development, and efforts to eradicate poverty*," 2018. Available: https://www.ipcc.ch/report/sr15/mitigation-pathways-compatible-with-1-5c-in-the-context-of-sustainable-4-development/
[86] M. Martín-Gamboa, D. Iribarren, and J. Dufour, "Environmental impact efficiency of natural gas combined cycle power plants: A combined life cycle assessment and dynamic data envelopment analysis approach," *Sci. Total Environ.*, vol. 615, pp. 29–37, 2018.

Appendix

Copyright Permission

Thesis similarity is entirely due to the seven published works of the candidate that are derived from this thesis. Consequently, equations, crucial information, notations, and illustrations that could not be revised without losing important essence of the work have been maintained. Thesis similarity with each of these published works is listed below:

Paper 1: F. Razi, I. Dincer, and K. Gabriel, "Process Improvement and Analysis of an Integrated Four-Step Copper–Chlorine Cycle Modified with a Flash Vaporization Process for Hydrogen Production", Energy and Fuels, vol. 35, No. 10, p. 9038–9046, 2021.

Similarity: 4%

Paper 2: F. Razi, I. Dincer, and K. Gabriel, "Exergoenvironmental analysis of the integrated copper-chlorine cycle for hydrogen production", Energy, vol. 226, p. 120426, 2021.

Similarity: 4%

Paper 3: F. Razi, I. Dincer, and K. Gabriel, "Exergoeconomic analysis of a new integrated copper-chlorine cycle for hydrogen production," International Journal of Hydrogen Energy, vol. 45, No. 55, p. 30042-30055, 2020.

Similarity: 3%

Paper 4: F. Razi, I. Dincer, and K. Gabriel, "A Specific exergy costing assessment of the integrated copper-chlorine cycle for hydrogen production," International Journal of Hydrogen Energy, vol. 45, No. 56, p. 31425-31439, 2020.

Similarity: 3%

Paper 5: F. Razi, I. Dincer, and K. Gabriel, "Thermal management of a new integrated copper-chlorine cycle for hydrogen production," Energy Conversion and Management, vol. 212, p. 112629, 2020.

Similarity: 3%

Paper 6: F. Razi, I. Dincer, and K. Gabriel, "A multi-objective optimization of the integrated copper-chlorine cycle for hydrogen production," Computers and Chemical Engineering, vol. 140, p. 106889, 2020.

Similarity: 2%

Paper 7: F. Razi, I. Dincer, and K. Gabriel, "Energy and exergy analyses of a new integrated thermochemical copper-chlorine cycle for hydrogen production," Energy, vol. 205, p. 117985, 2020.

Similarity: 1%